# SEISMIC RESPONSE OF THE UC PHYSICS BUILDING IN THE CANTERBURY EARTHQUAKES

**By**

**Samuel Alexander McHattie**

**August 2013**

A thesis submitted to the University of Canterbury

in partial fulfilment of the requirements

for the degree of Master of Engineering (Civil)

Supervised by Dr Brendon Bradley

Department of Civil and Natural Resources Engineering

College of Engineering

University of Canterbury

Christchurch, New Zealand

# ABSTRACT

The purpose of this thesis is to evaluate the seismic response of the UC Physics Building based on recorded ground motions during the Canterbury earthquakes, and to use the recorded response to evaluate the efficacy of various conventional structural analysis modelling assumptions.

The recorded instrument data is examined and analysed to determine how the UC Physics Building performed during the earthquake-induced ground motions. Ten of the largest earthquake events from the 2010-11 Canterbury earthquake sequence are selected in order to understand the seismic response under various levels of demand. Peak response amplitude values are found which characterise the demand from each event. Spectral analysis techniques are utilised to find the natural periods of the structure in each orthogonal direction. Significant torsional and rocking responses are also identified from the recorded ground motions. In addition, the observed building response is used to scrutinise the adequacy of NZ design code prescriptions for fundamental period, response spectra, floor acceleration and effective member stiffness.

The efficacy of conventional numerical modelling assumptions for representing the UC Physics Building are examined using the observed building response. The numerical models comprise of the following: a one dimensional multi degree of freedom model, a two dimensional model along each axis of the building and a three dimensional model. Both moderate and strong ground motion records are used to examine the response and subsequently clarify the importance of linear and non-linear responses and the inclusion of base flexibility. The effects of soil-structure interaction are found to be significant in the transverse direction but not the longitudinal direction. Non-linear models predict minor in-elastic behaviour in both directions during the 4 September 2010 $M_w$ 7.1 Darfield earthquake. The observed torsional response is found to be accurately captured by the three dimensional model by considering the interaction between the UC Physics Building and the adjacent structure. With the inclusion of adequate numerical modelling assumptions, the structural response is able to be predicted to within 10% for the majority of the earthquake events considered.

# ACKNOWLEDGEMENTS

I would like to express sincere gratitude to my supervisor Brendon Bradley for his continuous support throughout my masters. Brendon's work ethic and dedication to his career have provided me with great motivation and I could not have imagined having a better advisor and mentor.

I would also like to acknowledge my co-supervisor Jeff Clendon for providing me with much needed expertise and information about the Physics Building. I am extremely grateful for the foresight from Hamish Avery and GNS Science for setting up the instrumentation programme in the Physics Building, without which none of this research could have been done.

I would like to thank the Civil and Natural Resource Engineering Department at the University of Canterbury for their support and teaching throughout my undergraduate and postgraduate studies. Also, the funding provided from the UC Masters Scholarship is appreciated.

A very special thanks to my civil engineering colleagues at the University of Canterbury, in particular Varun Joshi, James O'Neill, Andrew Baird, Tobias Smith, Maxim Millen, Chris Watson, Dennis Pau, Zeinab Chegini, Lake Carter, Francesco Sarti, Gareth Morris, Matthew MacDonald, Harry Johnston, Daniel Moroder and Adi Ramakanth. Thank you for creating an awesome working environment and I will miss our daily coffee excursions. A further big thank you to my flatmates Marcus Burrows, Angus Grant, and Nick Dawe for making our three years of flatting very enjoyable.

The support from my family has been extremely important in turning me into the person I am today. I would especially like to thank my cousins Jemma Davies, for her help in proof-reading my work and Zack Johnson, for his Sketch Up expertise.

Finally, I would like to thank my parents Mary and Graeme McHattie for their undying support and encouragement during my 23 years. They have always ensured that I have had the opportunity to pursue my goals, and I dedicate this thesis to them.

# Table of Contents

# List of Figures

# List of Tables

# 1 INTRODUCTION

## 1.1 Overview

Instrumented buildings can be considered as full scale models, with the correct boundary and initial conditions, which are excited during earthquake events. They provide important system-level data on how real structures behave during earthquakes, which can be difficult, if not impossible, to obtain using sub-system-level laboratory experiments. To date, the majority of current data from instrumented buildings has been obtained from earthquakes in Japan and The United States. Recently, valuable data has been recorded from a number of instrumented buildings that were subjected to the Canterbury earthquakes and analysis of their results can yield additional insights, particularly in a New Zealand-specific context.

In 2006, the Physics Building section of the Rutherford Building at the University of Canterbury was instrumented with ten multi-directional accelerometers. These accelerometers recorded the earthquakes on 4 September 2010 and 22 February 2011, as well as the many subsequent events in the 2010-2011 Canterbury earthquake sequence. The data recorded from these events provides a unique opportunity to examine the behaviour of this structure under moderate and strong ground motions.

The ground motion data recorded can be directly examined to determine certain structural properties of the building using response spectra and frequency-domain techniques. These observed values can be compared with empirical code equations for the same parameters. This instrumental data also provides the ability to examine the predictive capabilities of numerical models by comparing the observed accelerations and displacements with those predicted by a numerical model. The New Zealand design standards prescribe several analysis methods including equivalent static, modal analysis and numerical response history analysis. The last of these methods is the focus of this thesis, in which various modelling assumptions will be scrutinized against the observed seismic response from the instrumental records.

## 1.2 Thesis Outline

The thesis is organised into the following eight chapters:

**Chapter 2** provides a review of previous research in two main areas. The first is seismic instrumentation and this is broken down into three further categories which look at (1) how and why seismic instrumentation is used; (2) past examples of seismically instrumented buildings; and (3) previous studies of the UC Physics Building using seismic instrumentation. The second main area of the literature review focuses on seismic design and prediction of building parameters and response. While this includes numerous design code methods, specific attention is given to numerical response history modelling. The last two sub sections of this chapter look methods for considering soil-structure interaction and non-linear effects, in order to improve the model's predictive capabilities.

**Chapter 3** provides background information on the UC Physics Building and its instrumentation. This includes how the building resists lateral loads and where the seismic instruments are located. The damage that was visible post-earthquakes and eye-witness accounts from people who were in the building during the earthquakes is also described.

**Chapter 4** examines how the building responded to ten of the larger earthquakes in the Canterbury earthquake sequence using the recorded accelerometer data. Amplitude parameters, such as peak floor acceleration and displacement, as well as duration parameters, such as significant duration, are discussed. The fundamental period of the structure is estimated using frequency-based techniques and other observed effects, including torsion and rocking are investigated.

**Chapter 5** looks at current seismic design practice and compares code predictions with the observed response. A one dimensional (1D) and two dimensional (2D) model is are developed in each orthogonal direction using simple design procedures. The predicted displacements from 1D and 2D fixed base numerical models are compared with the observations and reasons for the differences are discussed.

**Chapter 6** investigates how soil-structure interaction is accounted for in numerical modelling and updates the 1D and 2D fixed base models to allow for base flexibility. The SSI models account for soil degrading and the observed values are compared with two predictive methods for each event. The predicted displacements from 1D and 2D SSI models are compared with the fixed base models and observations and reasons for the differences are discussed.

**Chapter 7** introduces nonlinear effects into the model by considering simple non-linear constitutive models. The predicted non-linear behaviour is compared with observed damage from Chapter 3. This effect is added to the soil-structure interaction model in order provide the best predictions possible

using simple design methods. Finally, a three dimensional fixed base model is used to examine if the observed torsional behaviour can easily be predicted by a numerical model.

**Chapter 8** summarizes the key findings of this research.

# 2 LITERATURE REVIEW

## 2.1 Overview

There are three main approaches for evaluating seismic behaviour and performance of structural systems:

1. Laboratory testing of full or reduced-scale models of a structure or one or more of its sub-assemblies.
2. Numerical and/or analytical prediction.
3. Observations of seismic responses from instrumented structures.

This research will consider both numerical/analytical predictions and analysis of instrumentation recordings to assess the seismic behaviour of the UC Physics Building at the University of Canterbury. As this research covers a wide range of earthquake engineering topics, a brief but broad literature review is detailed below which covers the following areas:

- Seismic instrumentation
- Observed response of instrumented buildings in past earthquakes
- Previous research on the dynamic response of the UC Physics Building
- Adequacy of prescriptions in design guidelines
- Accuracy of response history analysis
- Soil-structure interaction effects
- Non-linear behaviour and constitutive models.

## 2.2 Instrumentation

The main objective of a seismic instrumentation array for structural systems is to improve understanding of the behaviour, and potential for damage, of structures under the dynamic loads imposed by earthquakes. As a result of this increased understanding, design and construction practices can be modified so that future earthquake damage is minimized (Celebi, 2001). An instrumentation array should provide sufficient data to reconstruct the response of the structure in enough detail to compare with the response predicted by mathematical models.

To obtain a useful dataset from an instrumented building, sensors must be placed in a certain configuration in order to capture important response outputs. Multiple horizontal sensors aligned vertically in a building can show relative lateral displacements and modal shapes associated with the principal sway vibration modes, whilst two parallel sensors on the same floor can be utilized to investigate both torsion and rocking response. Schematic illustrations of these configurations are shown in Figure 2-5 (a) and (b), respectively. The observed data can also be used to find important building dynamic parameters such as fundamental period, frequency ratios and periods of torsion and rocking motion (Li & Mau, 1997).

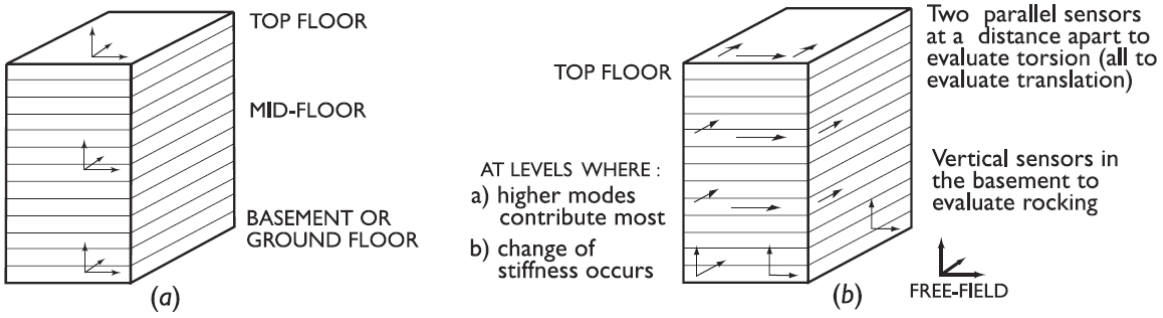


Figure 2-1: Recommended location of seismic instrumentation (from Celebi (2001)).

## 2.3 Observed response of instrumented structures in past earthquakes

The majority of analyses from instrumented building recordings in English literature have primarily examined horizontal accelerations using results from the 1994 Northridge earthquake. The Northridge earthquake, which occurred in Southern California, had a moment magnitude ($M_w$) of 6.7 and caused ground motion accelerations of up to 1.8g to be recorded (Vahdani & Wikstrom, 2002). Naeim (2000) used observed data from 20 instrumented buildings and found results for the natural periods, base shears, mode shapes and torsion. Ventura *et al.* (2003) performed a detailed analysis of two buildings affected by the Northridge earthquake where the pseudo-spectral velocity was calculated at different floors, and modal periods could clearly be seen. They also performed a modal analysis to find the first six modes (first and second translational modes in both horizontal axes and two torsion modes) for each building. Aldea *et al.* (2007) also used results obtained from seismic instrumentation to identify the modal periods for a building in Bucharest. They used a transfer function to find the first three translational periods of the structure in each direction as well as first two torsional periods. Aldea et al considered earthquake data from 12 events ranging in magnitude from 4.3 to 6.0 and averaged the results to find the periods.

In New Zealand, the GeoNet Instrumentation Project, operated by GNS Science, had focused on expanding the number of instrumented buildings. The program currently consists of six instrumented buildings in Wellington and one building in Christchurch, Levin, Napier and Nelson. As well as having the instrumented buildings all over the country, there is also variety in the types of buildings being instrumented. This includes numerous timber, steel and reinforced concrete buildings as well as the base-isolated Wellington Hospital and a post-tensioned timber building. Since the 4 September 2010 Darfield earthquake, several buildings have been instrumented in the Christchurch CBD (Beskhyroun *et al.*, 2012). The University of Auckland placed instruments in three damaged buildings using Micro Electro-Mechanical Systems (MEMS) accelerometers. Beskhyroun *et al.* (2012) were able to identify the mode shapes and fundamental periods in these buildings.

## 2.4 Previous research on the dynamic response of the UC Physics Building

One of the buildings in the GeoNet Instrumentation Project is the UC Physics Building at the University of Canterbury (Uma *et al.*, 2011). A diagram of the building with locations of the 10 multidirectional accelerometers is shown in Figure 2-2.

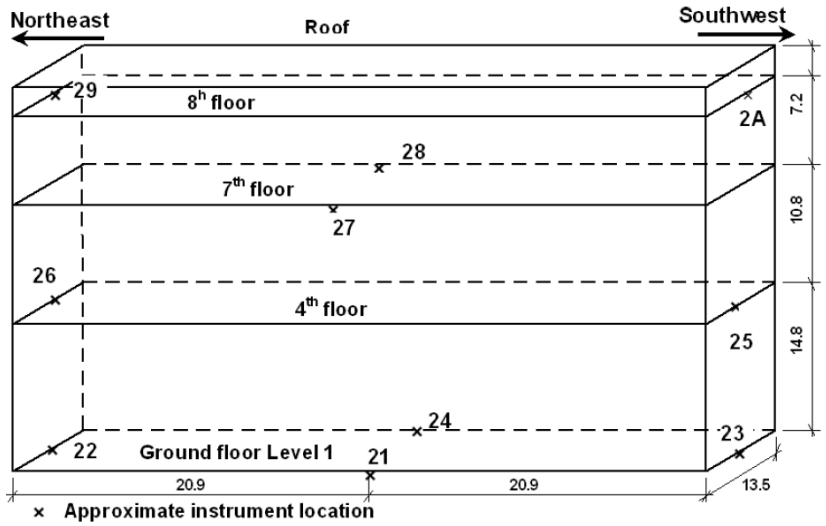


Figure 2-2: Locations of accelerometers in the UC Physics Building (from Zhao and Uma (2011))

The Rutherford Building is an eight-storey reinforced concrete building that was constructed in 1966 and designed by the Ministry of Works. The building is split into three distinct superstructures, each of which is separated by a seismic gap. The Chemistry Building is at the southwest end, the Physics Building at the northeast end, and the stairwell and lift shafts in the centre. The structural design of the two end buildings is almost identical with the exception of the Chemistry Building being longer in the longitudinal direction.

The Rutherford Building was dynamically tested with a small amplitude steady state vibrator by Reay (1970). Reay predicted the dynamic response with a theoretical analysis which he later compared to the results obtained using a vibration exciter. Soil-structure interaction was also examined but it was determined that the effects of this were hard to estimate with any degree of certainty. Reay found the resonant frequencies and equivalent damping ratios of the first five modes for the structure. These frequencies were 2.65 Hz and 8.6 Hz for the transverse direction, 3.24 Hz for the longitudinal direction, and 3.15 Hz and 11.7 Hz for torsion. During the same time period, one of the shear walls in the Chemistry Building was dynamically tested by Johnstone (1970). Johnstone (1970) found that the fundamental period of the translational motion in the end shear wall was 3Hz. Both Johnstone (1970) and Reay (1970) found that the rotation of the base during the dynamic excitation, as a result of base rotation, was significant and resulted in large displacements with a linear profile over the structure's height, with up to half of the displacement on the eighth floor resulting directly from base rotation.

The UC Physics Building has experienced a number of strong ground motions from earthquakes since the 4 September 2010 $M_w$ 7.1 Darfield earthquake, providing a large database of recorded accelerations of engineering significance (GeoNet, 2012). The ground motions experienced in Christchurch from the Darfield earthquake showed many complex effects from both source and site. There was evidence of forward directivity and basin effects which increased the long period motion of the earthquake (Bradley, 2011a). The effects of this earthquake on reinforced concrete (RC) buildings in Christchurch City were minimal and most buildings built after the 1970s performed well, whilst pre-1970s designs led to some brittle failures (Pampanin *et al.*, 2011). The 22 February 2011 earthquake in Christchurch was the second largest magnitude earthquake in the Canterbury earthquake sequence. This earthquake resulted in severe ground motion intensities in the city due to its close proximity. Basin effects were again experienced as well as soft soil effects, both of which increased the long period ground motion amplitudes experienced (Bradley, 2011b). The effect of the earthquake on the city was catastrophic with 182 deaths, the majority of which came from the collapse of two mid rise RC buildings (Kam *et al.*, 2011). Of the 833 RC buildings that were inspected in Christchurch shortly after the 22 February 2011 earthquake, 441 were given a green tag, 257 were given a yellow tag and 135 were given a red tag. The number of damaged buildings in this earthquake was significantly higher than the 4 September 2010 earthquake where 90% of RC buildings were given green tags (Kam *et al.*, 2011). There was also many significant geotechnical issues that occurred during the 22 Fberuary2011 earthquake which included: numerous areas of the city having liquation, differential settlements and tilting; punching settlements of structures with shallow foundations (Cubrinovski *et al.*, 2011). However, the liquefaction was most severe for residential areas located to the east of the CDB,

A preliminary analysis of the seismic response of the UC Physics Building in the 4 September 2010 earthquake was performed by Zhao and Uma (2011). They identified soil-structure interaction,

torsion and rocking motions of the foundation during the earthquake. This data was used to calculate the fundamental frequency for rocking about both horizontal axes, and the transverse mode. These values were found to be 1.6 Hz, 2.3 Hz and 2.1 Hz, respectively. The peak inter-storey drift was also found to be 0.3% and 0.15% in the transverse and longitudinal directions.

Butt and Omenzetter (2012) also used the instrumented UC Physics Building to investigate soil-structure-foundation interaction. They used recorded ground motion data from several earthquakes including the September 2010 and February 2011 records to find the first three mode shapes, damping ratios and periods of the structure. They inferred that the fundamental period appeared to increase with time, implying a gradual loss of stiffness in the structure.

The results of Zhao and Uma (2011) and Butt and Omenzetter (2012) provide preliminary analyses of the structural response during the earthquakes. However, there is clearly scope for a more detailed analysis. The analysis by Zhao and Uma was only carried out for the 4 September 2010 earthquake, whereas those performed by Butt and Omenzetter only included a small subset of earthquakes. Butt and Omenzetter used a relatively new technique to identify the modes, so a more reliable identification technique such as a Fourier transform is required to confirm their findings. Furthermore, neither of the aforementioned studies compared the observed building response with code prescriptions or numerical modelling. The observed building response can be utilised to scrutinise the adequacy of NZ design code prescriptions for fundamental period, response spectra and floor acceleration amplification. Also the response of the building cannot be properly understood without a numerical model of the structure. In this research, numerical models will be developed which include adequate assumptions based on the observed behaviour. This can provide further insight into the response of all floors (in addition to the instrumented floors) as well as any soil-structure interaction and damage as a result of non-linear behaviour. By comparing the observed response with predictions from numerical models can provide extremely valuable information on how current modelling techniques compare with actual observed data.

## 2.5 Adequacy of prescriptions in seismic design guidelines

The Australian/New Zealand Design Standards are the principal protocols to which engineers design buildings in New Zealand. The standard that considers earthquake loading is Part 5 (NZS, 2004), and includes empirical equations for parameters such as fundamental period and floor accelerations as well as many analytical methods for the seismic design of a structure. Figure 2-3 shows the relationship between the building height and prescribed fundamental period for a frame and wall system. These prescribed values can be compared with the observed period in both directions.

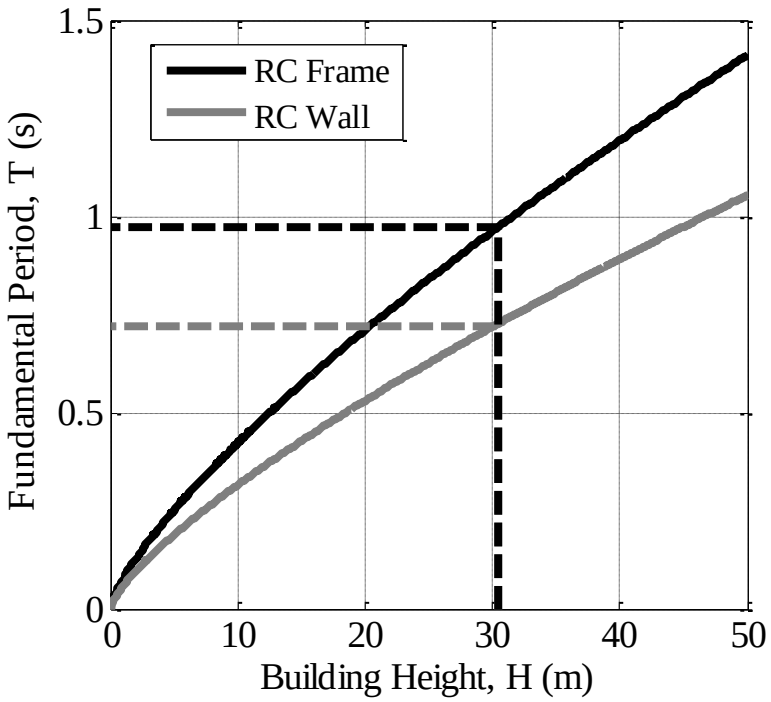


Figure 2-3: Prescribed code equations for fundamental period with height.

Section 8 of NZS1170.5 describes how to calculate the loading for the design of non-structural components of a building in an earthquake. This is usually performed by calculating the peak floor acceleration based on a prescribed equation and designing the part for this level of demand. The prescribed equations for the ratio of peak floor acceleration to peak ground acceleration with respect to height from the NZ standard NZS1170.5, European standard Eurocode-8 (2009) and American standard ASCE/SEI7-05 (2006) are shown in Figure 2-4. It is interesting to note that the prescribed acceleration amplification is not depend on the building type or fundamental period. It appears that the NZ code is very conservative compared with the other two codes. These equation can be compared with peak floor acceleration profiles observed from the UC Physics Building.

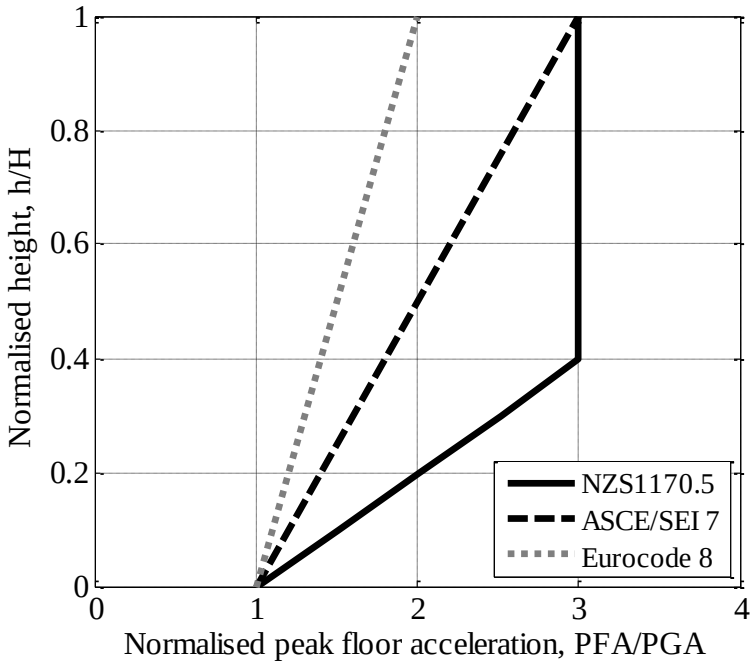


Figure 2-4: Prescribed code equations for amplification of acceleration with height.

## 2.6 Accuracy of response history analysis

The best example of using strong ground motion data in comparison with design was performed by Llera and Chopra (1995). Eight instrumented building responses from the 1994 Northridge earthquake were examined to extract useful information on the building properties and performance. They then constructed a linear model based on conventional design techniques for each building and compared the predictions with observations. Finally, they improved the models using state of the art practices to explain discrepancies with conventional linear modelling. This analysis procedure is also adopted in this research to understand the response of the UC Physics Building and how it compares with New Zealand design procedures. This type of analysis has not been performed for a New Zealand-based structure before.

It is more common for complex numerical analyses to be performed on buildings that have already been built and the engineer is required to understand how the structure resists earthquake loads. Only irregular or very tall structures are required to use a numerical analysis in the design process. Typically seismic instrumentation and numerical modelling are used in tandem so that the model can be validated based on the observed response. Once the model is validated it is then typically used perform further analysis on the building. Some examples of seismic instrumentation used in the validation of numerical models are detailed below.

Michel and Gueguen (2006) used acceleration recordings from a magnitude 4.6 earthquake in France to validate their lumped mass model of a 13-storey reinforced concrete building. They validated their model by comparing the observed acceleration time-series at the top of the structure with that predicted by the model. This validation allowed them to use the model to predict building performance in future earthquake scenarios.

Wallace *et al.* (1999) developed a time-series analysis methodology for tilt-up buildings using a series of simple 2D models to evaluate connection forces and deformations, as well as demand in the roof diaphragm, for a given ground motion. They used data from the response of an instrumented tilt-up building to validate their model so that it could be used for other designs.

Two reinforced concrete buildings, built in 1957 in Mexico City, were instrumented in order to better understand their how they were still able to resist earthquake loads. Cuevas (2000) used instrumented data from the 1994 Northridge earthquake to validate a 3D finite element model, which he then used to confirm how the buildings were resisting the earthquake motion.

The numerical models in the above paragraphs used state of the art modelling techniques in order to make their model as accurate as possible. In this research, the aim is to show the effect adding increasing complex design assumptions has on the accuracy of the predictions produced by the model. The main two effects that are examined in this research are the inclusion of soil-structure interaction and non-linear behaviour. Information of these two effects is provided in the following two sections.

## 2.7 Soil-structure interaction effects

In general, when an engineer develops a numerical model of a structure, they would assume that the model has a fixed base boundary condition. This however, is only the case if the structure is constructed on a rock or stiff soil site. Most structures in New Zealand urban areas are actually built on relatively soft soils which affect how the building reacts. Buildings on soft soils can have large horizontal, vertical and rotational movements at the base as a result of non-linear soil behaviour. A fixed base model does not allow for this and can cause the model to inadequately predict the displacement and acceleration responses. A background of soil-structure interaction modelling is detailed below.

Seismic soil-structure interaction (SSI) is the dynamic interaction between the soil and structure that arises during ground shaking. This interaction is able to change the seismic response of the structure by increasing or decreasing shear forces depending on the specific soil/structural conditions. As a result, an accurate seismic evaluation of structures cannot be carried out by considering the structure alone as is commonly done in conventional design practice. A fixed base model does not accurately

represent the behaviour of the global soil-structure system. The two mechanisms of interaction that take place between the structure and soil are inertial interaction and kinematic interaction (Stewart *et al.*, 1999a, 1999b).

The kinematic response depends on the ability of the foundation to follow the movement of the soil and thus based on its relative stiffness, the higher the foundation rigidity, the larger the kinematic effect on the incoming excitation. The oscillation experienced by the foundation will become the input motion for the superstructure. This effect is significant for embedded foundations as well as piles, and is equal to zero for shallow foundations subjected to horizontal motion, as there is no movement restriction of the free field motion in the latter case.

The inertial response is due to the presence of the structural mass under the action of the input motion; inertial forces arise causing new shear forces and overturning moments at the base level. Since the foundation can translate and rotate, the dynamic response of the structure depends on the amount of compliancy of the soil. Moreover, both structure and soil interact providing a feedback mechanism between each other (Kausel, 2010).

Since the UC Physics Building has shallow footings, the kinematic effects will be minimal and the main soil-structure interaction will come from inertial effects, therefore, only these effects will be considered in the chapters herein. A system commonly employed for simplified analysis of inertial interactions, shown in Figure 2-5, consists of a single-degree-of-freedom structure of height $h$ on a flexible foundation medium represented by the rotational springs $k_u$ and $k_\Theta$ . This simple system can be viewed as a model of a single-storey building, or more generally, as an approximate model of a multi-storey building that is dominated by the fundamental mode response. In the latter case, $h$ is interpreted as the distance from the base to the centroid of the inertial forces associated with the fundamental mode.

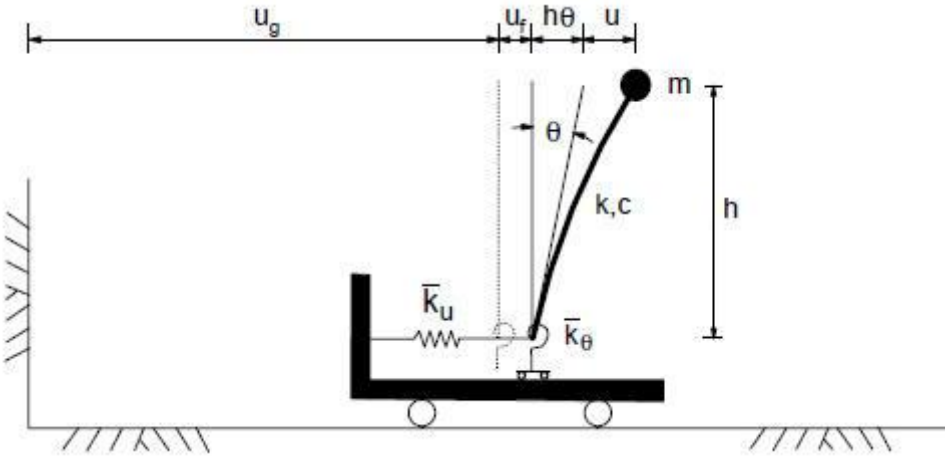


Figure 2-5: Simplified Model for Analysis of Inertial Interaction (from Stewart *et al.* (1999a)).

Traditionally, SSI has the effect of increasing the natural period and the damping of the soil-structure system, depending on dimensionless parameters like stiffness, slenderness and mass ratios (Wolf, 1998). In addition, while the overall displacement tends to increase because of the foundation flexibility, the maximum structural distortion tends to reduce. Typically, these effects are more significant as the structure becomes relatively rigid with respect to the foundation soil. These general trends, obtained through an equivalent linear approach, have been recently reviewed (Stewart *et al.*, 1999a) and compared (Stewart *et al.*, 1999b) with SSI effects empirically evaluated through system identification analyses for a broad range of sites. In general, it was found that the equivalent linear approach was reasonably accurate.

The impedance of the soil is a complex frequency-dependent dynamic number, that can be physically modelled through dynamic springs and dashpots; the former reflects the stiffness and the inertia of the supporting soil and the latter both radiation and material damping, due to wave scattering from the foundation and hysteretic behaviour of the soil, respectively. The dynamic response of rigid footings has been extensively investigated to include various aspects such as a range of footing geometries, foundation embedment, soil visco-elasticity and layering. User-friendly tables for calculating the frequency-dependent impedances for different conditions have been gathered by Gazetas (1991).

An alternative method of representing the stiffness of soil beneath a shallow foundation for two dimensional models is provided by, for example, FEMA (2000). Instead of uniform stiffness across the foundation, the footing is divided into zones of different stiffness as illustrated in Figure 2-6. The ends of the footing are represented by zones of relatively high stiffness over one-sixth of the footing width. The stiffness of these zones uses the formulations of Gazetas (1991) and is based on the vertical stiffness of a B x B/6 footing, while the stiffness of the middle zone is based on an infinitely long strip.

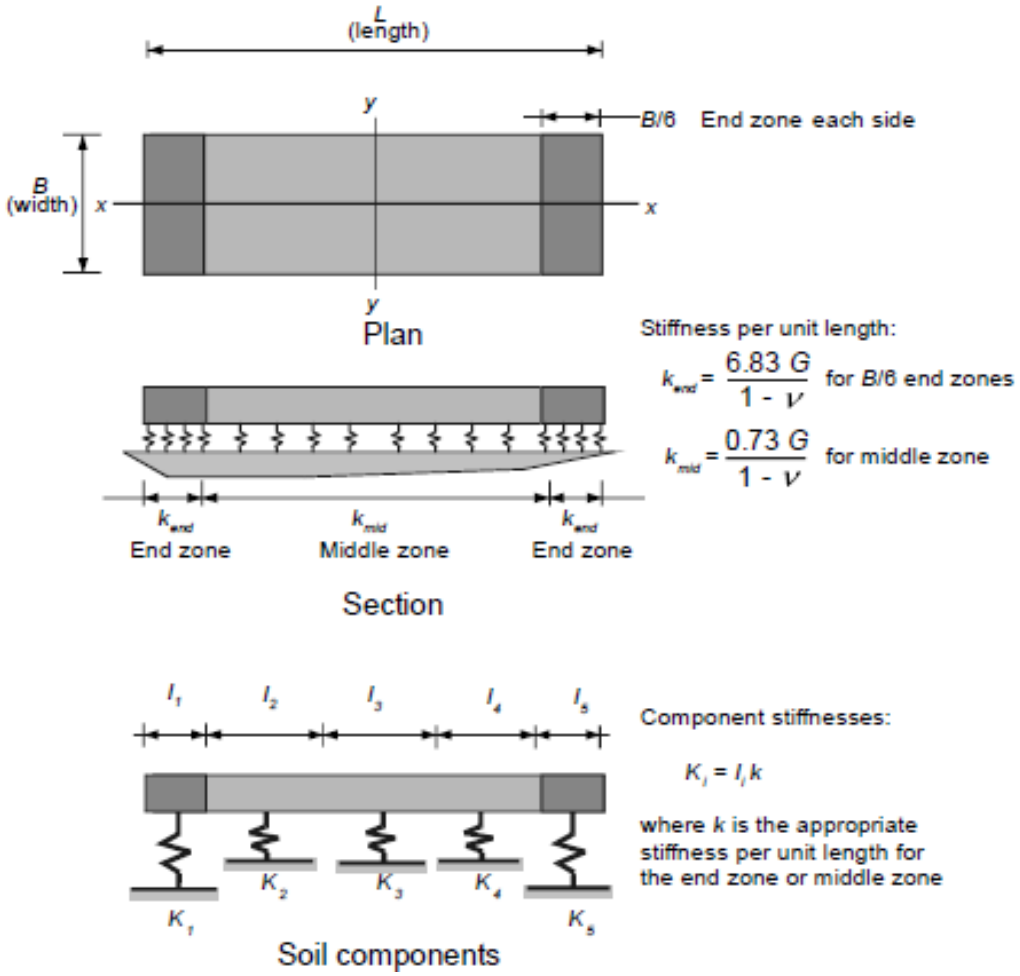


Figure 2-6: Diagram of Winkler soil-structure interaction model (FEMA273 (2000)).

where , $G_s$ is the shear modulus of the soil, and $\nu$ is the soil Poisson's ratio.

## 2.8 Non-linear behaviour and constitutive models

Numerical models of structures can also be modified to allow for nonlinear material behaviour. This, combined with foundation flexibility, should provide the best predictions based on real structural behaviour. However, it can be difficult to decide on which non-linear model is best suited for each specific element as well as defining the parameters in each model (Chopra, 2000). If the wrong model is chosen, or the parameters are defined incorrectly, then the resulting non-linear model can significantly over- or under-predict the actual behaviour. A brief background on non-linear structural modelling is described below.

A constitutive model defines the relationship between applied loading (moment or force) and the corresponding deformation (curvature or displacement) for a certain material. This relationship depends on both the type of material being modelled and the dimensions of the element. The simplest way to model the non-linear behaviour of reinforced concrete (RC) is to use a bi-linear relationship shown in Figure 2-7 (a). This model is defined by the initial stiffness and the yield point of the material (yield force ($F_y$) or moment ($M_y$)). The unloading and reloading stiffness of this model is the same as the initial stiffness. The area enclosed in this loop is equal to the energy dissipated by the material during each cycle of loading and this behaviour is called material or hysteretic damping.

Although the bi-linear model captures the basic non-linear behaviour of RC, there are other, more complicated models, that are available which do a better job. One of these models is the Modified Takeda Model (Takeda *et al.*, 1970) and is shown in Figure 2-7 (b). This model tries to incorporate the combined behaviour of the steel and concrete in a RC section. Typically, once the concrete has yielded in compression in one direction (i.e. cracked), it is much weaker when it is reloaded in that direction and only has the strength of the cracked section. The degradation of the unloading response increases the ductility of the section, providing a more realistic response (Stojadinovic & Thewalt, 1996).

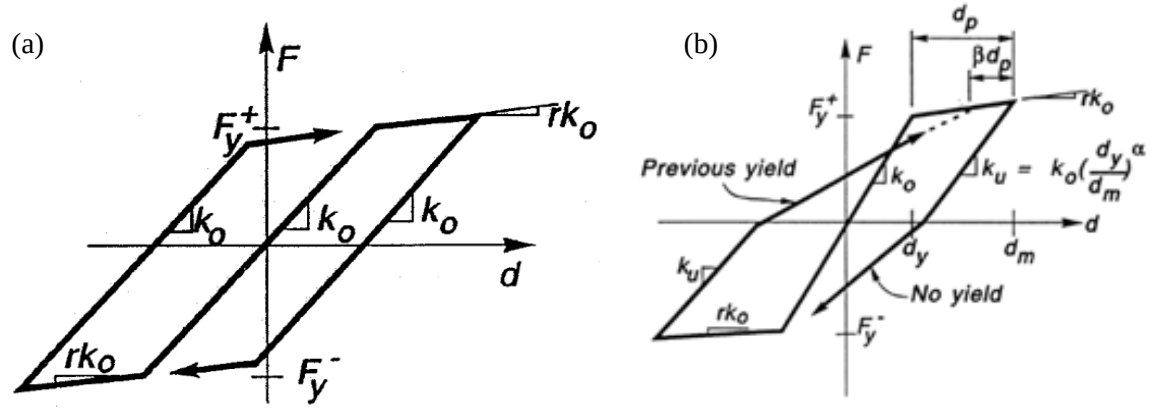


Figure 2-7: Constitutive models representing the non-linear behaviour of reinforced concrete using a (a) bi-linear and (b) Takeda relationship (after Carr (2004)).

Some of the parameters in a constitutive model have a strong influence on the structural response so must be selected carefully (Otani, 1984). These parameters include the yield level and the 'fatness' of the hysteresis loop. The post-yielding stiffness has a medium influence and the initial stiffness has a low influence for high ductility demands. However, for earthquakes which do not yield the material, the initial stiffness is very important.

Once the constitutive model has been selected, it must be determined where the non-linear behaviour can occur. Typically, the location of the non-linear behaviour is limited to the regions at the ends of the beams where it is most likely to occur. This is known as concentrated or lumped plasticity and it is most commonly used due to its simplicity. Two examples of this type of modelling are shown in Figure 2-8 (a) and (b). The other way to model plastic behaviour is to make the element have distributed plastic zones, as shown in Figure 2-8 (d) and (e). This allows the plastic behaviour to occur anywhere in the element as long as the yield force (or moment) is reached. This type of modelling can be more accurate, although it is more time-consuming to set up and is also more computationally expensive to run. The final option involves combining the two methods and include a defined region in which plasticity can occur. This is known as a finite hinge zone and is shown in Figure 2-8 (c). The length of this is zone is determined by material properties and is usually defined in material codes. This zone behaves like a distributed plasticity model but because it is only defined in a small region, it is not as computationally expensive and can be just as accurate if the region is defined correctly. However, the section between the two hinge zones remains linear elastic.

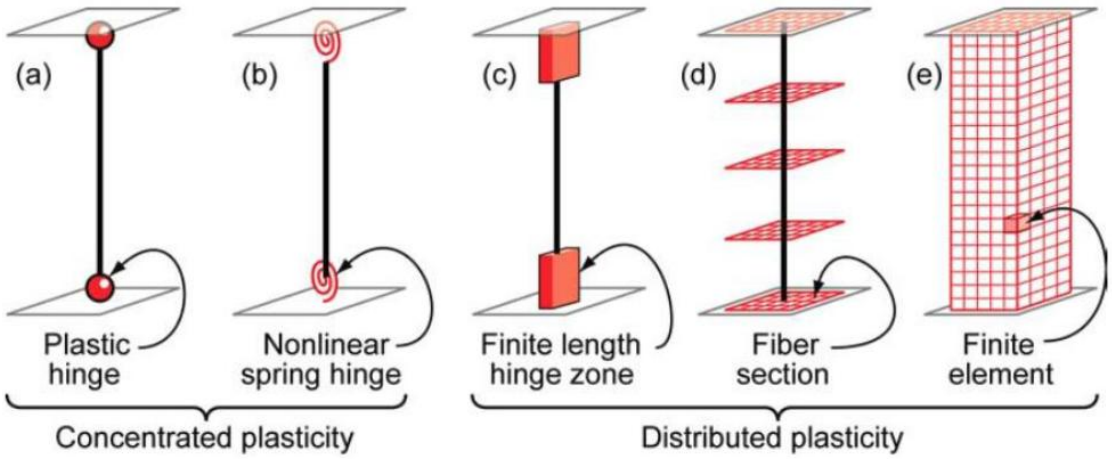


Figure 2-8: Concentrated and distributed plasticity models (after.Deierlein *et al.* (2010)).

In addition to material non-linearity's, geometric non-linearity's can also occur in a structure where the structural elements undergo significant displacements, thereby changing the geometry of the structure. These effects include P-delta and large-displacement effects, which cause increased moments due to the dead loads of the structure not being perfectly aligned down the column or walls. They become

more significant as the structure approaches failure and therefore will not be considered in this research, as the observed displacements of the UC Physics Building were relatively small for all events.

Non-linear modelling can be very useful, if it is done correctly, as it can identify the elements in a structure that are most likely to show non-linear behaviour resulting in damage. This was performed for a damaged building in the 1994 Northridge earthquake by Roger and Jirsa (1998). They used the structure's instrumented response to validate their model which was subsequently used to identify how and when the structure failed.

## 2.9 References

Aldea, A., Albota, E., Demetriu, S., & Kashima, T. (2007). *Seismic Response of a Low-Code High-Rise RC Building in Bucharest*. Paper presented at the International Symposium on Strong Vrancea Earthquakes and Risk Mitigation, Bucharest.

ASCE/SEI7-05. (2006). Minimum design loads for buildings and other structures. *ASCE Standard No. 007-05, 388pp*.

Beskhyroun, S., Ma, Q. T., Wotherspoon, L., & Davidson, B. J. (2012). *Experimental Modal Identification of Structures under Earthquake Excitation*. Paper presented at the 2012 NZSEE Conference. Paper 066

Bradley, B. A. (2011a). A Critical Analysis of Strong Ground Motions Observed in the 4 September 2010 Darfield Earthquake. *Bulletin of the New Zealand Society for Earthquake Engineering,* **44**(4), *pp. 181-194*.

Bradley, B. A. (2011b). Near-Source Strong Ground Motions Observed in the 22 February 2011 Christchurch Earthquake. *Department of Civil and Natural Resources Engineering, University of Canterbury*, **82**(6), *853-865*.

Butt, F., & Omenzetter, P. (2012). *Pre and post-earthquake dynamic analysis of an RC building including soil-structure interaction*. Paper presented at the 2012 NZSEE Conference. Paper 022

Carr, A. (2004). 2D RUAUMOKO: inelastic three-dimensional dynamic analysis program. Christchurch, NZ: University of Canterbury - Department of Civil Engineering.

Celebi, M. (2001). Current Practice and Guildlines for USGS Instrumentation of Buildings Including Federal Buildings. *Prepared for COSMOS (Consortium of Organizations for Strong-Motion Observation Systems) Workshop on Structural Instrumentation*.

Chopra, A. K. (2000). *Dynamics of Structures*. Upper Saddle River, NJ: Prentice-Hall, Inc

Cubrinovski, M., Bradley, B., Wotherspoon, L., Green, R., Bray, J., Wood, C., . . . Wells, D. (2011). Geotechnical Aspects of the 22 February 2011 Christchurch Earthquake. *Bulletin of the New Zealand Society For Earthquake Engineering*, **44**(4), *205-226*.

Cuevas, N. R. (2000). *Structural Models For Two Iinstrumented Buildings With Soil Structure Interaction*. Paper presented at the 12th World Conference on Earthquake Engineering. Paper No. 0144

Deierlein, G. G., Reinhorn, A. M., & Willford, M. R. (2010). Nonlinear structural analysis for seismic design (pp. 36pp): NIST GCR 10-917-5.

Eurocode-8 (2009). *Design of structures for earthquake resistance. Part 1: General rules seismic actions and rules for buildings.*

Federal Emergency Management Agency. (2000). *Prestandard and Commentary for the Seismic Rehabitation of Buildings. FEMA356.* Washington, D.C.

Gazetas, G. (1991). Foundation Vibrations. In H. Y. Fang (Ed.), *Foundation Engineering Handbook, 2nd Edition* (Chapter 15. pp. 553-593): Kluwer / Springer.

GeoNet. (2012). GeoNet strong motion building records,Retrieved from ftp://ftp.geonet.org.nz/building/

Johnstone, P. G. (1970). *The Stress Distribution in a Shear Wall.* Doctor of Philosophy in Civil Engineering, University of Canterbury, Christchurch, New Zealand.

Kam, W. Y., Pampanin, S., & Elwood, K. (2011). Seismic Performance of Reinforced Concrete Buldings in the 22 Feburary Christchurch (Lyttelton) Earthquakes. *Bulletin of the New Zealand Society for Earthquake Engineering,* **44**(4), *239-278*.

Kausel, E. (2010). Early historyofsoil–structureinteraction. *Soil DynamicsandEarthquakeEngineering,* **30**, *822-832*.

Li, Y., & Mau, S. T. (1997). Learning from Recorded Earthquake Motion of Buildings. *Journal of Structural Engineering,* **123**(1), *62-69*.

Llera, J. C. D. l., & Chopra, A. K. (1995). *Evaluation of Seismic Code Provisions Using Strong-Motion Building Records From the 1994 Northridge Earthquake.* Paper presented at the California Geological Survey - SMIP95 Seminar, San Francisco.

Michel, C., & Gueguen, P. (2006). *Dynamic Behaviour of The First Instrumented Building in France: The Grenoble City Hall*. Paper presented at the First European Conference on Earthquake Engineering and Seismology. Paper No. 941

Naeim, F. (2000). *Learning from Structural and Nonstructural Seismic Performance of 20 Extensively Instrumented Buildings*. Paper presented at the 12 WCEE 2000.

Standards New Zealand. (2004). *Part 5: Earthquake actions - New Zealand. NZS 1170.5.*

Otani, S. (1984). *Hysteresis Model of Reinforced Concrete for Earthquake Response Analysis*. Paper presented at the 8 WCEE, San Francisco.

Pampanin, S., Kam, W. Y., Tasligedik, A. S., Gallo, P. Q., & Akguzel, U. (2011). *Considerations on the seismic performance of pre-1970s RC buildings in the Christchurch CBD during the 4th Sept 2010 Canterbury earthquake: was that really a big one?* Paper presented at the Ninth Pacific Conference on Earthquake Engineering. Paper 179

Reay, A. M. (1970). *Dynamic Characteristics of Civil Engineering Structures.* Doctor of Philosophy in Civil Engineering, University of Canterbury, Christchurch, New Zealand.

Roger, Y., & Jirsa, J. O. (1998). Nonlinear Analyses of an Instrumented Structure Damaged in the 1994 Northridge Earthquake. *Earthquake Spectra,* **14**(2).

Stewart, J. P., Seed, R. B., & Fenves, G. L. (1999a). Seismic soil-structure interaction in buildings. I: Analytical aspects. *J. Geotech. & Geoenv. Engrg., ASCE,* **125 (1)**, *pp 26-37*.

Stewart, J. P., Seed, R. B., & Fenves, G. L. (1999b). Seismic soil-structure interaction in buildings. II: Empirical findings. *J. Geotech. & Geoenv. Engrg, ASCE,* **125 (1)**, *pp 38-48*.

Stojadinovic, B., & Thewalt, C. R. (1996). *Energy Balannced Hysteresis Models*. Paper presented at the 11 WCEE, Acapulco.

Takeda, T., Sozen, M. A., & Nielsen, N. N. (1970). Reinforced Concrete Response to Simulated Earthquakes. *ASCE, Journal of the Structural Division,* **96**(No. ST12).

Uma, S. R., King, A., Cousins, J., & Gledhill, K. (2011). The Geonet Building Instrumentation Programme. *Bulletin of the New Zealand Society for Earthquake Engineering,* **44**(1).

Vahdani, S., & Wikstrom, S. (2002). Response of the Tarzana strong motion site during the 1994 Northridge earthquake. *Soil Dynamics and Earthquake Engineering,* **22**(9–12), *837–848*.

Ventura, C. E., Laverick, B., Brincker, R., & Andersen, P. (2003). Comparison of Dynamic Characteristics of Two Instrumented Tall Buildings.

Wallace, J. W., Stewart, J. P., & Whittaker, A. S. (1999). Building Vulnerability Studies: Modeling and Evaluation of Tilt-up and Steel Reinforced Concrete Buildings *PEER Report 1999/13* Pacific Earthquake Engineering Research Center: College of Engineering University of California, Berkeley.

Wolf, J. P. (1998). Simple Physical Models for Foundation Dynamics. In Z. Chuhan & J. P. Wolf (Eds.), *Dynamic Soil-Structure Interaction*: Elsevier Science B.V.

Zhao, J. X., & Uma, S. R. (2011). *A preliminary analysis on the response of an instrumented building during the 2010 Darfield earthquake - significant effects of soil-structure interaction and nonlinear response*. Paper presented at the Ninth Pacific Conference on Earthquake Engineering. Paper 068

# 3 UC PHYSICS BUILDING

## 3.1 Overview

This chapter provides background information about the UC Physics Building, including the structural layout and detailing of members. The location of the seismic instrumentation is also provided. A detailed visual inspection was performed on the building after the earthquakes and the associated damage is identified. A summary of eye witness accounts from people who were inside the building during the earthquakes is also provided.

## 3.2 Background

The Rutherford Building is an eight-storey reinforced concrete building, which was designed by the Ministry of Works and constructed in 1966. The building is split into three sections, each of which is separated by a seismic gap of approximately 80 mm. The Chemistry Building is the section at the southwest end of the Rutherford Building, the Physics Building is the northeast section, and the stairwell and lift shafts, referred to as the Link Building herein, are located in the centre of the Rutherford Building. The orientation of the building is shown in Figure 3-1, where it can be seen that the longitudinal axis is aligned with an approximate northeast to southwest bearing. The structural design of the Physics and Chemistry buildings is almost identical, with the exception of the Chemistry Building being longer in the longitudinal direction.

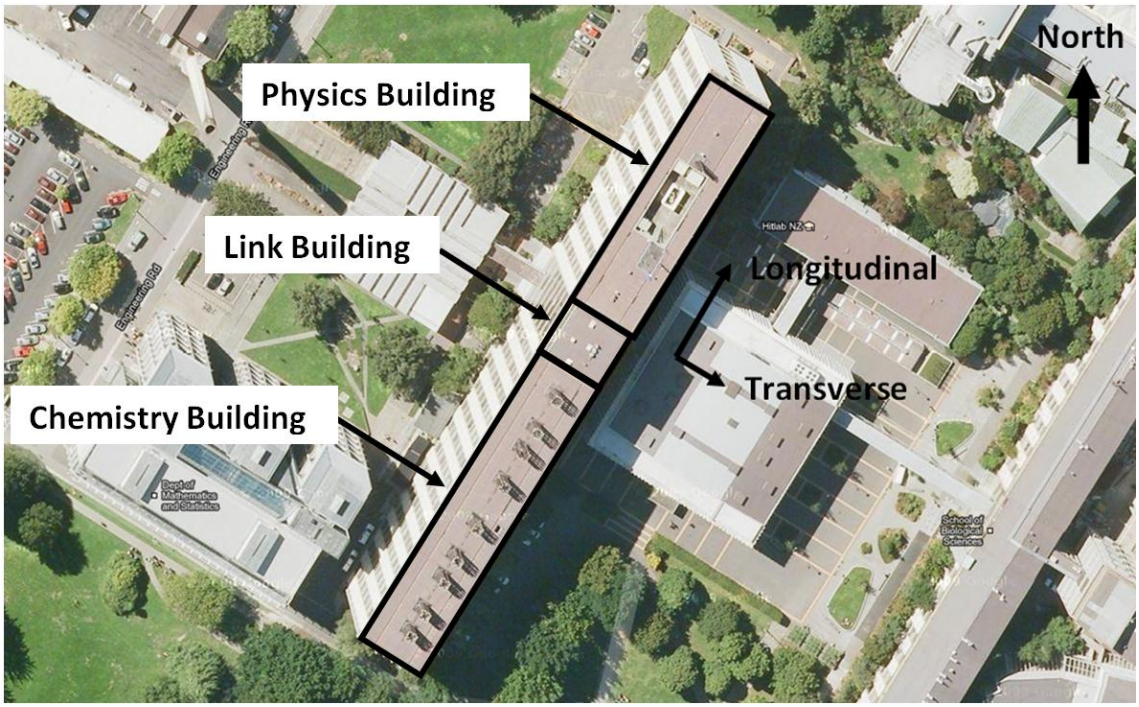


Figure 3-1: Aerial photo showing location and orientation of the building

A three-dimensional schematic of the Physics Building showing key structural element is illustrated in Figure 3-2. The structural layout of the building is described in the following section.

Figure 3-2: 3D schematic illustration of the UC Physics Building

## 3.3 Structural Layout

### 3.3.1 Overall layout

The overall size of the Physics Building floor plan is 58.2m by 15.0m. The total height of the building is 30.5m with an inter-story height of 3.8m. The foundations are shallow pad footings with a total depth of 2.4m. The main dimensions are shown in Figure 3-3.

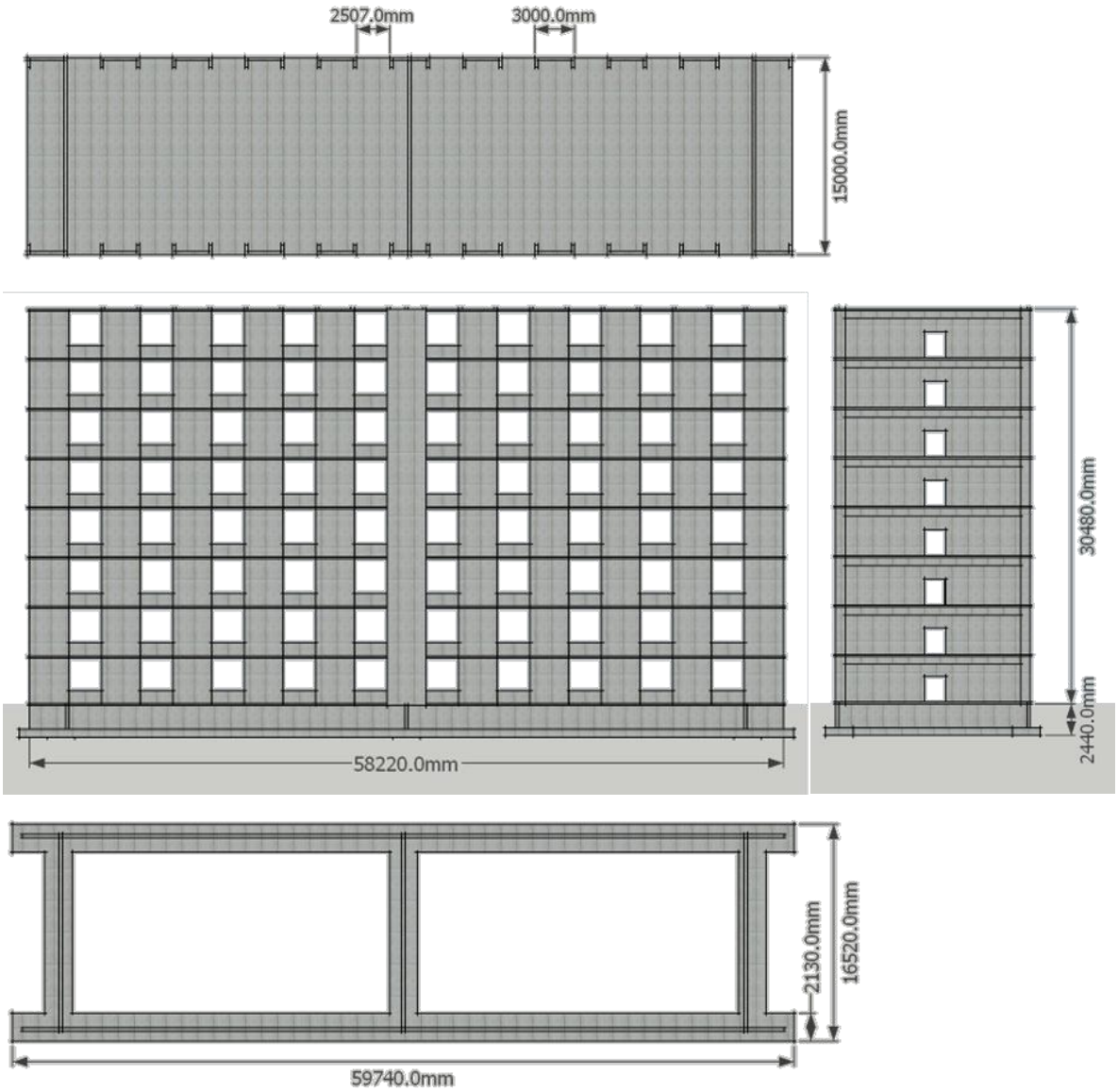


Figure 3-3: Physics Building plan and elevation views.

### 3.3.2 Element reinforcing details

The dimensions of reinforcement detailing for the key structural elements are shown in Figure 3-4 to Figure 3-9. Figure 3-4 shows the dimensions of the one of the end shear walls. The central gap in the shear wall is for the corridor on each floor. This divides the longitudinal reinforcement into two main zones that are approximately 5.2m and 8.1m long. As a result, the wall can be idealized as a coupled wall system with a short beam between the two walls on each floor.

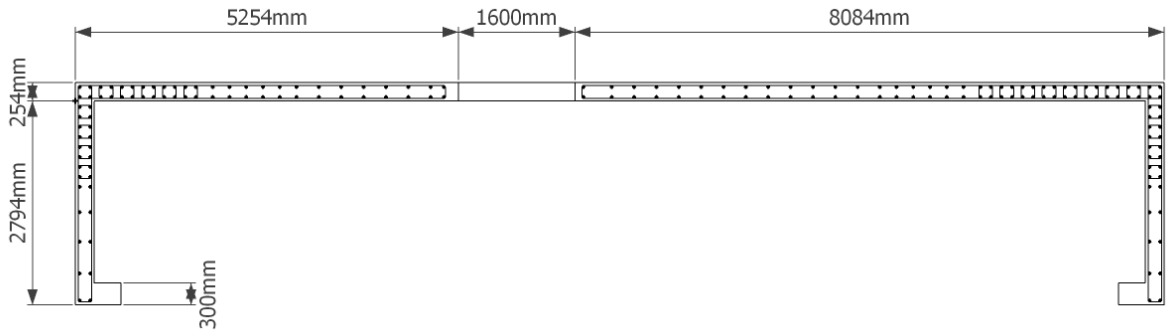


Figure 3-4: Dimensions of transverse shear wall.

The reinforcement for the shorter coupled wall is shown in Figure 3-5. It can be seen that 19mm longitudinal diameter bars are used for all of the longitudinal reinforcement with various spacing, the smallest spacing being close to the corner in both directions. This zone also has additional transverse reinforcement as illustrated.

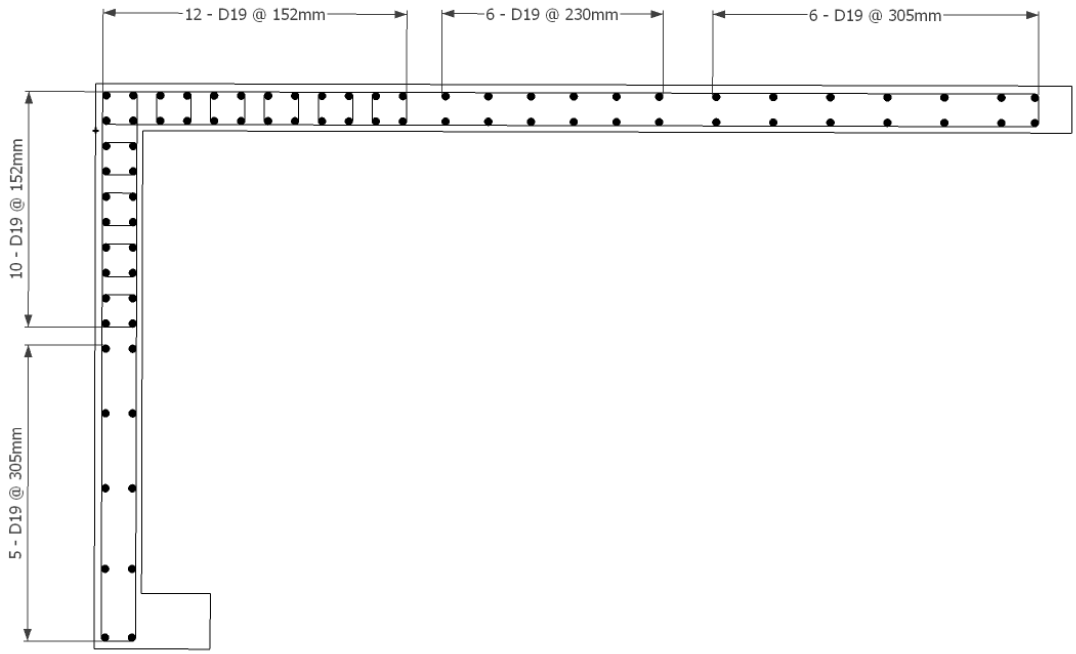


Figure 3-5: Reinforcing of smaller end of shear wall.

The reinforcing for the longer coupled wall is shown in Figure 3-6. Similar to the shorter coupled wall, the reinforcing in the corner is again closer in spacing and has additional transverse reinforcement.

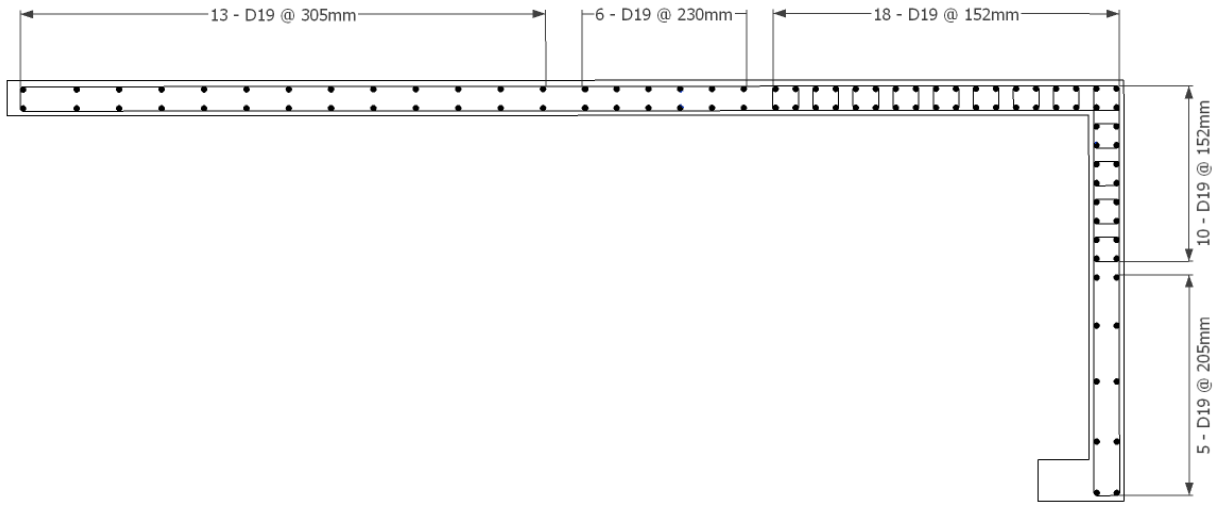


Figure 3-6: Reinforcing of larger end of shear wall.

The reinforcing and dimensions for the shear wall coupling beam are shown in Figure 3-7. It can be seen that this zone has a thicker 25.4mm diameter bar than the 19mm bars in the shear walls themselves, consistent with the fact that the coupling beam zone in a coupled wall system tends to attract high levels of stress that can cause this zone to fail in shear.

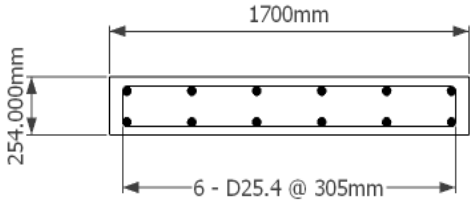


Figure 3-7: Dimensions and reinforcing for coupling beam in the shear wall.

The longitudinal lateral load resisting system is made up of a frame system which has U-shaped walls and deep beams. The dimensions and reinforcing for the walls are shown in Figure 3-8. The ends of the walls have minimal reinforcing so most of the moment resistance comes from the thin wall section. The reinforcing bars are also smaller in this wall with a diameter of 12.7mm.

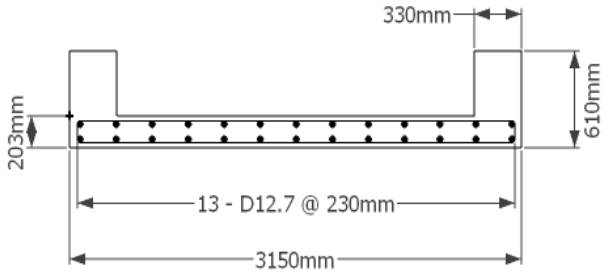


Figure 3-8: Dimensions and reinforcing for longitudinal walls.

The dimensions and reinforcing for the beams in the longitudinal direction are shown in Figure 3-9. The reinforcing bars have a smaller diameter of 12.7mm in comparison with the transverse system and the bar spacing in this direction is also smaller.

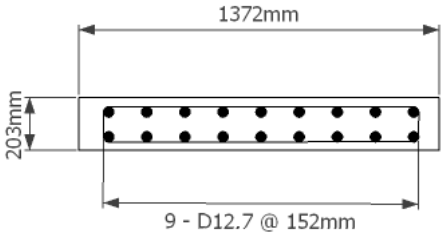


Figure 3-9: Dimensions and reinforcing for longitudinal beams.

### 3.3.3 Transverse load resisting system

The Physics Building is made up of 20 gravity frames positioned at 2.74m centres along the longitudinal axis of the building, as shown in Figure 3-10. In addition to the frames, the building is stiffened with three shear walls; one near each end and one in the middle of the building. The gravity loads are distributed evenly between the frames based on tributary area. For small lateral forces, the frames and shear walls will provide resistance, however, larger lateral loads will be resisted by the shear walls only. The reason for this is can be understood from the schematic in Figure 3-10, where the lateral stiffness of the frames is much smaller than the shear walls.

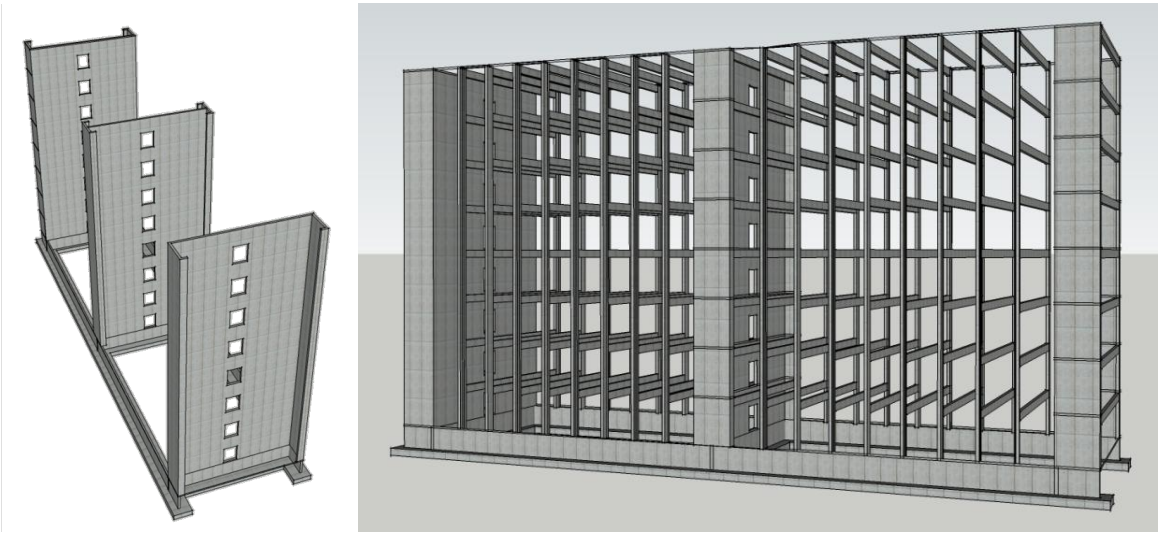

Figure 3-10: 3D view of transverse lateral resisting system depicting: (a) shear walls only; and (b) shear walls and gravity-designed frames

### 3.3.4 Longitudinal load resisting system

The lateral resistance of the structure in the longitudinal direction is made up of 11 small shear walls on each side equally spaced with a gap of 2.5m. The floors between the levels and frames provide an

almost rigid backbone to this system and allow most of the deformation to occur in the walls and beams. These frames are separated from the Link Building by a seismic gap of 80mm and are only connected through services and thin metal plates attached to each floor. The two parallel systems are shown in Figure 3-11 where the 'beam' elements in the frames are made up from a combination of the spandrel beams and floor slab. It is worth noting that the combination of walls and beams in this system act together as a frame system rather than a series of connected walls.

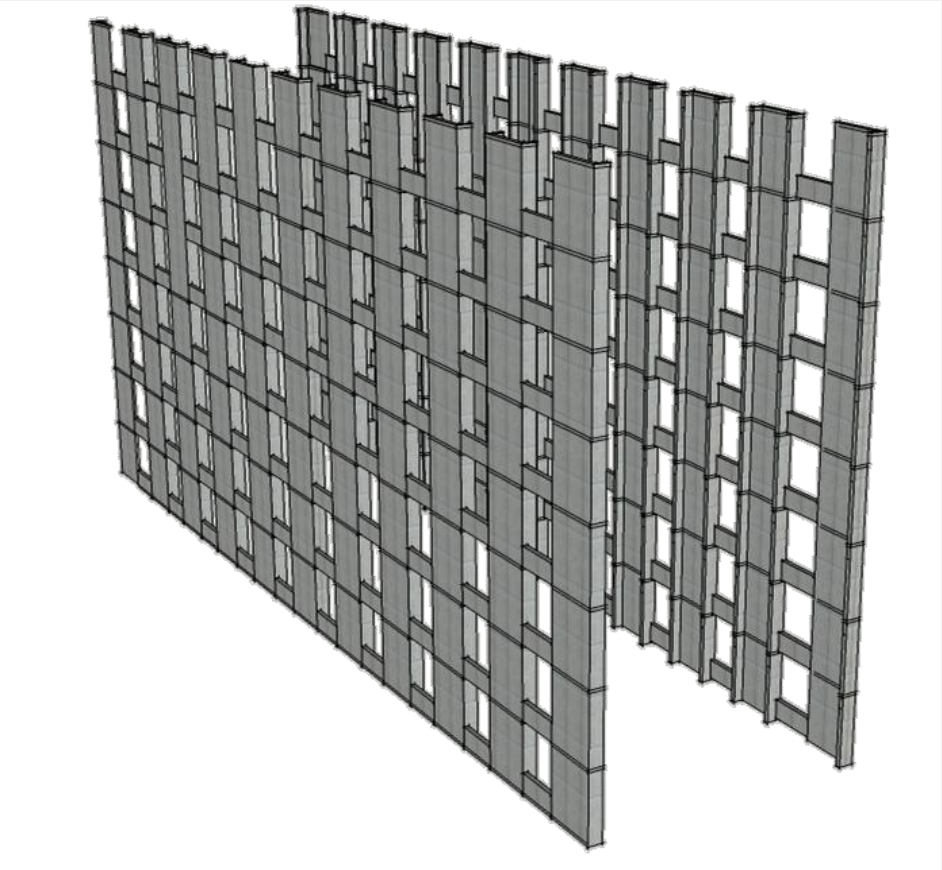

Figure 3-11: 3D view of longitudinal lateral resisting system.

### 3.3.5 Foundations

The foundation system of the Physics Building is a simple shallow pad footing that runs below the longitudinal frame system as well as under each shear wall. The footings are 2.4m deep and have a base, which is 610mm deep and 2.1m wide, as shown in Figure 3-12. The volume enclosed by the foundations is filled with compacted gravels.

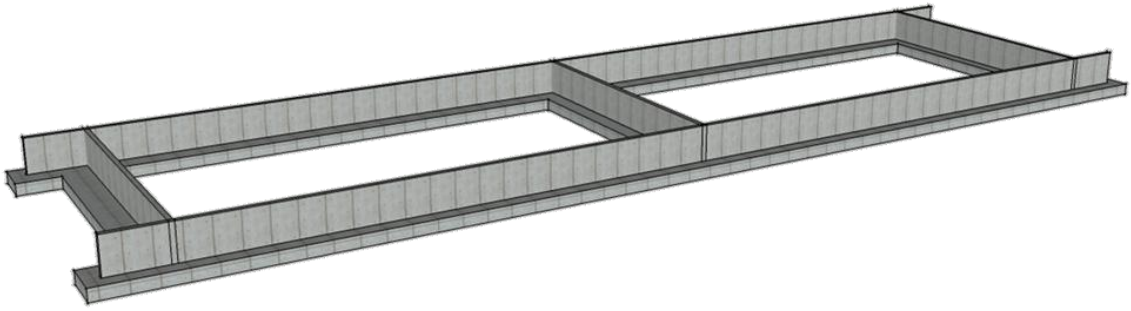

Figure 3-12: 3D view of foundation system.

The foundation system under the entire Rutherford Building is a continuous system which, unlike the rest of the building, has no seismic gap between each section. However, the foundations under the Link Building and Chemistry Building are twice as deep and are not filled with gravel. It should also be noted that the Chemistry and Link building foundations are fully embedded in soil while the Physics Building foundations are only partially embedded due to slopping ground around the Rutherford Building. A photo of the inside of the Chemistry Building's foundations is shown in Figure 3-13.

Figure 3-13: Photo from inside the Chemistry Buildings foundations.

## 3.4 Seismic Instrumentation

The Physics Building section of the University of Canterbury's Rutherford Building was instrumented in 2006 by GNS Science with 10 multi-directional accelerometers (Uma *et al.*, 2011). Figure 3-14 depicts the locations of the accelerometers, which are all positioned on the three transverse shear walls of the structure with four on the first floor, two on the fourth floor, two on the seventh floor and two on the eighth floor. There are three on each of the end shear walls with one at the base of the shear wall, one half way up and one at the top of the wall. In the middle of the building, there are also two on either side of the shear wall at the base and two three-quarters of the way up. Photos of each of the accelerometers are shown in Figure 3-15.

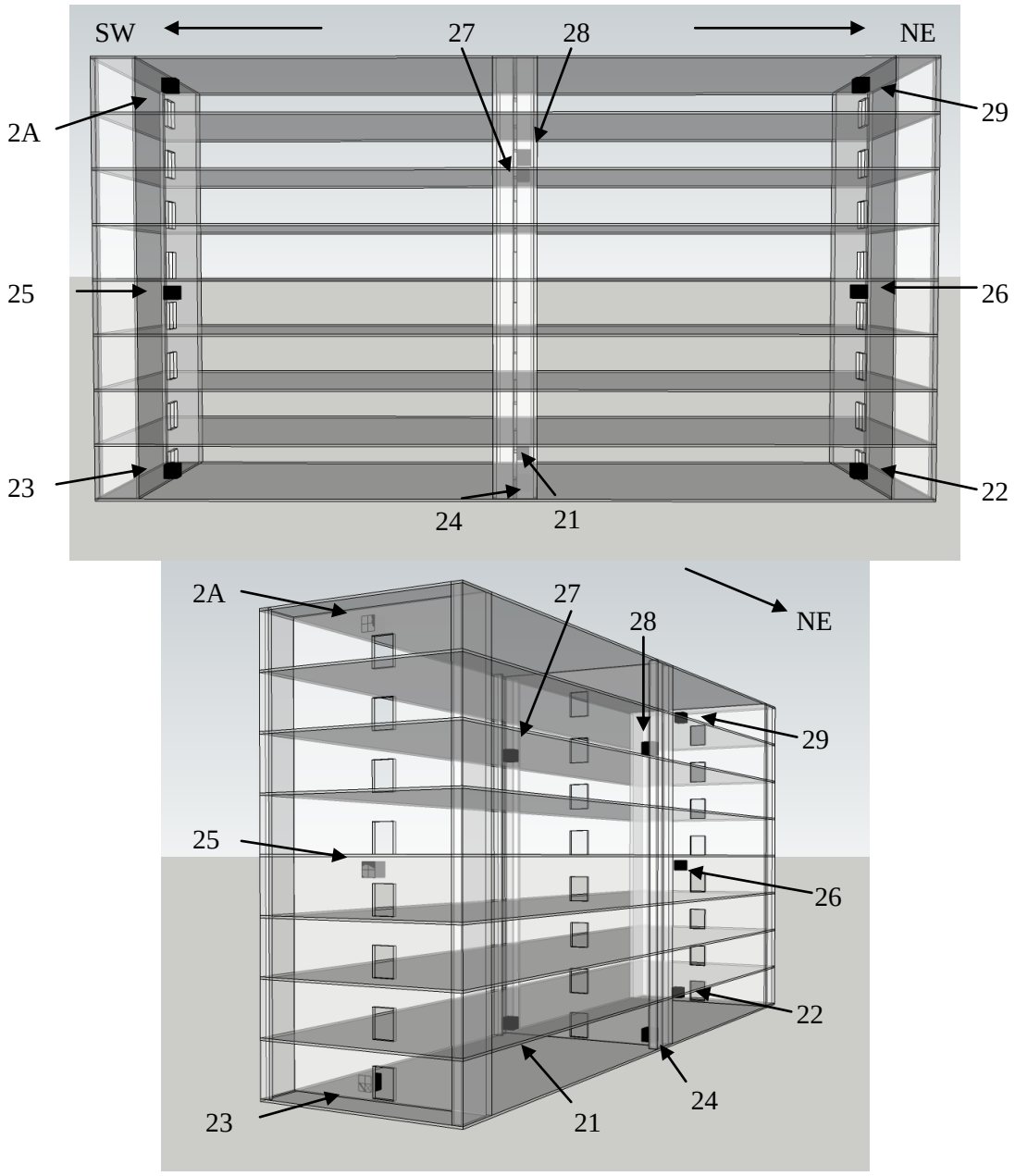


Figure 3-14: 3D view of the seismic instrumentation locations.

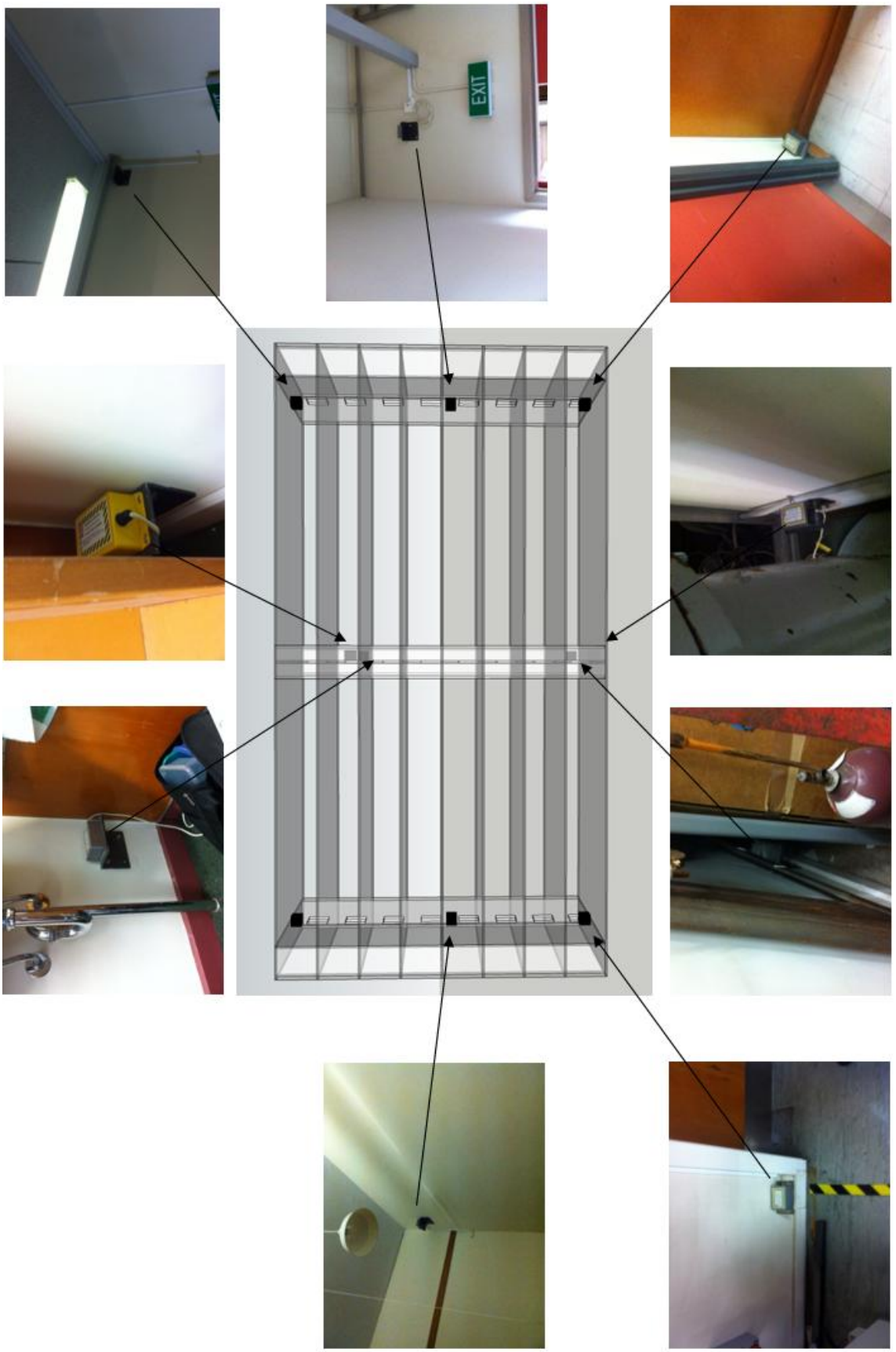


Figure 3-15: Photos of all accelerometers and their location in the Physics Building.

The accelerometer layout is such a way that:

- The lateral response from each end of the building can be easily found based on collectively examining the three accelerometers that are aligned vertically at each end of the building.
- The relative responses from both ends of the structure can also be compared in order to examine if there was any torsional response in the transverse direction.
- The four accelerometers on the first floor can be used to examine any rocking behaviour by comparing the vertical records from opposing accelerometers.
- The two accelerometers of the seventh floor can be used to examine any torsional behaviour in the longitudinal direction.

The ten accelerometers each have three data channels - one for each orthogonal direction (NE-SW, NW-SE and vertical), all recording ground motion accelerations at 200Hz. The accelerometers are set on a trigger to start recording once 0.004g of acceleration is reached within the 0.1-5Hz frequency range. When the shaking has stopped, the raw data is automatically uploaded to the GeoNet website (GeoNet, 2012), where it can be downloaded in ASCII text format.

## 3.5 Visual Inspection and Eye Witness Accounts

### 3.5.1 Visual Inspection

A visual inspection was undertaken on the building after the Canterbury earthquake sequence in order to find any signs of obvious physical damage, which can subsequently provide insight when performing structural analyses to understand the building response during these events. The main observed damage was found in the connection between the Link and Physics buildings, where the thin steel plates separating the two buildings had undergone some warping and in some places had come loose from its connections, as shown in Figure 3-16.

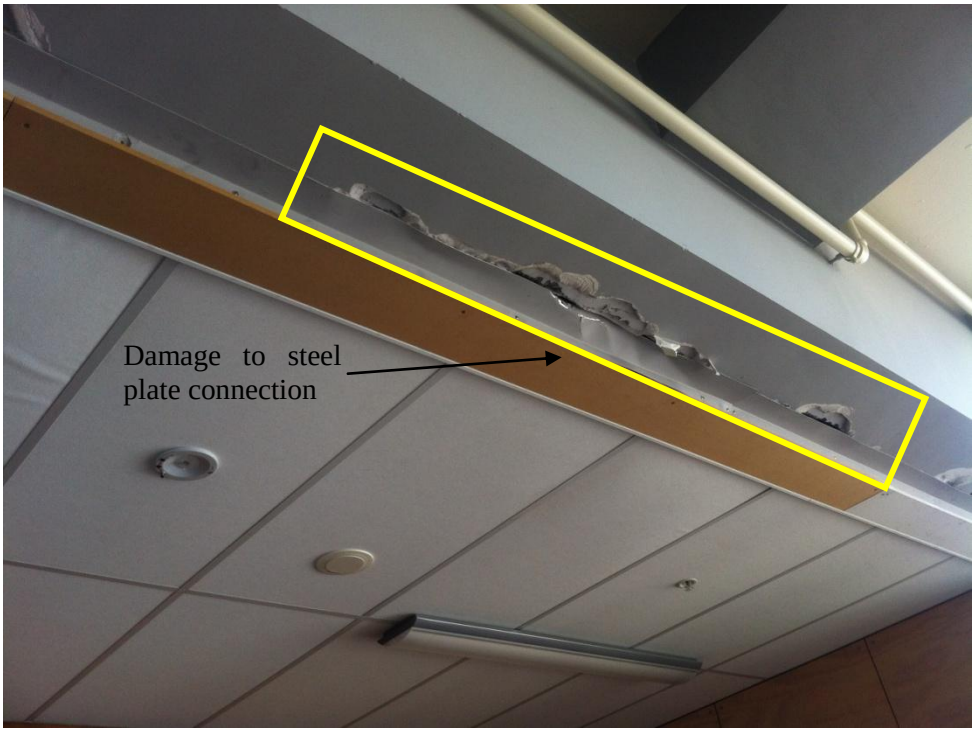


Figure 3-16: Photo of damage in the seismic gap between the Physics and Link Buildings.

Other physical damage observed included cracking in the beam-column joints in the transverse frame system. The worst of this is shown in Figure 3-17 in eighth floor frame.


Figure 3-17: Photo of cracking in eighth floor beam-column joint which can be seen in the warping of the surface paint.

There was no obvious visible damage to the outside of the Physics Building except for at the base of the foundation system, which is exposed at the end of the Physics Building. There was some cracking and signs of differential settlement as shown in Figure 3-18, however it is hard to determine if this occurred due to gravity settlement before the earthquakes.


Figure 3-18: Photo of cracking in the foundations.

The remainder of the observed damage was mostly to non-structural elements, such as plaster walls, as shown in Figure 3-19 from the first floor. There was also large spalling at the far end of the Chemistry Building, however the damage to the Link and Chemistry buildings was not investigated in detail.

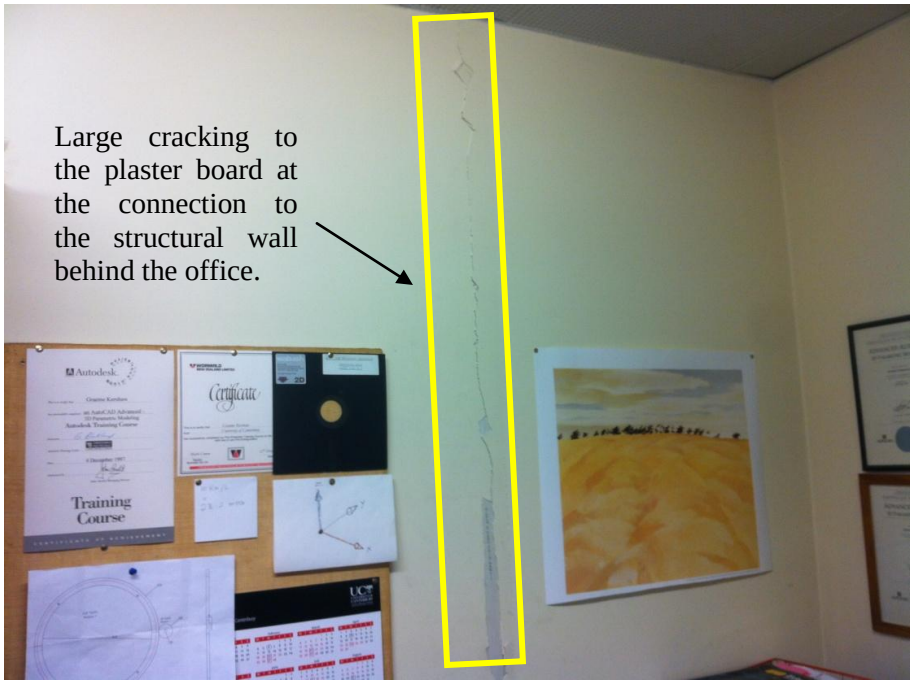


Figure 3-19: Photo of cracking in the plaster board.

In order to gain an idea of the overall damage to the building, a full inspection of the building was undertaken (Jeff Clendon personal communication, 2013). The main areas of interest where damaged occurred were the floor slab (shown in Figure 3-20); the shear walls (shown in Figure 3-21); and the spandrel beams (shown in Figure 3-22). These figures show the areas where cracks were found in the specified component.

The key points to be taken from these figures are:

- The majority of the cracks in the floor slabs were observed in the connection between the floor and the longitudinal walls.
- There was also cracking in the spandrel beams suggesting that there could have been some rotation occurring in the connections to the longitudinal walls.
- There was significant cracking at the base (first two levels) of the shear walls, while the rest of the wall had very few cracks.
- The small coupling beams that connect the two smaller walls, which make up the transverse shear wall, had diagonal cracking on all beams. This suggests that there was a large amount of shear being transferred across the beam from one wall to the other.

The observed damage from this chapter forms the basis of the non-linear modelling (found in Chapter 7) where the aim of the modelling is to try and replicate the observed damage caused in the zones.


Figure 3-20: Picture of reported floor damage after 22 February 2011 earthquake (Jeff Clendon personal communication, 2013). Note: The green lines correspond to observed cracks larger than 0.2mm while the red lines correspond to observed cracks less than 0.2mm wide.

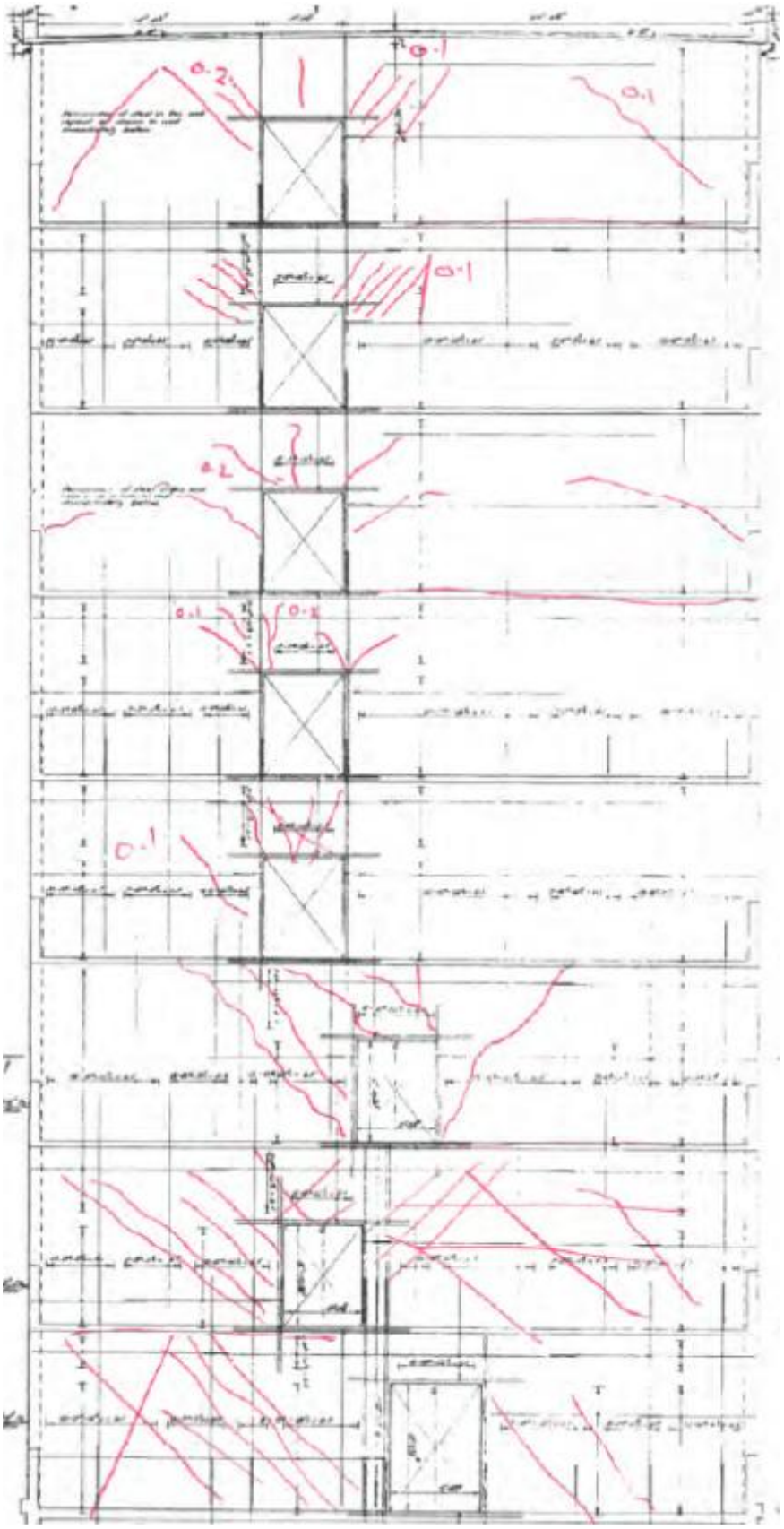

Figure 3-21: Picture of reported shear wall damage after 22 February 2011 earthquake (Jeff Clendon personal communication, 2013). Note: The red lines correspond to observed cracks less than 0.2mm wide.

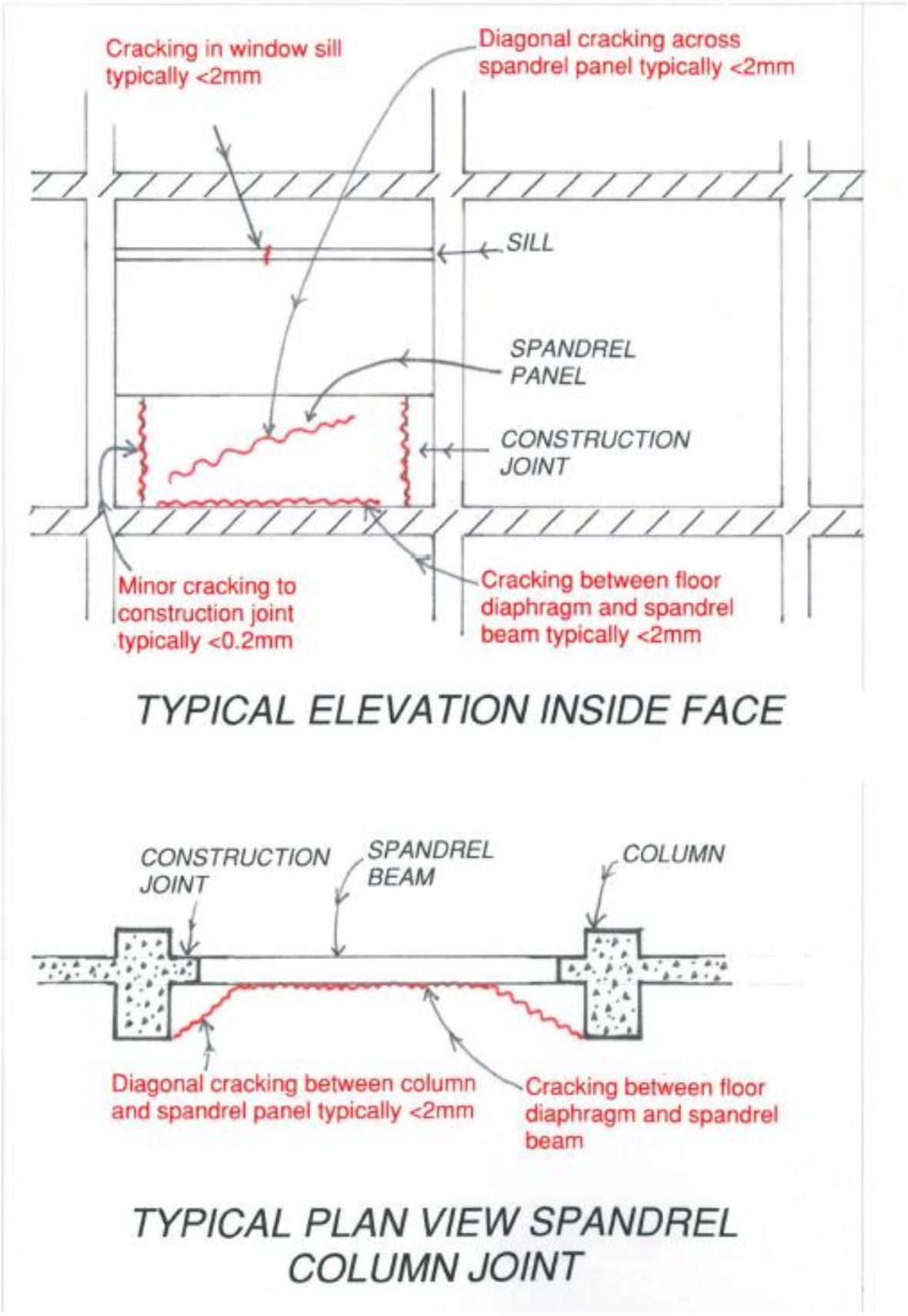


Figure 3-22: Picture of reported spandrel damage after 22 February 2011 earthquake (Jeff Clendon personal communication, 2013).

### 3.5.2 Eye Witness Accounts

Due to most of the earthquakes occurring during office hours, there were a large number of people who witnessed the response of the building in the earthquakes from inside. Six people who were inside the building during the earthquakes were interviewed. A summary of their responses is detailed below:

- People on the first and second floors described the 22 February 2011 earthquake as a VI on the Modified Mercalli Intensity (MMI) scale (Table 3-1), whereas people on the 6th and 7th floor described it as a VIII.
- People on the first floor also felt the first earthquake on the 13 June 2011 and described it as a V on the MMI scale and said it was definitely smaller compared with the 22 February 2011 earthquake.
- While being evacuated to the lawn after the 22 February 2011 earthquake, a number of people also noticed that the Physics Building and the Link Building were moving out of phase in both the longitudinal and transverse directions during one of the aftershocks. One person also stated that a service pipe that ran between the two buildings had failed in shear.
- A Lab Technician on the first floor noticed that the floor had bowed between the shear walls and also between the outside walls. Evidence of this came to light by placing a steel ball on the floor in different locations and observing it rolling quickly towards the corner in which it was placed closer to.

Table 3-1: Definitions of MMI scale for levels V, VI, VII and VIII (Kramer, 1996) given to witnesses.

| MMI | Description of observed level of shaking |
|---|---|
| V | Felt by nearly everyone, many awakened; some dishes, widows, etc., broken; a few instances of cracked plaster; unstable objects overturned; disturbances of trees, piles, and other tall objects sometimes noticed; pendulum clocks may stop. |
| VI | Felt by all, many frightened and run outdoors; some heavy furniture moved; a few instances of fallen plaster or damaged chimneys; damage slight. |
| VII | Everybody runs outdoors; damage negligible in buildings of good design and construction, slight to moderate in well-built ordinary structures, considerable in poorly built or badly designed structures; some chimneys broken; noticed by persons driving motor cars. |
| VIII | Damage slight in specially designed structures, considerable in ordinary substantial buildings, with partial collapse, great in poorly built structures; panel walls thrown out of frame structures; fall of chimneys, factory stacks, columns, monuments, walls; heavy furniture over-turned; sand and mud ejected in small amounts. |

## 3.6 References

GeoNet. (2012). GeoNet strong motion building records,Retrieved from ftp://ftp.geonet.org.nz/building/

Kramer, S. L. (1996). *Geotechnical Earthquake Engineering*. Upper Saddle River, NJ 07458: Prentice Hall, Inc

Uma, S. R., King, A., Cousins, J., & Gledhill, K. (2011). The Geonet Building Instrumentation Programme. *Bulletin of the New Zealand Society for Earthquake Engineering*, **44**(1).

# 4 OBSERVED INSTRUMENTAL RESPONSE

## 4.1 Overview

This chapter examines the observed instrumented response of the UC Physics Building during the 2010-11 Canterbury earthquakes. Direct analysis of accelerometer time-series is used to obtain response amplitude and duration parameters such as: peak floor acceleration, velocity and displacement; significant, bracketed and uniform durations. Ratios of the observed response parameters are also examined for the upper floors and the ground floor to directly determine the response of the structure.

Frequency-based ground motion parameters are examined using both response-spectral and Fourier-spectral analyses to identify the principal vibration periods of the structure (in three orthogonal directions). Comparisons between both response-spectral and Fourier-spectral methods, for all considered earthquake events, are used to develop confidence in the obtained vibration periods. The magnitude and vibration periods of torsion and rocking modes of the structure are also examined on the basis of the instrumental responses.

## 4.2 Summary of events considered

The 2010-2011 Canterbury earthquake sequence involved multiple moderate-to-large magnitude events which occurred in close proximity to urban Christchurch and the UC Physics Building (Kaiser *et al.* (2012) & Gledhill *et al.* (2011)). As a result of this close proximity, multiple strong ground motion records have been recorded from these events (Bradley (2011) & Bradley (2012)), and from the UC Physics Building array, in particular (Zhao & Uma, 2011) have presented results for 4 September 2010 earthquake. On the basis of strong motion amplitudes and sufficient quality instrumental responses for events in the Canterbury earthquake sequences, a total of ten events were considered for detailed analysis presented herein. A summary of the earthquakes considered and their source-to-site distance from the UC Physics Building is provided in Table 4-1. The location of the epicentres of the considered earthquakes is shown in Figure 4-1, as well as the location of the UC Physics Building in order to provide a visual representation of the source-to-site distance for each earthquake.

Table 4-1 Summary of earthquake events considered. Mw values are obtained from Gledhill *et al.* (2011)

| **Earthquake** | **Magnitude, $M_w$** | **Source to site distance, $R_{Rup}$ (km)** | **PGA (g)** |
|---|---|---|---|
| 04 September 2010 - 04:35 | 7.2 | 33.8 | 0.30 |
| 19 October 2010 - 11:32 | 4.8 | 11.6 | 0.08 |
| 26 December 2010 - 10:30 | 4.7 | 6.8 | 0.09 |
| 22 February 2011 - 13:50 | 6.2 | 10.4 | 0.25 |
| 16 April 2011 - 17:49 | 5.0 | 19.4 | 0.05 |
| 13 June 2011 - 13:01 (1) | 5.3 | 14.2 | 0.15 |
| 13 June 2011 - 14:20 (2) | 6.0 | 13.6 | 0.16 |
| 09 October 2011 - 20:34 | 4.9 | 17.5 | 0.03 |
| 23 December 2011 - 13:58 (1) | 5.8 | 17.7 | 0.14 |
| 23 December 2011 - 15:18 (2) | 5.9 | 14.8 | 0.17 |

Note: the (1) and (2) correspond to the first and second events on the respective date.

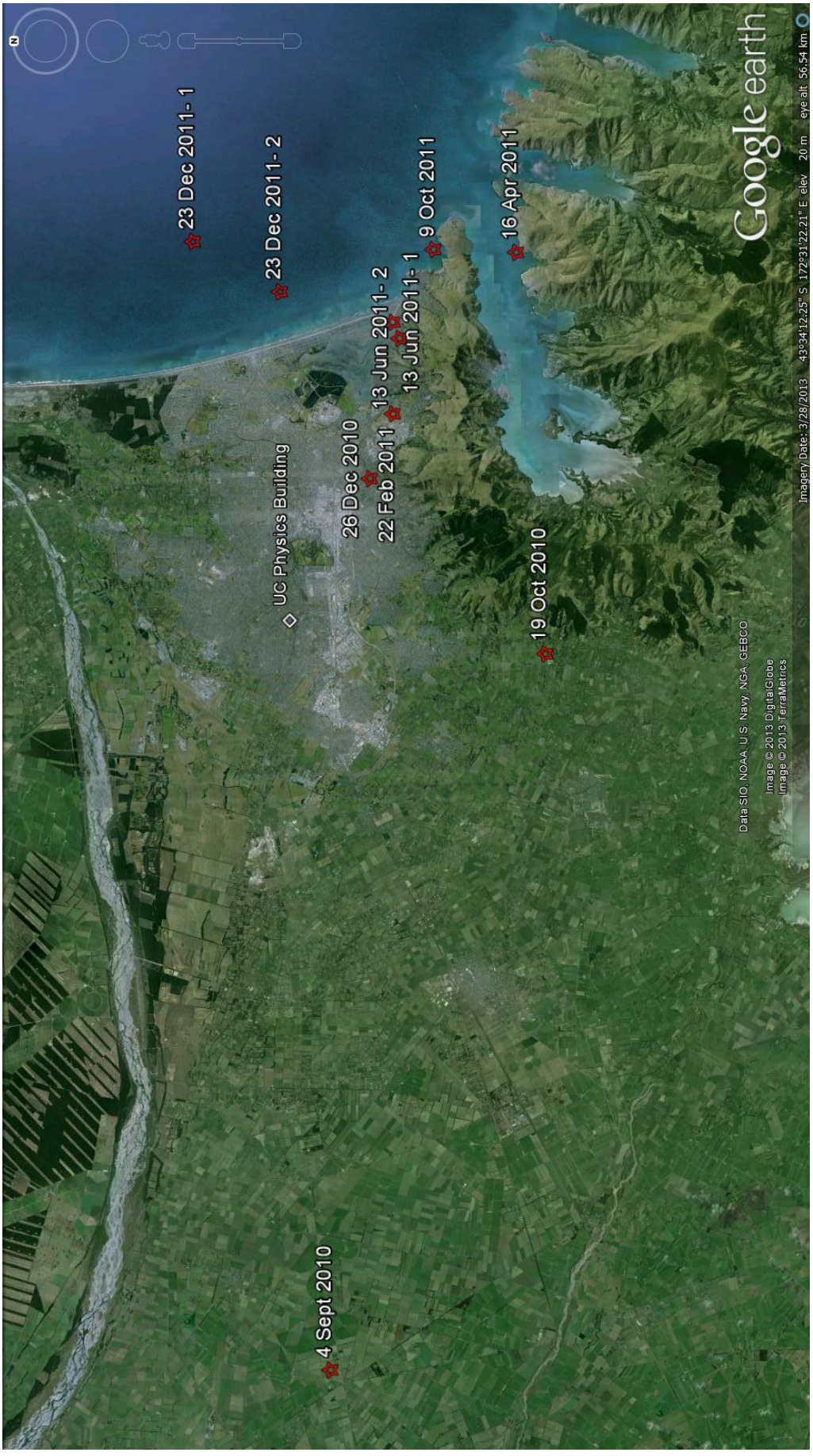


Figure 4-1: Epicentral locations for considered earthquakes relative to the location of the UC Physics Building

## 4.3 Processing of ground motion records

Raw data from the accelerometer array was downloaded from GeoNet (2012) in the form of a single file for each earthquake with all channels grouped together. Each component was processed using a baseline correction and applying filters to the frequency domain representation of the ground motion (Boore & Bommer, 2005). The purpose of the baseline correction and filtering is to remove any non-physical noise that is not considered to be from the earthquake-induced ground motion and to also remove any offsets from the delayed triggering.

As noted in Chapter 3, the installed accelerometers are triggered instruments. The nature of using an acceleration trigger (without a pre-triggering buffer) can result in un-natural spikes at the start of the record. These spikes cause large offsets in the velocity and displacement time-series owing to the integration of these errors (Boore & Bommer, 2005). Filtering is generally insufficient to remove these errors, so the use "padded zeros" at the start of the record is often utilized (Boore *et al.*, 2012). Herein, ten seconds of zeros were added to the acceleration record after the initial baseline correction. Once the baseline had been applied to the records, a frequency filter was used to remove the frequencies outside the desired frequency range. The frequency filter used was a fourth order Butterworth filter with corner frequencies of 0.2Hz and 25Hz (Boore & Akkar, 2003). This process was applied to all of the ground motion records in order to be consistent throughout the processing.

## 4.4 Characteristics of the observed seismic response of the UC Physics building.

In general, the severity of a ground motion is a function of its amplitude, frequency content and duration. Amplitude parameters considered in this study include peak floor accelerations (PFA), peak floor velocity (PFV) and peak floor displacement (PFD). For example, Figure 4-2 illustrates the acceleration, velocity and displacement time-series recorded on the first floor of the UC Physics Building during the 22 February 2011 earthquake in the longitudinal direction recorded from accelerometer 23 (refer to Figure 3-14 in the seismic instrumentation section of Chapter 3). It is worth noting that the peak amplitude values are the absolute values of acceleration, velocity and displacement. The relative displacement amplitudes are also calculated by subtracting the floor amplitudes by the amplitude recorded on the first floor. Relative displacement responses are examined in more detail in Chapter 5 as these are more important when modelling the structure.

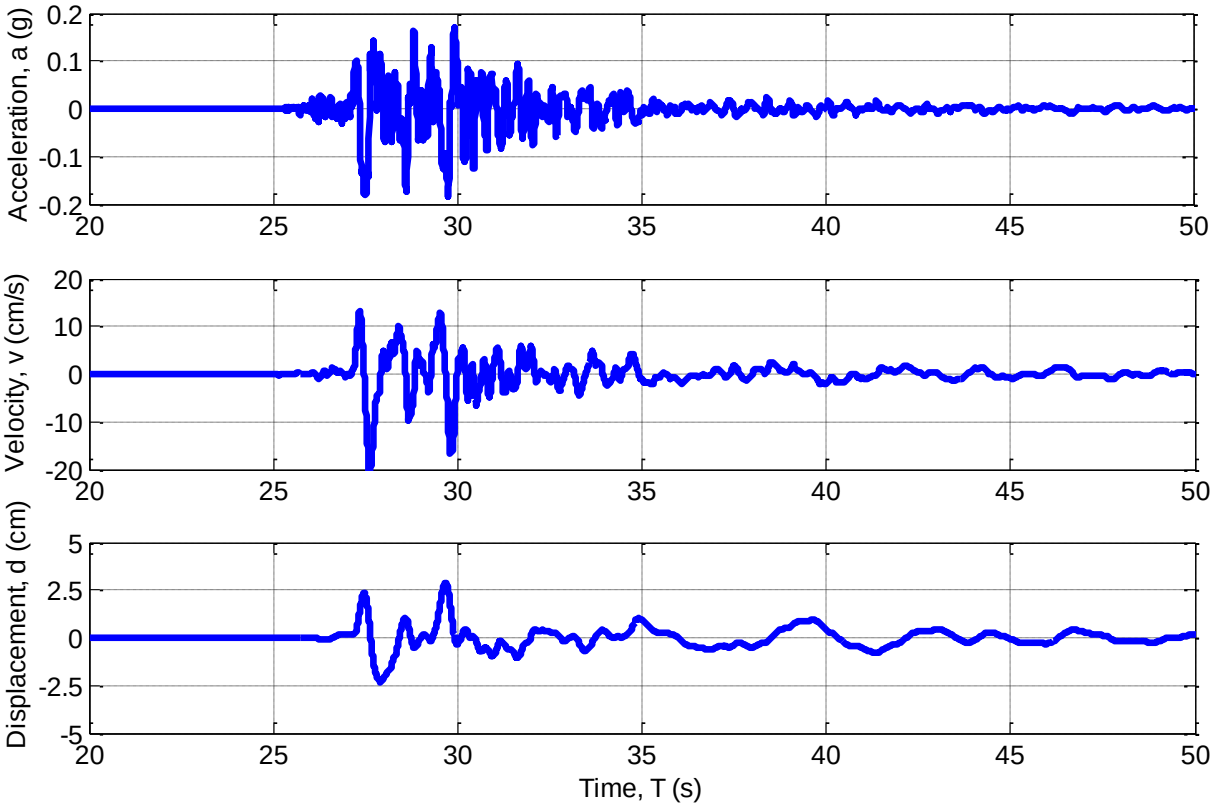


Figure 4-2: Observed acceleration, velocity and displacement time series from the first floor for the 22 February 2011 earthquake.

The observed ground motion amplitude parameters shown in Table 4-2 were found by averaging the accelerometers situated on the ground floor (accelerometers 23 and 24 (refer to Figure 3-14 in Chapter 3-4)). These values would approximately equal the free field amplitude values as the building has very shallow foundations so the kinematic interaction is not expected to be significant (Stewart *et al.*, 1999a, 1999b). It can be observed that the largest PFA, PFV and PFDs were recorded during the 4 September 2010 earthquake with values of 0.25g, 42.3cm/s and 12.5cm, respectively. This was followed by the amplitude parameters observed in the 22 February 2011 earthquake. Although the source-to-site distance is significantly greater in the former event, the peak amplitudes are larger than those observed in the former event principally due to its larger magnitude.

It should also be noted that PGA values greater than 0.1g were observed in six out of the ten earthquake events considered (refer to Table 4-2). The author is not aware of any other instrumented structures, whose earthquake-induced response has been documented (e.g. Aldea *et al.*, 2007; Butt & Omenzetter, 2012; Celebi, 1998; Limongelli, 2005; Michel & Gueguen, 2006; Skolnik *et al.*, 2006; Trifunac *et al.*, 2001; Ventura *et al.*, 2003), which have been repeatedly subjected to such a large number of strong ground motions.

Table 4-2: Observed amplitude ground motion parameters from Level 1 for the earthquake events considered.

| Earthquake | PFA (g) | | | PFV (cm/s) | | | PFD (cm) | | |
|---|---|---|---|---|---|---|---|---|---|
| | **Long** | **Trans** | **Vert.** | **Long** | **Trans** | **Vert.** | **Long** | **Trans** | **Vert.** |
| 4 September 2010 | 0.190 | 0.250 | 0.124 | 35.1 | 42.30 | 12.70 | 12.50 | 12.30 | 5.14 |
| 19 October 2010 | 0.062 | 0.055 | 0.033 | 3.50 | 3.79 | 1.81 | 0.63 | 0.45 | 0.34 |
| 26 December 2010 | 0.086 | 0.084 | 0.045 | 4.20 | 4.56 | 2.38 | 0.71 | 0.73 | 0.37 |
| 22 February 2011 | 0.180 | 0.190 | 0.110 | 21.7 | 10.60 | 6.50 | 2.83 | 2.34 | 0.99 |
| 16 April 2011 | 0.031 | 0.046 | 0.021 | 2.40 | 2.57 | 1.57 | 0.50 | 0.48 | 0.40 |
| 13 June 2011 (1) | 0.110 | 0.100 | 0.049 | 7.90 | 6.85 | 2.70 | 0.85 | 1.00 | 0.73 |
| 13 June 2011 (2) | 0.120 | 0.120 | 0.058 | 23.2 | 13.40 | 8.05 | 6.70 | 2.57 | 2.33 |
| 9 October 2011 | 0.017 | 0.026 | 0.010 | 2.00 | 1.50 | 0.60 | 0.34 | 0.21 | 0.15 |
| 23 December 2011 (1) | 0.098 | 0.109 | 0.052 | 10.0 | 7.85 | 4.72 | 2.74 | 3.35 | 2.05 |
| 23 December 2011 (2) | 0.097 | 0.150 | 0.066 | 8.20 | 13.00 | 5.70 | 2.38 | 2.42 | 1.10 |

In addition to the peak response amplitudes, duration-related seismic response parameters are also worth examining because they indicate the potential for resonance and cumulative inelastic response to occur. Table 4-3 presents the 5-95% Significant duration, $D_{s5-95}$, Bracketed duration, $D_B$, and Uniform duration, $D_U$ (see Bommer and Martinez-Pereira (1999) for further detail) of the recorded ground motion on the first floor during each of the events. It can be seen in Table 4-3 that the largest duration parameters were observed in the 4 September 2010 earthquake, followed by those of the 22 February 2011 event, which is consistent with these events having the largest magnitudes (and therefore rupture durations). The significant duration was similar in both the longitudinal and transverse directions, however was typically longer in the vertical direction. This implies that it takes less time to build up 5-95% of the energy (Arias intensity (Arias, 1970)) in the horizontal direction than it does in the vertical direction. The duration parameters of bracketed and uniform durations were found using a triggering acceleration of 0.01g.

Table 4-3: Observed duration ground motion parameters from level 1. $Ds_{5\text{-}95}$=5-95% significant duration; $D_B$=bracketed duration; $D_U$ = uniform duration

| Earthquake | $Ds_{5\text{-}95}$ (s) | | | $D_B$ (s) | | | $D_U$ (s) | | |
|---|---|---|---|---|---|---|---|---|---|
| | **Long** | **Trans** | **Vert.** | **Long** | **Trans** | **Vert.** | **Long** | **Trans** | **Vert.** |
| 4 September 2010 | 27.1 | 20 | 22.9 | 91.5 | 88.3 | 60.4 | 31.4 | 24.1 | 18.5 |
| 19 October 2010 | 8.5 | 9.2 | 14.8 | 9.0 | 10.6 | 6.00 | 3.9 | 4.2 | 1.4 |
| 26 December 2010 | 6.0 | 6.8 | 7.0 | 8.3 | 9.0 | 6.2 | 4.2 | 4.1 | 2.0 |
| 22 February 2011 | 6.2 | 7.9 | 7.3 | 42.1 | 41.8 | 14.5 | 9.1 | 10.2 | 6.3 |
| 16 April 2011 | 12.2 | 13.1 | 15.5 | 10.6 | 15.1 | 6.7 | 3.0 | 4.5 | 0.66 |
| 13 June 2011 (1) | 8.7 | 8.6 | 17.6 | 17.3 | 19.6 | 18.1 | 7.4 | 8.0 | 3.7 |
| 13 June 2011 (2) | 12.7 | 14.3 | 17.6 | 25.7 | 32.7 | 20.9 | 12.7 | 11.9 | 8.22 |
| 9 October 2011 | 15.1 | 15.3 | 22.0 | 3.6 | 7.5 | 0.0 | 0.74 | 0.86 | 0.0 |
| 23 December 2011 (1) | 11.0 | 15.0 | 23.8 | 21.6 | 23.8 | 24.9 | 8.7 | 11.8 | 6.1 |
| 23 December 2011 (2) | 10.7 | 11.2 | 16.2 | 21.0 | 22.3 | 18.0 | 9.6 | 9.7 | 5.4 |

### 4.4.1 Longitudinal direction

Figure 4-3 (a) shows the PFA values on the first, fourth and eighth floors for all earthquakes in the longitudinal direction versus normalised height of the structure, obtained by averaging the response from each shear wall. The instrument IDs are 23, 25 and 2A for the SW shear wall and 22, 26 and 29 for the NE shear wall (refer to Figure 3-14 in Chapter 3-4). The response of the 4 September 2010 and 22 February 2011 earthquakes are highlighted in this figure by the use of different colours. It can be seen that the highest PFA values on most levels occurred during the 22 February 2011 earthquake with an acceleration of 0.76g observed on the eighth floor. It is also worth noting that all but two of the PFA values on the eighth floor are greater than 0.1g.

Similar to Figure 4-3 (a), Figure 4-3 (b) and Figure 4-3 (c) illustrate the PFV, and PFD values, respectively, obtained in the longitudinal direction during the considered events. The largest PFV and PFD values occurred during the 4 September 2010 earthquake. The 22 February 2011 earthquake caused the second and third largest responses in the two figures, respectively. In contrast, Figure 4-3 (d) illustrates that the peak relative floor displacements increase with height, and the largest relative displacement response occurred during the 22 February 2011 earthquake.

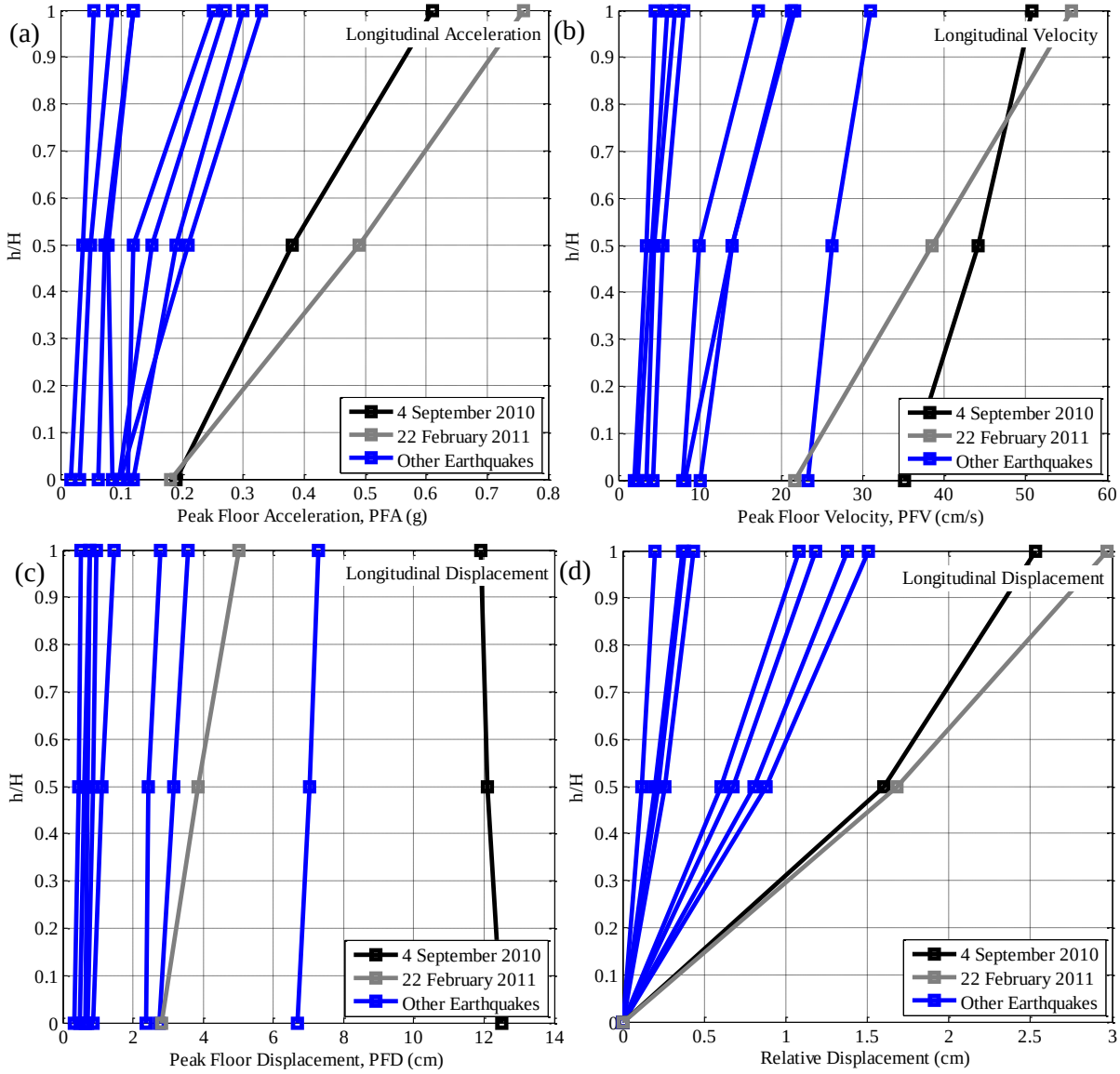


Figure 4-3: Longitudinal amplitudes for (a) peak floor acceleration, (b) peak floor velocity, (c) peak floor displacement and (d) relative displacement versus normalised height.

### 4.4.2 Transverse direction

The PFAs in the transverse direction obtained by averaging the three accelerometers on each shear wall, are shown in Figure 4-4 (a). Therefore any effect of torsion is neglected by taking the average response. Similar to the results in Figure 4-3 (a) for the longitudinal direction, the PFA values tend to increase up the structure. The largest PFA response was observed during the 4 September 2010 earthquake while, the 22 February 2010 earthquake had the second largest response. The largest acceleration observed during the 4 September 2010 earthquake was 0.61g on the eighth floor. The PFV and PFD responses in the transverse direction can be in Figure 4-4 (b) and Figure 4-4 (c), respectively. The largest response in both velocity and displacement profiles occurred during the 4 September 2010 earthquake. The velocity response during the 4 September 2010 response was twice as large as any other earthquake while the displacement response was at least three times larger than

any other displacement response. The maximum relative displacement response in the transverse direction is shown in Figure 4-4 (d) for all earthquake events. In general, the peak relative displacements in the transverse direction are larger than the those in Figure 4-3 (d) for the longitudinal direction. The largest response occurred during the 4 September 2010 earthquake which was twice as large as the response of any other earthquake event.

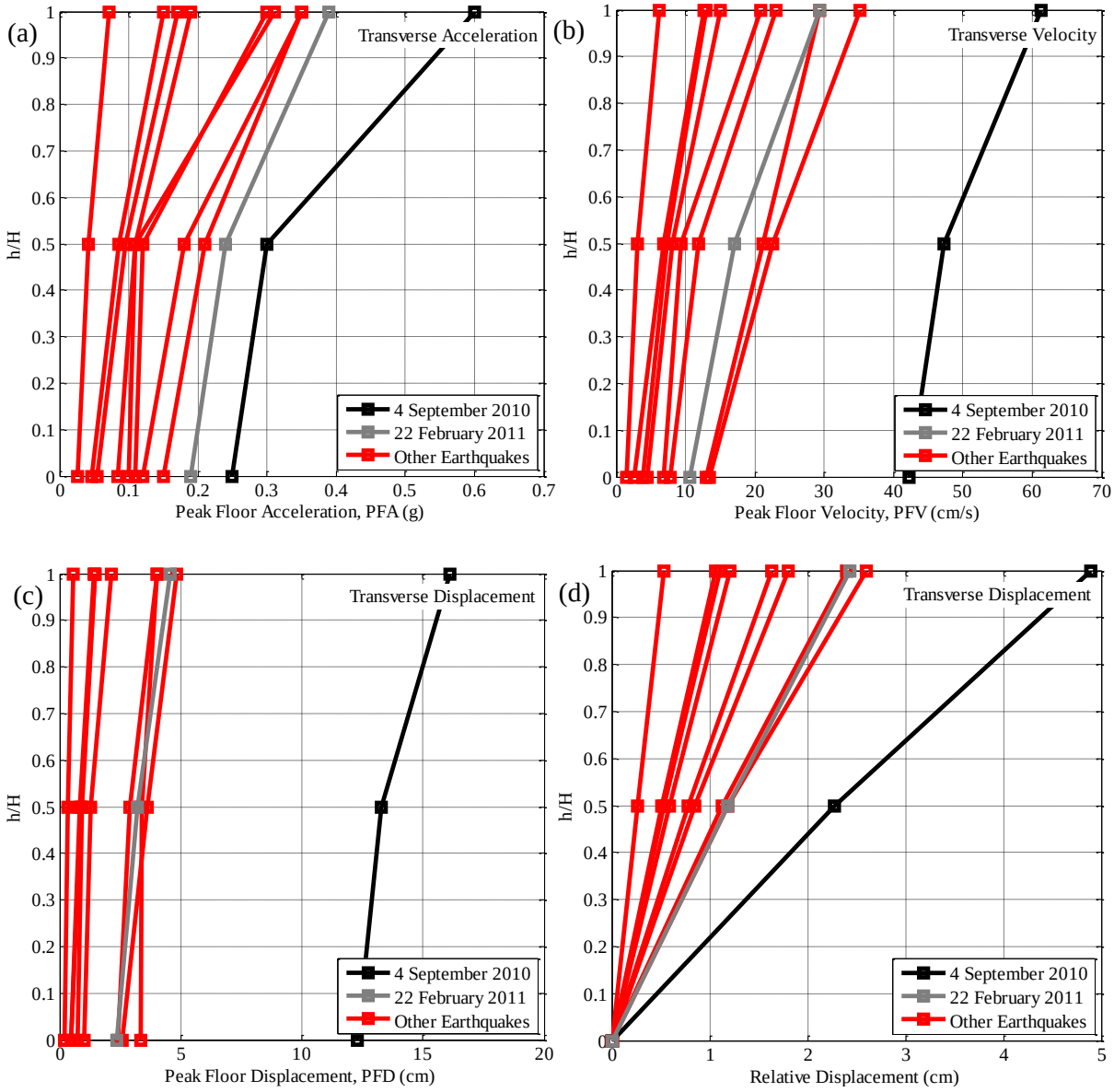


Figure 4-4: Transverse amplitudes for (a) peak floor acceleration, (b) peak floor velocity, (c) peak floor displacement and (d) relative displacement versus normalised height.

### 4.4.3 Vertical direction

The PFA's observed in the vertical direction obtained by averaging the three accelerometers on each shear wall, are shown in Figure 4-5 (a). The magnitude of the PFA's are significantly less than in both horizontal directions with the maximum observed acceleration only 0.18g on the eighth floor. It

is interesting to note that the increase in acceleration between the eighth floor and first floor is approximately equal to 1.5 while in both horizontal directions it was greater than 2. The PFV and PFD profiles are shown in Figure 4-5 (b) and Figure 4-5 (c), respectively.. It can be seen that both PFV and PFD values are very consistent with height, a result of the vertical vibration modes having high frequencies. In general, the peak relative displacements in the vertical direction were all very small (less than 0.3 cm). The peak relative displacements from the 22 February 2011 earthquake were significantly larger with a difference of up to 3cm on the eighth floor.

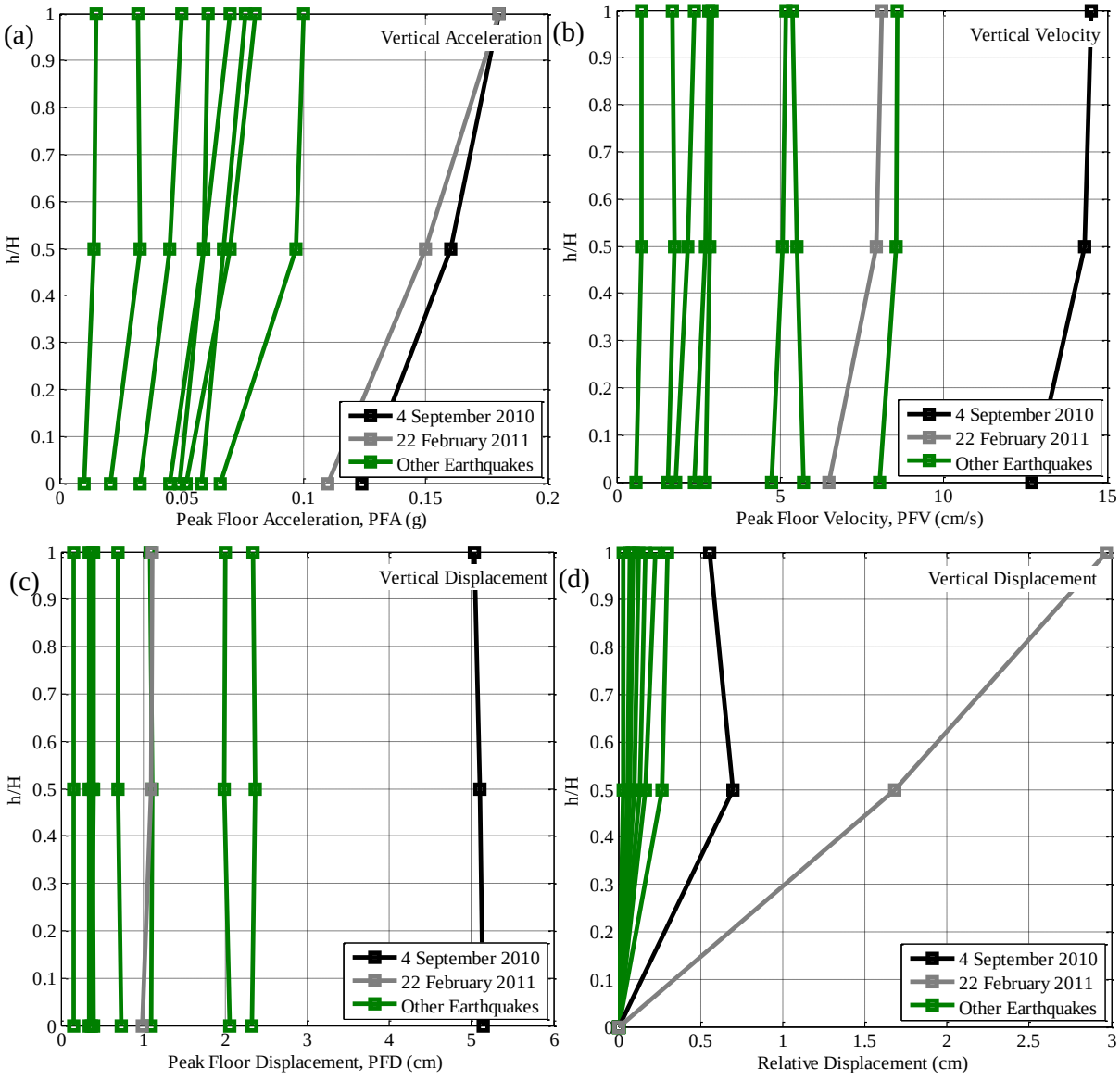


Figure 4-5: Vertical amplitudes for (a) peak floor acceleration, (b) peak floor velocity, (c) peak floor displacement and (d) relative displacement versus normalised height.

### 4.4.4 Base rotation

Significant base rotation occurs predominantly as a result of horizontal building translation. While base rotation is always present, to some extent, generally significant base rocking only occurs if the structure has shallow foundations and the soil below the building is relatively soft. Both these conditions are met by the UC Physics Building so it would be suspected that the building would rock under strong ground motion excitation. Using small-amplitude forced-vibration testing, Reay (1970) found that up to 30% of the transverse roof displacement, and 8% of the longitudinal roof displacement, resulted directly from the base rocking.

Rocking can occur about both axes, however it is typically more predominant in the direction of the smaller foundation length. Figure 4-6 shows the response of the two pairs of parallel vertical accelerometers at the base of the structure as well as the difference between the two pairs for the 22 February 2011 earthquake (i.e. accelerometers 22 and 23 in the longitudinal direction, and accelerometers 21 and 24 in the transverse direction (refer to Figure 3-14 in the seismic instrumentation section of Chapter 3)).

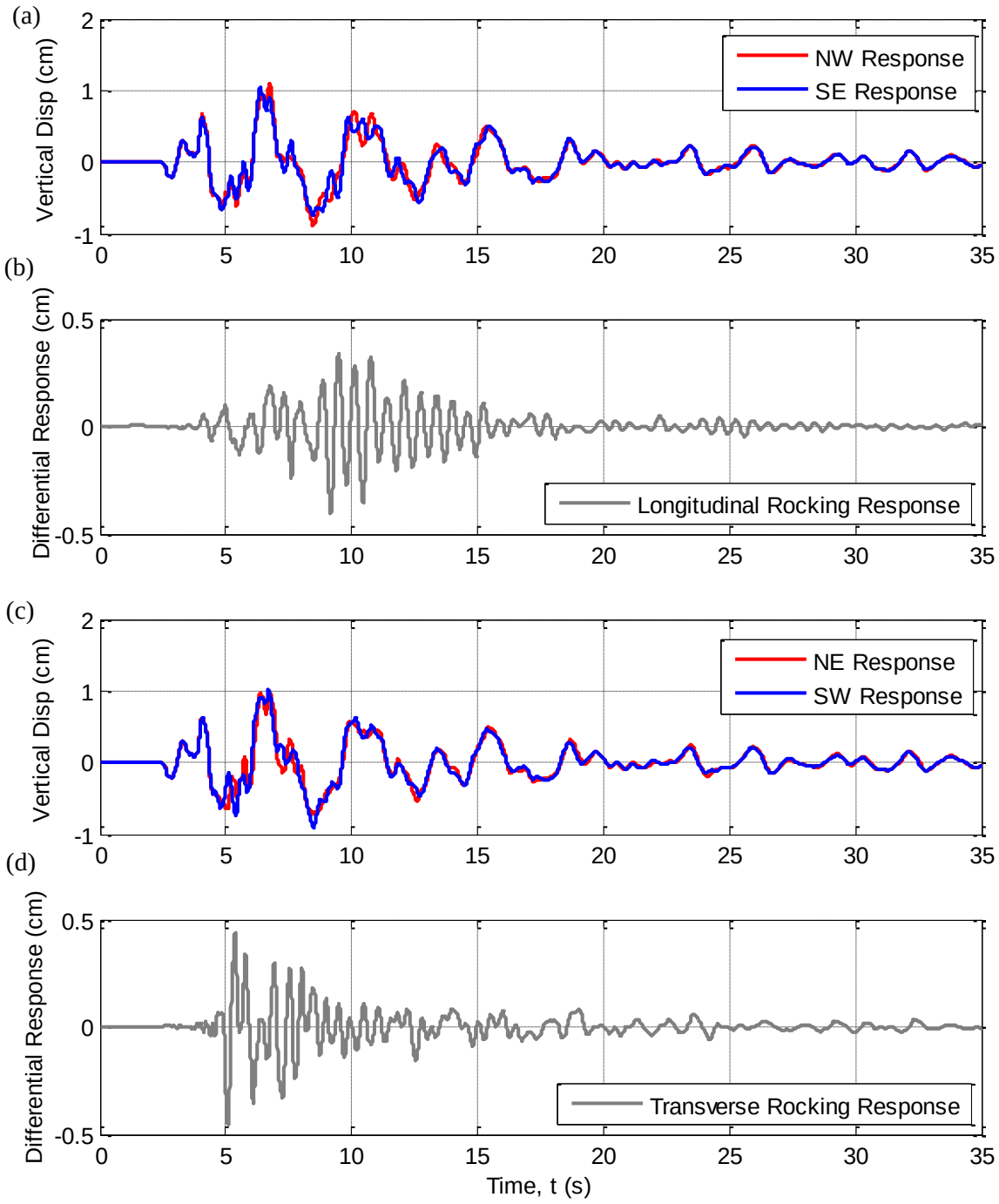


Figure 4-6: Comparison of observed vertical displacement response of the four accelerometers from the 1st floor: (a) and (b) for the longitudinal response; and (c) and (d) for the transverse response for the 22 February 2011 earthquake.

Table 4-4 shows the maximum rocking angle calculated in each direction. The rocking angle is taken as the difference between the two parallel accelerometers divided by the distance between them. This distance is 52.1 m in the longitudinal direction and 15.0 m in the transverse direction. As expected, maximum rocking occurred during the 4 September 2010 earthquake, which also has the maximum relative displacement amplitude values as shown previously in this chapter (e.g. Figure 4-4). These values are very similar to those computed by Zhao and Uma (2011) which were $0.19*10^{-3}$ rad and

$1.2*10^{-3}$ rad in the longitudinal and transverse directions, respectively. The rocking in the transverse direction is roughly ten times larger than in the longitudinal direction, even though the longitudinal direction is only three times longer in length. The modelling of this effect is performed in Chapter 6 in both the longitudinal and transverse directions.

Table 4-4: Maximum rocking angle about each axis.

| **Earthquake** | **Angle (rad) $*10^{-3}$** | |
|---|---|---|
| | **Longitudinal** | **Transverse** |
| 4 September 2010 | 0.17 | 1.0 |
| 19 October 2010 | 0.014 | 0.11 |
| 26 December 2010 | 0.0088 | 0.076 |
| 22 February 2011 | 0.087 | 0.27 |
| 16 April 2011 | 0.014 | -* |
| 13 June 2011 (1) | 0.035 | -* |
| 13 June 2011 (2) | 0.075 | -* |
| 9 October 2011 | 0.0065 | -* |
| 23 December 2011 (1) | 0.046 | 0.16 |
| 23 December 2011 (2) | 0.037 | 0.27 |

*Vertical acceleration records not available for these earthquakes.

### 4.4.5 Torsional deformation

The UC Physics Building has a very regular design so it would not be expected that any torsional behaviour would normally occur. However, due to the fixity to the Link Building (as described in Chapter 3), there is a possibility of accidental torsion. This interaction with the Link Building at the SW end caused reduced acceleration and displacement responses relative to those at the NE end of the building. The transverse displacement response series for the eighth and fourth floors is shown in Figure 4-7. This figure shows the response from each shear wall (NE and SW) and the difference between the two on the fourth and eighth floors. It can clearly be seen that the NE shear wall response is larger than the SW shear wall response.

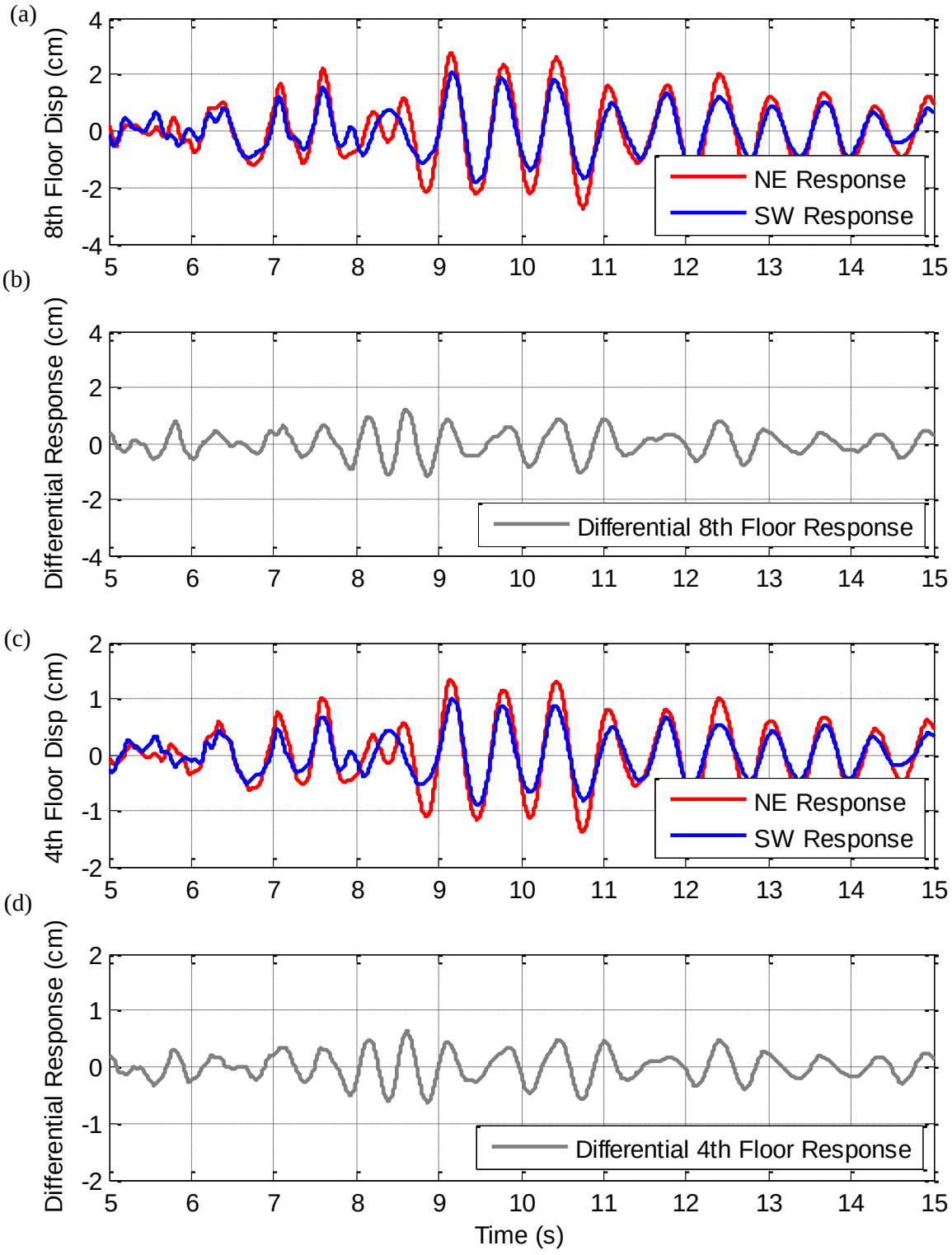


Figure 4-7: Comparison of the observed transverse displacement response series of the eighth and fourth floor for the two end shear walls in the 22 February 2011 earthquake: (a) and (b) for the eighth floor response; and (c) and (d) for the fourth floor response.

A torsional mode can also occur in the longitudinal direction as a differential movement between the two frame systems. This can be measured by comparing the two accelerometers on the either side of the middle shear wall on the seventh floor (accelerometers 27 and 28 (refer to Figure 3-14 in the

seismic instrumentation section of Chapter 3)). The longitudinal displacement response series for the accelerometers is shown in Figure 4-8. The response of the two sides of the building is very similar with 0.3 cm being the maximum difference in responses. As this difference is very small, torsion in this direction is not considered further herein.

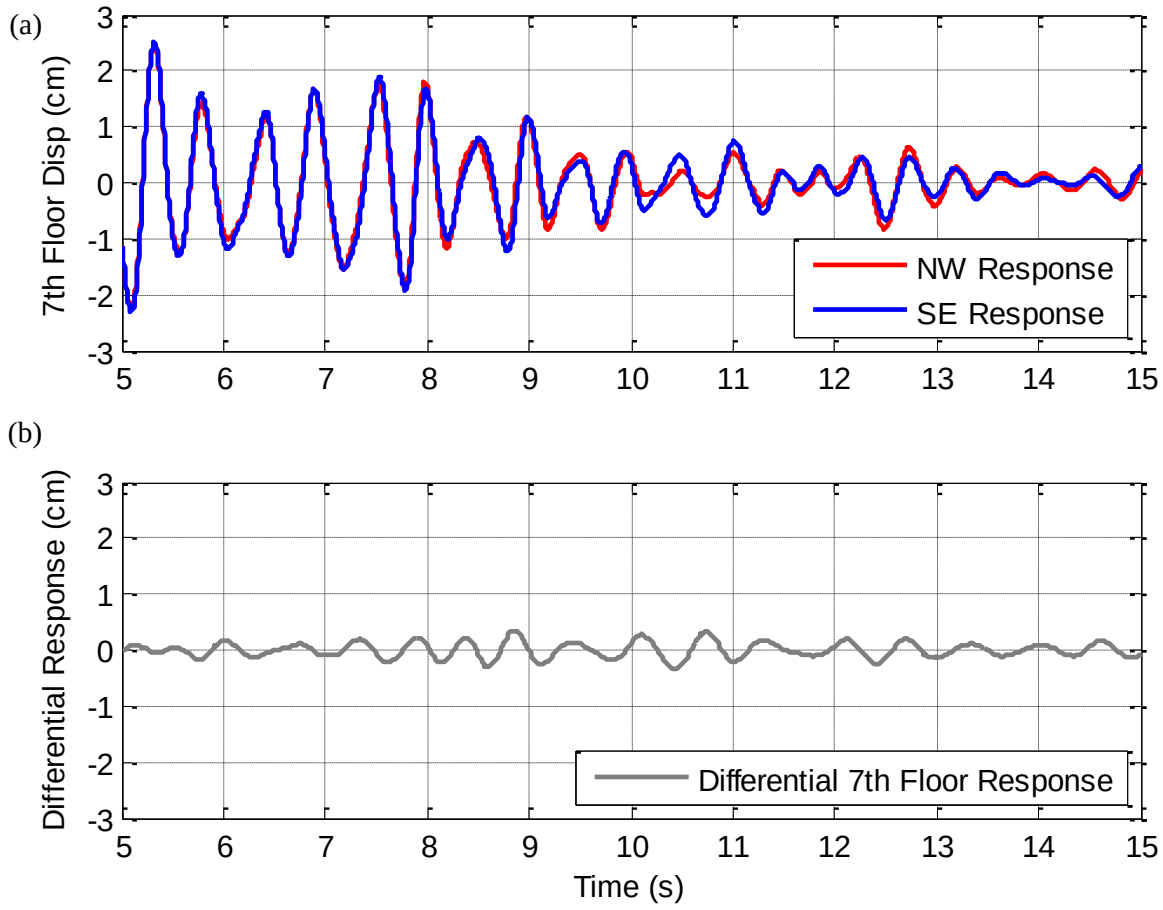


Figure 4-8: Comparison of the observed longitudinal displacement response series of the seventh floor for the middle shear wall in the 22 February 2011 earthquake.

The maximum torsion angle is considered to be the maximum difference in transverse shear wall displacements divided by the distance between the two shear walls. For example, the maximum differential eighth floor displacement during the 22 February 2011 earthquake was 1.21 cm. The distance between the two shear walls is 52.1m, therefore the maximum torsion angle was:

$$\text{Maximum torsional angle } = \frac{1.21}{52.1 \times 100} = 0.233 \text{ x } 10^{-3} \text{ rad}$$

Another parameter that can be examined is the percentage of the torsional displacement over maximum displacement. This is taken as the maximum differential displacement on the eighth floor divided by the maximum displacement on the eighth floor. Using the same example from the 22

February 2011 earthquake, the maximum eighth floor displacement was 2.75 cm. Therefore the maximum torsion displacement percentage was:

$$\text{Maximum torsion displacement percentage } = \frac{1.21}{2.75} \times 100 = 44\ \%$$

Table 4-5 shows the maximum torsion angle and maximum percentage of torsional displacement over relative displacement on the first floor and eighth floor for all earthquake events. The torsion angle on the first floor was calculated using the same method as described above. The average torsion angle on the first floor was 18%. This is a significant amount of torsion for the ground floor and could be due to the connection to the Link Building or the sloping ground which reduces the embedment depth of the foundations from the SW end to the NE end. It can be seen that the torsional displacement percentage on the eighth floor is, on average, 38%. This is quite high and shows that torsion plays a significant role in the displacement of the structure. The modelling of this effect is performed in Chapter 7.4 by connecting a3D model of the Physics Building and a 1D model of the Link Building.

Table 4-5: Maximum torsion angle on the1st and 8th floors.

| | **First Floor** | | **Eighth Floor** | |
|---|---|---|---|---|
| **Earthquake** | **Max Angle (rad)*$10^{-3}$** | **Max Torsion Disp (%)** | **Max Angle (rad)*$10^{-3}$** | **Max Torsion Disp (%)** |
| 4 September 2010 | 0.214 | 9 | 0.477 | 41 |
| 19 October 2010 | 0.0230 | 27 | 0.097 | 37 |
| 26 December 2010 | 0.0290 | 21 | 0.127 | 49 |
| 22 February 2011 | 0.0919 | 19 | 0.233 | 44 |
| 16 April 2011 | 0.0197 | 20 | 0.075 | 32 |
| 13 June 2011 (1) | 0.0417 | 22 | 0.163 | 42 |
| 13 June 2011 (2) | 0.0877 | 18 | 0.211 | 37 |
| 9 October 2011 | 0.0089 | 23 | 0.030 | 26 |
| 23 December 2011 (1) | 0.0548 | 9 | 0.163 | 44 |
| 23 December 2011 (2) | 0.0514 | 11 | 0.151 | 30 |
| **Average** | | **18** | | **38** |

## 4.5 Structural vibration parameters obtained from spectral analysis techniques

The principal structural vibration parameter that can be obtained from spectral techniques is the dominant vibration period. In order to identify such vibration periods, the recorded time series of the eighth and first floor responses are utilised. The two main engineering spectral analysis techniques are Fourier analysis (Kramer, 1996) and response-spectral analysis (Biot, 1941). The application of these methods and a comparison of the obtained results is discussed in this section.

### 4.5.1 Response-spectral analysis

An empirical estimate of the frequency response function of the structure between two locations m and n, can be obtained by taking the ratio between the pseudo-spectral accelerations (or spectral displacements), as given by:

$$SR_{m-n}(T) = \frac{SA_m(T)}{SA_n(T)} \quad (4\text{-}1)$$

where $SA_n(T)$ and $SA_m(T)$ are the pseudo-spectral accelerations at locations n and m, respectively.

Herein, where the intention is to identify the predominant translational vibration properties of the UC Physics Building, the spectral ratio is obtained from the eighth floor and the first floor responses in each orthogonal direction (and hence the spectral ratio is denoted as $SR_{8-1}$). Because, the dynamic response of the building can be considered to act as a signal filter, where frequencies that are close to the dynamic modal frequencies are amplified to a greater extent than those at other frequencies, then this spectral ratio can be used to identify such modal periods. For earthquake-induced ground motions, which have a broad range of frequencies, the maximum ratio should occur at the predominant period in each orthogonal direction considered (Ventura *et al.*, 2003). In this chapter, the spectral ratios have been examined at both ends of the structure (accelerometers 23 and 2A for the SW shear wall and 22 and 29 for the NE shear wall), in order to determine if there is a different response at each end.

#### *4.5.1.1 Longitudinal direction*

Figure 4-9 (a) shows the $SR_{8-1}$ values at the north-east end, and Figure 4-9 (b) at the south-west end for vibration in the longitudinal direction. Both figures show the spectral ratio from each earthquake in grey and the average response from all earthquakes in black. For both the NE and SW ends of the structure, all earthquakes produce a similar response for periods greater than 0.2 seconds, while there is some variation for periods less than this. This variation is speculated to be the result of both higher modal periods, as well as a reduced signal to noise ratio (the cut-off filter period used was 0.04 seconds).

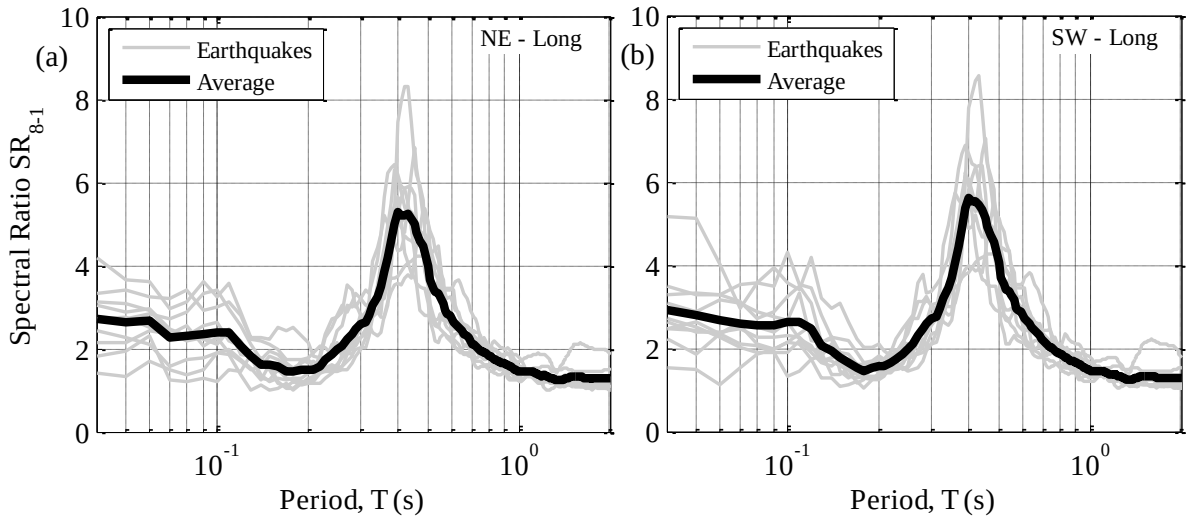


Figure 4-9: Ratio of pSA between the eighth and first floors in the longitudinal direction at the (a) NE and (b) SW end.

Figure 4-10 provides a direct comparison between the average SR values for the NE and SW directions depicted in Figure 4-9, in which it can be seen that the responses are very similar. This suggests that the response in the longitudinal direction is very regular in plan, with little effects of torsional motion in this direction (as shown in previously in Figure 4-8). It can also be seen that both average SR's reach their maximum values at a period of approximately 0.4 seconds. The specific maximum value of these spectral ratios at the NE and SW ends, which is taken to be equal to the fundamental vibration period in that orthogonal direction, can be found in Table 4-6.

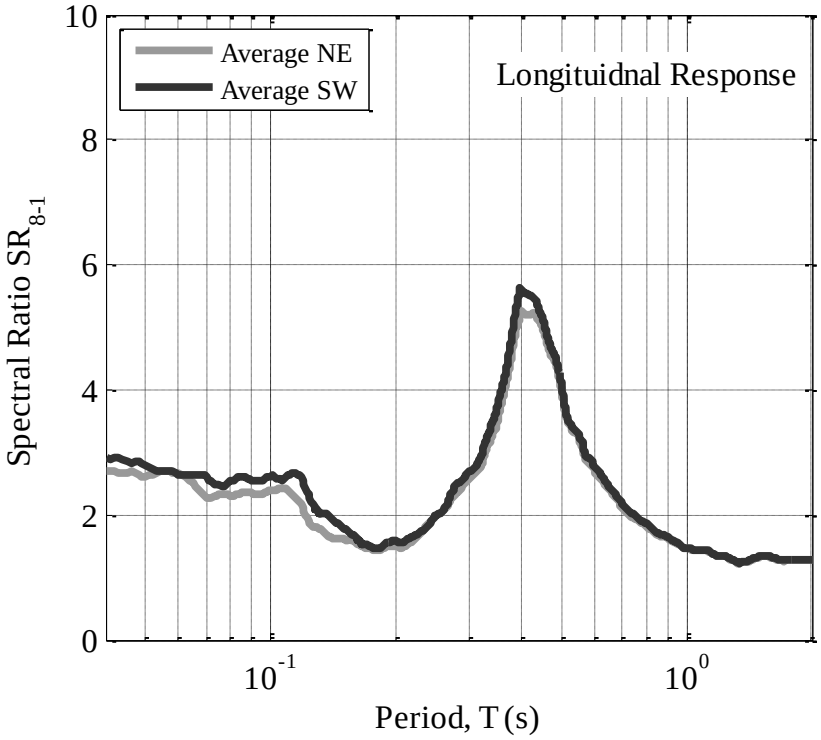


Figure 4-10: Comparison of spectral ratios between the NE and SW ends in the longitudinal direction.

#### *4.5.1.2 Transverse direction*

Similar to the results in the longitudinal direction, the SR's in the transverse direction can be found in Figure 4-11 (a) and (b) for the NE and SW ends of the building, respectively. Again, it can be seen that the SR's from each earthquake in both cases are again very similar for all periods. However, there appears to be a difference between the two shear walls in the size of the ratio and the location of the peak response.

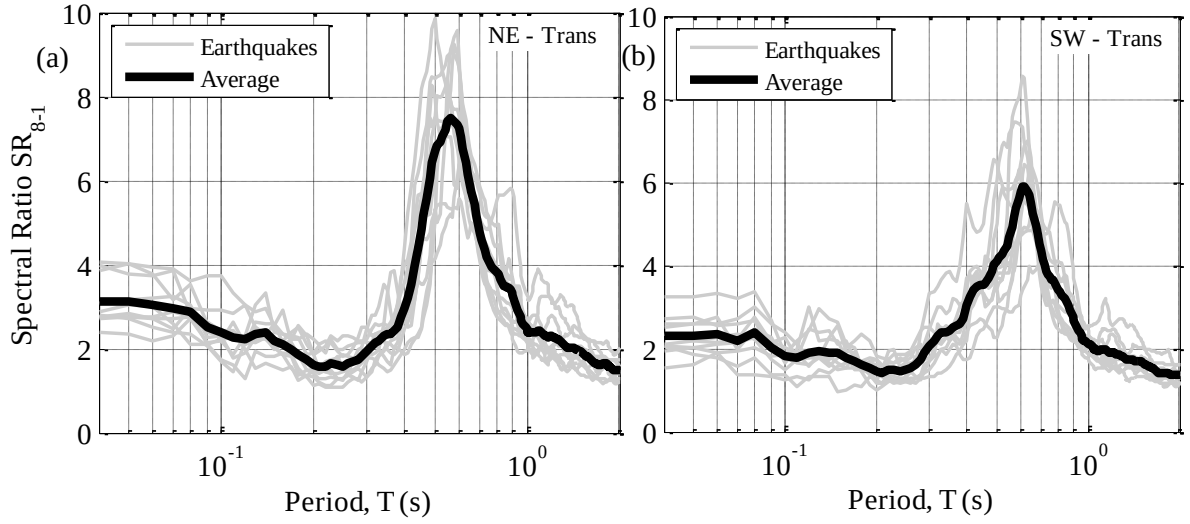


Figure 4-11: Ratio of pSA between the eighth and first floors in the transverse direction at the (a) NE and (b) SW end.

Figure 4-12 provides a comparison of the average SR's for transverse vibration at the NE and SW ends of the building. It can be seen that there is a clear difference in the average SR values in the transverse direction between the north-east and south-west ends, with the average SR at the NE end being larger than the SW end and it also appears that there is a slight difference in fundamental period. As explained in Chapter 3, there is a seismic gap between the Physics Building and the Link Building, however, the buildings are attached through a continuous foundation system as well as the many services that run between the buildings. There are also metal plates which connect the building over the seismic gap. These various connections could possibly have some effect, which reduces the response of the SW end. This restraint can also causes torsional effects in the building which are further examined in Chapter 7.

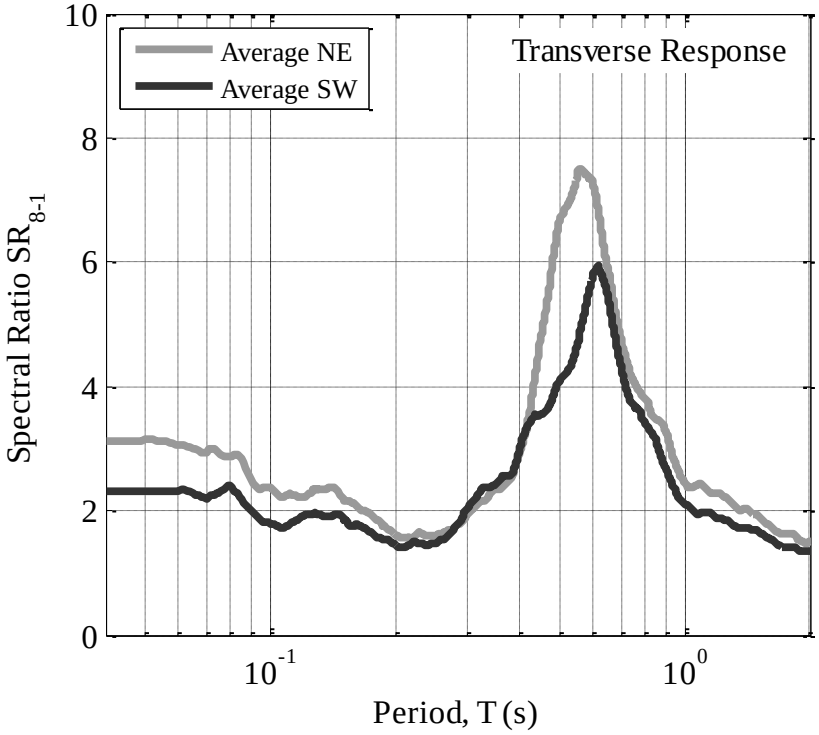


Figure 4-12: Comparison of spectral ratios between the NE and SW ends in the transverse direction.

#### *4.5.1.3 Vertical direction*

The SR's for vertical response of both ends of the building are examined in Figure 4-13. Vertical accelerations typically have more high frequency motion as compared with horizontal motion. The vertical period of the structure is smaller than the horizontal periods and also has a smaller spectral ratio compared with the horizontal ratios. However, there is still a small peak at around 0.08 seconds which could be caused by the building responding in the vertical mode.

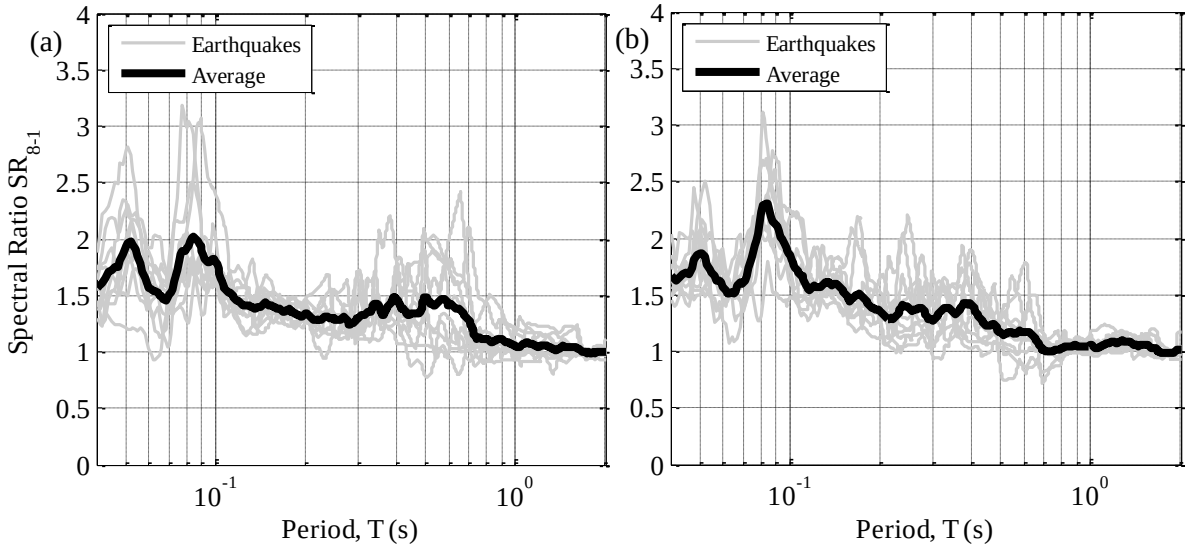


Figure 4-13: Ratio of pSA between the eighth and first floors in the vertical direction at the (a) NE and (b) SW end.

The average vertical ratios are compared in Figure 4-14 where both ends appear to react in a similar way. As explained previously, there is no clear increase in SR at the fundamental period but it is suspected to be in the range below 0.1 seconds.

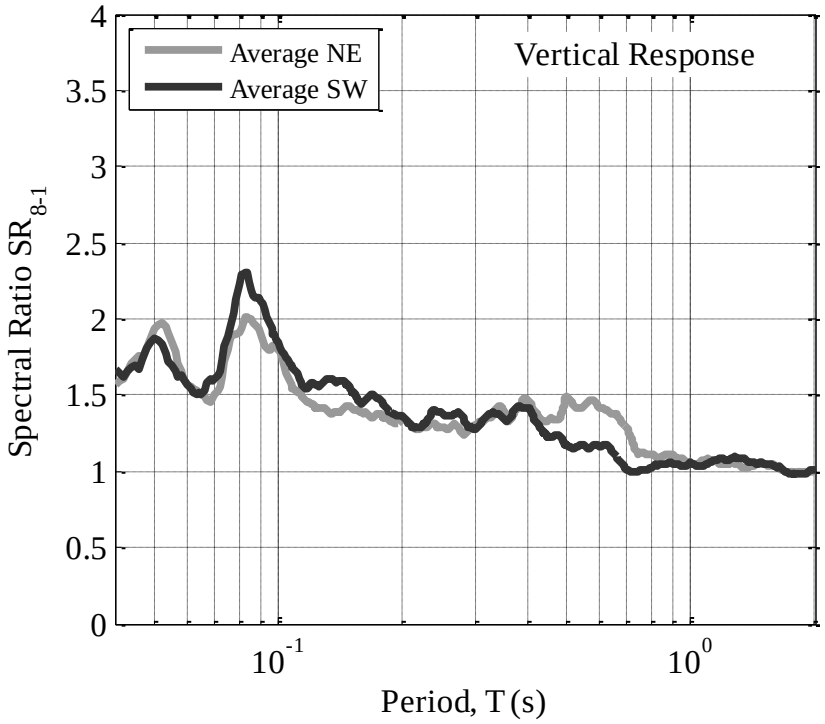


Figure 4-14: Comparison of spectral ratios between the NE and SW ends in the vertical direction.

#### *4.5.1.4 Base rotation*

The period of the base rotational motion was found by subtracting the parallel acceleration records from the first floor of the building (i.e. accelerometers 22 and 23 in the longitudinal direction, and accelerometers 21 and 24 in the transverse direction (refer to Figure 3-14 in the seismic instrumentation section of Chapter 3)) and then performing a spectral analysis on the differential acceleration record. The fundamental period of the rocking motion was considered to be the period associated with the largest spectral acceleration. The results from this analysis are shown in Figure 4-15 for the transverse and longitudinal rocking.

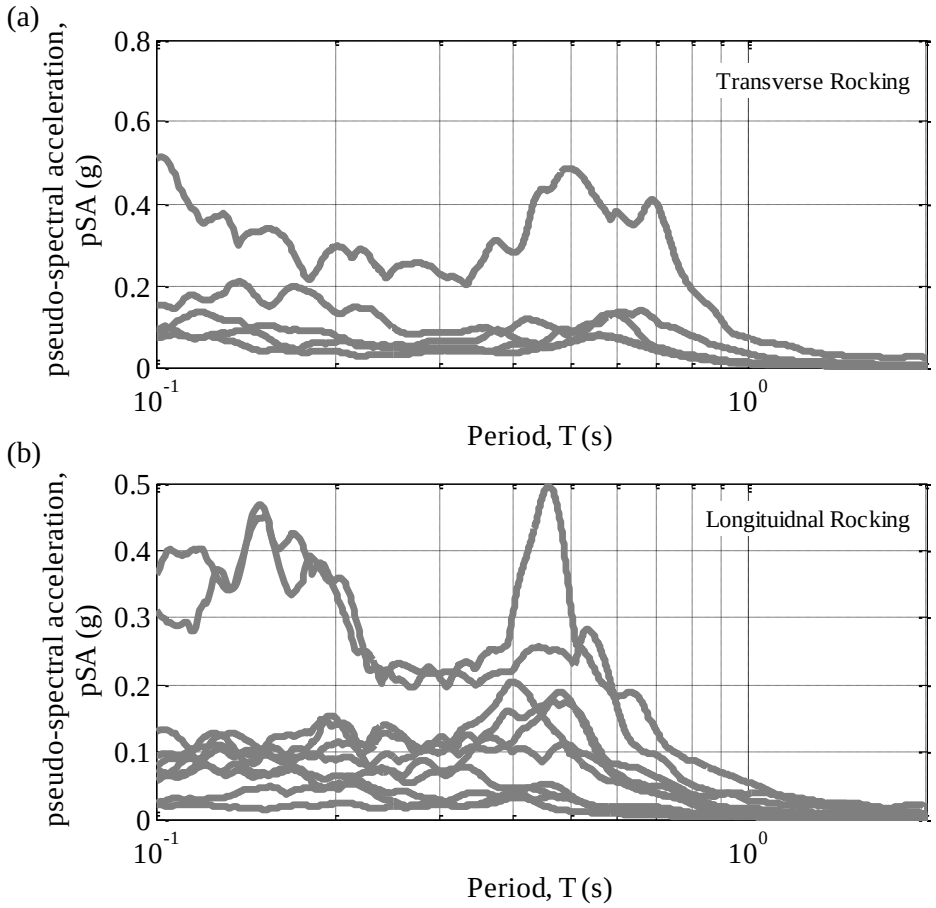


Figure 4-15: Spectral response amplitude for rocking in the (a) transverse and (b) longitudinal directions.

The fundamental period results from these analyses can be found in Table 4-6. The period of base rotation around the transverse axis was 0.45 seconds. This is very similar to the fundamental period of the building translational deformation in this direction which again confirms that the rotation of the base occurs as a result of the motion of the building. In the transverse direction, the period of base rotation was equal to 0.58 seconds. This is again very close to the transverse translational period of 0.59 seconds.

#### *4.5.1.5 Torsional deformation*

As shown previously in Section 4.4.5, the torsional motion is predominately in the transverse direction. Therefore, in order to calculate the torsional fundamental period, the differential movement of the eighth floor and first floor was examined. This involved subtracting the transverse acceleration response from eighth floor of the two shear walls (accelerometers 29 and 2A) and performing a spectral analysis on the differential acceleration record. This was also applied to the two first floor accelerations records (accelerometers 22 and 23) and again performing a spectral analysis. The ratio between the eighth and first floors was found and the period corresponding to the maximum ratio was considered to be the fundamental period of the torsional motion. The spectral ratio for all ten

earthquake events is shown in Figure 4-16. The results from the spectral analysis can be found in Table 4-6. The value of the fundamental period varies significantly between earthquakes events indicating that there may be multiple torsional modes of importance, or interaction of the torsional modes with translational modes.

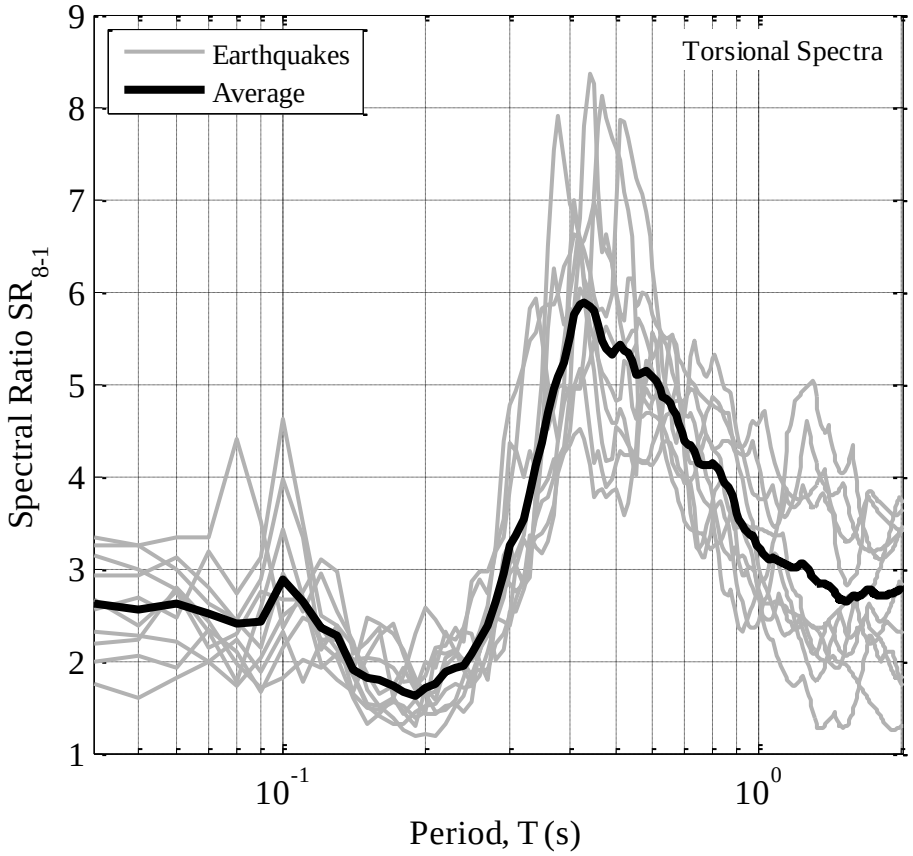


Figure 4-16: Spectral ratio between the eighth and first floor torsional responses.

#### *4.5.1.6 Summary of vibration periods obtained from response spectral ratios*

The fundamental period in each direction of the structure as well as the rocking and torsion motion was found for each earthquake using a response spectra analysis. The results for this can be found in Table 4-6. In the longitudinal direction, the average period for both directions was 0.42 seconds. The fundamental period inferred at both ends of the building were the same for each event but varied between events. In the transverse direction, the average fundamental period was 0.58 seconds and 0.62 seconds for the NE and SW ends, respectively. This difference in periods was due to the fixity of the SW end as explained earlier (Chapter 3.3). The difference in fundamental periods between the ends of the building for the same event also varied. The vertical period was 0.06 seconds and 0.08 seconds for the NE and SW ends, respectively. These values are close to the cut-off period of 0.04 seconds, so a more accurate method is required to find the true fundamental period. The periods of the rocking motion about each axis were 0.45 seconds and 0.58 seconds for the longitudinal and

transverse directions respectively. These values were both very close to their respective translational fundamental periods. On average the torsional period was 0.50 seconds, however, there was significant variance between events.

Table 4-6: Fundamental periods of the building from spectral analysis.

| | **Tm (s)** | | | | | | | | |
|---|---|---|---|---|---|---|---|---|---|
| | **Longitudinal** | | **Transverse** | | **Vertical** | | **Rocking** | | **Torsion** |
| | **NE** | **SW** | **NE** | **SW** | **NE** | **SW** | **Long** | **Trans** | **Trans** |
| 4 September 2010 | 0.36 | 0.36 | 0.60 | 0.72 | 0.05 | 0.04 | 0.46 | 0.50 | 0.37 |
| 19 October 2010 | 0.43 | 0.44 | 0.56 | 0.65 | 0.05 | 0.08 | 0.33 | 0.56 | 0.41 |
| 26 December 2010 | 0.40 | 0.40 | 0.56 | 0.49 | 0.09 | 0.09 | 0.45 | 0.56 | 0.51 |
| 22 February 2011 | 0.47 | 0.47 | 0.58 | 0.65 | 0.05 | 0.05 | 0.53 | 0.59 | 0.47 |
| 16 April 2011 | 0.39 | 0.39 | 0.50 | 0.63 | 0.08 | 0.08 | 0.46 | -* | 0.44 |
| 13 June 2011 (1) | 0.49 | 0.48 | 0.63 | 0.62 | 0.08 | 0.09 | 0.37 | -* | 0.73 |
| 13 June 2011 (2) | 0.45 | 0.45 | 0.55 | 0.59 | 0.09 | 0.08 | 0.47 | -* | 0.66 |
| 9 October 2011 | 0.39 | 0.39 | 0.57 | 0.58 | 0.08 | 0.08 | 0.41 | -* | 0.38 |
| 23 December 2011 (1) | 0.39 | 0.39 | 0.59 | 0.61 | 0.05 | 0.08 | 0.48 | 0.59 | 0.42 |
| 23 December 2011 (2) | 0.43 | 0.43 | 0.61 | 0.66 | 0.05 | 0.10 | 0.40 | 0.66 | 0.60 |
| **Average** | **0.42** | **0.42** | **0.58** | **0.62** | **0.06** | **0.08** | **0.45** | **0.58** | **0.50** |

*Vertical acceleration records not available for these earthquakes.

### 4.5.2 Fourier analysis

A Fourier analysis converts an acceleration time-series into the frequency domain. Each frequency has a Fourier amplitude which represents the contribution of each frequency to the acceleration record. When two Fourier series are divided, the result is what is known as a transform function. The transfer function is a property of the system, and represents the amplification (or de-amplification) of frequencies between the two locations where the acceleration records were measured. Typically, empirical transfer function analysis is conducted in a soil profile to try and understand how the different soil layers change the ground motion record and to identify the fundamental period of each layer (Kramer, 1996). The same process can also be applied to structural responses to identify the fundamental period of the structure (e.g. Trifunac *et al.* (2001)). A Fourier analysis is considered to be more accurate than a spectral analysis because it identifies the frequencies of the motion directly; however, the process can take longer to compute and is also dependent on how the Fourier spectra is smoothed. The equation for the Fourier Spectral Ratio (FSR) is given by:

$$FSR_{m-n}(T) = \frac{FAS_m(T)}{FAS_n(T)} \qquad (4\text{-}2)$$

where $FAS_n(T)$ and $FAS_m(T)$ are the Fourier amplitudes at locations n and m, respectively. The Fourier responses of the two floors were 'smoothed' before taking the ratio using a function developed by (Ohmachi, 1998) with a bandwidth value of 20. In this chapter, the Fourier spectral ratios have been examined at both ends of the structure (accelerometers 23and 2A for the SW shear wall and 22 and 29 for the NE shear wall), in order to determine if there is a different response at each end.

#### *4.5.2.1 Longitudinal direction*

In order to try and capture the total response of the building, the Fourier Spectral Ratio ($FSR_{8-1}$) between the first and eighth floor records is taken. Figure 4-17 (a) shows the $FSR_{8-1}$ values at the north-east end, and Figure 4-17 (b) at the south-west end for vibration in the longitudinal direction. Both ends have similar responses for all earthquakes and the fundamental period is clearly visible. There is also a second peak around 0.12 seconds which could be the second mode of the structure in this translational direction. The average responses from each end of the building are compared in Figure 4-18. The response at each end was very similar with a period of approximately 0.4 seconds.

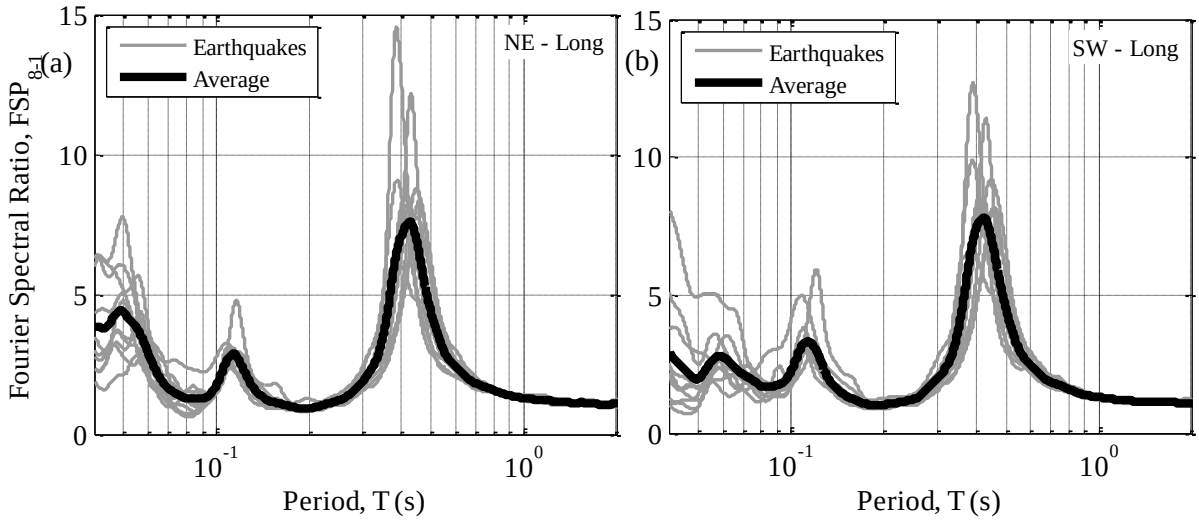


Figure 4-17: Ratio of Fourier amplitude between the eighth and first floors in the longitudinal direction at the (a) NE and (b) SW end.

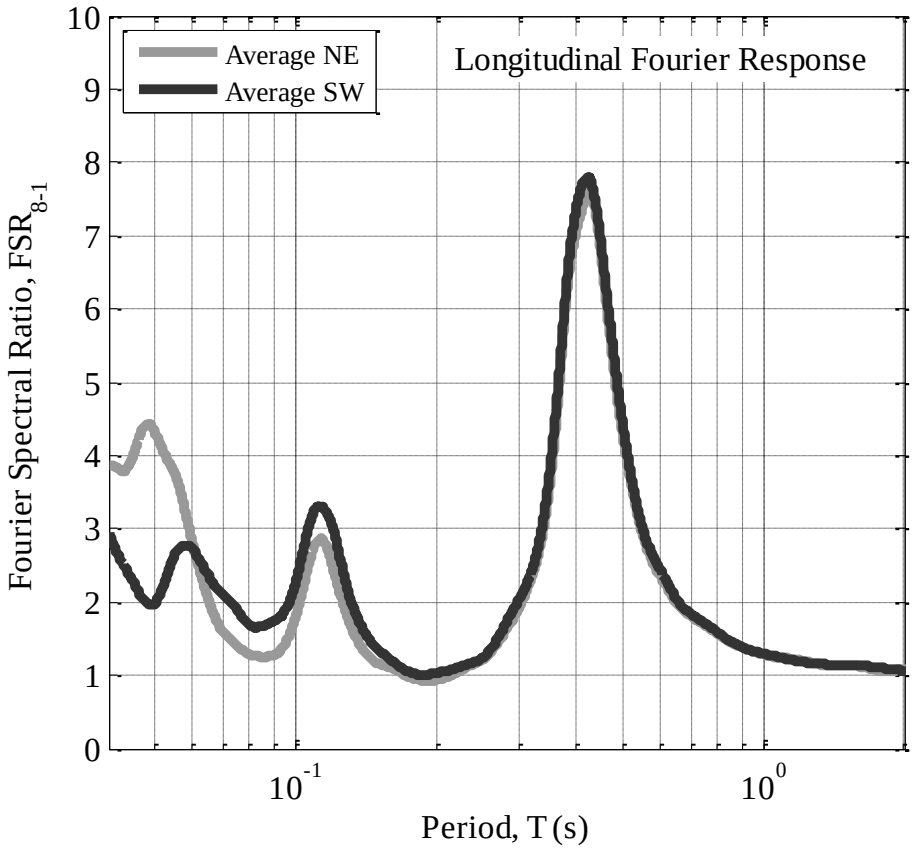


Figure 4-18: Comparison of Fourier amplitude ratios between the NE and SW ends in the longitudinal direction.

### *4.5.2.2 Transverse direction*

Figure 4-19 (a) shows the $FSR_{8-1}$ values at the north-east end (accelerometers 22 and 29), and Figure 4-19 (b) at the south-west (accelerometers 23 and 2A) end for vibration in the transverse

direction. There is a clear peak at around 0.6 seconds at both ends, however, the response is smaller at the SW end and the period is slightly larger. The average transfer functions for the transverse direction are compared in Figure 4-20. The difference in the end responses are more visible in this figure where it can be seen that the interaction with the Link Building causes another response peak at about 0.42 seconds which could correspond to the fundamental period of the Link Building. There is also another slight peak at around 0.15 seconds which could again be the second translational mode. It is worth noting that the spectral shape produced from the Fourier analysis for the transverse and longitudinal directions is different to that produced by the pseudo-spectral analysis. The Fourier spectra has two peaks which correspond to the first and second modes, while the pseudo spectral analysis only has one peak.

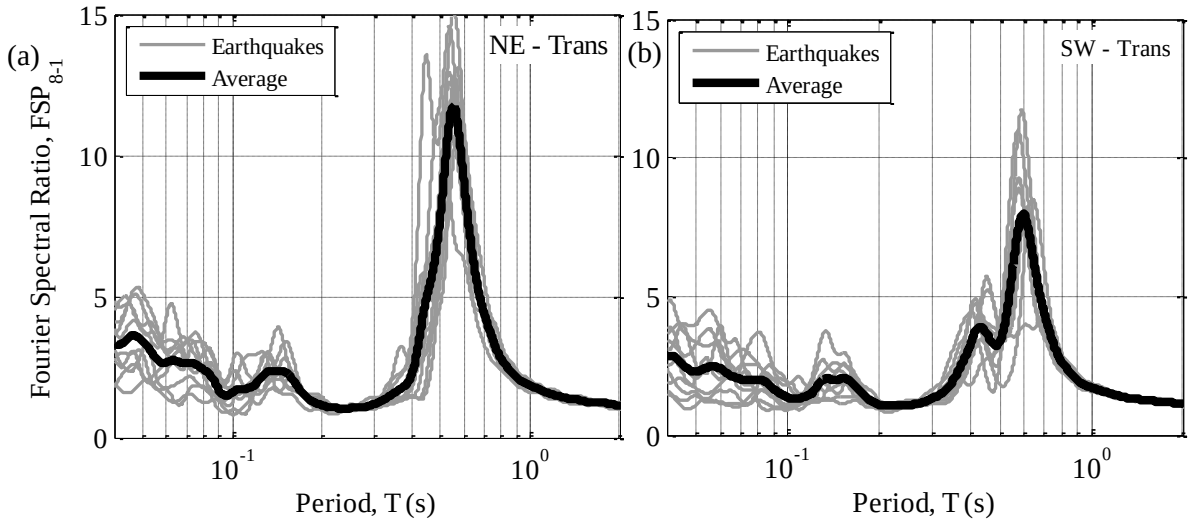


Figure 4-19: Ratio of Fourier amplitude between the eighth and first floors in the transverse direction at the (a) NE and (b) SW end.

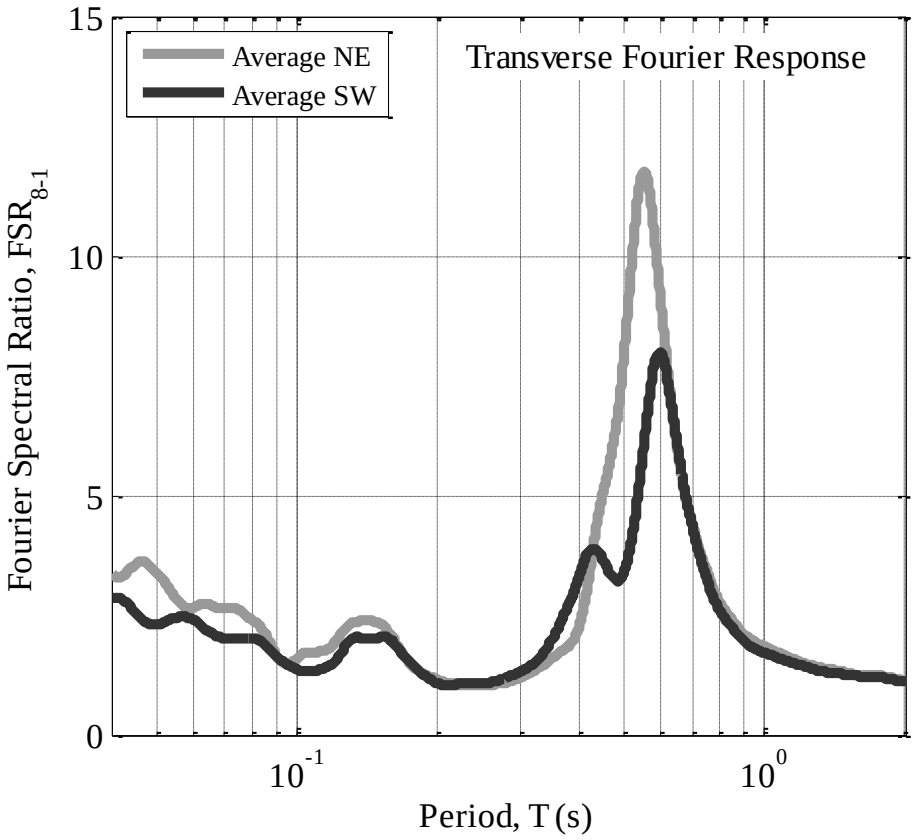


Figure 4-20: Comparison of Fourier amplitude ratios between the NE and SW ends in the transverse direction.

#### *4.5.2.3 Vertical direction*

The ratio of vertical Fourier amplitudes can be found in Figure 4-21. The responses at each end are again very similar with the largest peak occurring at approximately 0.09 seconds. The average vertical transfer functions found in Figure 4-22 are very similar at both ends. The second peak in this figure could correspond to the second vertical mode, however, it is very close to the cut off frequency so a more detailed analysis would be required in order to identify this.

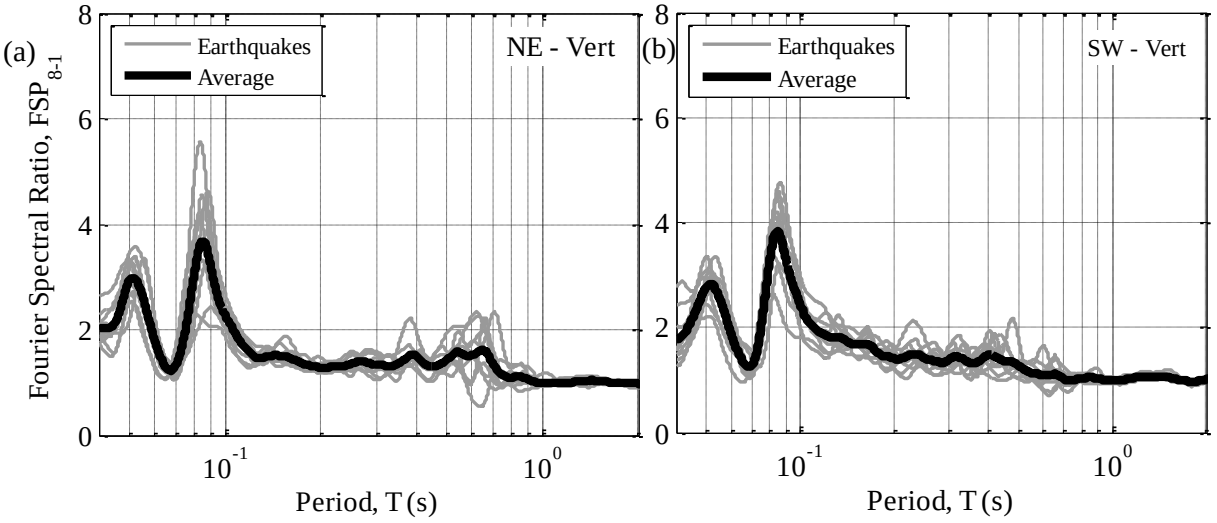


Figure 4-21: Ratio of Fourier amplitude between the eighth and first floors in the vertical direction at the (a) NE and (b) SW end.

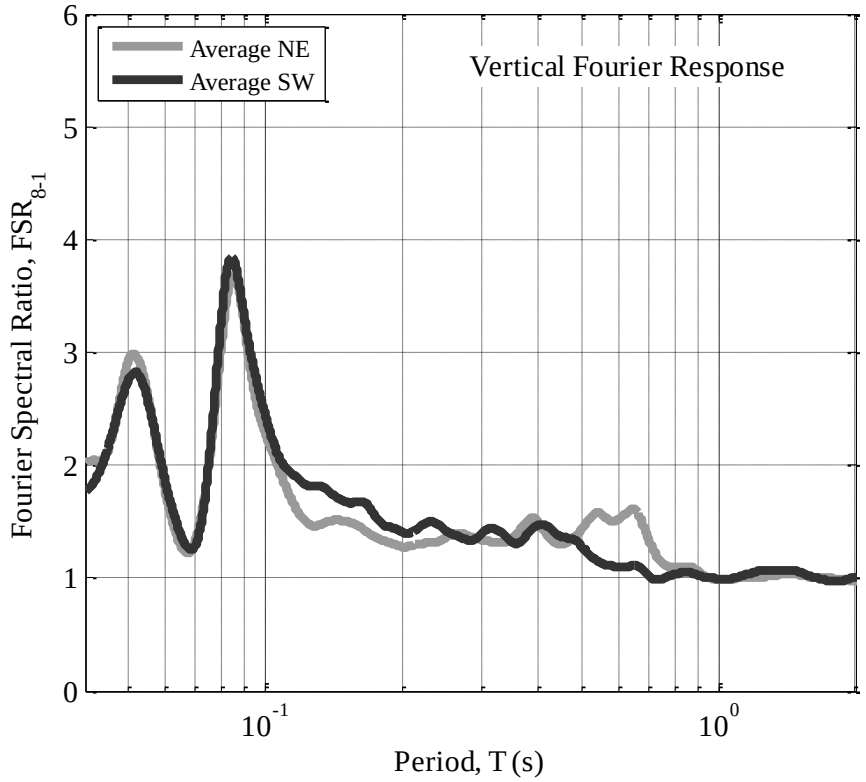


Figure 4-22: Comparison of Fourier amplitude ratios between the NE and SW end in the vertical direction.

#### *4.5.2.4 Base rotation*

The period of the base rotational motion was found by subtracting the parallel acceleration records from the first floor of the building (i.e. accelerometers 22 and 23 in the longitudinal direction, and accelerometers 21 and 24 in the transverse direction (refer to Figure 3-14 in the seismic

instrumentation section of Chapter 3)) and then performing a Fourier analysis on the differential acceleration record.

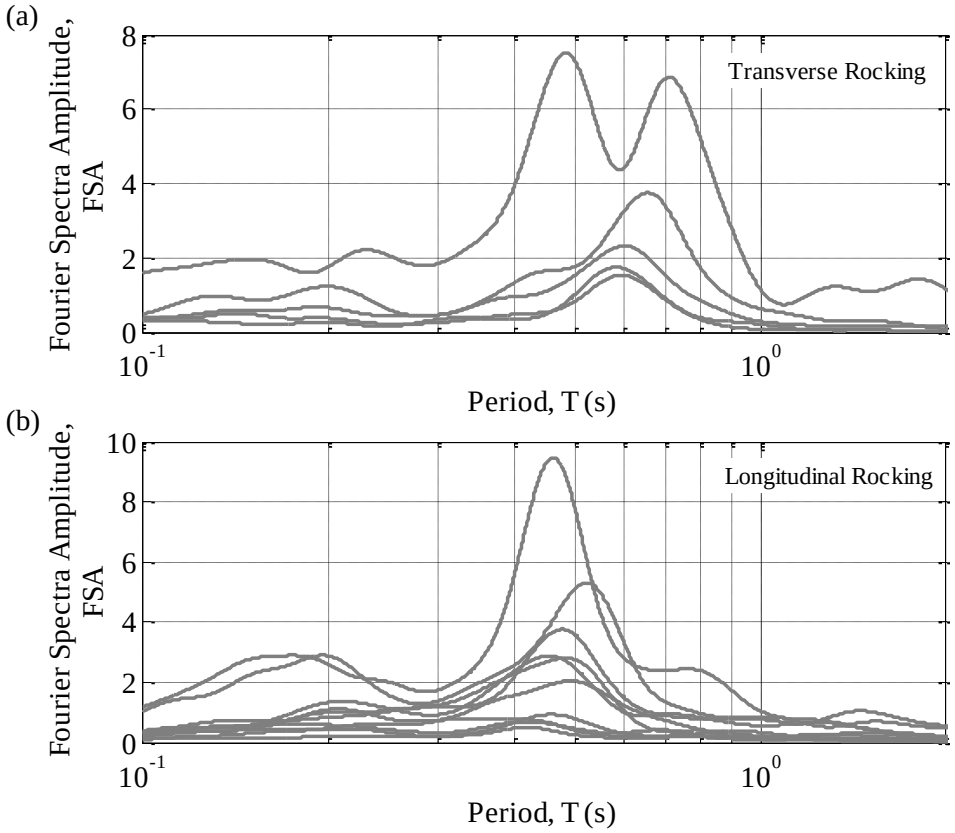


Figure 4-23: Fourier response amplitude for rocking in the (a) transverse and (b) longitudinal directions.

The period associated with the maximum Fourier amplitude was considered to be the period of the rocking motion. The results from these analyses can be found in Table 4-7. The period of rocking along the longitudinal axis was 0.44 seconds and in the transverse direction, the period of rocking was equal to 0.63 seconds.

#### *4.5.2.5 Torsional deformation*

As shown previously in Section 4.4.5, the torsional motion is predominately in the transverse direction. Therefore, in order to calculate the torsional fundamental period, the differential movement of the eighth floor and first floor was examined. This involved subtracting the transverse acceleration response from eighth floor of the two shear walls (accelerometers 29 and 2A) and performing a Fourier analysis on the differential acceleration record. This was also performed on the two first floor accelerations records (accelerometers 22 and 23) and again applying a Fourier analysis. The ratio between the eighth and first floors was found and the period corresponding to the maximum ratio was considered to be the fundamental period of the torsional motion. The Fourier spectral ratio for all ten earthquakes is shown in Figure 4-24. The results from the spectral analysis can be found in Table 4-7.

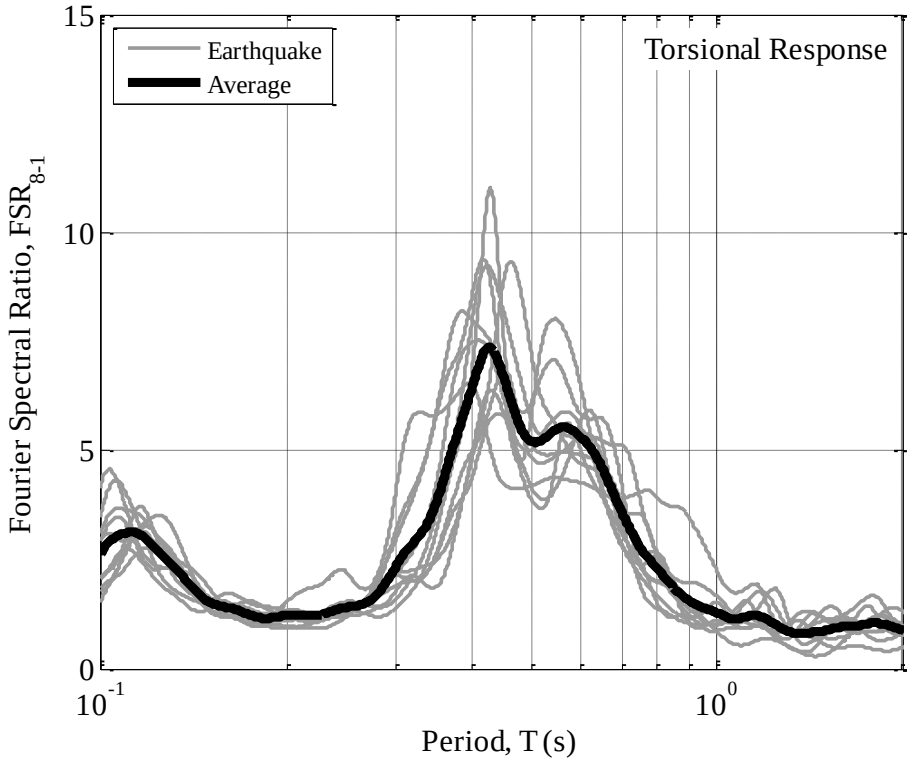


Figure 4-24: Fourier spectral ratio between the eighth and first floor torsional responses.

#### *4.5.2.6 Summary of vibration periods obtained from Fourier spectral ratios*

The fundamental period in each direction of the structure as well as the rocking and torsion motion was found for each earthquake using a Fourier-spectra analysis  The results for this can be found in Table 4-7.  The fundamental period of the longitudinal mode was on average 0.42 seconds for both NE and SW ends.  The fundamental period in the transverse direction varied between ends however was on average it was 0.54 seconds and 0.61 seconds for the NE and SW ends respectively. This could be due to torsional effects as explained previously.  The vertical period, was on average, 0.08 seconds. The periods of the rocking motion about each axis were 0.44 seconds and 0.63 seconds for the longitudinal and transverse directions respectively. These values were both very close to their respective translational fundamental periods. On average the torsional period was 0.43 seconds.

Table 4-7: Fundamental period of the building from Fourier Analysis.

| | Tm (s) | | | | | | | | |
|---|---|---|---|---|---|---|---|---|---|
| | Longitudinal | | Transverse | | Vertical | | Rocking | | Torsion |
| | NE | SW | NE | SW | NE | SW | Long | Trans | Trans |
| 4 September 2010 | 0.39 | 0.39 | 0.52 | 0.70 | 0.05 | 0.05 | 0.46 | 0.69 | 0.42 |
| 19 October 2010 | 0.41 | 0.41 | 0.45 | 0.58 | 0.08 | 0.08 | 0.33 | 0.58 | 0.38 |
| 26 December 2010 | 0.39 | 0.39 | 0.54 | 0.58 | 0.08 | 0.08 | 0.41 | 0.60 | 0.42 |
| 22 February 2011 | 0.46 | 0.46 | 0.58 | 0.64 | 0.06 | 0.09 | 0.52 | 0.65 | 0.46 |
| 16 April 2011 | 0.41 | 0.41 | 0.54 | 0.60 | 0.09 | 0.08 | 0.46 | -* | 0.42 |
| 13 June 2011 (1) | 0.45 | 0.45 | 0.55 | 0.60 | 0.08 | 0.08 | 0.49 | -* | 0.43 |
| 13 June 2011 (2) | 0.45 | 0.45 | 0.57 | 0.61 | 0.08 | 0.08 | 0.48 | -* | 0.45 |
| 9 October 2011 | 0.39 | 0.39 | 0.54 | 0.57 | 0.08 | 0.08 | 0.42 | -* | 0.41 |
| 23 December 2011 (1) | 0.43 | 0.42 | 0.56 | 0.59 | 0.09 | 0.08 | 0.47 | 0.60 | 0.43 |
| 23 December 2011 (2) | 0.43 | 0.43 | 0.55 | 0.60 | 0.05 | 0.09 | 0.44 | 0.66 | 0.44 |
| **Average** | **0.42** | **0.42** | **0.54** | **0.61** | **0.07** | **0.08** | **0.44** | **0.63** | **0.43** |

*Vertical acceleration records not available for these earthquakes.

### 4.5.3 Comparison between response and Fourier-spectral analyses

Table 4-8 shows a summary of the fundamental periods calculated in each orthogonal direction and for the rocking and torsion modes calculated using both analytical methods. The period in the longitudinal direction was equal to 0.42 seconds for all cases, therefore this value was considered to be very accurate. In the transverse direction, both analyses found that the SW end had a larger period, equal to approximately 0.62 seconds, whilst the NE end was about 0.56 seconds. Therefore, the average for the building in this direction can be taken as 0.59 seconds. The vertical period was equal to roughly 0.08 seconds in both cases. The periods of the foundation rotation were 0.45s and 0.61s in the longitudinal and transverse directions, respectively. These are very close to the translational period in their respective directions. There was large variability in the torsional period and it is suspected to be somewhere between the two translational periods (0.42s and 0.59s), however it is difficult to determine the exact value.

Table 4-8: Comparison of fundamental periods calculated from spectral and Fourier analyses.

| | Tm (s) | | | | | | | | |
|---|---|---|---|---|---|---|---|---|---|
| | Longitudinal | | Transverse | | Vertical | | Rocking | | Torsion |
| | NE | SW | NE | SW | NE | SW | Long | Trans | Trans |
| Spectral Analysis | 0.42 | 0.42 | 0.58 | 0.62 | 0.06 | 0.08 | 0.45 | 0.58 | 0.50 |
| Fourier Analysis | 0.42 | 0.42 | 0.54 | 0.61 | 0.07 | 0.08 | 0.44 | 0.63 | 0.43 |
| **Average** | **0.42** | **0.42** | **0.56** | **0.62** | **0.07** | **0.08** | **0.45** | **0.61** | **0.47** |
| **Combined Average** | **0.42** | | **0.59** | | **0.08** | | **0.45** | **0.61** | **0.47** |

## 4.6 Conclusions

This chapter has provided a detailed overview of the observed response of the UC Physics Building from 10 ground motions generated in the Canterbury earthquake sequence. The key points from this chapter are:

- Ten of the largest earthquake events from the 2010-11 Canterbury earthquake sequence were selected in order to understand the seismic response of the UC Physics Building. This included the two largest events of the 4 September 2010 earthquake with a magnitude of 7.2 and the 22 February 2011 earthquake with a magnitude of 6.2.
- The largest PGA, PGV and PGDs were recorded during the 4 September 2010 earthquake and were found to be 0.25g, 42.3cm/s and 13.5cm respectively. The 22 February 2011 earthquake had the second highest values and had a PGA of 0.19g. Six out of the ten ground motions selected had PGA values greater than 0.1g.The 4 September 2010 earthquake had the longest significant duration which was equal to 27.1s in the longitudinal direction. The largest level of acceleration recorded in the building was on the eighth floor during the 22 February 2011 earthquake and it was equal to 0.76g. The largest floor acceleration, velocity and displacement recorded during the 4 September 2010 earthquake was 0.61g, 61.2cm/s and 16.1cm respectively. Rocking behaviour was observed in the building during the earthquakes with the maximum angle of rocking equal to $1x10^{-2}$ rads in the transverse direction and $1.9x10^{-3}$ rads in the longitudinal direction during the 4 September 2010 earthquake. Torsional behaviour was also observed in the building during the earthquakes. The maximum angle of torsional movement was observed during the 4 September 2010 earthquake and was equal to $48\ x10^{-3}$ radians.
- The fundamental period of the building was found in each orthogonal direction using both a pseudo-spectral and Fourier analysis. Both analytical methods produced the same result in the longitudinal direction where the fundamental period was found to be 0.42s. In the transverse direction, there was more variation between the methods as well as between the ends of the building. It was found that on average the fundamental period in the transverse direction of the south-west end of the building was 0.62s, whilst the north-east end had a period of 0.56s. The fundamental period of the rocking motion was found to be 0.61s in the transverse direction and 0.45s in the longitudinal direction. These periods were very similar to the fundamental period of the translational motion in each direction. The period of the torsional motion was found to lie in the range of 0.43s to 0.50s.
- In general, the response-spectra and Fourier spectra analyses produced the same fundamental period, however, the second translation period was able to be identified in the Fourier analysis and not in the response-spectra analysis.

## 4.7 References

Aldea, A., Albota, E., Demetriu, S., & Kashima, T. (2007). *Seismic Response of a Low-Code High-Rise RC Building in Bucharest*. Paper presented at the International Symposium on Strong Vrancea Earthquakes and Risk Mitigation, Bucharest.

Arias, A. (1970). *A measure of earthquake intensity, in Seismic Design for Nuclear Power Plants*. R. J. Hansen. MIT Press: Cambridge, MA.p. 438–483.

Biot, M. A. (1941). A mechanical analyzer for the prediction of earthquake stresses. *Bulletin of the Seismological Society of America*, **31**, *151-171*.

Bommer, J. J., & Martinez-Pereira, A. (1999). The effective duration of earthquake strong motion. *Journal of Earthquake Engineering*, **3**, *127-172*.

Boore, D. M., & Akkar, S. (2003). Effect of causal and acausal filters on elastic and inelastic response spectra. *Earthquake Engineering & Structural Dynamics*, **32**, *1729-1748*.

Boore, D. M., & Bommer, J. J. (2005). Processing of strong-motion accelerograms: needs, options and consequences. *Soil Dynamics and Earthquake Engineering*, **93**(115).

Boore, D. M., Sisi, A. A., & Akkar, S. (2012). Using Pad-Stripped Acausally Filtered Strong-Motion Data. *Bulletin of the Seismological Society of America*, **102**, *751-760*.

Bradley, B. A. (2011). Near-Source Strong Ground Motions Observed in the 22 February 2011 Christchurch Earthquake. *Department of Civil and Natural Resources Engineering, University of Canterbury*, **82**(6), *853-865*.

Bradley, B. A. (2012). Strong ground motion characteristics observed in the 4 September 2010 Darfield, New Zealand earthquake. *Soil Dynamics and Earthquake Engineering*, **42**(32-46).

Butt, F., & Omenzetter, P. (2012). Evaluation of Seismic Response Trends from Long-Term Monitoring of Two Instrumented RC Buildings Including Soil Structure Interaction. *Advances in Civil Engineering*.

Celebi, M. (1998). *The Loma Prieta, California, Earthquake of October 17, 1989-Building Structures*.

GeoNet. (2012). GeoNet strong motion building records,Retrieved from ftp://ftp.geonet.org.nz/building/

Gledhill, K., Ristau, J., Reyners, M., Fry, B., & Holden, C. (2011). The Darfield (Canterbury, New Zealand) Mw 7.1 Earthquake of September 2010: A Preliminary Seismological Report,. *Seismological Research Letters*, **82**(378-386).

Kaiser, A., Holden, C., Beavan, J., Beetham, D., Benites, R., Celentano, A., . . . Zhao, J. (2012). The Mw 6.2 Christchurch earthquake of February 2011: preliminary report. *New Zealand Journal of Geology and Geophysics*, **55**(67-90).

Kramer, S. L. (1996). *Geotechnical Earthquake Engineering*. Upper Saddle River, NJ 07458: Prentice Hall, Inc

Limongelli, M. P. (2005). Performance Evaluation of Instrumented Buildings. *ISET Journal of Earthquake Technology, Paper No. 455,* **42**(2-3), *47-61*.

Michel, C., & Gueguen, P. (2006). *Dynamic Behaviour of The First Instrumented Building in France: The Grenoble City Hall*. Paper presented at the First European Conference on Earthquake Engineering and Seismology. Paper No. 941

Ohmachi, K. K. T. (1998). Ground-Motion Characteristics Estimated from Spectral Ratio between Horizontal and Vertical Components of Microtremor. *Bulletin of the Seismological Society of America,* **88**(1), *228-241*.

Reay, A. M. (1970). *Dynamic Characteristics of Civil Engineering Structures.* Doctor of Philosophy in Civil Engineering, University of Canterbury, Christchurch, New Zealand.

Skolnik, D., Lei, Y., Yu, E., & Wallace, J. W. (2006). Identification, Model Updating, and Response Prediction of an Instrumented 15-Story Steel-Frame Building. *Center for Embedded Network Sensing, University of California*.

Stewart, J. P., Seed, R. B., & Fenves, G. L. (1999a). Seismic soil-structure interaction in buildings. I: Analytical aspects. *J. Geotech. & Geoenv. Engrg., ASCE,* **125 (1)**, *pp 26-37*.

Stewart, J. P., Seed, R. B., & Fenves, G. L. (1999b). Seismic soil-structure interaction in buildings. II: Empirical findings. *J. Geotech. & Geoenv. Engrg, ASCE,* **125 (1)**, *pp 38-48*.

Trifunac, M. D., Ivanovic, S. S., & Todorovska, M. I. (2001). Apparent periods of a building. I:Fourier Analysis. *ASCE Journal of Structural Engineering*.

Ventura, C. E., Laverick, B., Brincker, R., & Andersen, P. (2003). Comparison of Dynamic Characteristics of Two Instrumented Tall Buildings.

Zhao, J. X., & Uma, S. R. (2011). *A preliminary analysis on the response of an instrumented building during the 2010 Darfield earthquake - significant effects of soil-structure interaction and nonlinear response*. Paper presented at the Ninth Pacific Conference on Earthquake Engineering. Paper 068

# 5 COMPARISON OF OBSERVATIONS WITH DESIGN CODE EXPRESSIONS AND FIXED-BASE LINEAR MODELS

## 5.1 Overview

The main objective of this chapter is to compare typical design assumptions with the observed response of the UC Physics Building. Initially, the observed results from Chapter 4 are compared with prescribed code equations for spectral acceleration, peak floor acceleration, fundamental period and deflected shape. Secondly, the observed deflections are compared with conventional dynamic modelling techniques. In conventional modelling, the designer typically assumes that the structure is linear elastic and the model has a fixed base. These assumptions are examined in this chapter using both one dimensional (1D) and two dimensional (2D) models of the UC Physics Building. The predictive capabilities of the 1D fixed base models are compared with the observations and predictions from the 2D models. Finally, reasons for the differences in predictive capabilities of the 1D and 2D models are discussed.

## 5.2 Comparison of observations with design codes

NZS1170.5 (2004): Part 5, is the New Zealand code for designing structures against earthquake loadings. The code prescribes many equations for important design parameters including spectral acceleration demands, height-wise variation of peak floor accelerations, fundamental period and deflected shape. The empirical equations for all of these parameters can be compared with the observations from the UC Physics Building so the accuracy of each can be examined for this specific case study.

### 5.2.1 Response spectra

NZS1170.5 (2004) prescribes an equation for the pseudo-spectral acceleration (pSA) as a function of fundamental period, which is used to determine the lateral design forces for a structure. The site hazard factor, C(T), is an estimate of spectral acceleration and is based on the buildings location, soil type and return period for a design earthquake. Typical values used for design in central Christchurch are an earthquake with a return period of 1/500 years and soil class D.

The design spectra and observed response-spectra for the 10 earthquakes is shown in Figure 5-1 for the (a) longitudinal direction, (b) transverse direction and (c) vertical direction based on the accelerometer records on the first floor of the UC Physics building (i.e. accelerometers 21-24 in Figure 3-14). It should be noted that the horizontal design spectra is the same in both directions while vertical design spectra is simply the horizontal spectra multiplied by 0.7. It can be seen that the 4 September 2010 and 22 February 2011 earthquakes produce spectral values above the design level for certain periods. The site hazard factor used for the design spectra has since been updated from a value of 0.22, to a value of 0.3 after the initial 4 September 2010 earthquake. If the design spectra is calculated based on this vale, then all the events are within the design spectra.

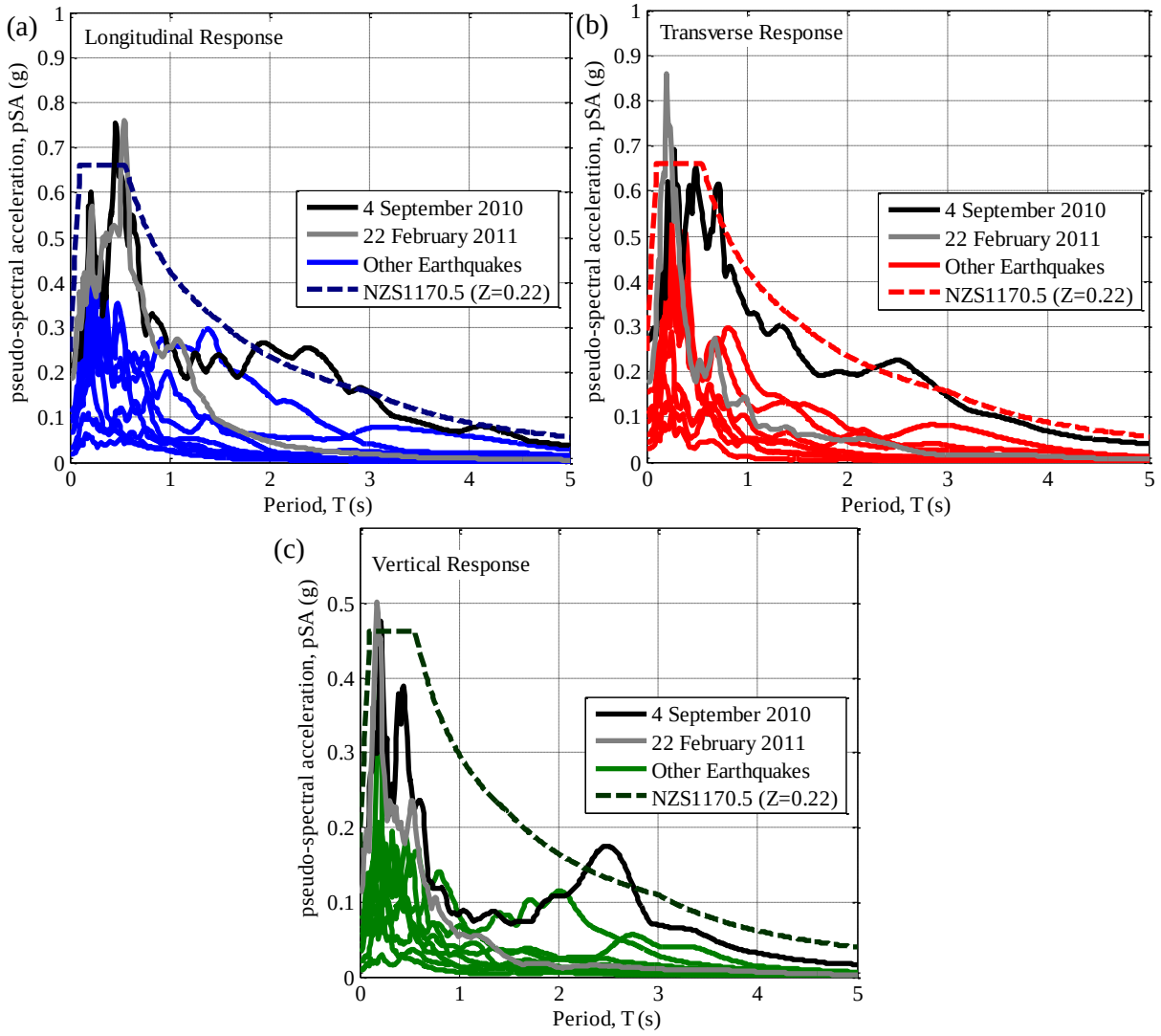


Figure 5-1: Comparison of pseudo-spectral acceleration from observations and design earthquake in the (a) longitudinal, (b) transverse and (c) vertical direction.

### 5.2.2 Peak floor acceleration profile

The observed maximum values of the horizontal absolute acceleration data can also be compared with Section 8 (Requirements for Parts and Components) of NZS1170.5 (2004) which prescribes an empirical formula for the amplification of peak horizontal floor accelerations with respect to the height of the building. The equation is represented by the black line in Figure 5-2 applied to the UC Physics Building. It can be seen that a maximum ratio of three, as prescribed by the code, provides a good match with the eighth floor average observation. However, all observations from the fourth floor are within the prescribed line, suggesting that the code is over-conservative for this particular structure (i.e. for structures with similar vibration periods). It should be noted that this data pertains to one building with two fundamental periods in each direction and that the code equation covers all buildings with all periods. The American code (ASCE/SEI7-05, 2006) and European code (Eurocode

8 (2009)) prescriptions are also illustrated for reference. These codes are less conservative compared with the NZ code and the Eurocode under-predicts most of the observed eighth floor acceleration ratios.

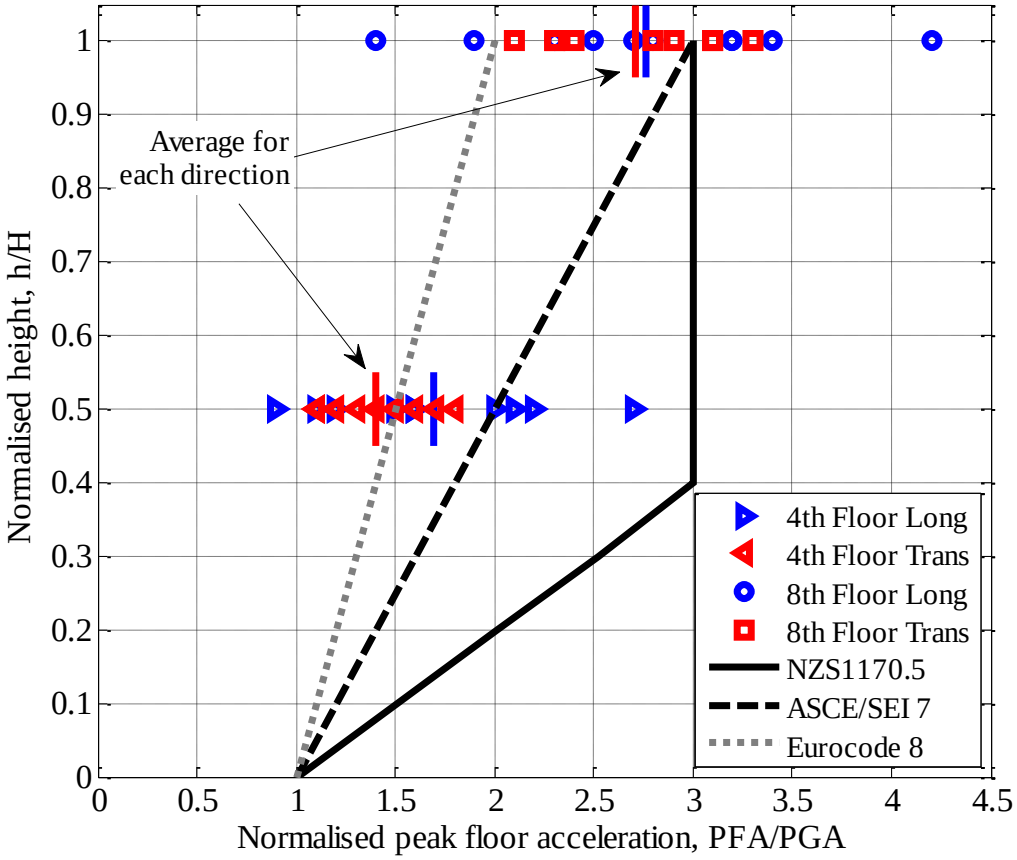


Figure 5-2: NZS1170.5 prescription for peak floor acceleration with respect to the normalized height of the building.

### 5.2.3 Fundamental period

An estimate of the fundamental period of a structure can also be made using NZS1170.5 (2004). The estimated fundamental period is used in the initial stages of design in order to calculated the lateral design forces on the structure. The period is found using the following empirical equation (described in more detail in Chapter 2.5):

$$T_1 = 1.0\, k_t h_n^{0.75} \quad for\ the\ serviceability\ limit\ state \tag{6-1}$$

The longitudinal direction consists of a moment resisting frame structure, therefore:

$$k_t = 0.075 \quad for\ moment\ resisting\ concrete\ frames$$

$$h_n = 30.4\ m$$

$$T_1 = 0.075\ x\ 30.4^{0.75} = 0.97\ s$$

This is much larger than the longitudinal period of 0.42 s based on the instrumental observations (i.e. Table 4-8 in Chapter 4).

The transverse direction consists of three concrete shear walls, therefore:

$$k_t = \frac{0.075}{\sqrt{A_c}}\ for\ structures\ with\ concrete\ shear\ walls$$

$$where\ A_c = \sum A_i(0.2 + \frac{l_{wi}}{h_n})^2$$

$$A_i = 3.75\ m^2$$

$$l_{wi} = 15.0\ m$$

$$k_t = \frac{0.075}{\sqrt{1.8}}$$

$$T_1 = 0.056\ x\ 30.4^{0.75} = 0.72\ s$$

This is larger than the transverse period of 0.59 s based on the instrumental observations (i.e. Table 4-8 in Chapter 4).

Clearly, the above comparisons illustrate that these predictions are not very accurate. However, they are prescribed to be used only as an initial estimate and a more accurate method should be used in the actual design.

### 5.2.4 Displacement based assessment

Displacement based design (DBD) is an alternative method to the force based design method prescribed in NZS1170.5 (2004). Instead of calculating the horizontal forces to be applied to the model, a displacement profile is estimated for the structure (Priestley *et al.*, 2007). The structure is converted into an equivalent single degree-of-freedom (SDOF) model with an effective height and mass. The fundamental period of the model is typically estimated from the effective SDOF model, however, in this case the fundamental period of the UC Physics Building is already known from the observations. Therefore a displacement based assessment (DBA) can be performed on the structure using the known fundamental period and calculating the effective height. The displacement at the effective height is then estimated based on the spectral displacement at the fundamental period for the

ground motion event considered. The effective height of the structure can be found in both directions using the following equation (Priestley *et al.*, 2007):

$$H_e = \frac{\sum_{i=1}^{n}(m_i \Delta_i H_i)}{\sum_{i=1}^{n} m_i \Delta_i} \quad (6\text{-}2)$$

The parameters for this equation are calculated in Table 5-1 for the longitudinal direction. The deflected shape in the table (δi) is based on the typical DBD prescribed equation for frames (Priestley *et al.*, 2007). The magnitude of the deflected shape (Δi) is not important, as the resulting effective height normalises the displacement value.

Table 5-1: Displacement Based Design for the Frame System (Longitudinal)

| **Storey, i** | **Height, Hi (m)** | **Mass, mi (tonnes)** | **δi** | **Δi (cm)** | **mi×Δi** | **mi×Δi²** | **mi×Δi×Hi** |
|---|---|---|---|---|---|---|---|
| 8 | 30.4 | 346.5 | 1 | 0.471 | 163 | 77 | 4958 |
| 7 | 26.6 | 346.5 | 0.91 | 0.429 | 149 | 64 | 3954 |
| 6 | 22.8 | 346.5 | 0.81 | 0.382 | 133 | 51 | 3021 |
| 5 | 19 | 346.5 | 0.70 | 0.331 | 115 | 38 | 2179 |
| 4 | 15.2 | 346.5 | 0.58 | 0.275 | 95 | 26 | 1446 |
| 3 | 11.4 | 346.5 | 0.45 | 0.213 | 74 | 16 | 843 |
| 2 | 7.6 | 346.5 | 0.31 | 0.147 | 51 | 7 | 387 |
| 1 | 3.8 | 346.5 | 0.16 | 0.076 | 26 | 2 | 100 |
| **Sum** | | **2772** | | | **805** | **281** | **16889** |

The effective height in the longitudinal direction is equal to:

$$H_e = \frac{16889}{805} = 21.0m$$

The corresponding values for the transverse direction are shown in Table 5-2.The prescribed deflected shape (Δi) in this case is for a wall.

Table 5-2: Displacement Based Design for the Wall System (Transverse)

| **Storey, i** | **Height, Hi (m)** | **Mass, mi (tonnes)** | **Δi (cm)** | **mi×Δi** | **mi×Δi²** | **mi×Δi×Hi** |
|---|---|---|---|---|---|---|
| 8 | 30.4 | 346.5 | 0.62 | 213 | 132 | 6490 |
| 7 | 26.6 | 346.5 | 0.50 | 174 | 87 | 4619 |
| 6 | 22.8 | 346.5 | 0.39 | 135 | 53 | 3080 |
| 5 | 19 | 346.5 | 0.29 | 99 | 28 | 1882 |
| 4 | 15.2 | 346.5 | 0.19 | 67 | 13 | 1014 |
| 3 | 11.4 | 346.5 | 0.11 | 39 | 4 | 449 |
| 2 | 7.6 | 346.5 | 0.05 | 18 | 1 | 139 |
| 1 | 3.8 | 346.5 | 0.01 | 5 | 0 | 18 |
| **Sum** | | **2772** | | **751** | **318** | **17692** |

The effective height in the transverse direction is equal to:

$$H_e = \frac{17692}{318} = 23.6m$$

Figure 5-3 shows the displacement response-spectra for the 4 September 2010 earthquake while Figure 5-4 shows the displacement spectra for the 22 February 2011 earthquake. These figures show the fundamental periods for the longitudinal and transverse directions and corresponding spectral displacements for both earthquakes. The transverse values are shown in grey while the longitudinal values are in black.

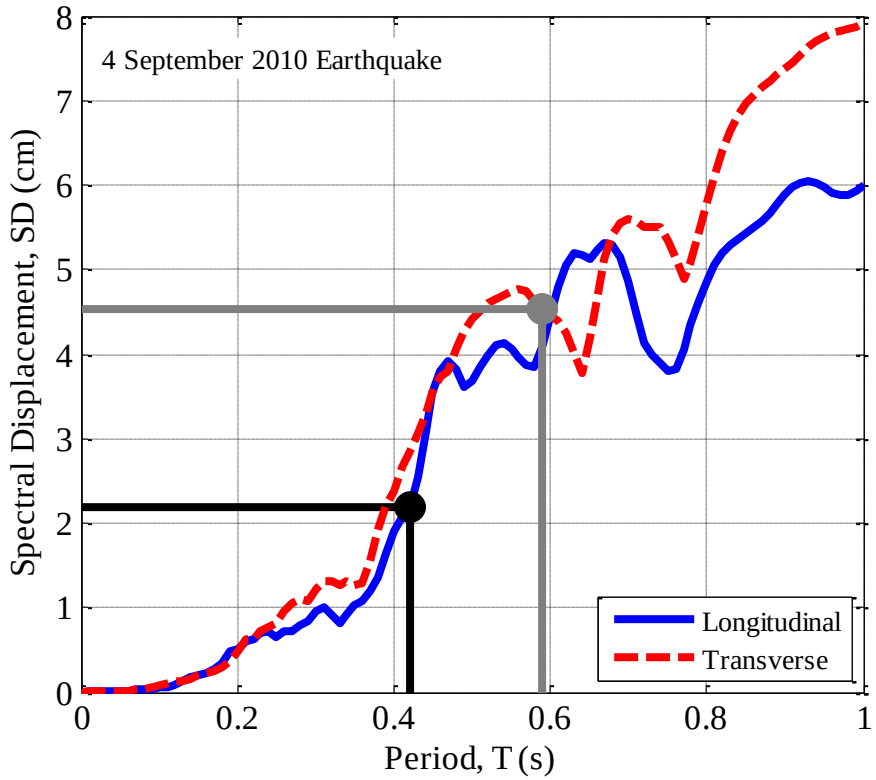


Figure 5-3: Spectral displacement for the 4 September 2010 earthquake.

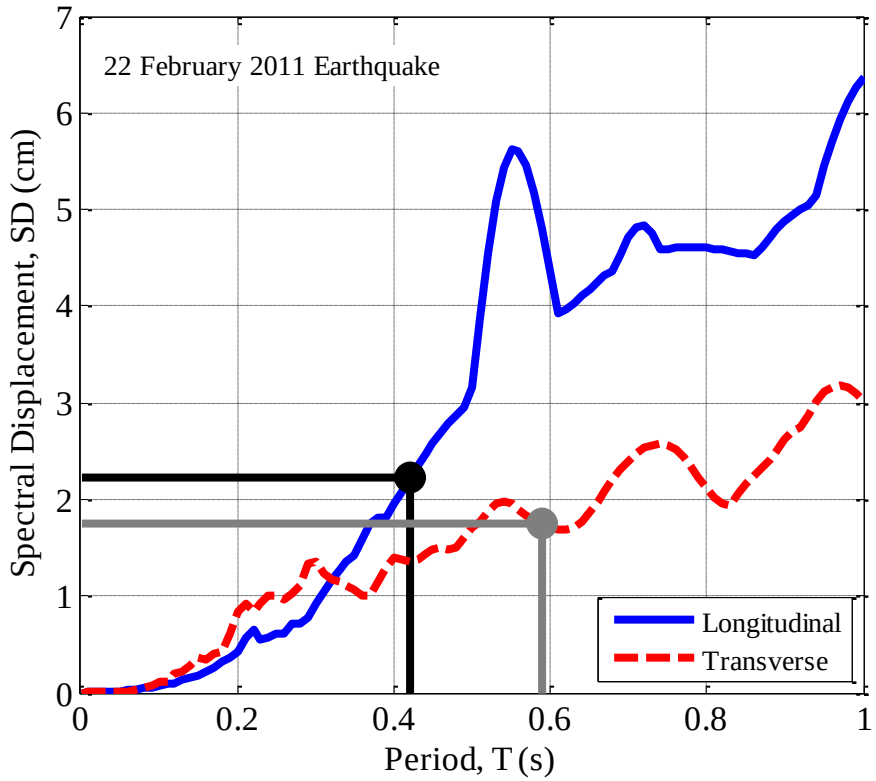


Figure 5-4: Spectral displacement for the 22 February 2011 earthquake.

An estimate of the relative deflections for an earthquake event can be calculated based on the DBA approach. The known deflected shape profile for the frame or wall system (Priestley *et al.*, 2007) is projected through the spectral displacement at the effective height. This is shown in Figure 5-5 for the longitudinal direction for the 4 September 2010 earthquake. The green square is the spectral displacement at the effective height and the black line is the prescribed deflected shape for a frame system. The observed relative displacements from the 4 September 2010 earthquake are represented by the circles positioned at their location in the building (i.e. the fourth, sixth and eighth floors). The thin circles on the fourth and eighth floors are the observed displacements from each shear wall (i.e. accelerometers 25 and 2A for the SW wall and 26 and 29 for the NE wall). The thin circles in the sixth floor are from the two accelerometers on the middle shear wall (i.e. accelerometers 27 and 28). The thicker circle is the average of the two observed displacements on each floor.

The predicted deflected shape in Figure 5-5 is a very good estimate of the observations considering it is based on a SDOF model. This suggests that the longitudinal system behaves like a frame even though it is made up of 11 small shear walls and beams.

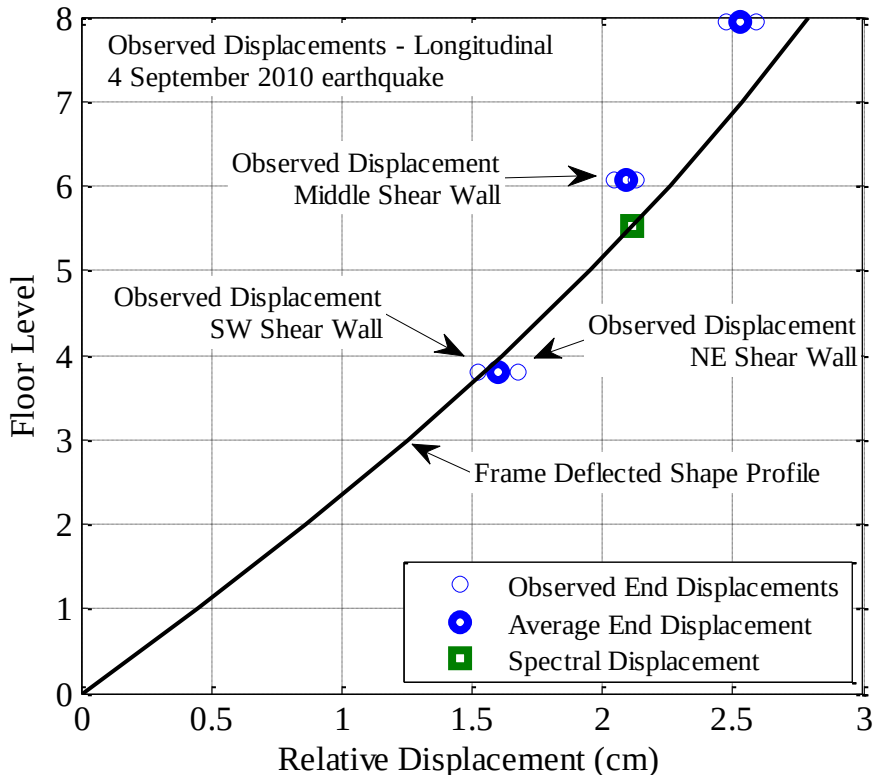


Figure 5-5: Observed longitudinal displacements compared with the displacement based assessment (DBA) prediction for the 4 September 2010 earthquake.

Figure 5-6 shows the relative displacements in the transverse direction for the 4 September 2010 earthquake. It also shows the spectral displacement at the effective height for the transverse system and the corresponding projected deflected shape for a wall system. The predicted deflected shape in

for the transverse direction does not match the observations as well as the longitudinal direction. This suggests that the system is not behaving like a single wall or there could be other effects occurring such as soil-structure interaction or non-linear behaviour. Neither of these two effects are accounted for in this model.

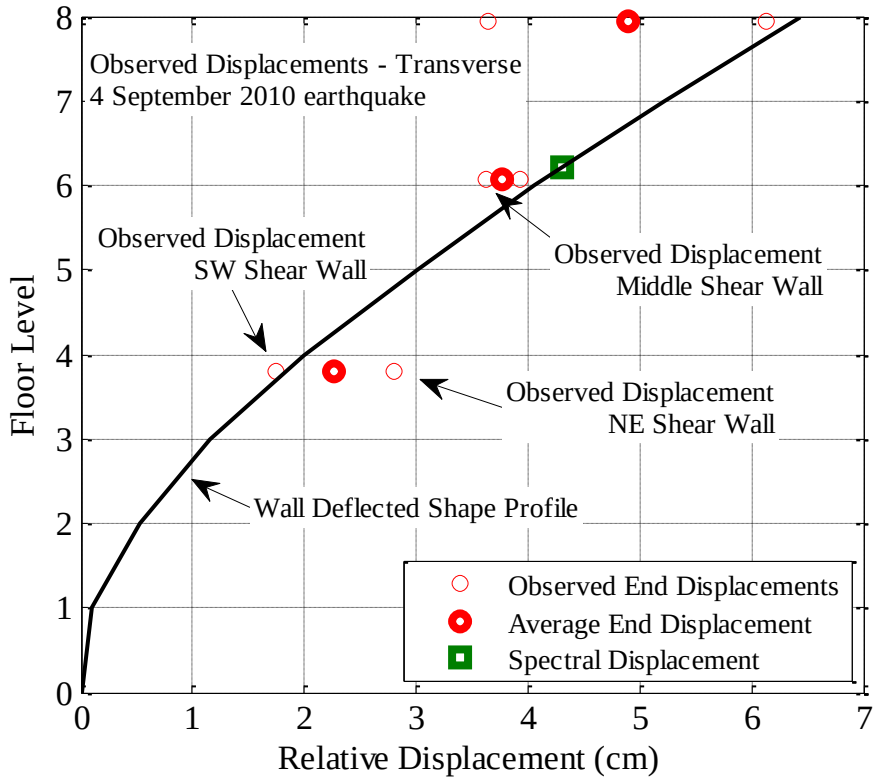


Figure 5-6: Observed transverse deflected shape and spectral displacement for 4 September 2010 earthquake.

The comparison between observations and spectral displacements can be performed for all earthquakes by normalising the displacements from each event by the average eighth floor observed displacement. This is shown in Figure 5-7 for the longitudinal direction and in Figure 5-8 for the transverse direction. These figures only show the normalised spectral displacement and not the corresponding deflected shape.

It can be seen in Figure 5-7 that the normalised observed deflected shape from each earthquake is very similar with all observations on one floor within 10% of each other. The spectral displacements also match the observations relatively well; however they have a larger distribution covering about 30% of the normalised scale.

The comparison of normalised displacements in the transverse direction are shown in Figure 5-8. Again, it can be seen that the average normalised observed deflected shape from each earthquake is very similar, with averages within 10% on the fourth and sixth floors. The spectral displacements at the effective height fit the normalised deflected shape but again have a wide range of 30%.

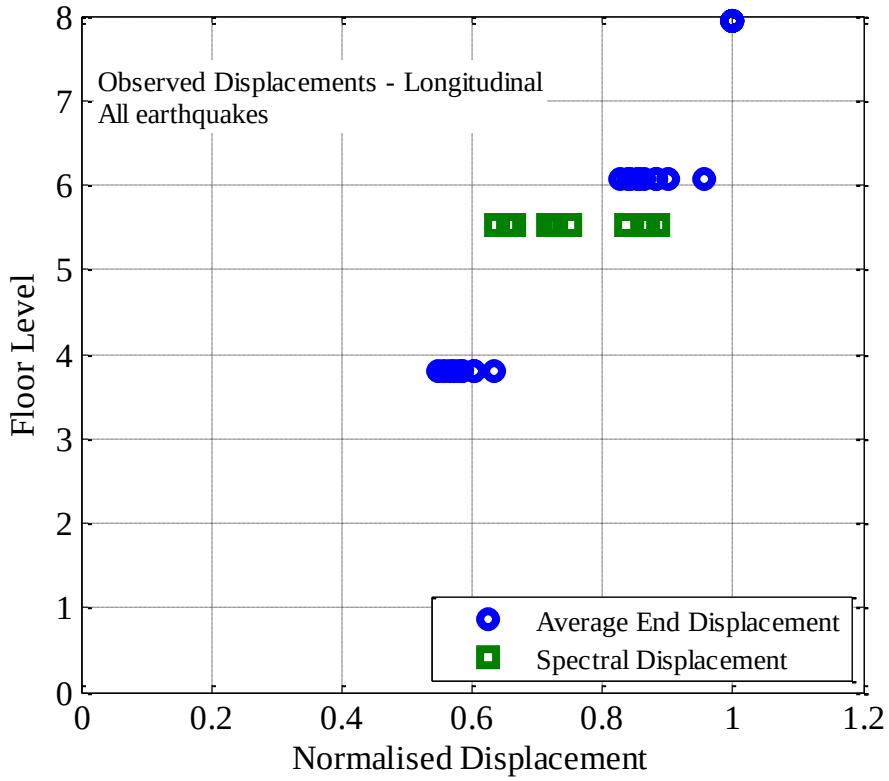


Figure 5-7: Observed longitudinal deflected shape and spectral displacement for all earthquakes.

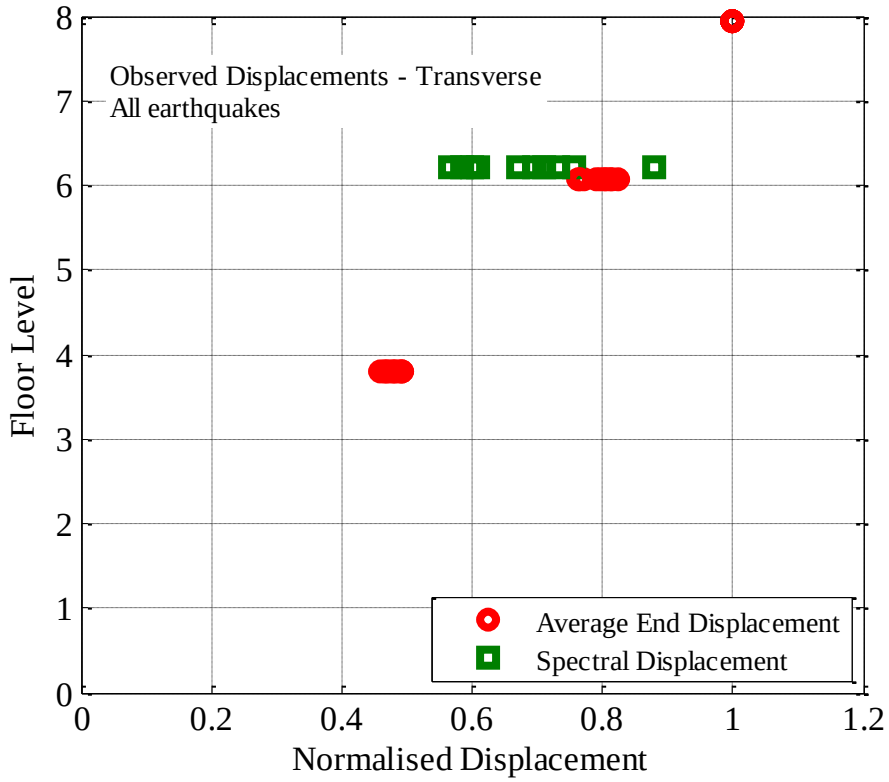


Figure 5-8: Observed transverse deflected shape and spectral displacement for all earthquakes.

## 5.3 MDOF one dimensional fixed base model

A one dimensional (1D) model simplifies a structure to exist entirely along one axis, which can comprise either a single degree-of-freedom (SDOF) or a multi degree-of-freedom (MDOF) system (Clough & Penzien, 2003). The first of these was discussed in the previous section as used in DBA. A MDOF model is a more accurate way to represent a structure, as each floor is represented as a lumped point with mass, connected between floors by a single element with stiffness. A MDOF model for the UC Physics Building is shown in Figure 5-9 that has eight nodes and eight elements which represent the eight floors of the structure. This model can be used to represent both transverse and longitudinal directions of the structure, with the relevant stiffness of the elements being represented in each direction. Both MDOF models initially have a fixed base and linear elastic elements, as these are simple approximations which are usually made in design. The same approach was also used by (Llera & Chopra, 1995) who compared observed instrumental results from the 1994 Northridge earthquake with linear models in order to examine typical design modelling.

Figure 5-9: 1D MDOF Model of the UC Physics building

The MDOF model can provide displacement predictions for all eight floors of the structure which can be compared with the three floors with observed displacements. All models were created using the modelling program (OpenSees, 2011). Response history analyses were performed on the model and the peak response on each level recorded. These values are compared with peak responses observed during the corresponding earthquake event. The observed displacement time series on the three instrumented floors can also be compared with the displacement predicted by the model on the same floors to check that the model is behaving correctly throughout the ground motion. The average of the recorded ground motions on the first floor of the structure was used as the input excitation in the analyses.

In the longitudinal direction, it was assumed that the structure would act as a frame with rigid diaphragms, therefore each floor would remain horizontal (Chopra, 2000). As a result, the rotation of each floor is constrained to zero. In the transverse direction, the system behaves like a wall, therefore it cannot be assumed that the floors remain horizontal. To allow for this, the rotations at each floor in the transverse model are not constrained.

### 5.3.1 Model properties

The two main properties required for the MDOF model are the mass at each floor and element stiffness. These were calculated based on the structural drawings. The mass of the structure was calculated using the volumes of the structural members. The concrete density was assumed to be 2400 kg/m$^3$ while the volumes of each of the members were calculated based on the member sizes described in Chapter 3. The density of concrete was multiplied by the total volume to find the permanent actions (dead load) of the structure per floor. The loading combination used was equal to dead load plus the live load (G + Q) instead of the design loadings (1.2G + 1.5Q) as the model was used for comparison rather than design (NZS1170.0 (2002a)). The loading of the contents were calculated based on NZS1170.1 (2002b) using a distributed load equal to 3kPa. This was prescribed in Table 3.1 of the code with the specified use of the floor defined as either a laboratory or institutional assembly area. The total mass per floor was calculated to be roughly 1,000,000kg. The stiffness of each element was calculated based on the geometric properties of each section. However. the stiffness was then adjusted so that the fundamental period of the model was equal to the observed period. Typical values of effective stiffness were equal to 20-30% of the gross stiffness. This process was also used by (Roger & Jirsa, 1998) in order to keep the analysis simple by not having different factors for columns, beams and walls.

### 5.3.2 Calculation of damping

Rayleigh damping (e.g. Chopra, 2000) was utilized, requiring specification of a target level of viscous damping and two periods which are to have the target level of damping. The first two modal periods of the structure were used as the input periods and the level of target damping was varied in order to find the best match between the model and the observed damping during ground motion excitation. This was done by varying the level of damping using 2%, 6% and 8% and comparing the predicted eighth floor response history with the observed response as shown in Figure 5-10. It can be seen, in the t=8-18s time window, that the model with 6% damping behaves the closest to the observations. This was also the case in the transverse direction, so 6% damping was also used in the model. A similar approach was taken by (Radoičić & Jovanović, 2013) to identify the structural damping.

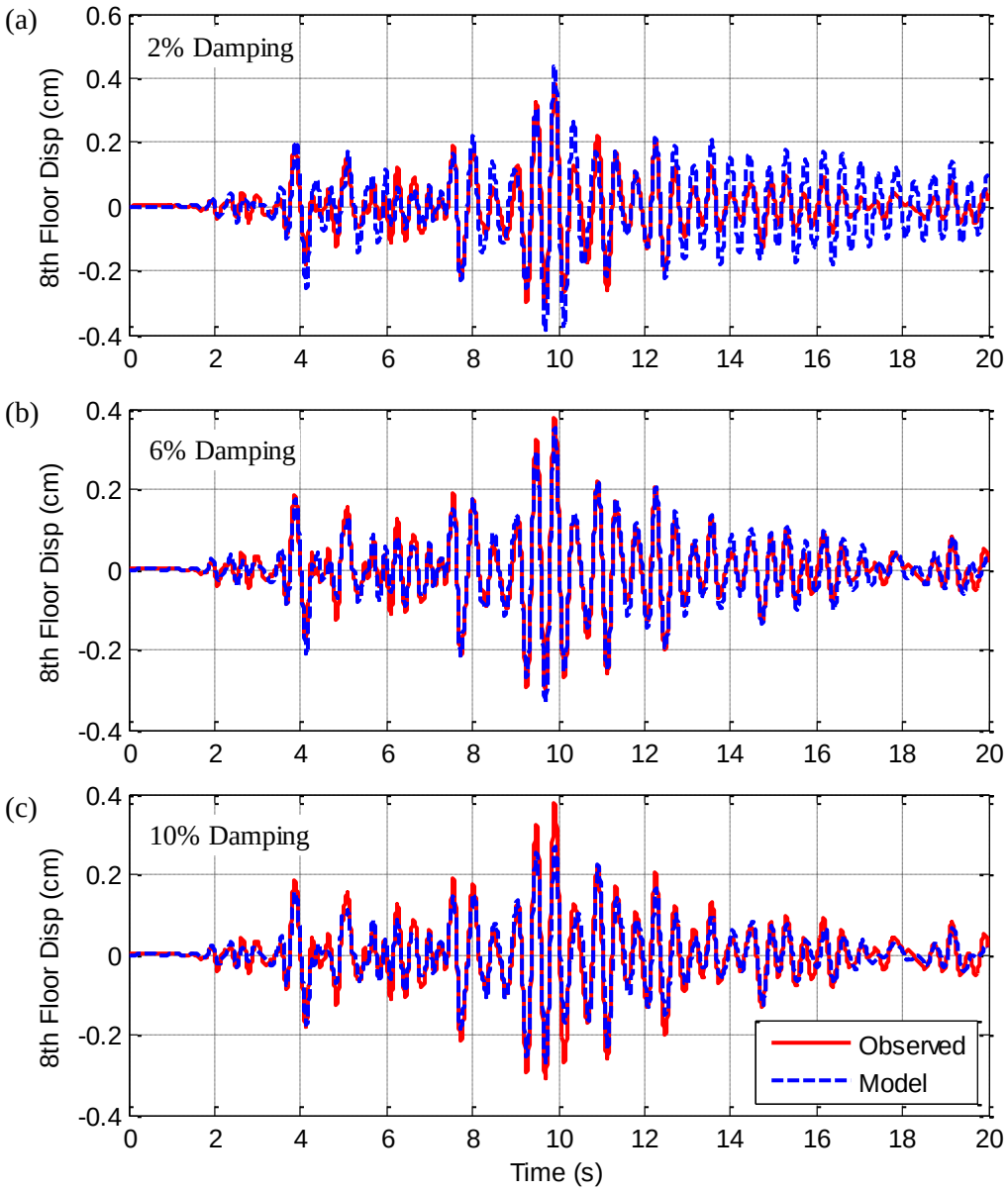


Figure 5-10: Eighth floor displacement time histories of the 1D longitudinal model comparing damping percentages of: (a) 2%; (b) 6%; and (c) 10%

### 5.3.3 1D fixed base prediction vs observations

#### *5.3.3.1 Longitudinal direction*

The displacement time-series of the model and observations can be compared at the fourth, sixth and eighth floors. For example, these comparisons are shown in Figure 5-11 in the longitudinal direction for the 16 April 2011 earthquake. As this event produced relatively small ground motions at the location of the UC Physics Building, it would be expected that the response of the building would be very similar to that of a fixed base, linear model. The response of the building to the 4 September 2010 and 22 February 2011 earthquakes is investigated in Chapters 6 and 7 as these chapters examine the soil-structure interaction and non-linear effects which are a result of large ground motion intensity.

It can be seen in the figure that the model predicts the response at the three heights very well and it appears that the level of damping and period of the model match the observed response. The maximum response on the sixth and eighth floors were slightly under-predicted on the large cycle at t=10s.

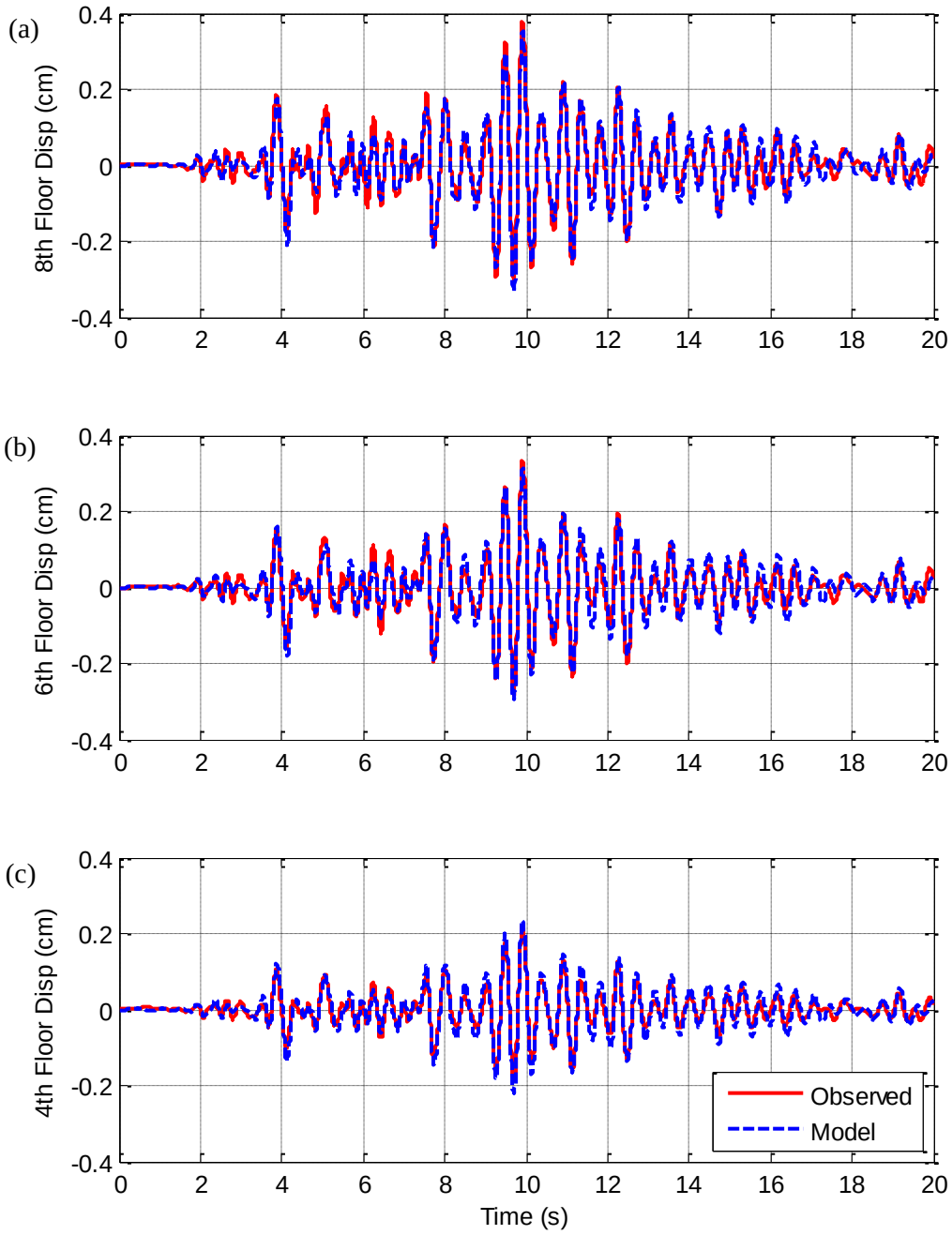


Figure 5-11: Comparison between the displacement time histories of the observations and 1D longitudinal fixed base model for the 16 April 2011 earthquake: (a) 8$^{th}$; (b) 6$^{th}$; and (c) 4$^{th}$ floor responses.

The under-prediction of the eighth and sixth floors can be more clearly seen in Figure 5-12 which compares the maximum observed displacements and the maximum predicted displacement envelope

in the longitudinal direction for the 16 April 2011 earthquake. The SDOF prediction is also very close to the MDOF predicted response.

The stiffness of the model is an important parameter when determining the fundamental period and hence the displacement of the structure. The stiffness was chosen in order to match the observed period, and therefore in order to show the sensitivity of the model to a change in stiffness, it was varied by ±10%. This variation caused a change in displacement which is represented by the shaded grey area in Figure 5-12. This variation is quite large and it covers all observed results.

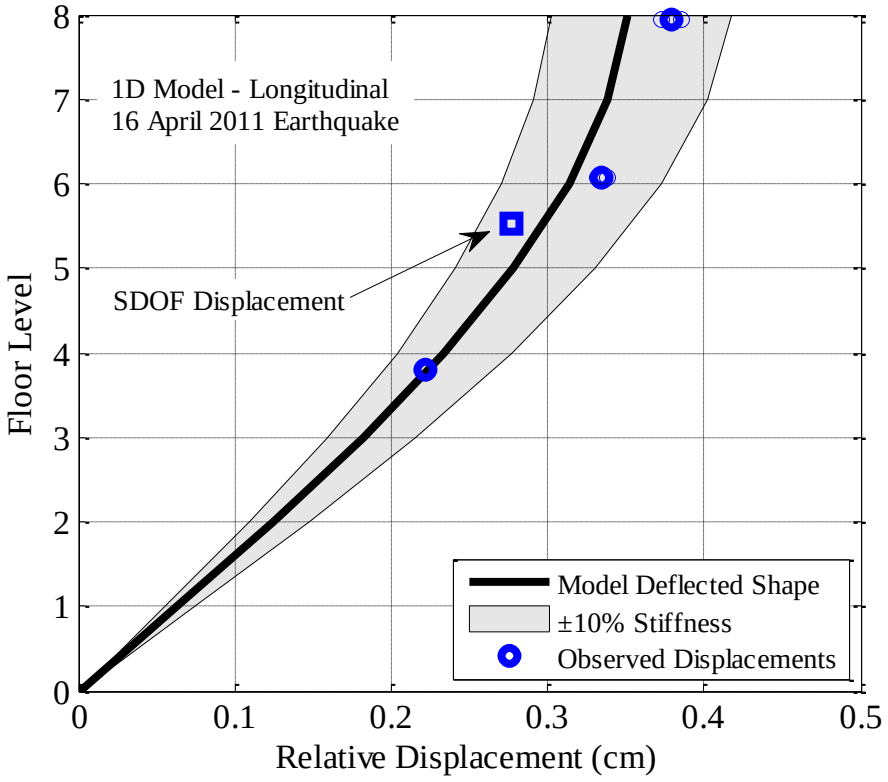


Figure 5-12: Comparison of the maximum deflected shape between observations and 1D longitudinal fixed base model for the 16 April 2011 earthquake.

The comparison between predicted and observed responses for all earthquakes can be better seen by normalising all displacements from each event by the predicted eighth floor displacement. This is shown in Figure 5-13 for the longitudinal direction. The variation of the blue circles shows the range in the predicted response, with the range equal to 40% (±20%) on the eighth floor. The deflected shape of the model passes through the range of observations (blue circles) near the average (green triangle), on the three observed floors suggesting that this model is a good fit for most events.

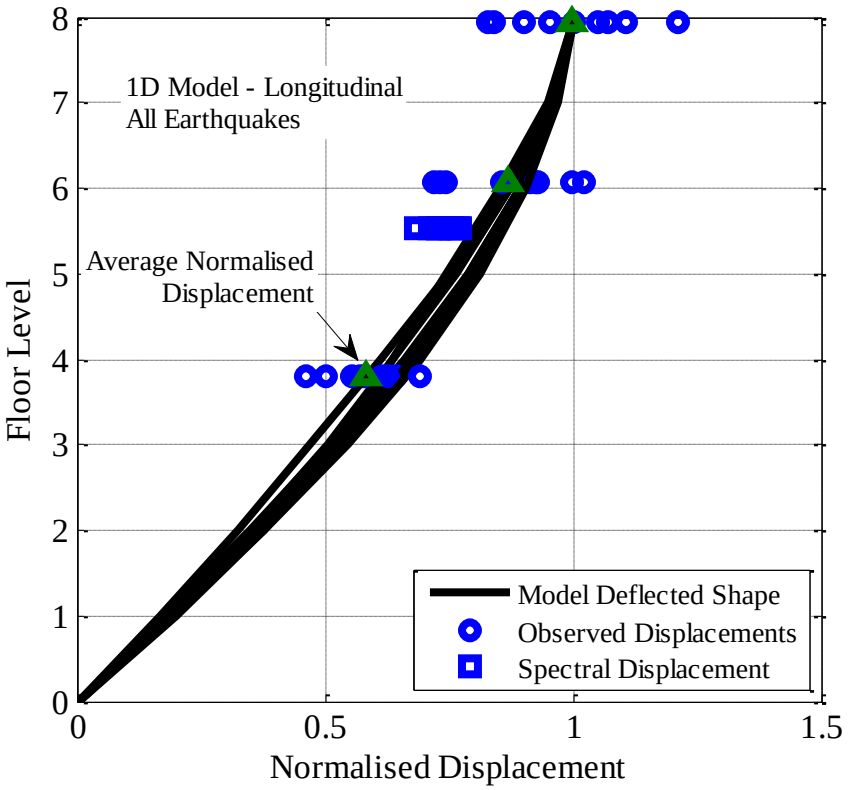


Figure 5-13: Comparison of the normalised maximum deflected shape between observations and the 1D longitudinal fixed base model for all earthquakes.

#### *5.3.3.2 Transverse direction*

The predicted response of the transverse 1D model was initially compared with the observations for the 16 April 2011 earthquake. This event was again used as this it produced relatively small ground motions at the location of the UC Physics building and it would be expected that the response of the building would be very similar to that of a fixed base, linear model. The transverse response of the building to the 4 September 2010 and 22 February 2011 earthquakes is investigated in Chapters 6 and 7 as these chapters examine the soil-structure interaction and non-linear effects which are a result of large ground motion intensity. The displacement response histories for the predictions and observations on the fourth, sixth and eighth floors are shown in Figure 5-11. The model provides very good predictions for eighth floor response however, the fourth and six floor responses are under-predicted. It appears that the fundamental period of the model matches the observed period.

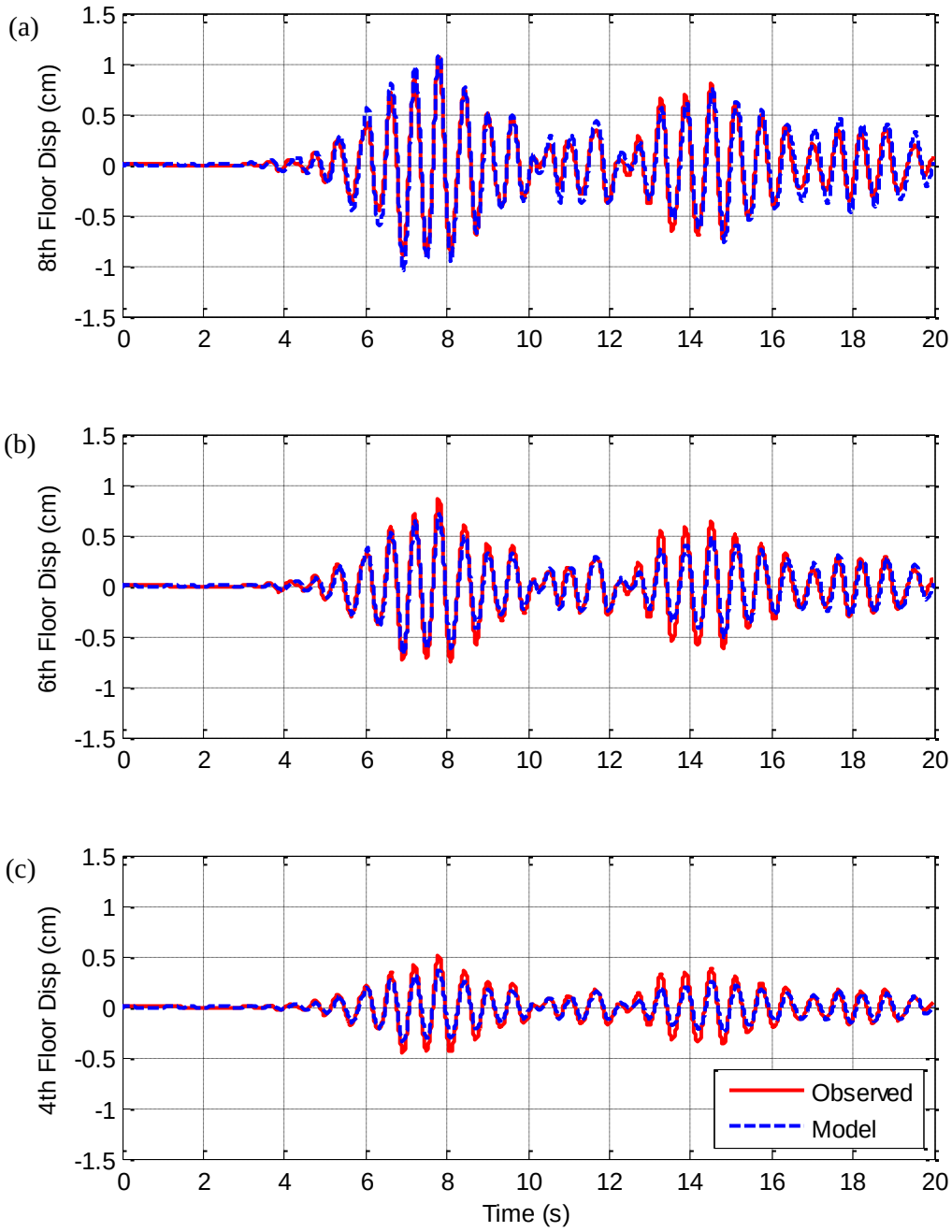


Figure 5-14: Comparison between the displacement time histories of the observations and 1D transverse fixed base model for the 16 April 2011 earthquake: (a) 8th; (b) 6th; and (c) 4thfloor responses. Note: the observed response is the average response of the two accelerometers on each floor.

The difference between the prediction and model can be more clearly seen by comparing the maximum displacement response profile. This is shown in Figure 5-15 for the 16 April 2011 earthquake. This figure shows how the maximum displacements on the fourth and sixth floors are significantly under-predicted, while the eighth floor displacement prediction is very close to the observations. The SDOF prediction is also very close to the MDOF prediction.

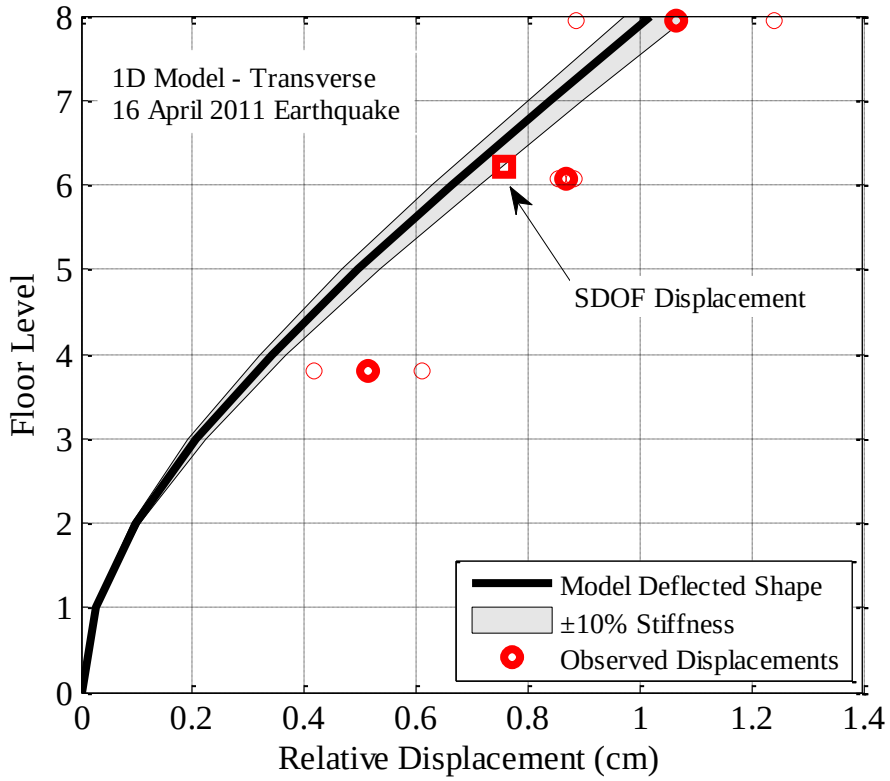


Figure 5-15: Comparison of the maximum deflected shape between observations and the 1D transverse fixed base model in the 16 April 2011 earthquake.

The normalised response of the model for all earthquakes in the transverse direction is shown in Figure 5-16. It can be seen that the eighth floor prediction on average is very close to the observations while the sixth and fourth floor are significantly under-predicted. It is therefore evident that the 1D MDOF model for the transverse direction cannot predict the full displacement profile of the structure when it is assumed to behave as a fixed-base cantilever wall. Possible solutions to the under-prediction of fourth and sixth floors are investigated in Chapters 6 and 7 where the effect of SSI and non-linear elements are incorporated into the model.

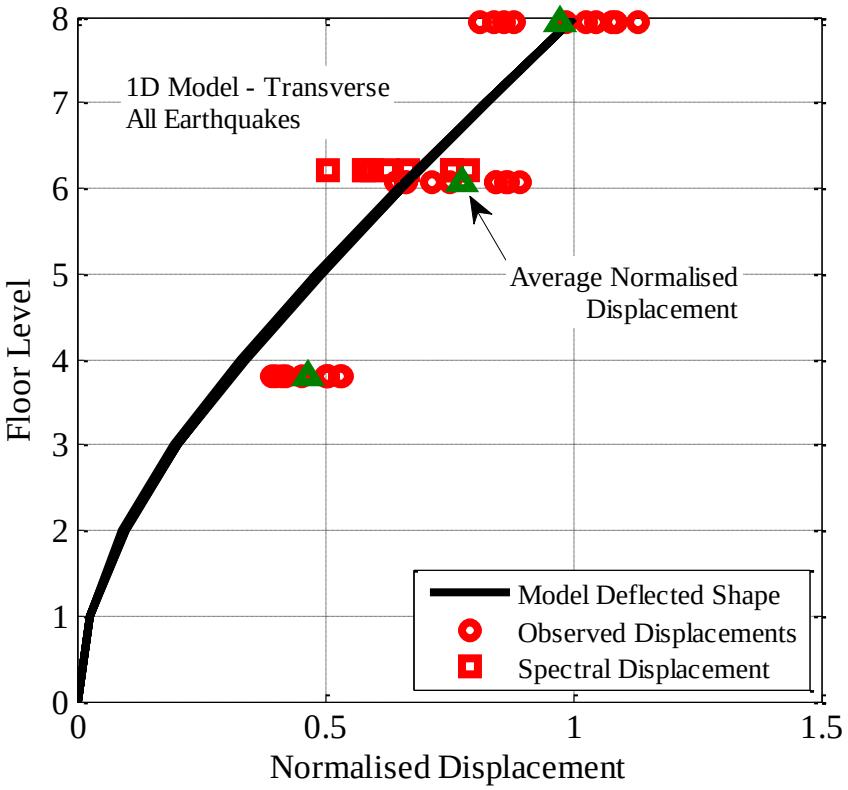


Figure 5-16: Comparison of the normalised maximum deflected shapes between observations and the 1D transverse fixed base model for all earthquakes.

## 5.4 MDOF two dimensional fixed base model

A two dimensional (2D) model represents the building in a more realistic way compared with the 1D model, as it represents each structural member individually as either a vertical element or a horizontal element. This interaction between the vertical and horizontal elements can add the complexity required to better predict the deflected shape of the structure. The longitudinal model in Figure 5-17 (a) consists of eleven columns and eight floors. This allows for the stiffness of each element to be modelled more accurately and the mass to be spread across all the nodes on each floor. The 2D transverse model shown in Figure 5-17 (b) consists of two vertical elements and eight floors. This resembles a coupled wall and beam system.

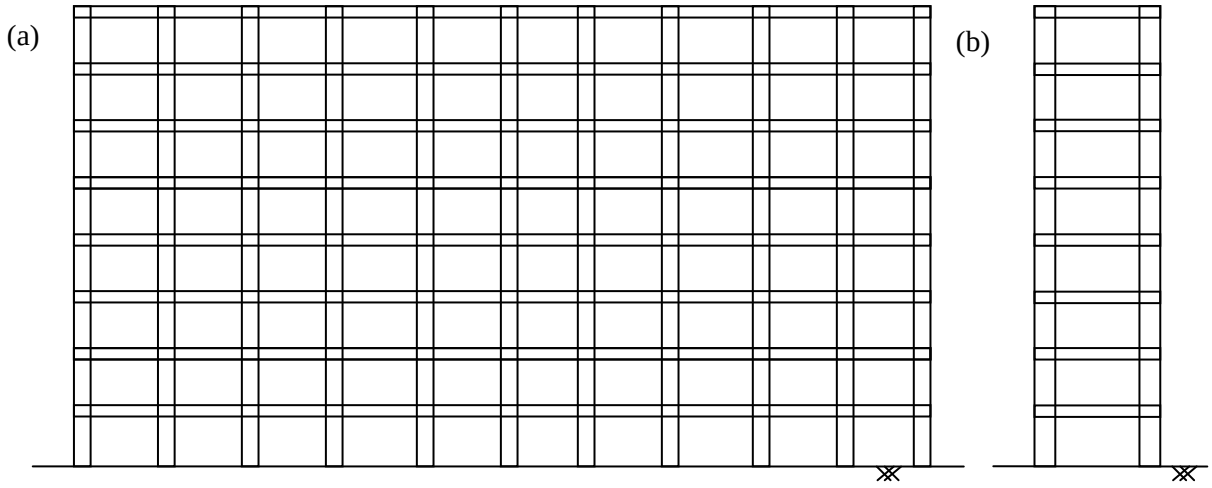


Figure 5-17: 2D schematic of the (a) longitudinal and (b) transverse direction models.

### 5.4.1 Model properties

The floor mass of the 2D model is still the same as the 1D model, however there are 11 nodes per floor in the longitudinal direction and 2 per floor in the transverse direction for the mass to be distributed amongst based on tributary area. The stiffness of the frame can be more accurately modelled as individual members rather than lumped together as one element. This allows for better comparison with the prescribed effective section properties from Table C6.6 in NZS3101 (2006) shown in Table 5-3. The percentage of effective second moment of inertia for the different beam, column and wall members varies with axial load, steel strength and design ductility.

Table 5-3: Effective section properties (Table C6.6) prescribed by NZS3101 (2006)

| Type of member | Ultimate limit state | | Serviceability limit state | | |
|---|---|---|---|---|---|
| | $f_y$ = 300 MPa | $f_y$ = 500 MPa | $\mu$ = 1.25 | $\mu$ = 3 | $\mu$ = 6 |
| **1 Beams** | | | | | |
| (a) Rectangular ¶ | 0.40 $I_g$ (use with $E_{40}$) § | 0.32 $I_g$ (use with $E_{40}$) § | $I_g$ | 0.7 $I_g$ | 0.40 $I_g$ (use with $E_{40}$)§ |
| (b) T and L beams ¶ | 0.35 $I_g$ (use with $E_{40}$) § | 0.27 $I_g$ (use with $E_{40}$) § | $I_g$ | 0.6 $I_g$ | 0.35 $I_g$ (use with $E_{40}$)§ |
| **2 Columns** | | | | | |
| (a) $N^*/A_g f_c' > 0.5$ | 0.80 $I_g$ (1.0 $I_g$)‡ | 0.80 $I_g$ (1.0 $I_g$)‡ | $I_g$ | 1.0 $I_g$ | As for the ultimate limit state values in brackets |
| (b) $N^*/A_g f_c' = 0.2$ | 0.55 $I_g$ (0.66 $I_g$)‡ | 0.50 $I_g$ (0.66 $I_g$)‡ | $I_g$ | 0.8 $I_g$ | |
| (c) $N^*/A_g f_c' = 0.0$ | 0.40 $I_g$ (0.45 $I_g$)‡ | 0.30 $I_g$ (0.35 $I_g$)‡ | $I_g$ | 0.7 $I_g$ | |
| **3 Walls** ¶ | | | | | |
| (a) $N^*/A_g f_c' = 0.2$ | 0.48 $I_g$ | 0.42 $I_g$ | $I_g$ | 0.7 $I_g$ | As for the ultimate limit state values |
| (b) $N^*/A_g f_c' = 0.1$ | 0.40 $I_g$ | 0.33 $I_g$ | $I_g$ | 0.6 $I_g$ | |
| (c) $N^*/A_g f_c' = 0.0$ | 0.32 $I_g$ | 0.25 $I_g$ | $I_g$ | 0.5 $I_g$ | |

In order to be consistent, it was decided that the same percentage of stiffness of both the walls and beams would be used in order to again match the model period with the observed period. A similar process was adopted by (Roger & Jirsa, 1998) when modelling an instrumented building in the 1994

Northridge earthquake. They also decided to match the model fundamental period with the observations by adjusting the effective stiffness to 35% of the total stiffness for all beams and columns. Roger and Jirsa found that using the same percentage of stiffness reduction for all beams and columns was sufficient to provide satisfactory results, however, the results would have been improved if different factors had been used for the beams and columns.

The percentage of gross stiffness used in this study was 21.1% and 28.5% in the longitudinal and transverse directions, respectively. It is hard to make direct comparison with Table 5-3 as the level of earthquake demand was between serviceability and ultimate limit states and the design ductility is unknown. However, the calculated values are slightly lower than those suggested for ultimate limit state, but still reasonable for a building that has been in operation for nearly 50 years. It is also worth noting that the addition of foundation flexibility to the models in Chapter 6 allows the percentage of gross stiffness in the transverse direction to be further increased to approximately 80% of the gross stiffness making it a better comparison with the design table.

### 5.4.2 2D fixed base prediction vs observations

#### *5.4.2.1 Longitudinal direction*

The displacement response history on the fourth, sixth and eighth floors for the longitudinal 2D fixed base model and observations is shown in Figure 5-18. The predicted response from the model matches the observations very well for all floors, particularly in the t=10-18 second region.

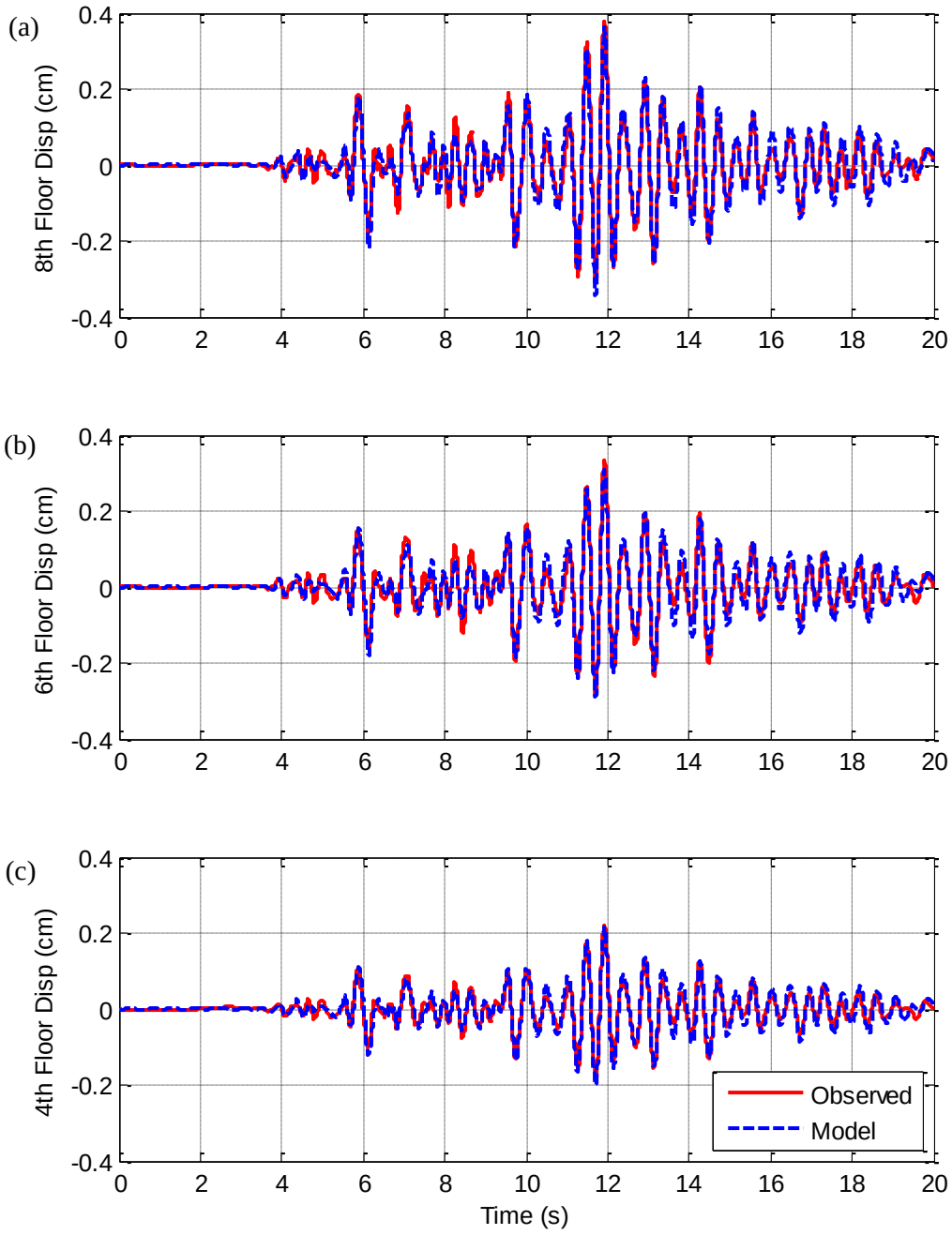


Figure 5-18: Comparison between the displacement time histories of the observations and 2D longitudinal fixed base model for the 16 April 2011 earthquake: (a) 8th; (b) 6th; and (c) 4th floor responses.

The maximum displacements from the 2D longitudinal model and observations are compared for the 16 April 2011 in Figure 5-19. This figure also shows the range of responses when the stiffness of all elements is adjusted by ±10%. This model appears to very accurately predict the peak response of the structure with all three observations within 5%. The variation in stiffness causes a large change in the predicted maximum response with the variation being up to 25% on the eighth floor.

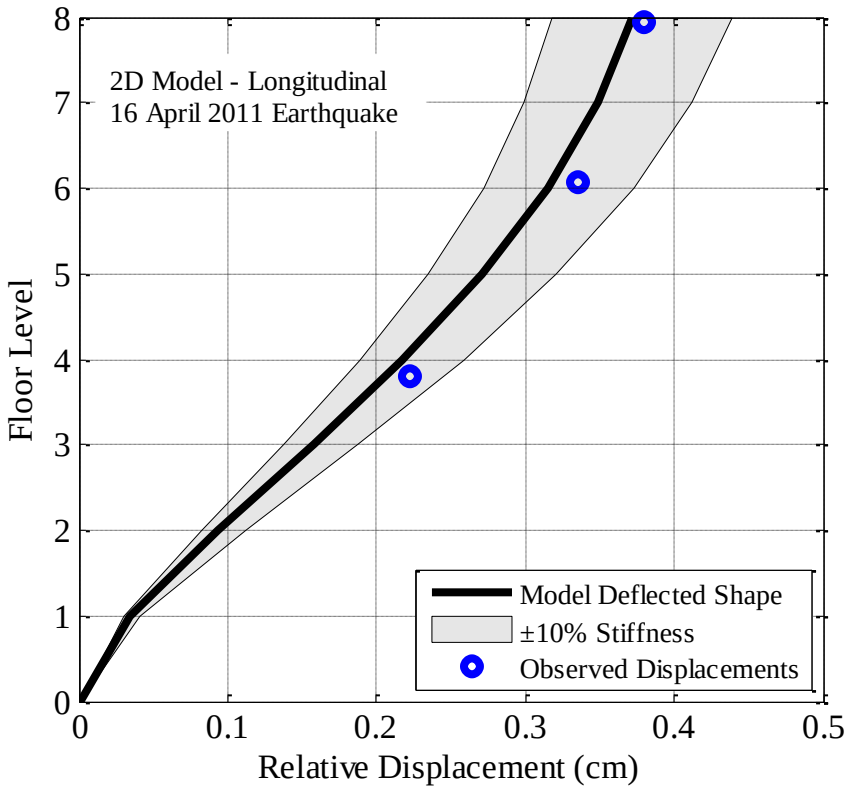


Figure 5-19: Comparison of the maximum deflected shapes between observations and the 2D longitudinal fixed base model for the 16 April 2011 earthquake.

The normalised predicted maximum displacements from the 2D longitudinal model are compared with observations in Figure 5-20. As with the 1D longitudinal model, the predicted displacement appears to be a good fit with the observed data with the predictions all passing through the average normalised observation.

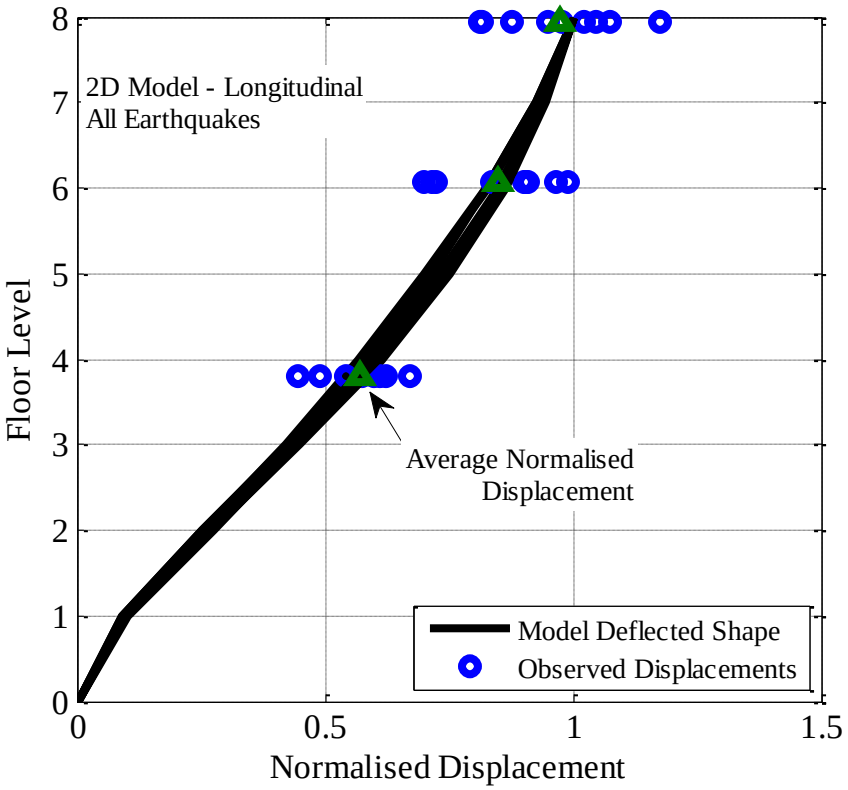


Figure 5-20: Comparison of the normalised maximum deflected shapes between observations and the 2D longitudinal fixed base model for all earthquakes.

#### *5.4.2.2 Transverse direction*

The predicted response of the transverse 2D model was initially compared with the observations for the 16 April 2011 earthquake. The predicted and observed displacement response of the fourth, sixth and eighth floors is shown in Figure 5-21. The 2D transverse model is able to predict the eighth floor response very well, however, the predicted response of the fourth and sixth floors is consistently slightly less than the observations. It is worth noting that, although the model is under-predicting the response, the period of the predicted and observed response appears to the same. Therefore suggesting that the under-prediction is not a result of the incorrect period in the model.

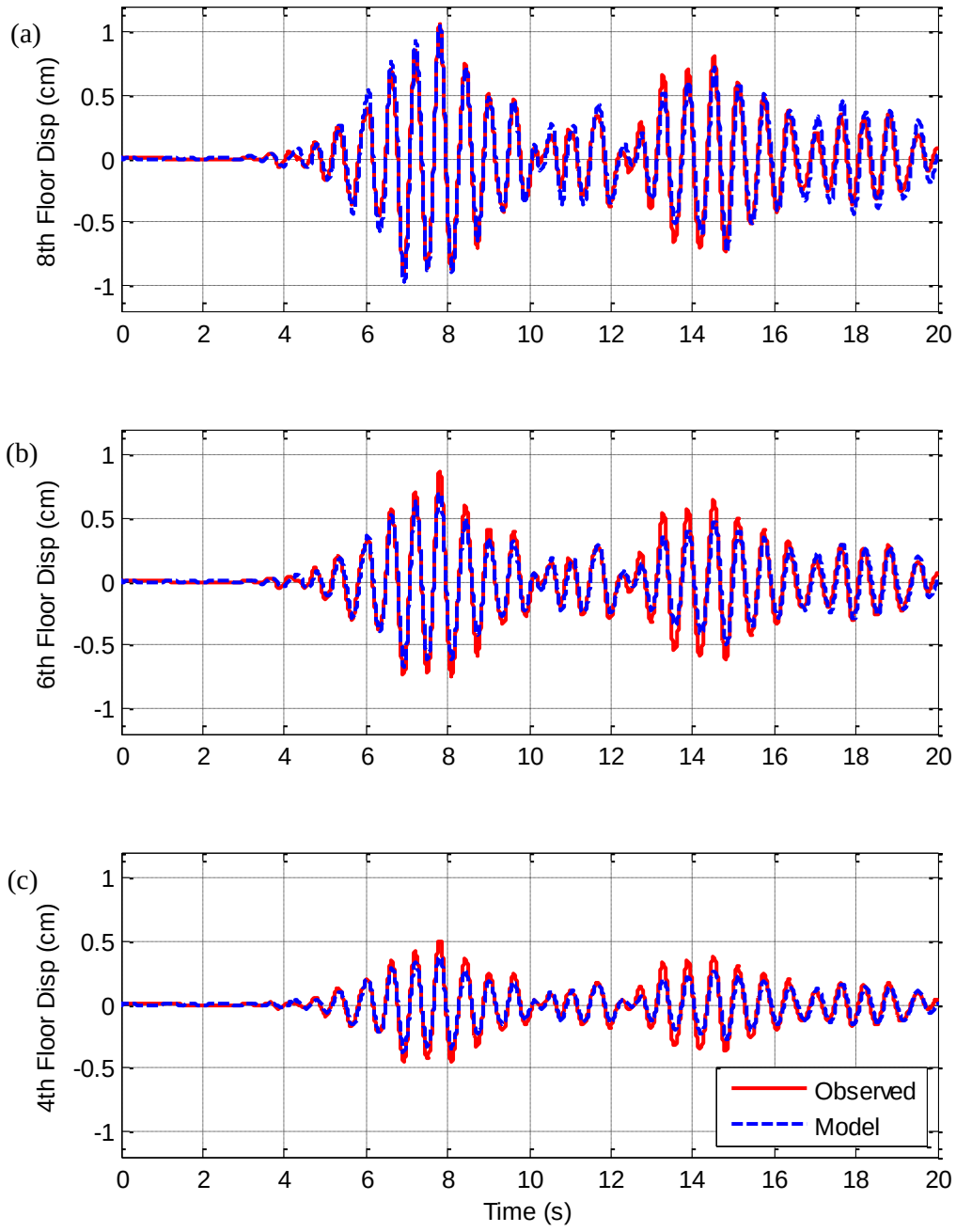


Figure 5-21: Comparison between the displacement time histories of the observations and 2D transverse fixed base model for the 16 April 2011 earthquake: (a) 8th; (b) 6th; and (c) 4th floor responses. Note: the observed response is the average response of the two accelerometers on each floor.

The comparison between the maximum displacement response of the 2D model and observations in the transverse direction for the 16 April 2011 earthquake is shown in Figure 5-22. It can be clearly seen in this figure that the transverse model again under-predicts the response of the fourth and sixth floors. The variation in displacement caused by the change in stiffness is also very small in this model, with the grey area barely noticeable compared with the black line.

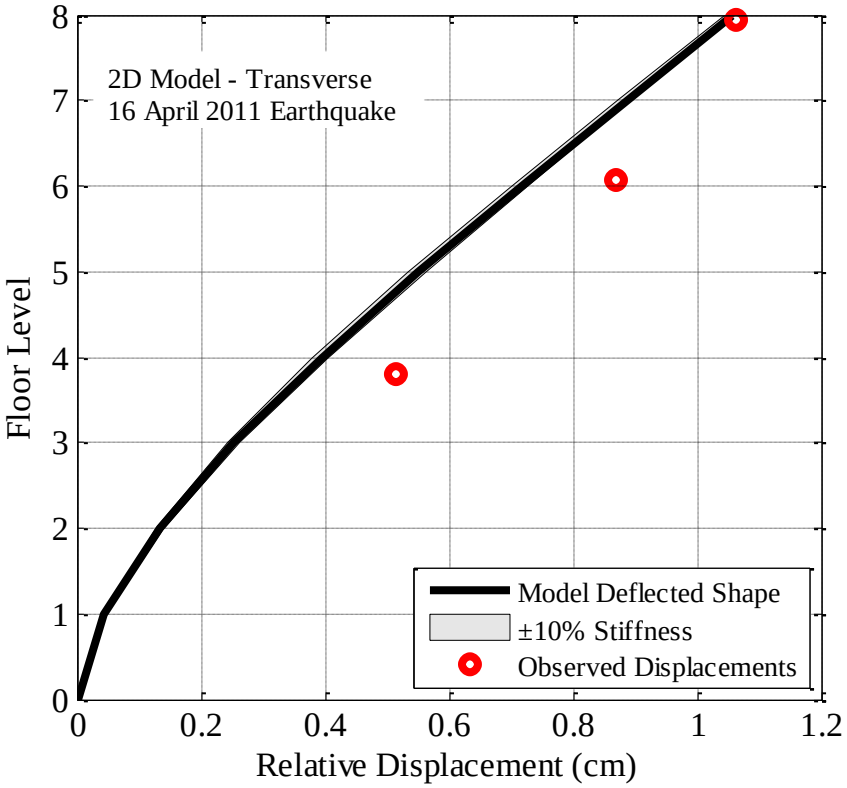


Figure 5-22: Comparison of the maximum deflected shapes between observations and the 2D transverse fixed base model for the 16 April 2011 earthquake.

The comparison between the normalised, observed and 2D predicted displacements in the transverse direction for all earthquakes is shown in Figure 5-23. There appears to be no improvement in the predicting capability from the 1D model, as the 2D model still under-predicts the fourth and sixth floor displacements for all earthquakes. It would appear that the assumption of a fixed base cantilever is not a good representation of the structure in the transverse direction. The displacement profile suggests that either the structure does not have a constant stiffness with height, or that some amount of rotation is occurring at the base. The latter is explored in Chapter 6 since this is believed to be the most likely reason for the poor comparison.

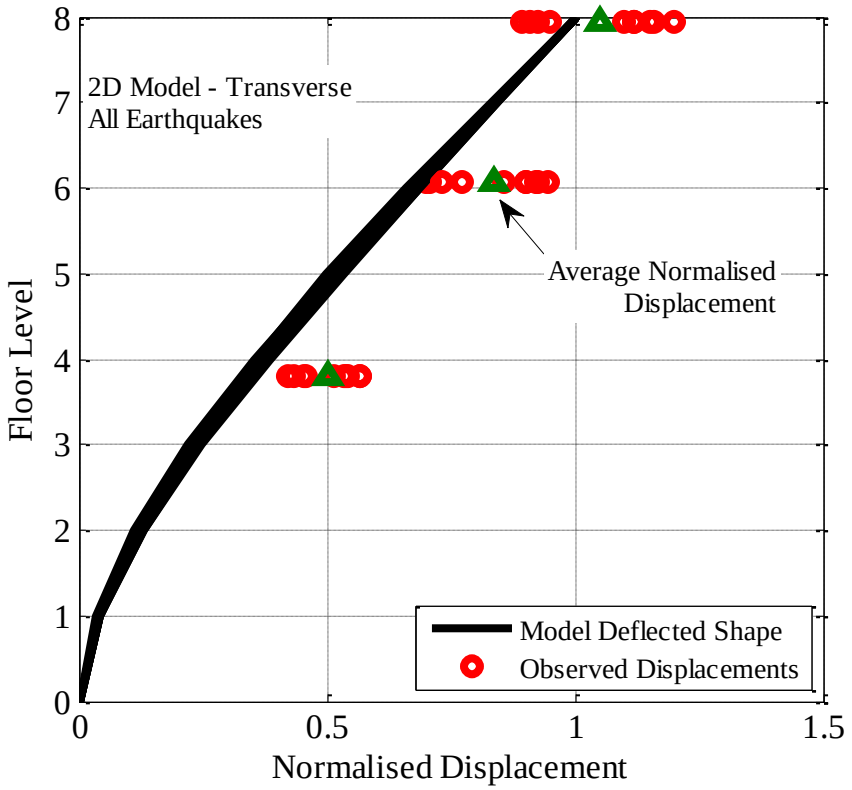


Figure 5-23: Comparison of normalised maximum deflected shape between observations and 2D longitudinal fixed base model for all earthquakes.

## 5.5 Comparison between 1D and 2D models

### 5.5.1 Longitudinal direction

The accuracy of the 1D and 2D models is compared by calculating the average error between observed and predicted displacement from each floor for all events. The errors can be found in Table 5-4 for longitudinal models. This table shows that both longitudinal models can very accurately predict the maximum deflected shape and the 2D model in fact slightly increases the predictive capability over the 1D model. The average floor error is within 6% for the three floors considered.

Table 5-4: Average percentage error of the 1D and 2D longitudinal fixed base models compared with observations.

| | **Longitudinal** | |
|---|---|---|
| | **1D FB** | **2D FB** |
| 8th Floor | -5.1% | -2.8% |
| 6th Floor | -2.3% | -4.0% |
| 4th Floor | +3.3% | -2.6% |
| **Average** | **3.6%** | **3.1%** |

Another way to compare the models is to plot the average predicted deflected shape from both models along with the normalised observed deflected shape. This is shown in Figure 5-24 for the two longitudinal models. It can be easily seen that the longitudinal models have different average deflected shapes however, they are both capable of predicting the peak displacements.

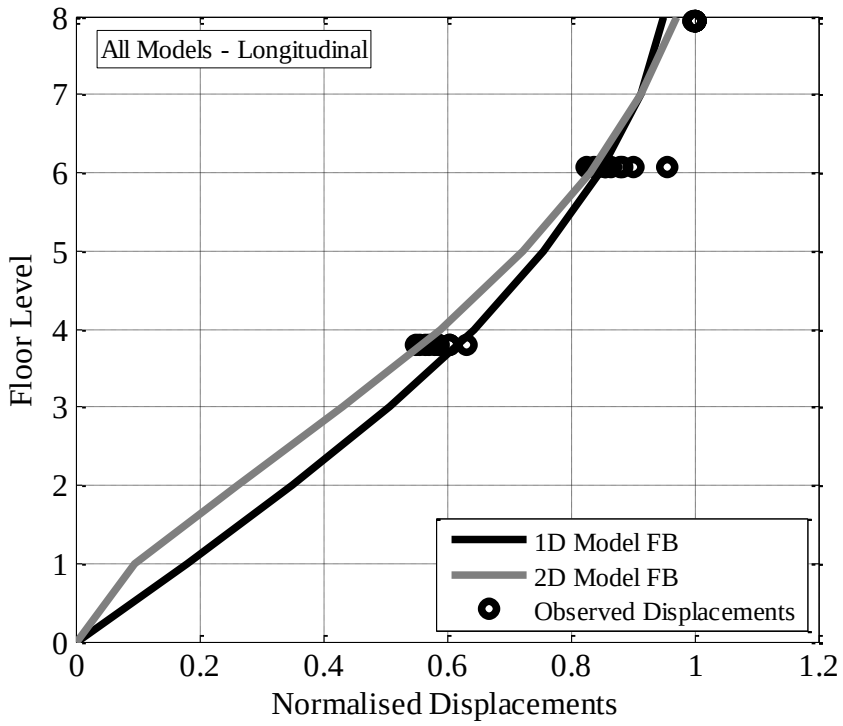


Figure 5-24: Comparison of the normalised maximum deflected shapes between 1D and 2D longitudinal fixed base models for all earthquakes.

### 5.5.2 Transverse direction

The accuracy of the 1D and 2D models is compared by calculating the average error between observed and predicted displacement from each floor in each event for both models. The errors can be found in Table 5-5 for both transverse models. This table shows that both transverse models under-predict the observations, on average, by 11-12%, however this error is much higher due to the inaccuracy in predicting the fourth and sixth floor displacements. The 2D model does not provide better predictions compared with the 1D model and is in fact on average worse at predicting the response in the transverse direction.

Table 5-5: Average percentage error of the 1D and 2D transverse fixed base models compared with observations.

| | **Transverse** | |
|---|---|---|
| | **1D FB** | **2D FB** |
| 8th Floor | -1.6% | -6.3% |
| 6th Floor | -15.4% | -15.5% |
| 4th Floor | -17.7% | -15.2% |
| **Average** | **11.6%** | **12.3%** |

The average predicted deflected shape from both transverse models along with the normalised observed deflected shape is shown in Figure 5-25. It can be easily seen from these graphs that both transverse models significantly under-predict the lower floors' displacement. The possible reason for this is investigated in Chapters 6 by adding base flexibility to account for SSI and in Chapter 7 by adding non-linear elements to the model.

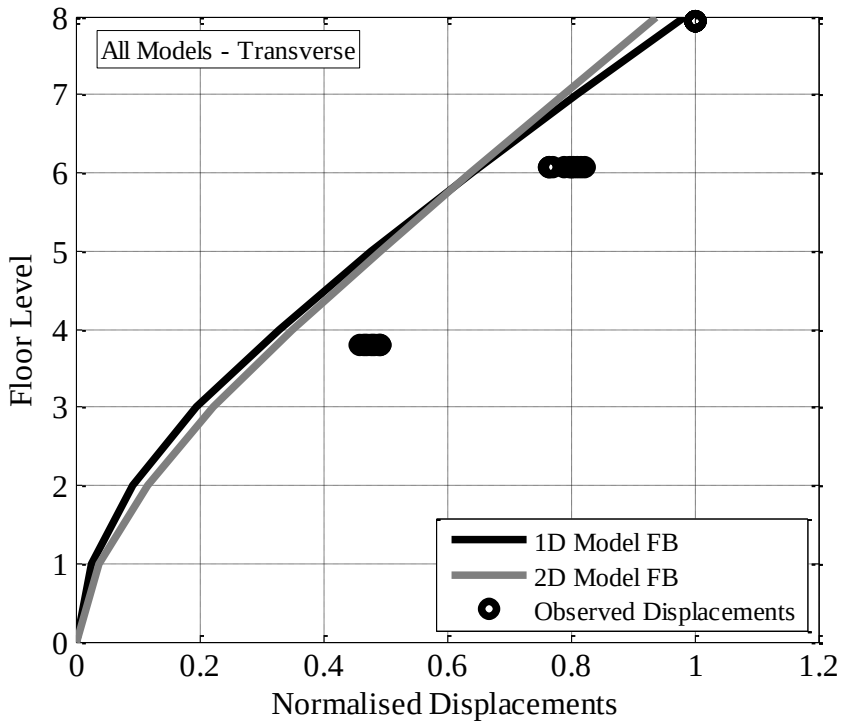


Figure 5-25: Comparison of the normalised maximum deflected shapes between 1D and 2D transverse fixed base models for all earthquakes.

## 5.6 Conclusions

This chapter has provided a detailed overview of conventional modelling practices in seismic design and assessment and how they compare with the observed behaviour of the UC Physics Building during the 2010-2011 Canterbury earthquakes. The key findings from this chapter are detailed below:

- The observed results from Chapter 4 were compared with prescribed code equations for spectral acceleration, peak floor acceleration, fundamental period and deflected shape. Response-spectra from the 4 September 2010 and 22 February 2011 earthquakes were greater than the design level in the longitudinal, transverse and vertical directions for some periods while all other events were less than the design level. The observed ratio of PFA/PGA versus height was compared with the prescribed equation in NZS1170.5, and it was found that the code equation is very conservative for the middle floors of this structure. An estimate of the fundamental period was calculated using the design equations for frame and wall systems, which represent the building in the longitudinal and transverse direction, respectively. The periods were estimated to be 0.97s and 0.72s in the longitudinal and transverse directions which are larger than the observed periods of 0.42s and 0.59s, respectively. The displacement based profile from the DBD process was very similar to observed deflected shape in the longitudinal direction. However, the displacement profile for a wall deflection was not a good representation for the transverse response.
- A multi-degree-of-freedom (MDOF) 1D model was developed to represent the structure in the longitudinal and transverse directions. The mass and stiffness of the structure was found using the structural drawings of the building. The effective stiffness required for the model period to match the observed period was 21% of the gross stiffness in the transverse direction and 28.5% in the transverse direction. The damping of the structure was estimated based on trial and error and comparing the resulting eighth model displacement time series with the observed eighth floor time series. It was found that the damping level was equal to 6% in both directions.
- The predictions from the 1D MDOF model in the longitudinal direction provided a good match with the data, while the transverse 1D MDOF model matched the observations on the eighth floor but under-estimated the deflections on the fourth and sixth floors. The average error from the two 1D MDOF models was 3.6% and 11.6% for the longitudinal and transverse models respectively.
- Finally, the building was represented with a 2D model in each direction. The maximum deflected shape predicted from the longitudinal 2D model provided improved predictions compared with the 1D model and the average percentage error was reduced to 3.1%. The transverse 2D model did not provide better predictions than the MDOF model and the average

percentage error was equal to 12.3%. Possible reasons for this are examined in the following two chapters, where soil-structure interaction and non-linearity's are investigated.

## 5.7 References

Eurocode 8 (2009). Design of structures for earthquake resistance. Part 1: General rules seismic actions and rules for buildings.

Standards Australia. (2002a). Part 0: General principles. AS/NZS 1170.0.

Standards Australia. (2002b). Part 1: Permanent, imposed and other actions. AS/NZS 1170.1.

ASCE/SEI7-05. (2006). Minimum design loads for buildings and other structures. ASCE Standard No. 007-05, 388pp.

Chopra, A. K. (2000). Dynamics of Structures. Upper Saddle River, NJ: Prentice-Hall, Inc

Clough, R. W., & Penzien, J. (2003). Dynamics of Structures. United States of America

Llera, J. C. D. l., & Chopra, A. K. (1995). Evaluation of Seismic Code Provisions Using Strong-Motion Building Records From the 1994 Northridge Earthquake. Paper presented at the California Geological Survey - SMIP95 Seminar, San Francisco.

Standards New Zealand. (2004). Part 5: Earthquake actions - New Zealand. NZS 1170.5.

Standards New Zealand. (2006). Part 1 - The Design of Concrete Structures. NZS3101.

OpenSees. (2011). Open System for Earthquake Engineering Simulation: OpenSees,Retrieved from http://opensees.berkeley.edu

Priestley, M. J. N., Calvi, G. M., & Kowalsky, M. J. (2007). Displacement-Based Seismic Design of Structures. Pavia, Italy: IUSS Press

Radoičić, G., & Jovanović, M. (2013). Experimental Identification of Overall Structural Damping of System. Journal of Mechanical Engineering, **59**(4), 260-268.

Roger, Y., & Jirsa, J. O. (1998). Nonlinear Analyses of an Instrumented Structure Damaged in the 1994 Northridge Earthquake. Earthquake Spectra, **14**(2).

# 6 EFFECT OF SOIL-STRUCTURE INTERACTION ON MODEL PREDICTION

## 6.1 Overview

This chapter examines the effects of soil-structure interaction (SSI) in the numerical model of the UC Physics Building in comparison with the observed response. The amount of base flexibility that is required to model SSI behaviour is calculated from the soil properties and foundation characteristics, obtained from cone penetrometer test (CPT) site investigation. The base flexibility is accounted for in the model by adding a series of springs, whose properties are a function of the soil shear stiffness, foundation depth, width, and height, (Gazetas, 1991). In one dimensional models, a rotational spring alone is used to model the base flexibility. In two dimensional models along the transverse direction, two parallel vertical springs with a rigid link can also be used to represent the rotational stiffness of the soil. Alternatively, the Winkler spring model is another method suggested by FEMA356 (2000) which has a series of vertical springs linked with a rigid beam. In this chapter, comparisons between the predictive capabilities of the fixed base and SSI models are examined for the 1D and 2D models considered in the previous chapter.

## 6.2 Idealizations of foundation deformation

Seismic soil-structure interaction (SSI) is the dynamic interaction between the soil and structure that arises during ground shaking. This interaction is able to change the seismic response of the structure by increasing or decreasing shear forces depending on the specific soil/structural conditions. As a result, a seismic evaluation of structures cannot be carried out by considering the structure alone as is commonly done in conventional design practice. A fixed base model does not accurately represent the behaviour of the global soil-structure system. The two mechanisms of interaction that take place between the structure and soil are inertial interaction and kinematic interaction (Stewart *et al.*, 1999a, 1999b).

The kinematic response depends on the ability of the foundation to follow the movement of the soil and thus based on its relative stiffness, the higher the foundation rigidity, the larger the kinematic effect on the incoming excitation. The oscillation experienced by the foundation will become the input motion for the superstructure. This effect is significant for embedded foundations as well as piles, and is equal to zero for shallow foundations subjected to horizontal motion, as there is no movement restriction of the free field motion in the latter case.

The inertial response is due to the presence of the structural mass under the action of the input motion; inertial forces arise causing new shear forces and overturning moments at the base level. Since the foundation can translate and rotate, the dynamic response of the structure depends on the amount of compliancy of the soil. Moreover, both structure and soil interact providing a feedback mechanism between each other (Kausel, 2010).

Since the UC Physics Building has shallow footings, the kinematic effects will be minimal and the main soil-structure interaction will come from inertial effects so therefore, only these effects will be considered herein. Soil-structure interaction models, such as that proposed by Wolf (1994), try to capture the complex SSI phenomena in a simple way by dividing the deformations into three basic components of horizontal, vertical and rotational movement. Each of these movements can be represented with a zero length spring at the base of the model. An example of this is shown in Figure 6-1 where $u_f$ is the displacement from the horizontal spring, $h_\theta$ is the displacement from the rotational spring and u is the flexural displacement from the element. Typically the translational displacement from the horizontal spring is relatively small compared with the horizontal displacement from the rotational spring (Moghaddasi *et al.*, 2012). Therefore only the rotational movement was considered in this analysis. For two dimensional models, the rotational stiffness can be modelling in a number of ways including a rotational spring with a rigid beam or a series of vertical springs with a rigid beam. Generally, a free field acceleration recording is required as an input for a SSI model, however, as this is not available, the first floor recordings are again used. This will introduce some error as the first

floor recording would have been influenced by the foundation response. Despite this, it is expected that the results will still provide some insight into the effects of SSI.

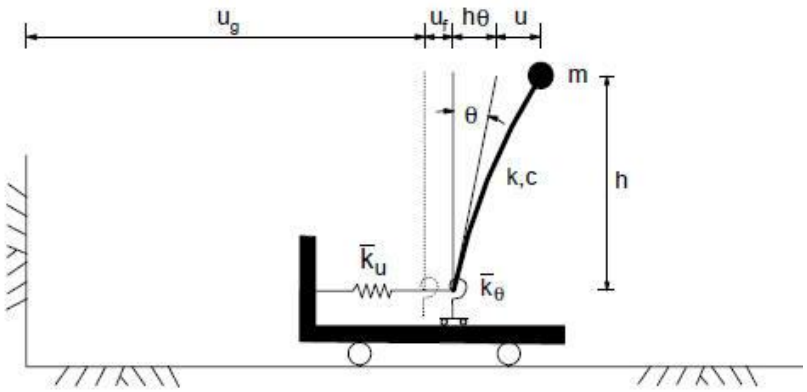


Figure 6-1: Schematic of SSI with horizontal and rotational springs (from Stewart *et al.* (1999a)).

Herein, springs representing SSI-related deformations were all assumed to be linear elastic in order to keep the model simple (see Gajan *et al.* (2010) for a practice orientated application of non-linear SSI analysis), with the subsequently obtained results suggesting that such models are highly efficient at improving the model prediction in comparison with the fixed base models.

## 6.3 Determination of soil parameters

### 6.3.1 CPT tests performed

Three cone penetrometer tests (CPT) performed in the vicinity of the Rutherford Building were available for determining soil properties, as shown in Figure 6-2. The data from the CPT002 was not used because the CPT did not go to a sufficient depth.

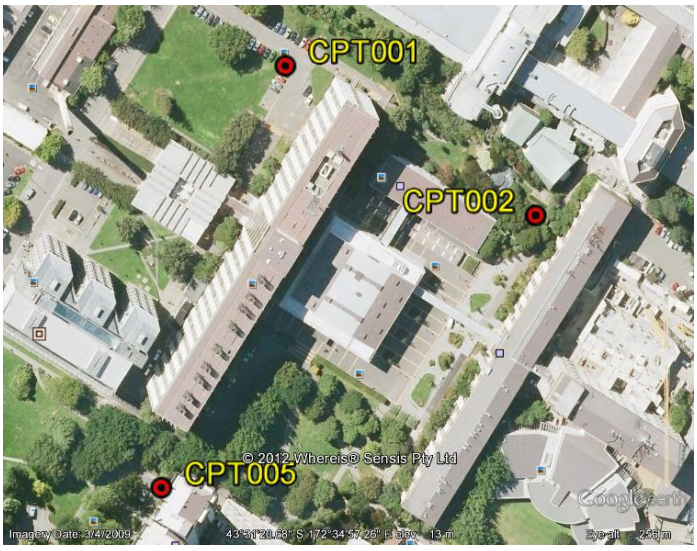


Figure 6-2: Location of CPT test sites around the Rutherford Building (courtesy of Davis Ogilvie Professionals).

### 6.3.2 Correlations between CPT and shear wave velocity, Vs

A CPT provides data on cone tip resistance and sleeve friction as the cone moves through the soil profile. It can also be used to find the ground water depth if it lies within the depth of soil profile tested. From this information, the total and effective stresses in the soil can be found, as well as the soil behaviour type index, Ic. Using the following equation, proposed by Robertson (2012), the shear wave velocity profile of the two test locations was found.

$$V_s = \left[\frac{\propto_{vs} (q_t - \sigma_v)}{p_a}\right]^{0.5} \quad m/s \qquad (5\text{-}1)$$

$$where \ \propto_{vs} = 10^{(0.55\, I_c + 1.68)} \quad (m/s)^2$$

where $q_t$ the is total cone resistance (MPa); $\sigma_v$ is the in-situ vertical stress, $p_a$ is atmospheric pressure (MPa), $I_c$ is the behaviour type index and $V_s$ is shear wave velocity (m/s).

As an example of the use of Equation (5-1), the results from CPT001 are shown in Figure 6-3 along with the inferred Vs values. The ground water table (GWT) is located at a depth of 1.9m. There is a clear change of shear wave velocity at a depth of 2.25m. The shear wave velocity is roughly 150 m/s above 2.25m, whilst it increases to roughly 250 m/s below 2.25m.

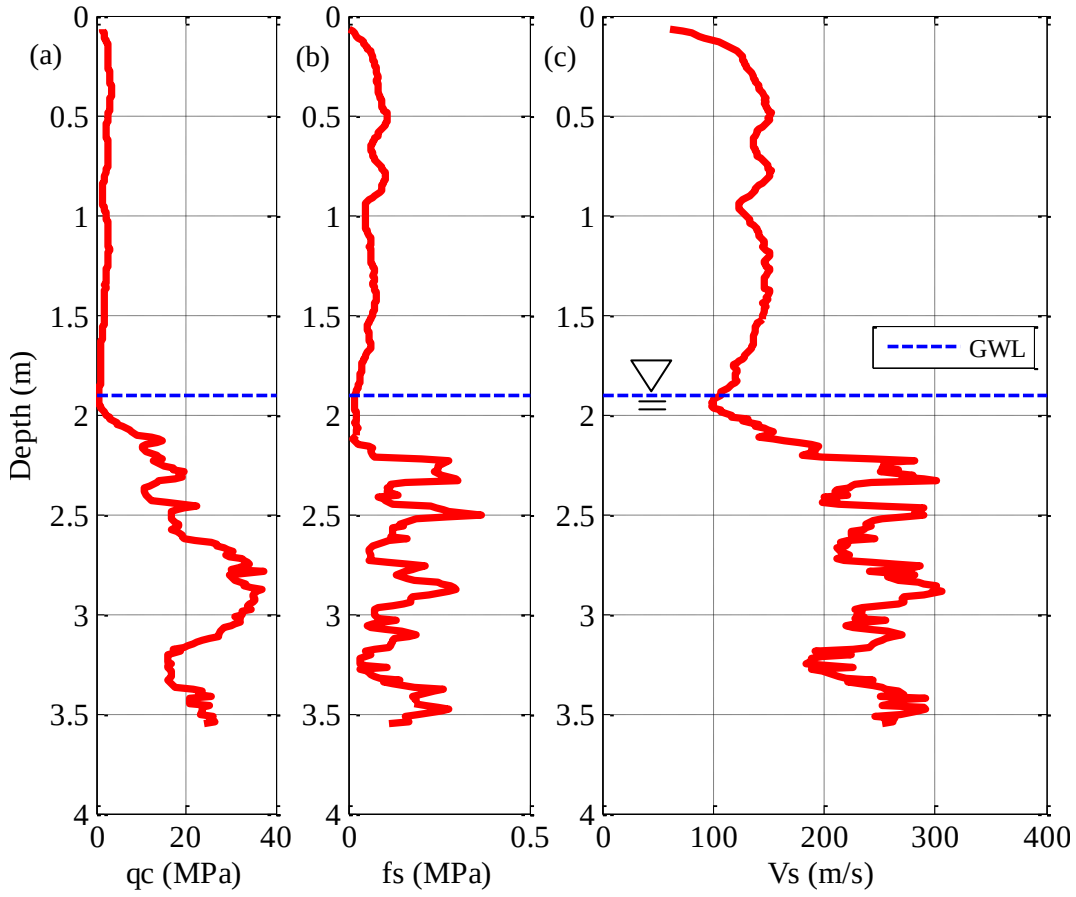


Figure 6-3: CPT test results from location CPT001 showing: (a) cone resistance; (b) sleeve friction; and (c) shear wave velocity.

The results from CPT005 are shown in Figure 6-4. The water table is located at a depth of 2.9m, however it is noted that the surface elevation of this site is 1m above the CPT001 site. The soil profile at this site is again divided into two different stiffness zones. Above approximately 3.5m, the average shear wave velocity is 125 m/s and below 3.5m, the average shear wave velocity is 250 m/s.

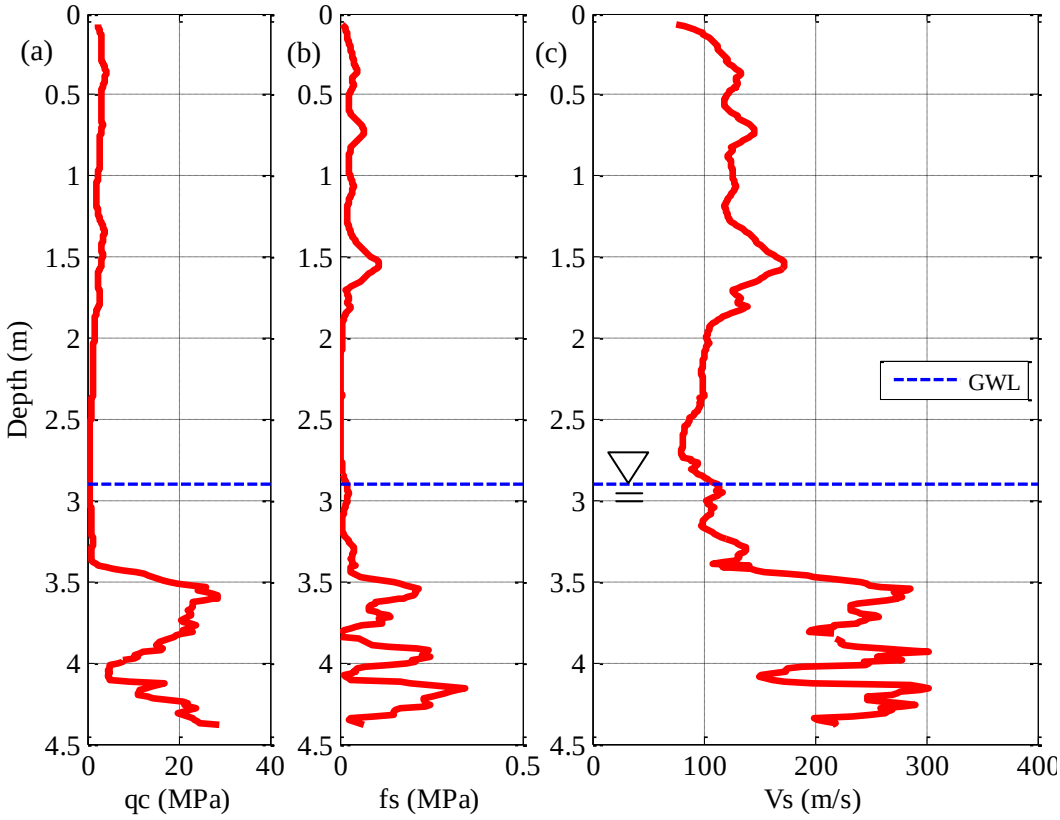


Figure 6-4: CPT test results from location CPT005 showing cone resistance, sleeve friction and shear wave velocity.

The depth of the foundations is 2.44m (Figure 3-3), therefore the second soil layer would be providing the resistance to vertical and rotational foundation movement at both site investigation locations. The following equation was used to convert from shear wave velocity to shear stiffness:

$$G = \rho V_s^{\,2} \qquad (5\text{-}2)$$

$$where\ the\ soil\ density, \rho = 1800\ kg/m^3 \quad (saturated\ soil)$$

$$shear\ wave\ velocity, V_s = 246\ m/s$$

$$therefore\ the\ shear\ modulus, G = 109\ MPa$$

### 6.3.3 Calculation of SSI spring stiffness

The vertical and rotational stiffness of the springs were calculated based on Gazetas (1991). The following equation was used to calculate the vertical stiffness of an arbitrarily shaped foundation on the surface of a homogeneous half space:

$$K_z = \frac{2GL}{1-\nu}(0.73 + 1.54\,\chi^{0.75}) \qquad (5\text{-}3)$$

$$where\ \chi = \frac{A_b}{4L^2}$$

where $2L$ is the length of the foundations (2L = 60m in the longitudinal direction and 16.5m in the transverse direction), $A_b$ is the bearing area of the foundations ( $A_b$ = 127.5 m$^2$ in the longitudinal direction and 35.1 m$^2$ in the transverse direction), $\nu$ is the Poisson's ratio ($\nu$ = 0.3) and the vertical spring stiffness values were calculated to be $K_z = 7.96 * 10^3\ N/m$ and $K_z = 2.72\ * 10^3\ N/m$, in the longitudinal and transverse directions, respectively.

The rotational stiffness was equal to:

$$K_{ry} = \frac{G}{1-\nu} I_{by}^{0.75}\left(3\,(\frac{L}{B})^{0.15}\right) \qquad (5\text{-}4)$$

where 2B is the foundation width (2B = 2.13 m in both directions) and $I_{by}$ is the second moment of inertia of the foundations about the axis of rotation ($I_{by} = 37.9 * 10^3\ m^4$ in the longitudinal direction and $7.4 * 10^3\ m^4$ in the transverse direction). The vertical spring stiffness values were calculated to be $K_z = 2{,}091 * 10^3\ Nm/rad$ and $K_z = 507\ * 10^3\ Nm/rad$, in the longitudinal and transverse directions, respectively.

These different stiffness values were then multiplied by a factor which allowed for the foundations to be partially or fully embedded in the ground. The embedded vertical stiffness was:

$$K_{z,emb} = K_{z,sur}\left[1 + \frac{1}{21}\frac{D}{B}(1 + 1.3\chi)\right] \times \left[1 + 0.2(\frac{A_w}{A_b})^{2/3}\right] \qquad (5\text{-}5)$$

where D is the depth of the foundations (D = 2.4m in both directions) and $A_w$ is the actual sidewall contact area ($A_w = 2 * (2L + 2B) * d = 150.9$ m$^2$ in the longitudinal direction and 45.4 m$^2$ in the transverse direction), d is the actual embedded depth of the foundations (d=D/2 for the UC Physics Building) and the embedded vertical spring stiffness values were calculated to be $K_{z,emb} = 9.16 * 10^3\ N/m$ and $K_{z,emb} = 3.17\ * 10^3\ N/m$ in the longitudinal and transverse directions, respectively.

The embedded rotational stiffness was equal to:

$$K_{ry,emb} = K_{ry,sur}\left\{1 + 0.92(\frac{d}{L})^{0.6}\left[1.5 + (\frac{d}{L})^{1.9}(\frac{d}{D})^{-0.6}\right]\right\} \quad (5\text{-}6)$$

where the embedded rotational spring stiffness values were calculated to be $K_{ry,emb} = 2.51 * 10^3 Nm/rad$ and $K_{ry,emb} = 734 * 10^3\ Nm/rad$ in the longitudinal and transverse directions, respectively.

### 6.3.4 Degradation of soil shear strength

The shear strength of soil does not remain constant when loaded dynamically. In fact, if the dynamic response of the soil is significant, shear strains can be large enough to result in non-linear response of the foundation soils resulting in a degradation of the shear strength. For simplicity, nonlinear soil response is accounted for using equivalent linear spring stiffness whereby one value of degraded shear strength is used. In an equivalent linear analysis, the shear modulus, G, is generally taken as a secant shear modulus. The relationship between shear strain and shear stress is based on a backbone curve as shown in Figure 6-5. The secant stiffness is the slope from the current shear stress and strain value to the origin. This is usually expressed as a percentage of the initial shear stiffness, $G_{max}$.

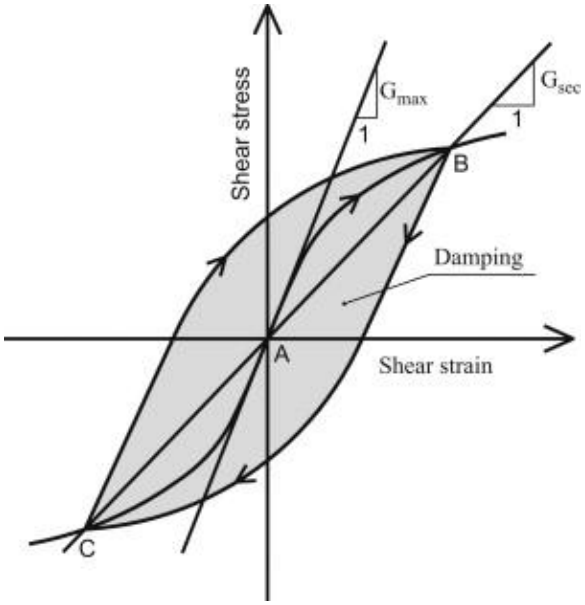


Figure 6-5: Shear Stress versus Shear Strain (Seed & Idriss, 1970).

New Zealand structural codes do not provide any information on how to account for this degraded shear modulus in SSI modelling. Therefore, two alternate methods are used to understand the expected strength degradation of the soil. The first is a very simple method is prescribed by FEMA356 (2000) which relates the peak spectral acceleration at the fundamental period to the effective shear modulus as shown in Table 6-1. It can be seen that the effective shear modulus also depends on the soil site class which is considered to be a level D for the Canterbury University area.

Table 6-1: Effective shear modulus ratio prescribed by Table4-7 from FEMA356 (2000).

| | Effective Peak Acceleration, $S_{XS}/2.5$ | | | |
|---|---|---|---|---|
| Site Class | $S_{XS}/2.5$ =0 | $S_{XS}/2.5$ =0.1 | $S_{XS}/2.5$ =0.4 | $S_{XS}/2.5$ =0.8 |
| A | 1.00 | 1.00 | 1.00 | 1.00 |
| B | 1.00 | 1.00 | 0.95 | 0.90 |
| C | 1.00 | 0.95 | 0.75 | 0.60 |
| D | 1.00 | 0.90 | 0.50 | 0.10 |
| E | 1.00 | 0.60 | 0.05 | * |
| F | * | * | * | * |

Note: Use straight-line interpolation for intermediate values of $S_{XS}/2.5$.

* Site-specific geotechnical investigation and dynamic site response analyses shall be performed.

The second method considered was developed by Paolucci *et al.* (2009) for the consideration of non-linear soil behaviour in the displacement-based design (DBD) method. Relationships between percentage of rotational stiffness and rotation have been developed and are used to predict the rotation of the base under the design level of earthquake loading. This is then further applied to predict the deflected shape in the DBD process. This method was applied to a wall system by Sullivan *et al.* (2010) and following the same process, it can be applied to the transverse wall system of the UC Physics Building. In the present study the observed rotations of the UC Physics building foundation for each event are already known (Chapter 4), therefore the percentage of rotational stiffness that should be used in design can be back-calculated. The degraded stiffness versus curvature (K-θ) curves depend of the ratio of maximum bearing capacity ($N_{max}$) over the applied bearing load (N*) and relative density of the soil ($\rho = 1800\ kg/m^3$). This can easily be calculated for the transverse shear wall as shown below:

$$N_{max} = \sigma_b \times A_{bearing} \tag{5-7}$$

where $\sigma_b$ is the bearing stress capacity, equal to 2.85 MPa (courtesy of Davis Ogilvie Professionals (2013)) and $A_{bearing}$ is the bearing area of the shear wall.

$$A_{bearing} = 60 \times 2.1 \times 2 + 12 \times 2.1 \times 3 = 327.6\ m^2$$

$$N_{max} = 934 \times 10^3\ kN$$

$$N^* = 8\ (floors) \times 1{,}000{,}000 \times 9.81\ (\frac{kN}{floor})$$

$$N^* = 78.5 \times 10^3\ kN$$

$$N^*/N_{max} = 12$$

Using this ratio of N*/N_max, the K-θ curve for the UC Physics Building can be found as shown in Figure 6-6. This figure also shows the maximum observed transverse rotations and their corresponding stiffness ratio.

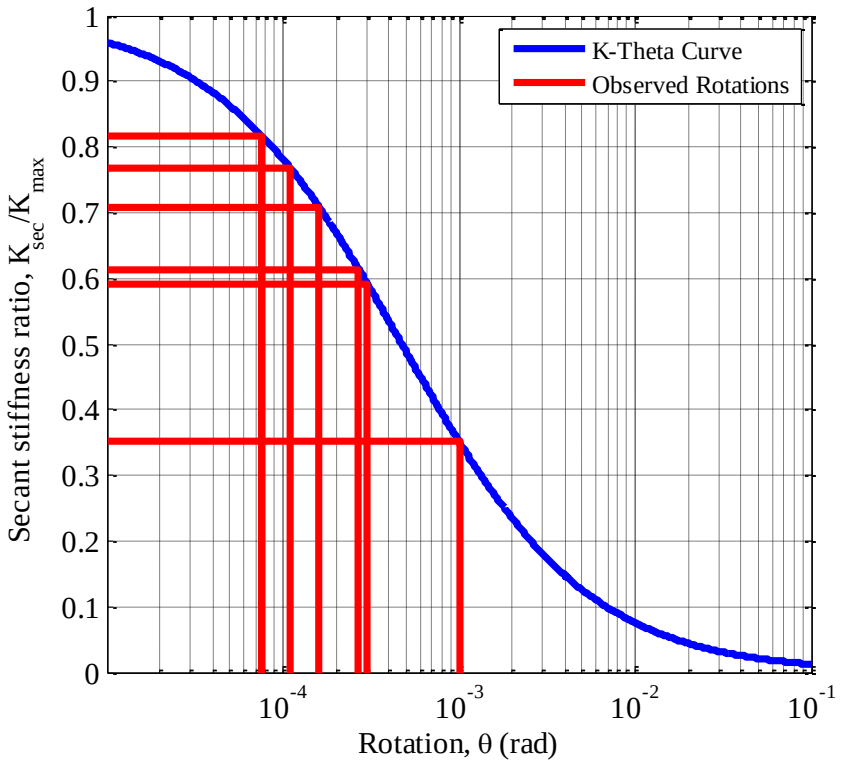


Figure 6-6: Secant stiffness ratio versus base rotation for UC Physics Building soil properties. Observed rotations are from the instrumental building response (refer to Table 4-4 in Chapter 4)

In the following SSI modelling sections, the spring stiffness's (calculated in Section 6.3.3) in the numerical model are reduced by a factor so that the maximum predicted base rotation matches peak observed rotation. This is adjusted for each model on an event by event basis so that there is a different reduction factor for each model and for earthquake. The percentage of degraded stiffness used in the model to match the observed rotations is considered to be the observed degraded shear modulus. These values can then be compared with the predicted reduction factors prescribed by FEMA356 (2000) in the longitudinal direction and with both FEMA356 (2000) and Paolucci *et al.* (2009) in the transverse direction.

## 6.4 One dimensional SSI models

The one dimensional fixed base models from Chapter 5 were adjusted to allow for SSI behaviour. This required the addition of a zero length rotational spring to the base of the model as shown in Figure 6-1. The rotational spring initially had the stiffness ($K_{ry,emb}$) calculated in Section 6.3.3 for each respective direction. As described in Section 6.3.4, there is expected to be some degradation of the shear modulus. Therefore, to account for this, the spring stiffness was reduced by a factor so that the predicted base rotation matched the observed base rotation. This process was performed for each earthquake event and the percentage of reduced stiffness required to match the observed rotations was compared with the predicted stiffness reduction by FEMA356 (2000).

By allowing for the base flexibility in the SSI model, there is an increase in the fundamental period of the model (Mylonakis & Gazetas, 2008). Therefore, in order to keep the fundamental period the same as the fixed base model, the stiffness of the structural elements was increased. This increase in stiffness ranged from 2-3% in the longitudinal direction and 28-120% in the transverse direction.

### 6.4.1 1D longitudinal SSI model

The percentage of rotational spring stiffness required to match the observed base rotation in the 1D longitudinal SSI model is shown in Figure 6-7. This value was 10% for the 4 September 2010 earthquake and 15% for all other events. As it can be seen in the figure, the observed reduction values are significantly less than the predicted reduction. This is because the calculated rotational spring stiffness from the Gazetas (1991) equations is very high due to large foundation length. In reality, the longitudinal foundation would not rotate as a uniform system therefore the calculated stiffness needs to be reduced by a large factor in order to match the observed rotations.

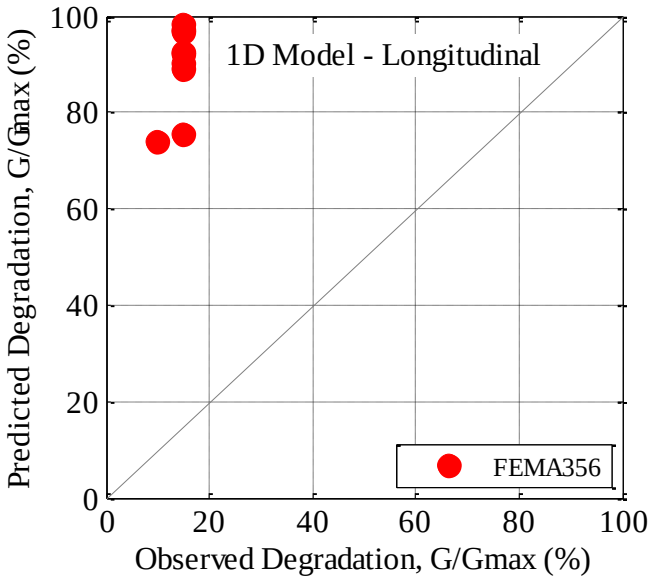


Figure 6-7: Predicted vs observed stiffness reduction for the 1D longitudinal model.

Figure 6-8 shows the displacement and rotational response history for the 1D SSI model compared with the observed response for the 22 February 2011 earthquake. This earthquake is used to illustrate the SSI response under a large amplitude ground motion. The model appears to match the initial large cycle displacement response, however, the predicted rotational response does not match as well.

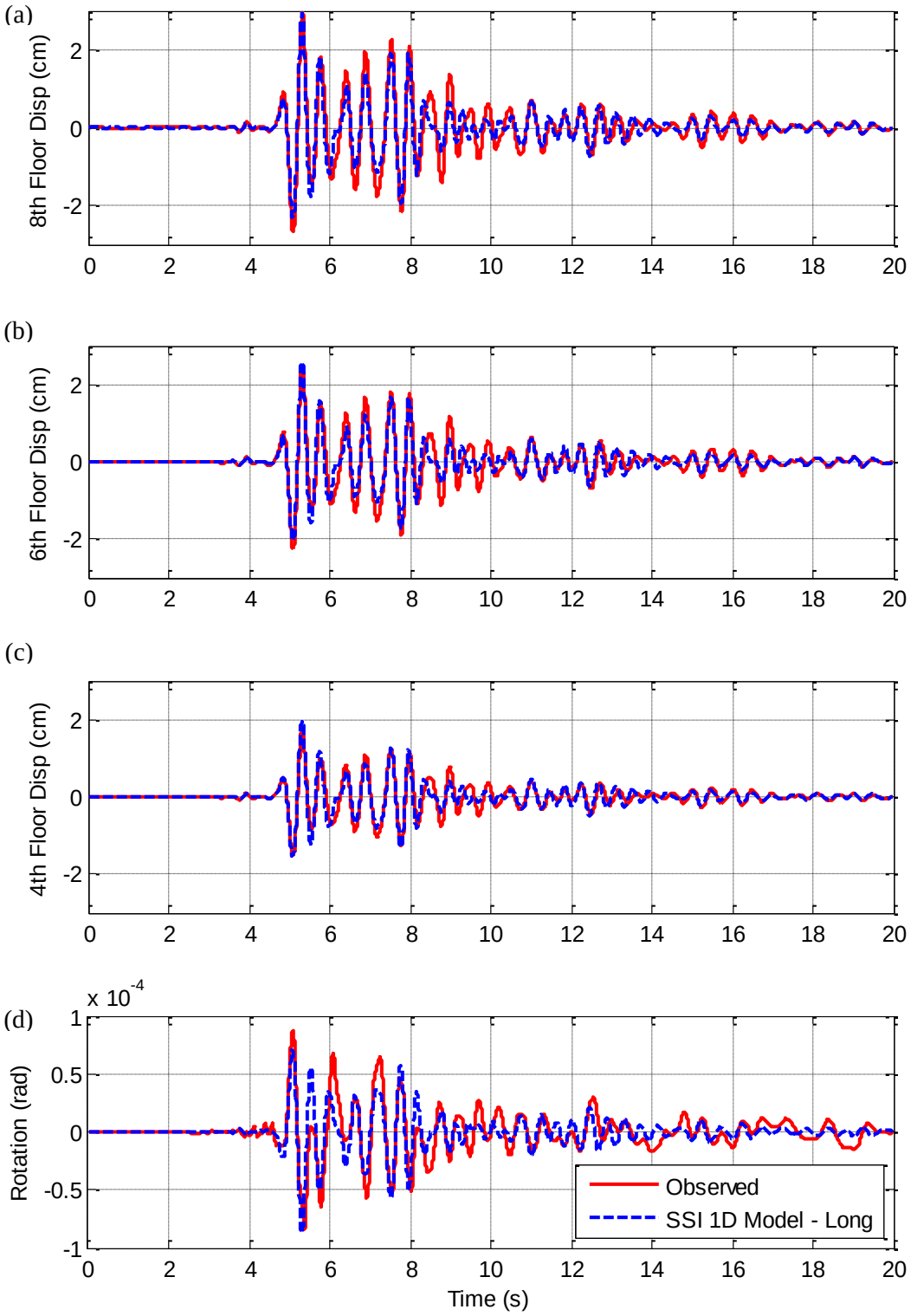


Figure 6-8: Comparison of the (a) 8th; (b) 6th, and (c) 4th floor responses and (d) .rotational response histories and the observations for 1D longitudinal SSI model in the 22 February 2011 earthquake.

In order to better understand the effect of the added base flexibility, the peak displacement responses from the 1D longitudinal SSI and fixed base models is shown in Figure 6-9. The solid black line shows the fixed base deflected shape and the dashed black line shows the displacement predicted from the SSI model. This figure also shows the maximum predicted roof displacement caused directly from the rotation at the base. This is calculated by multiplying the maximum angle of rotation at the base by the height of the building. As described earlier, the stiffness of the rotational spring was adjusted so that these values matched for most earthquake events. It can be seen that, even though the models have the same fundamental period, the SSI predicted roof displacement is 10% larger. This provides a better match for the maximum eighth floor displacement but not for the fourth and sixth floors which now over-predict the response.

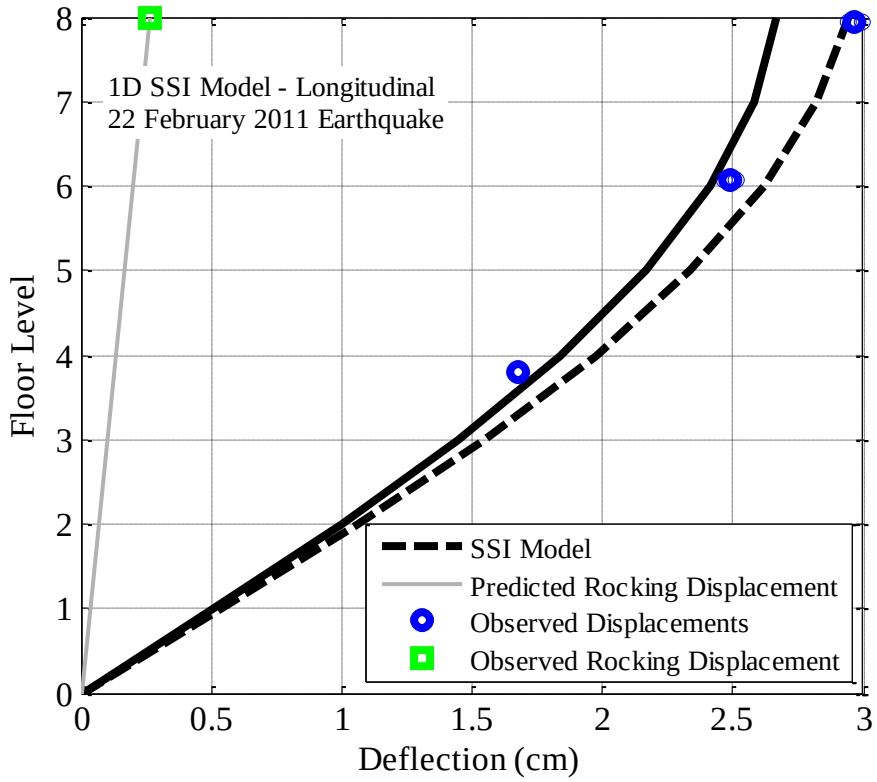


Figure 6-9: Comparison of the maximum deflected shape between observations and the 1D longitudinal SSI model for the 22 February 2011 earthquake.

The comparison between the normalised maximum displacements from the 1D longitudinal SSI model and the observations for all earthquakes is shown in Figure 6-10. It can be seen that the observed normalised roof displacements caused by base rotation line up with the roof displacement predicted by the model as the spring stiffness was calibrated so that the two matched. It can be seen that the normalised rotation is similar for all events and the SSI model now over-predicts the average displacement on all floors.

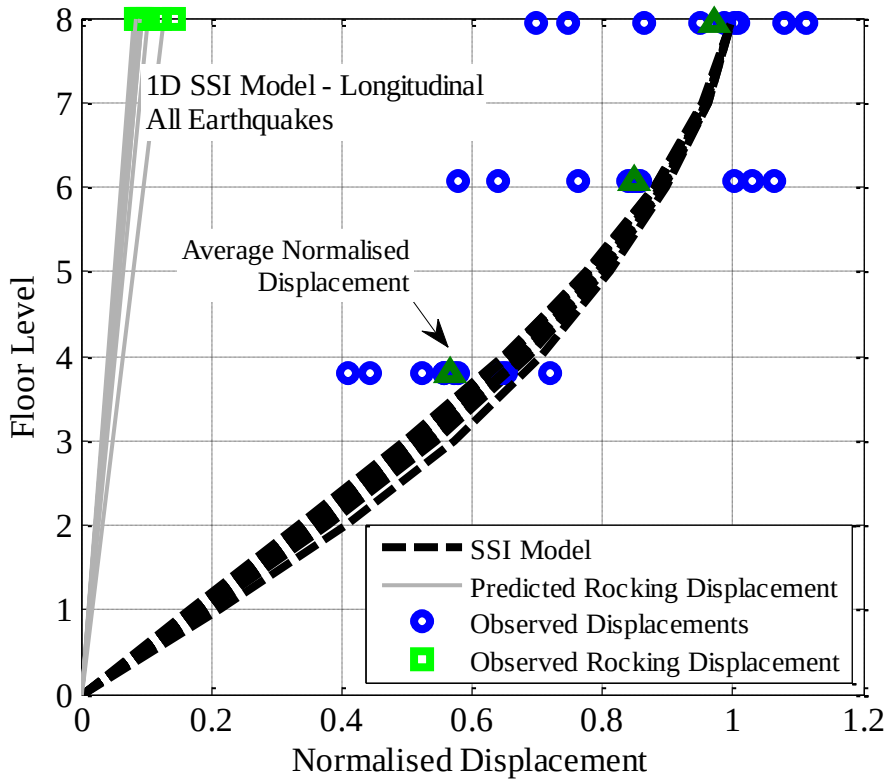


Figure 6-10: Comparison of the maximum deflected shape between observations and the 1D longitudinal SSI model for all earthquakes.

### 6.4.2 1D transverse SSI model

The percentage of rotational spring stiffness required to match the observed base rotation in the 1D transverse SSI model is shown in Figure 6-11. The observed degraded stiffness is compared with the predicted degraded stiffness from FEMA356 (2000) and Paolucci *et al.* (2009). The prescribed FEMA356 values under-predict the reduction for most events. This is because the predicted reduction is purely based on the spectral acceleration at the fundamental period and does not take into account the properties of the foundation or the structure. The predicted stiffness reduction from Paolucci *et al.* (2009) appears to be a better match with the observations with the four largest events almost perfectly predicted.

As described previously, the element stiffness had to be increased from the fixed base model in order to keep the period of the two models the same. The increase in element stiffness varied between events with the largest increase required for events with the largest spring stiffness reduction. For the smaller events, the fixed base element stiffness was increases by 26%. For the 4 September 2010 event the required increase in element stiffness was 220%.

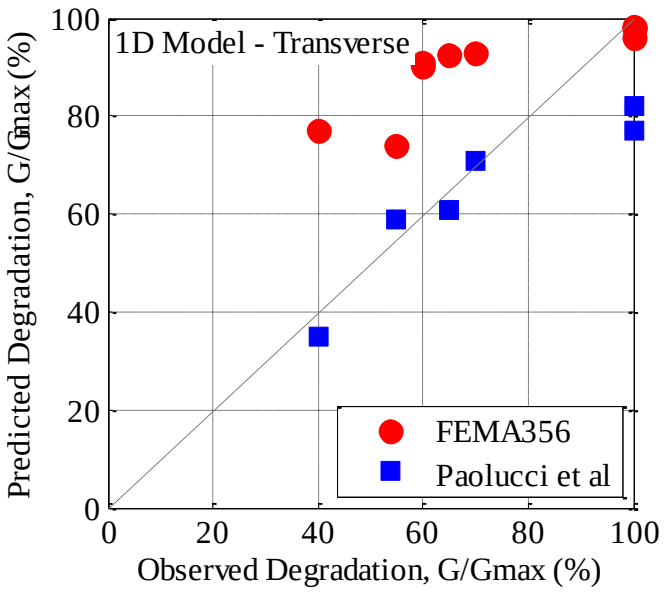


Figure 6-11: Predicted vs observed stiffness reduction for the 1D transverse model.

Figure 6-12 (a), (b) and (c) shows the displacement response histories for the 1D SSI model compared with the observed response for the 22 February 2011 earthquake. As mentioned previously, this earthquake was used to illustrate the SSI response under a large amplitude ground motion. The predicted displacement response on all floors matches the observed response very well for the entire ground motion except for slightly under-predicting the response between 9-11 seconds.

Figure 6-12 (d) compares the predicted and observed rotational response at the base of the model. The rotation predicted from the SSI model matches the observed base rotation very well. The observed rotation is calculated by subtracting the vertical responses of the two accelerometers on either side of the bottom shear wall divided by the distance between them (accelerometers 21 and 24 (refer to Figure 3-14 in Chapter 3)). It is interesting to note how accurately the rotational spring can predict the rotational response which suggests that SSI is present in the transverse response of the structure.

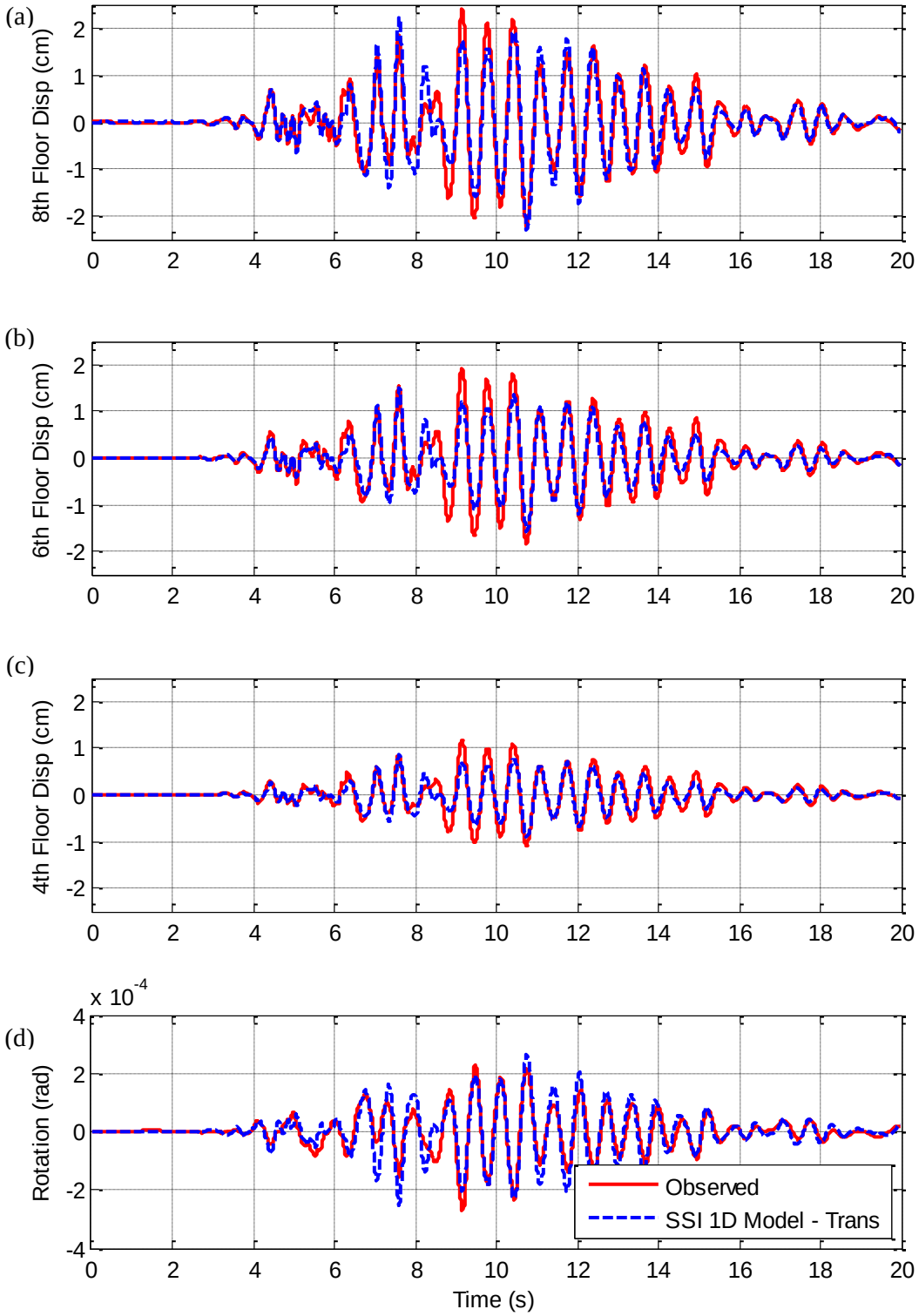


Figure 6-12: Comparison of the (a) 8th; (b) 6th, and (c) 4th floor responses and (d) .rotational response histories and the observations for 1D transverse SSI model in the 22 February 2011 earthquake.

The maximum displacement response of the 1D transverse SSI model is compared with the fixed base model for the 22 February 2011 earthquake in Figure 6-13. The SSI model has a different maximum deflected shape compared with the fixed base mode as the rotational spring allows for some initial

slope at the base of the model. This initial slope increases the displacements on all floors making the predicted response closer to the observations.

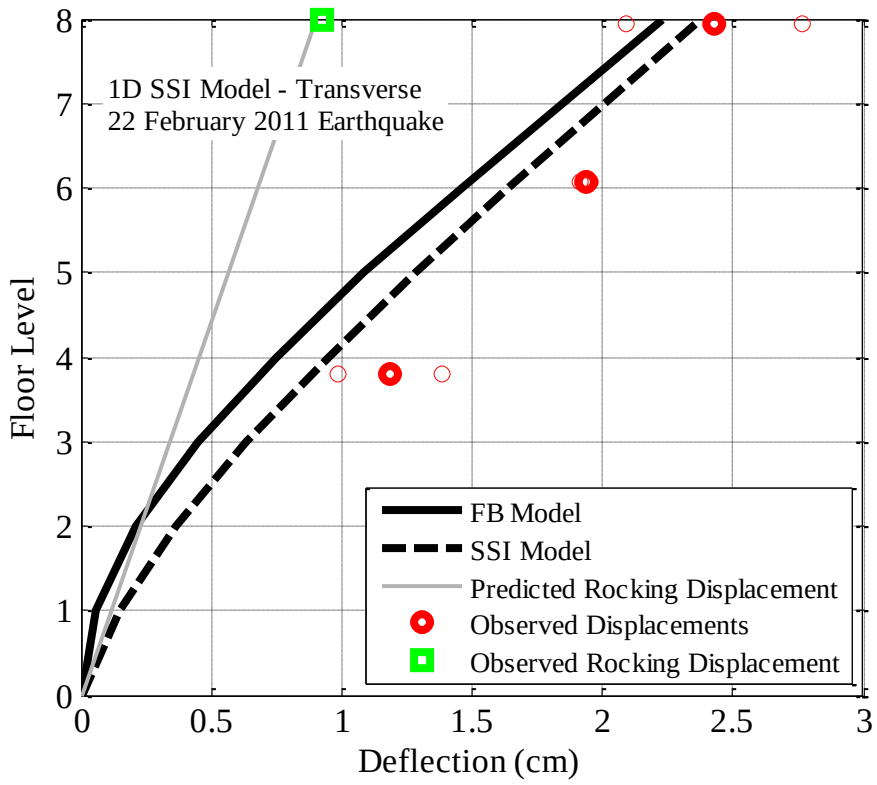


Figure 6-13: Comparison of the maximum deflected shape between observations and the 1D transverse SSI model for the 22 February 2011 earthquake. Note that the thin circles represent the observed end shear wall displacements while the thick circles represents the average of the two responses.

The comparison of normalised maximum deflected shape for the fixed base and SSI models in the transverse direction for all earthquakes is shown in Figure 6-14. The predicted and observed roof displacements caused by the base rotation are the same as the spring stiffness was calibrated based on this. The additional base flexibility results in increased predicted displacements for all floor which causes the model to over-predict the eighth floor response on average. The average response of the fourth and sixth floors is still under-predicted however, is now much closer compared with the fixed base model.

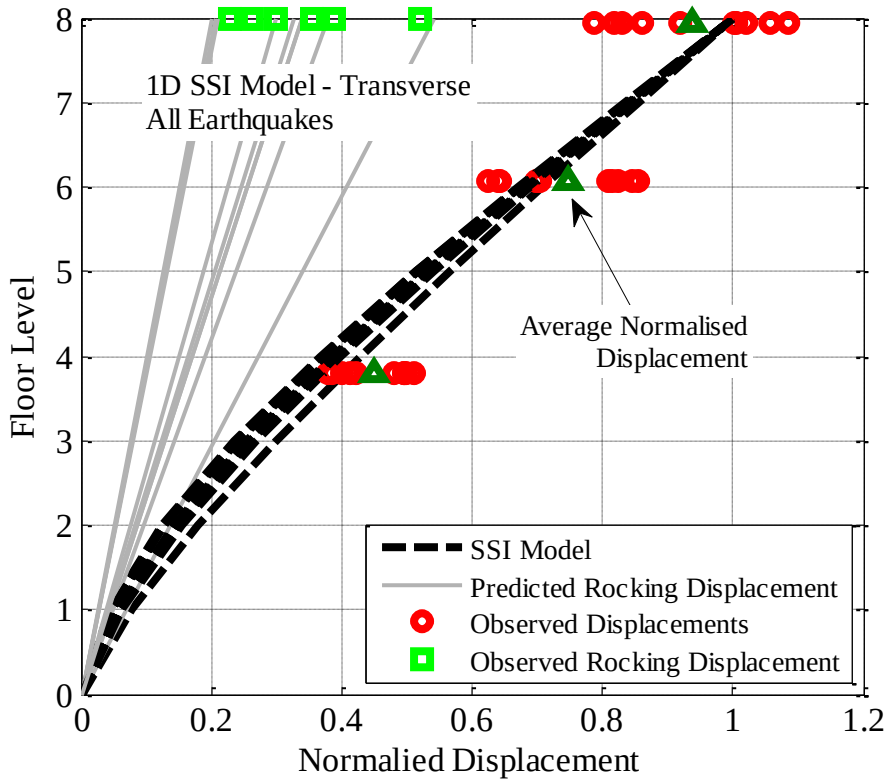


Figure 6-14: Comparison of the maximum deflected shape between observations and the 1D transverse SSI model for all earthquakes.

### 6.4.3 Comparison with 1D fixed base models

#### *6.4.3.1 Longitudinal direction*

The average percentage error the predictions is shown in Table 6-2 for the longitudinal fixed base and SSI models. It can be seen that the added base flexibility in the longitudinal SSI model does not allow for any increased predictions. In fact, the SSI models predictions are worse than the fixed base mode which suggests that there is minimal or no SSI in this direction.

Table 6-2: Average percentage error of the longitudinal 1D fixed base and SSI models compared with observations.

| | **1D FB** | **1D SSI** |
|---|---|---|
| 8th Floor | -5.1% | 3.5% |
| 6th Floor | -2.3% | 5.3% |
| 4th Floor | 3.3% | 8.5% |
| **Average** | **3.6%** | **5.8%** |

The comparison of the average normalised maximum deflected shape for the fixed base and SSI longitudinal models is shown in Figure 6-15. This figure clearly shows how the added base flexibility increases the predictions on all floors by a large amount causing it to over-predict the response.

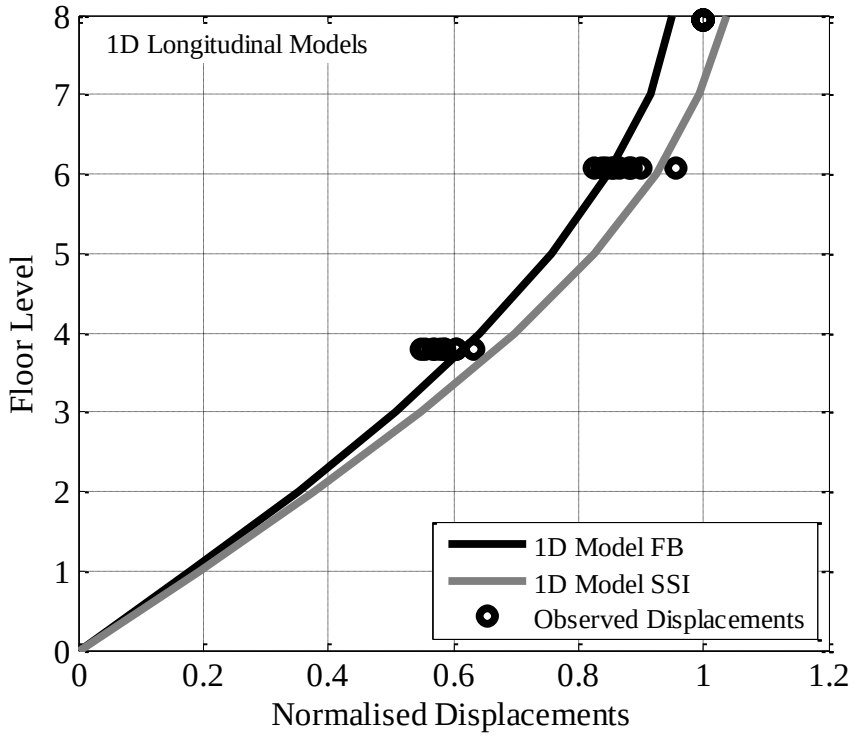


Figure 6-15: Comparison of the normalised maximum deflected shape between the 1D longitudinal fixed base and SSI models for all earthquakes.

### *6.4.3.2 Transverse direction*

The average percentage error the predictions is shown in Table 6-3 for the transverse fixed base and SSI models. It can be seen that the added base flexibility in the transverse SSI model allows for better predictions, particularly on the fourth and sixth floors, with the average error reducing to almost half of the error associated with the fixed base model. However, the SSI model still under-predicts the displacements of the fourth and sixth floors by 10% on average which suggests that there could be another effect, which is not accounted for in this model, causing this. Possible non-linear behaviour and torsional effects are investigated in Chapter 7 as a possible reason for this.

Table 6-3: Average percentage error of the transverse 1D fixed base and SSI models compared with observations.

| | **1D FB** | **1D SSI** |
|---|---|---|
| 8th Floor | -1.6% | 1.1% |
| 6th Floor | -15.4% | -9.8% |
| 4th Floor | -17.7% | -10.3% |
| **Average** | **11.6%** | **7.1%** |

The average response of the fixed base and SSI transverse model is shown in Figure 6-16. It can be seen that the SSI model increases the displacements of the lower floors while the eighth floor displacement remains very similar.

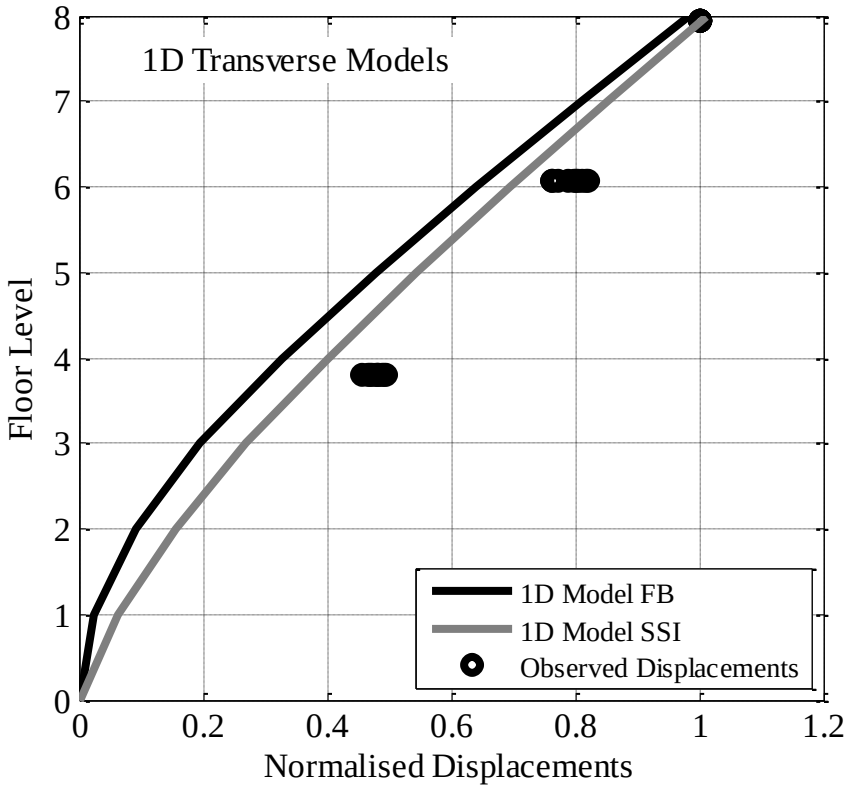


Figure 6-16: Comparison of the normalised maximum deflected shape between the 1D transverse fixed base and SSI models for all earthquakes.

## 6.5 Two dimensional SSI models

The two dimensional (2D) model of the UC Physics Building (refer to schematic figure in Chapter 5) has multiple bays, and therefore points of contact with the foundation. The rotation of the foundation can therefore, in theory, be more accurately modelled as the difference in vertical displacement between the ends of the foundation. Computers and Structures (1998) state that for major structures on soft soil, a one dimensional analysis is adequate. However, for major structural elements, such as the base of a shear wall, mass less elastic springs should be used to estimate the foundation stiffness.

### 6.5.1 2D longitudinal SSI model

In the longitudinal direction, it is expected that the foundation would not act as a rigid element because it is too long. This effect was evident in the 1D SSI modelling as the stiffness of the rotational spring had to be significantly decreased in order to match the observed rotation. Therefore, to try and model the SSI in the longitudinal direction, a vertical spring was placed at the base of each wall. This allows for individual vertical movement of each column but not a grouped rotation effect. However, group rotation can still occur under certain levels of loading, but is less likely. The percentage of vertical spring stiffness used in the 2D model is shown in Figure 6-17. The observed reduced stiffness's are compared with the predicted reduced stiffness by FEMA356. It can be seen that the predicted reduction factors are under-estimating the level of reduction however, it appears to be a better match compared with the 1D longitudinal SSI analysis. This can be attributed to how the SSI is modelled in 1D which assumes the whole foundation is rotating as a combined system. In order to keep the fundamental period equal to the observed period, the stiffness of the elements was also increased by 5-18% depending on the event. This resulted in the effective element stiffness increasing from 21.1% to 24.9% for the 4 September 2010 event

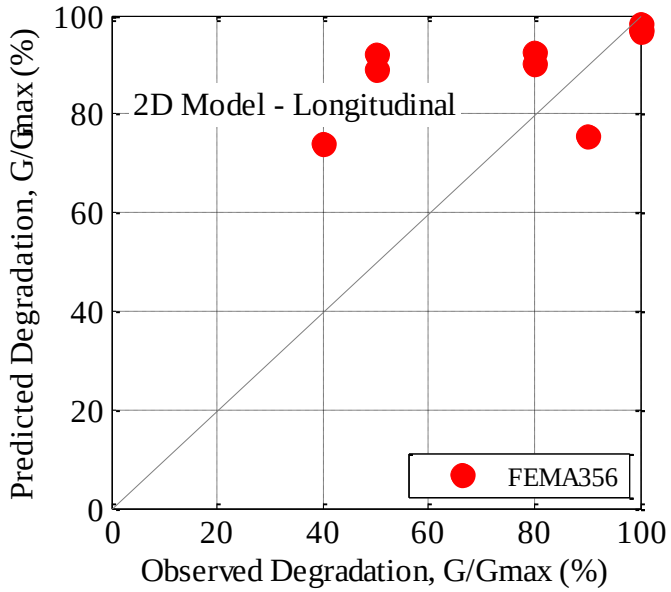


Figure 6-17: Predicted vs observed stiffness reduction for the 2D longitudinal model.

Figure 6-18 shows the displacement and rotational response histories for the 2D longitudinal SSI model compared with the observed response for the 22 February 2011 earthquake. This is very similar to the 1D SSI response however, the predicted base rotation is a result of the difference in vertical displacements of the outmost walls. This appears to still model the rotation reasonably well.

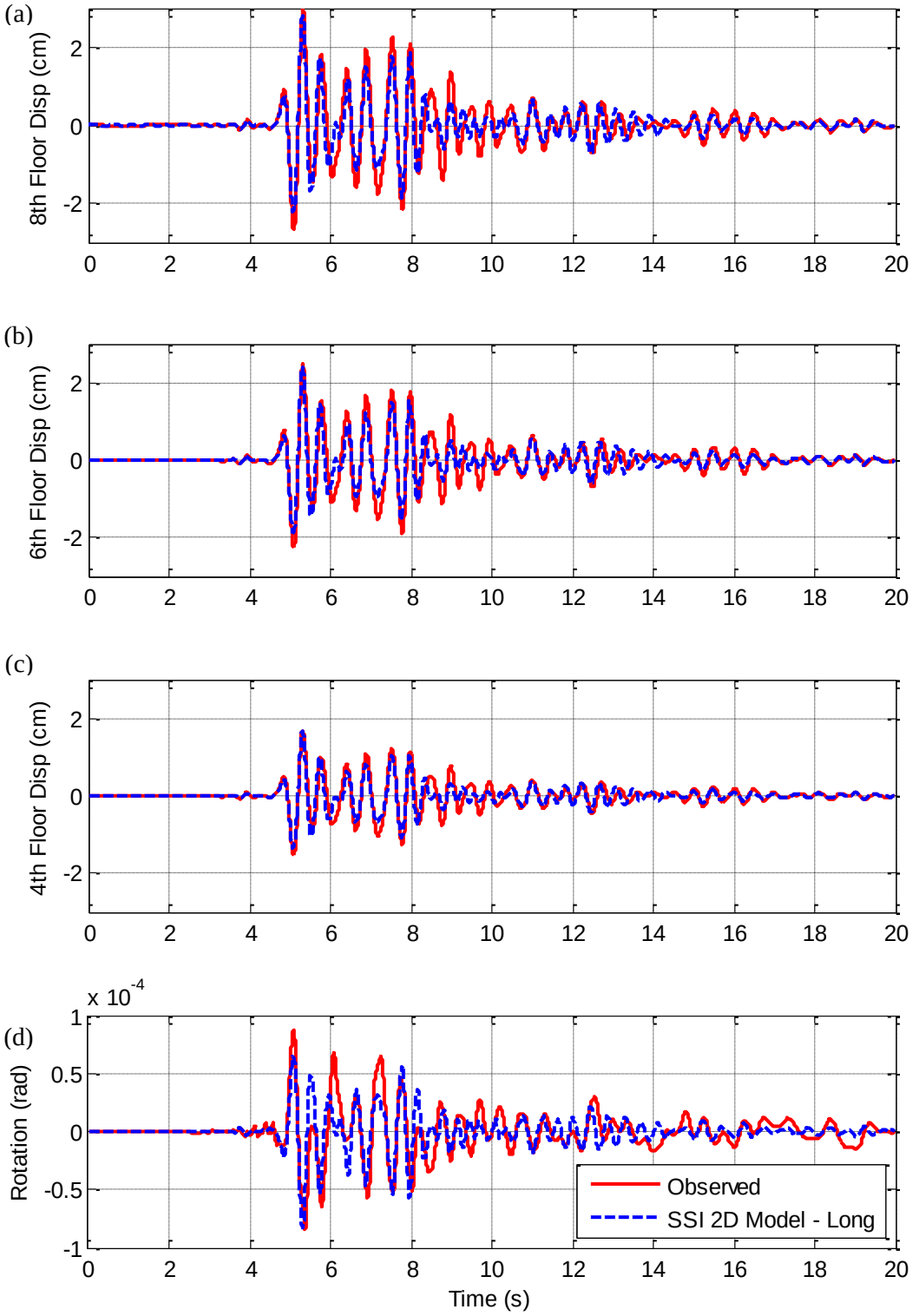


Figure 6-18: Comparison of the (a) 8th; (b) 6th, and (c) 4th floor responses and (d) .rotational response histories and the observations for 2D longitudinal SSI model in the 22 February 2011 earthquake.

The maximum predicted displacement from the 2D longitudinal SSI model is compared with the 2D fixed base model and observations from the 22 February 2011 earthquake in Figure 6-19. It can be seen that the effect of the base flexibility is very small in this case, as the maximum displacements on all floors except the eighth are almost identical.

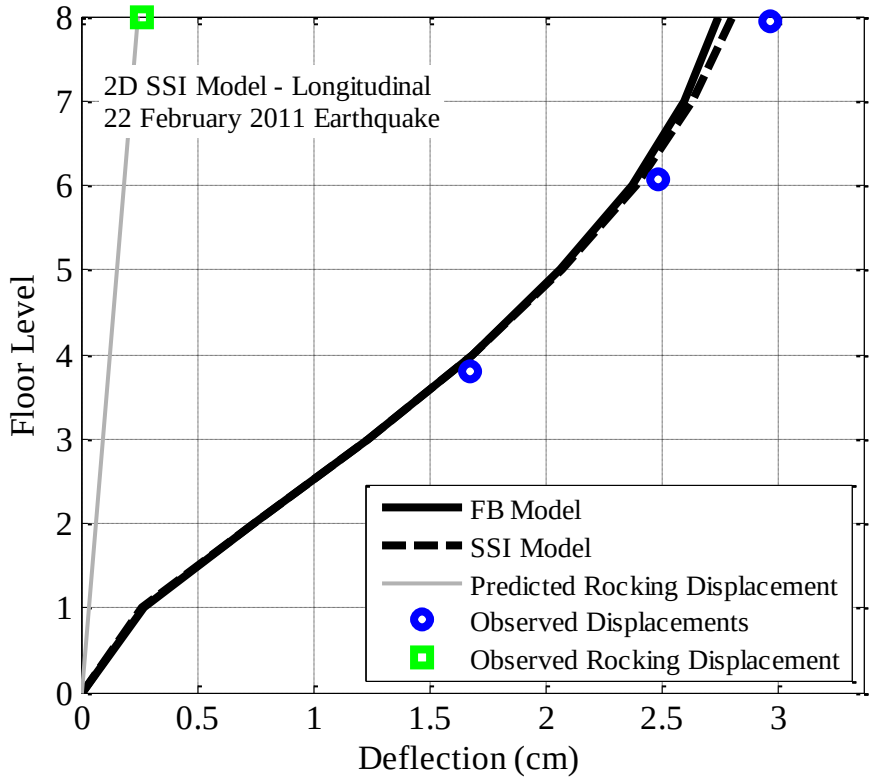


Figure 6-19: Comparison of the maximum deflected shape between observations and the 2D longitudinal SSI model for the 16 April 2011 earthquake.

The normalised comparison of maximum deflections from the 2D longitudinal SSI model for all earthquakes is shown in Figure 6-20. On average, the 2D SSI model under-predicts the observed displacement on all floors however, it is within 5% on all floors. The 2D SSI model provides better predictions compared with the 1D SSI model while still allowing for the observed level of rotation. The reason for this, as described previously, was due to how the SSI was being modelled with the 1D assuming full base rotation while the 2D allowed for individual vertical displacements under each wall. This also provided better comparison between predicted and observed degraded shear modulus.

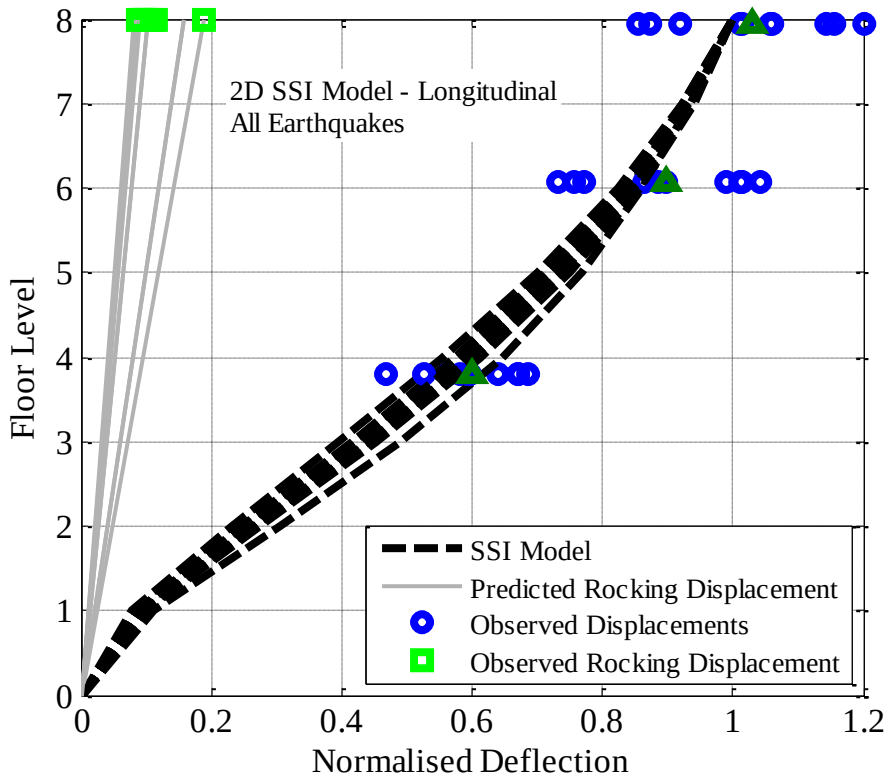


Figure 6-20: Comparison of the maximum deflected shape between observations and the 2D longitudinal SSI model for all earthquakes.

### 6.5.2 2D transverse SSI models

In the transverse direction, due to the short width of the foundations, it was assumed that the foundation system would act as a rigid beam. This allows the Gazetas (1991) springs, which are designed for 1D models, to be applied to the 2D model. There are many ways in which the rotational capacity of the soil can be represented with springs. However, in this study three of the more simple SSI methods were used.

The first SSI system was a single rotational spring in the centre of the base connected to the walls through rigid elements as shown in Table 6-4 (a). This allows for global rotation of the base, however it still uses a rotational spring to provide the rotational capacity of the soil. The second method was to represent the rotational soil resistance with a vertical spring under each wall with the 'upper node' of the two springs connected with a rigid element as shown in Table 6-4 (b). The stiffness of the vertical springs was calculated based on the rotational stiffness using the following relationships:

$$K_V = \frac{F}{\Delta} \tag{5-8}$$

where $K_V$ is the vertical stiffness, F is the applied force and Δ is the deflection.

$$K_R = \frac{M}{\theta} \tag{5-9}$$

where $K_R$ is the vertical stiffness, M is the applied moment and $\theta$ is the rotation.

$$M = F \times D \tag{5-10}$$

where D is the distance between the vertical and rotational springs.

$$\theta = \frac{\Delta}{D} \tag{5-11}$$

Combining these four equations to find a relationship between the vertical and rotational stiffness's:

$$K_V = \frac{K_R}{D^2} \tag{5-12}$$

The third method was a Winkler beam system, prescribed for example by FEMA (2000) (described in more detail Chapter 2) and is shown in Table 6-4 (c). The Winkler beam model used had ten vertical springs with middle and end spring stiffness's equal to:

$$K_{middle} = \frac{0.73G}{1-\nu} \times L \tag{5-13}$$

$$K_{end} = \frac{6.83G}{1-\nu} \times L \tag{5-14}$$

where L is length of the foundation, $K_{end}$ is the stiffness of the outmost spring at each end and $K_{middle}$ is the stiffness of the middle springs.

In order to provide a fair comparison, the Winkler spring stiffness's were multiplied by 2.9 so that the rotational capacity of the system matched the other methods based on equation 5-12. This accounts for the I-shaped foundations which increase the foundation stiffness. The stiffness's were further multiplied by a factor of 1.45 to account for the embedded foundations based on equation 5-6. The Winkler spring model also accounts the full width of the foundations. This meant the base of the model was 17m wide rather than just the distance between the two nodes which was 8.8m.

Table 6-4: Schematic drawings of the 2D SSI models considered.

| (a) Rotational Spring | (b) Vertical Springs | (c) Winkler Beam |
|---|---|---|
| 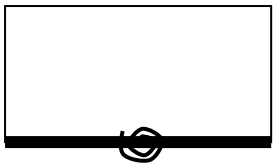 |  | 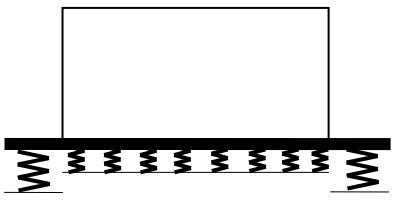 |

Following the same process described previously, the stiffness of the springs in the three 2D SSI models was adjusted until the model rotation matched the observed rotation. The observed degraded stiffness for the three the 2D SSI model was very similar for each event and the average of the values is compared with the predicted degraded stiffness from FEMA356 (2000) and Paolucci *et al.* (2009) in Figure 6-21. It appears that the FEMA356 (2000) prescription under-predicts the degraded stiffness while the Paolucci *et al.* (2009) method over-predicts the degradation.

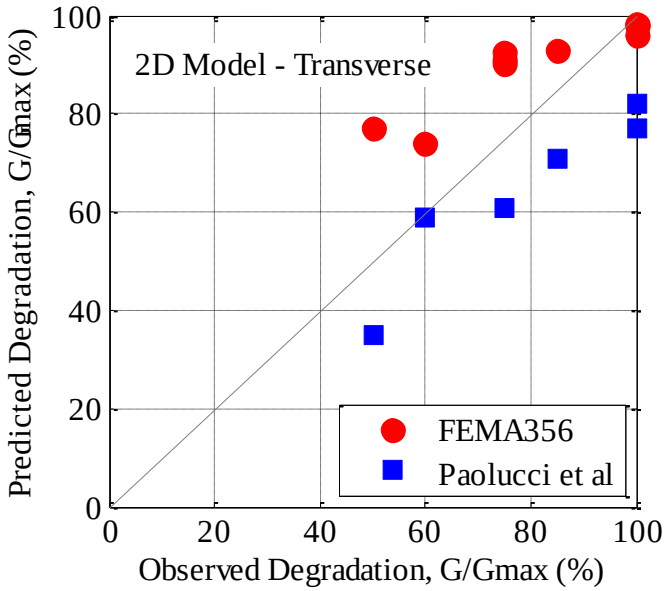


Figure 6-21: Predicted vs observed stiffness reduction for the 2D transverse models.

The stiffness of the elements in the three 2D SSI models was again increased in order to keep the period of the SSI model the same as the fixed base model. The increase in stiffness varied significantly between events with the smaller events requiring an increase in stiffness from 28.5% of the total stiffness to 80%. For events with a large degradation in spring stiffness, the increase in element stiffness was even larger with an increase to 240% of the total element stiffness required in order for the 4 September 2010 event to have a fundamental period of 0.59 seconds. This increased stiffness appears to be very high, however, on inspection of Table 4-6 (from the spectral analysis section of Chapter 4) it can be seen that the observed period of the 4 September 2010 earthquake was actually 0.66 seconds on average. This is larger than the event average period of 0.59 seconds and when the stiffness is adjusted to match this period, approximately 80% of total stiffness was again required. It is interesting to note that the increase percentage of total stiffness required in the SSI models proves to be a better match with the prescribed effective section properties from Table C6.6 in NZS3101 (2006) (described in Table 5-3 in Chapter 5). Effective stiffness's for serviceability limit state from NZS3101 ranged from 50% of $I_g$ to 100% of $I_g$ depending on the design ductility and axial force ratio.

#### *6.5.2.1 2D transverse SSI model - rotational spring*

The first transverse 2D SSI model examined was the rotational spring model. The spring initially had the same stiffness as the 1D SSI model however this stiffness was modified as shown in Figure 6-21. The displacement response history for the eighth, sixth and fourth floors are compared with the observed responses for the 22 February 2011 earthquake in Figure 6-22 (a), (b) and (c) respectively. The predictions from the 2D SSI model are very good for the majority of the response histories however the model under-predicts the displacements on the cycles between 8-10 seconds. This is very similar to the 1D SSI model response shown in Figure 6-12. The predicted rotational response in Figure 6-22 (d) also matches the observations well. This again demonstrates that there is rotational SSI motion in the transverse direction and that a rotational spring is capable of modelling this.

The comparison between the maximum displacement response predicted by the 2D transverse SSI model with a rotational spring and the observations from the 22 February 2011 earthquake is shown in Figure 6-23. The SSI model has increased displacements on all floors by approximately 0.1cm. However, the SSI model still under-predicts the observed displacements by a large amount (0.4 cm per floor).

A normalised comparison between predicted and observed response from the 2D transverse SSI model with a rotational spring for all earthquake events is shown in Figure 6-24. It can be seen that the normalised predicted rocking displacement matches the observed displacement for all events as the spring was calibrated for this. Even with this adjustment for SSI, the model still under-predicts the average observed displacement on all three floors.

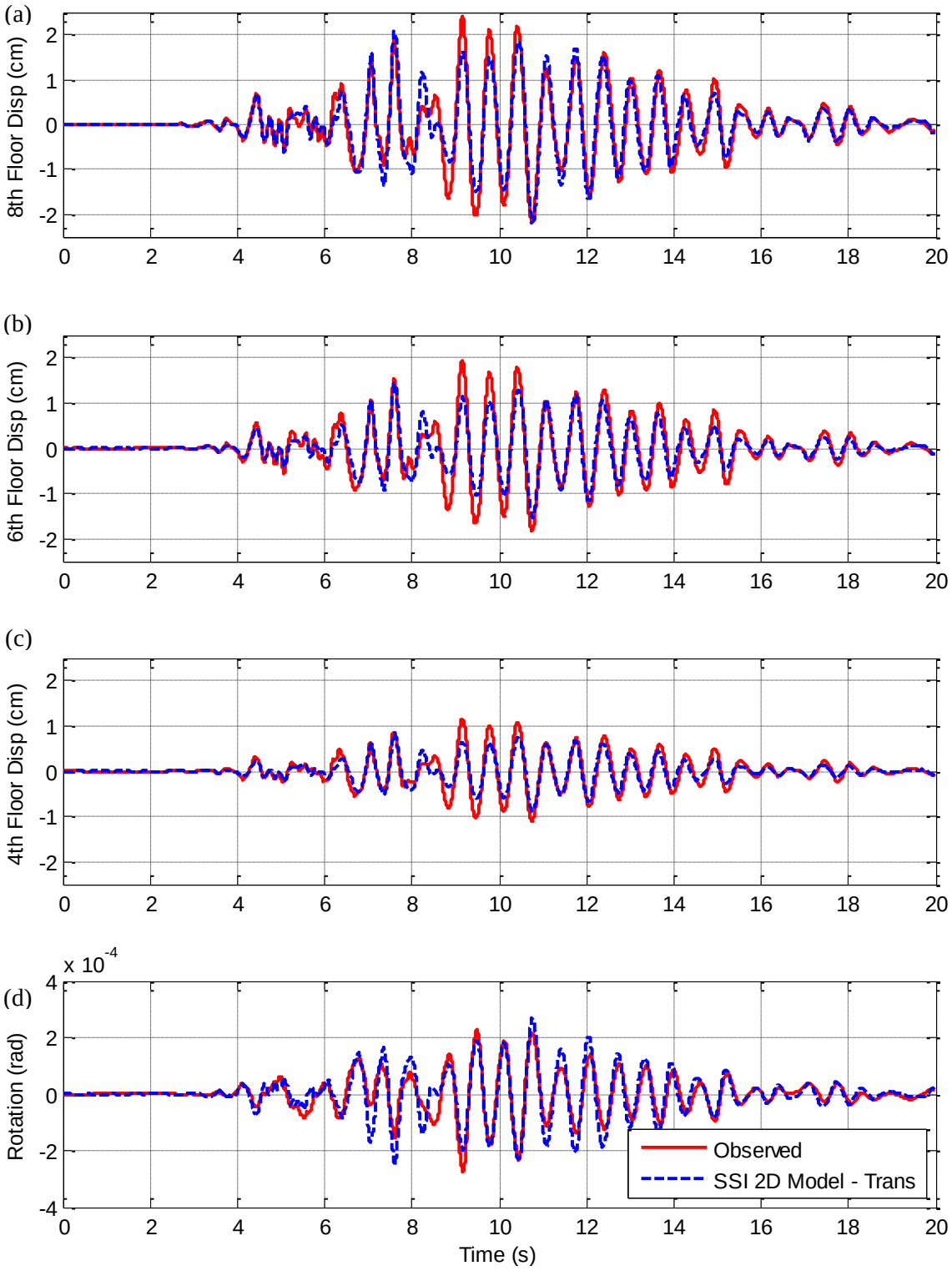


Figure 6-22: Comparison of the (a) 8th; (b) 6th, and (c) 4th floor responses and (d) .rotational response histories and the observations for 2D transverse SSI model with a rotational spring in the 22 February 2011 earthquake.

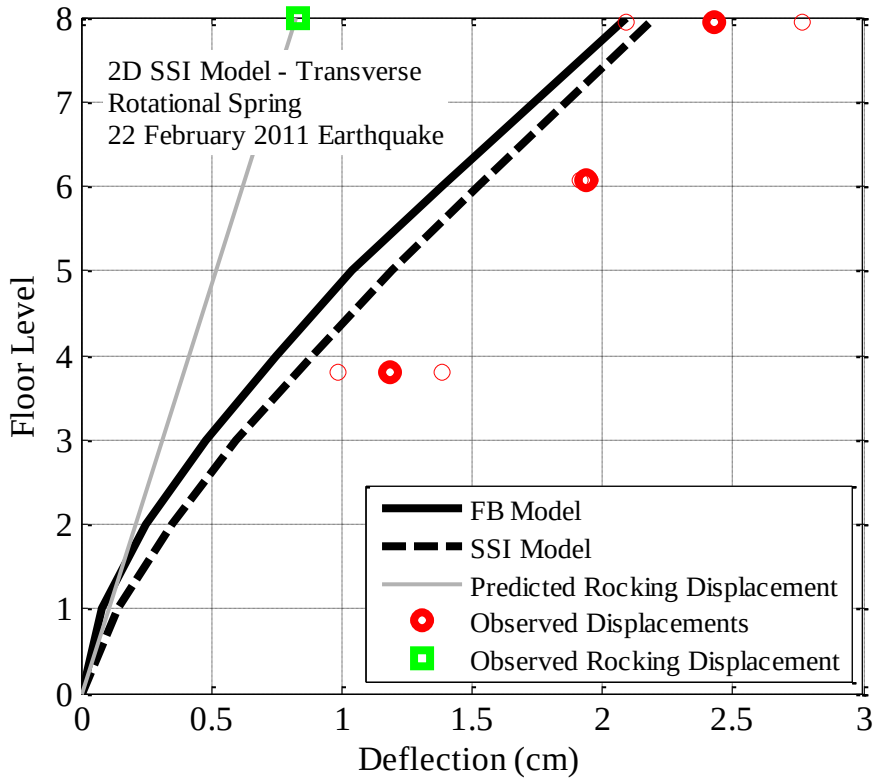


Figure 6-23: Comparison of the maximum deflected shape between observations and the 2D transverse SSI model with rotational springs only for the 22 February 2011 earthquake.

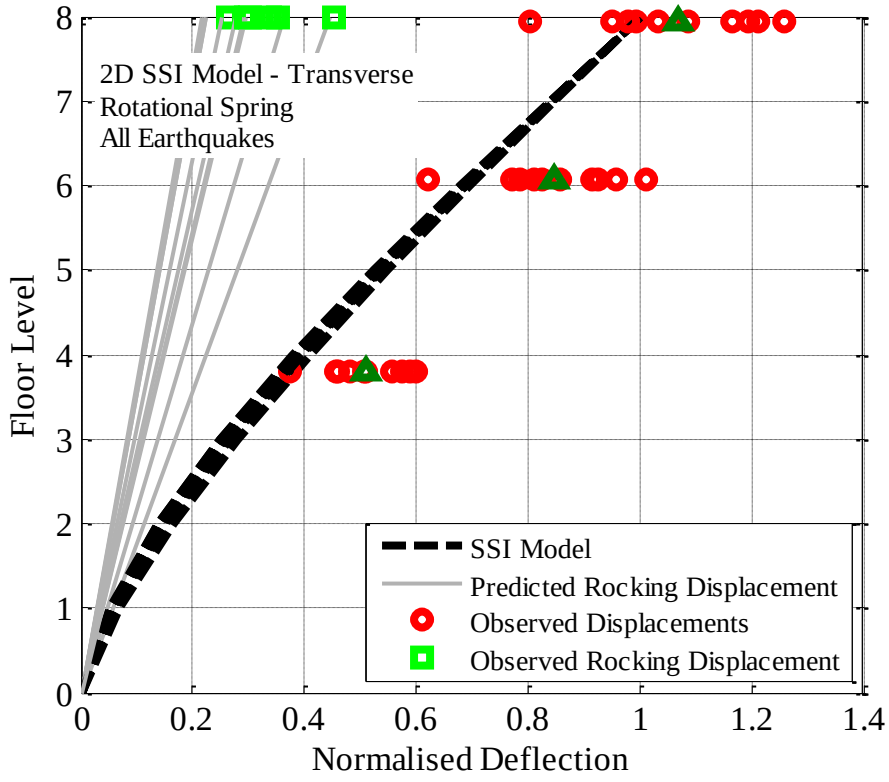


Figure 6-24: Comparison of the maximum deflected shape between observations and the 2D transverse SSI model with rotational springs only for all earthquakes.

#### *6.5.2.2 2D transverse SSI model - vertical springs*

The second transverse 2D SSI model examined was a system with two vertical springs connected with a rigid beam element. The stiffness of the vertical springs was determined using equation 5-12. It was expected that the response of this system would be very similar to the rotation spring system as it was calibrated based on this. The displacement response history for the eighth, sixth and fourth floors are compared with the observed responses for the 22 February 2011 earthquake in Figure 6-25 (a), (b) and (c) respectively. The predictions from the 2D SSI model are very similar to the rotational spring model with the model providing good predictions for the majority of the response histories while under-predicting the displacements on the cycles between 8-10 seconds. The predicted rotational response in Figure 6-25 (d) again matches the observations well suggesting that the SSI rotation can be modelled with either a rotational spring or two vertical springs.

The comparison between the maximum displacement response predicted by the 2D transverse SSI model with vertical springs and the observations from the 22 February 2011 earthquake is shown in Figure 6-26. The SSI model again increased displacements on all floors by approximately 0.1cm. However, the SSI model still under-predicts the observed displacements by a large amount (0.4 cm per floor).

A normalised comparison between predicted and observed response from the 2D transverse SSI model with vertical springs for all earthquake events is shown in Figure 6-27. The prediction of the eighth floor displacement from SSI model is on average the same as the observed eighth floor displacement. However, the predictions on the fourth and eighth floor are still less than the observations.

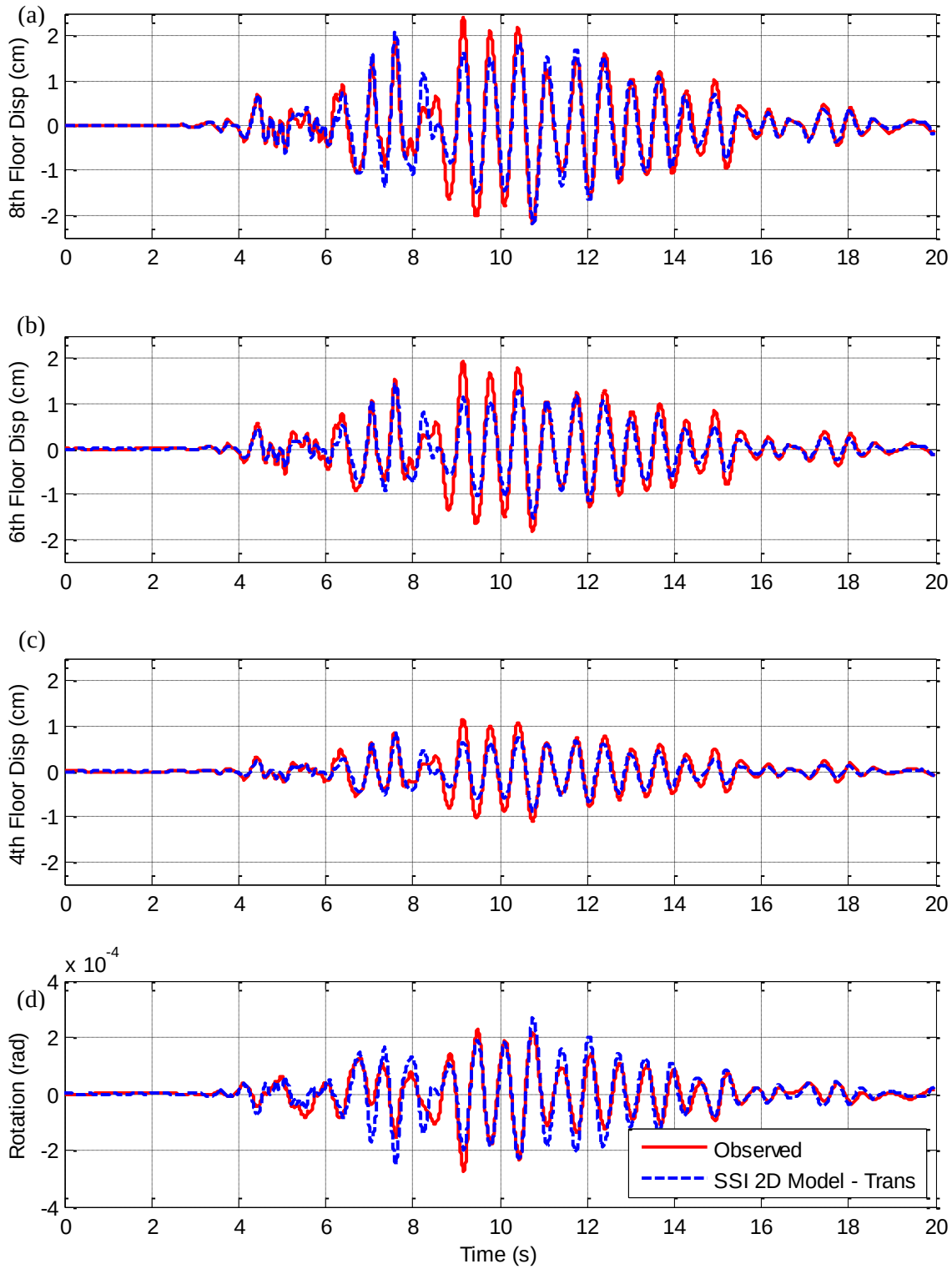


Figure 6-25: Comparison of the (a) 8th; (b) 6th, and (c) 4th floor responses and (d) .rotational response histories and the observations for 2D transverse SSI model with vertical springs in the 22 February 2011 earthquake.

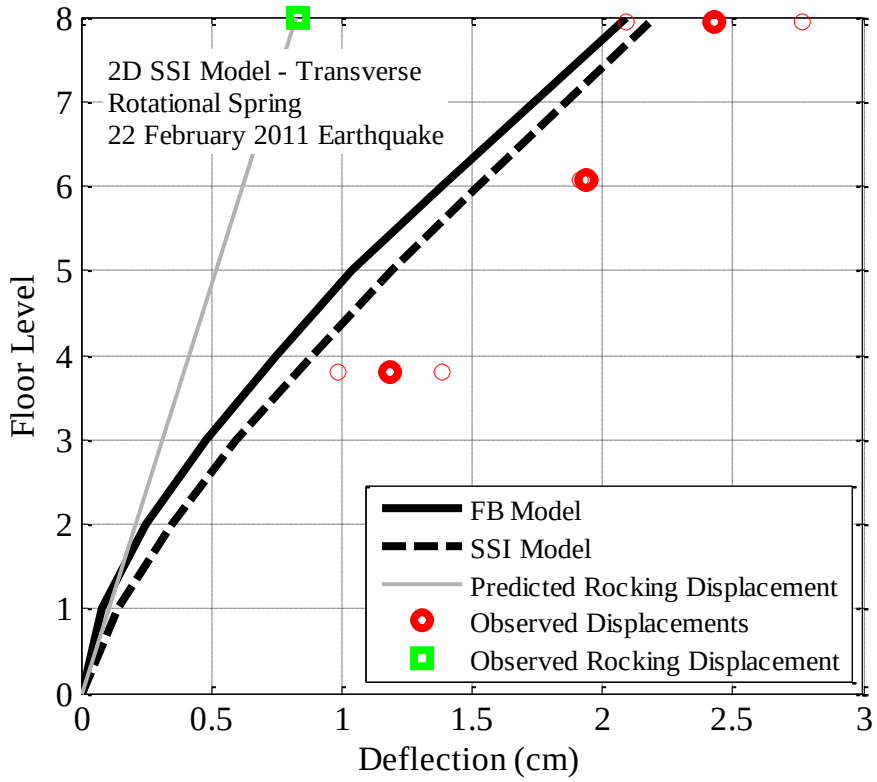


Figure 6-26: Comparison of the maximum deflected shape between observations and the 2D transverse SSI model with vertical springs only for the 22 February 2011 earthquake.

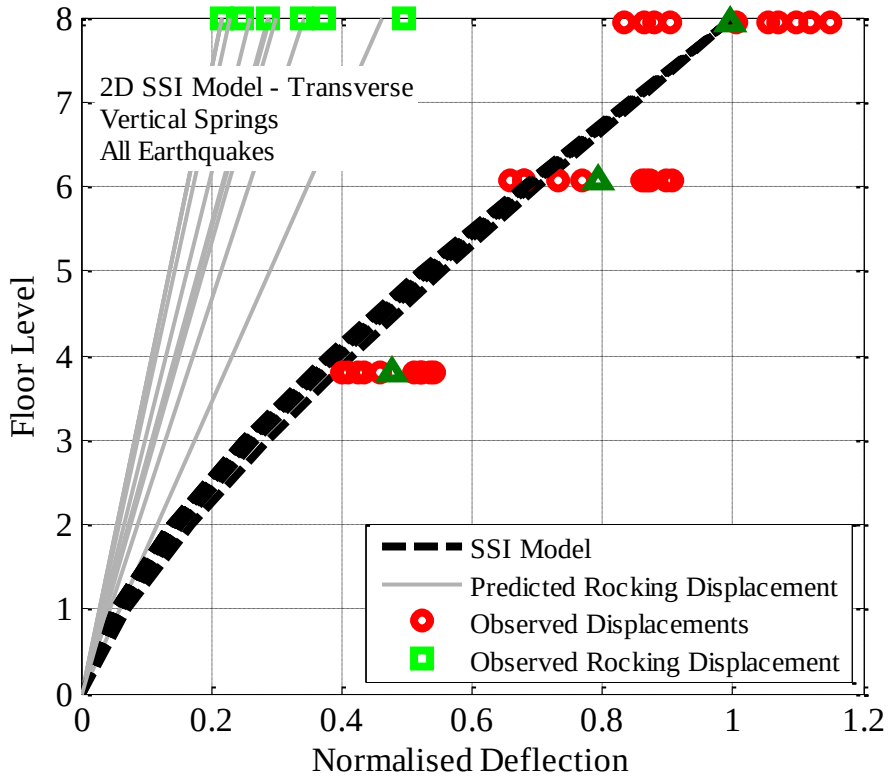


Figure 6-27: Comparison of the maximum deflected shape between observations and the 2D transverse SSI model with vertical springs only for all earthquakes.

#### *6.5.2.3 2D transverse SSI model - Winkler model*

The third transverse 2D SSI model examined was a system with Winkler springs connected with a rigid beam element. The stiffness of the Winkler springs was determined using equation 5-13 and 5-14. The displacement response history for the eighth, sixth and fourth floors are compared with the observed responses for the 22 February 2011 earthquake in Figure 6-28 (a), (b) and (c) respectively. The predictions from the 2D SSI model Winkler model are very similar to the two SSI models. The predicted rotational response in Figure 6-28 (d) again matches the observations well suggesting that the SSI rotation can be modelled with either a rotational spring or two vertical springs.

The comparison between the maximum displacement response predicted by the 2D transverse SSI model with Winkler springs and the observations from the 22 February 2011 earthquake is shown in Figure 6-29. The increase in displacements on all floors is approximately 0.2cm which is larger than the other two SSI models. However, the SSI model still under-predicts the observed displacements on all floors but is within 0.1cm on the eighth floor.

A normalised comparison between predicted and observed response from the 2D transverse SSI model with Winkler springs for all earthquake events is shown in Figure 6-30. The prediction of the eighth floor displacement from SSI model is on average slightly higher than the observed eighth floor displacement. The fourth and sixth floor predictions are still under-predicted however, they are now within 10% of the observed average.

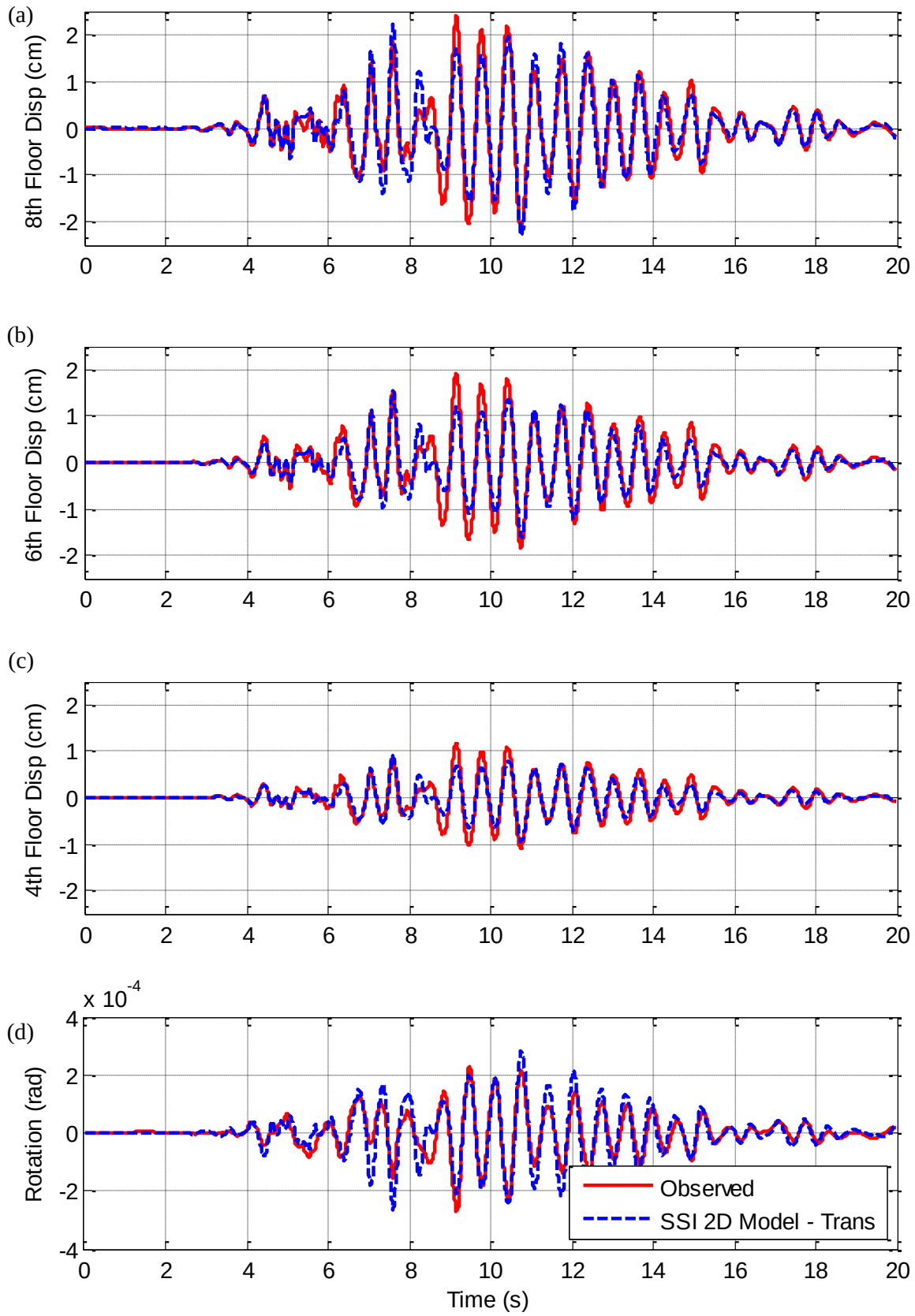


Figure 6-28: Comparison of the (a) 8th; (b) 6th, and (c) 4th floor responses and (d) .rotational response histories and the observations for 2D transverse SSI model with Winkler springs in the 22 February 2011 earthquake.

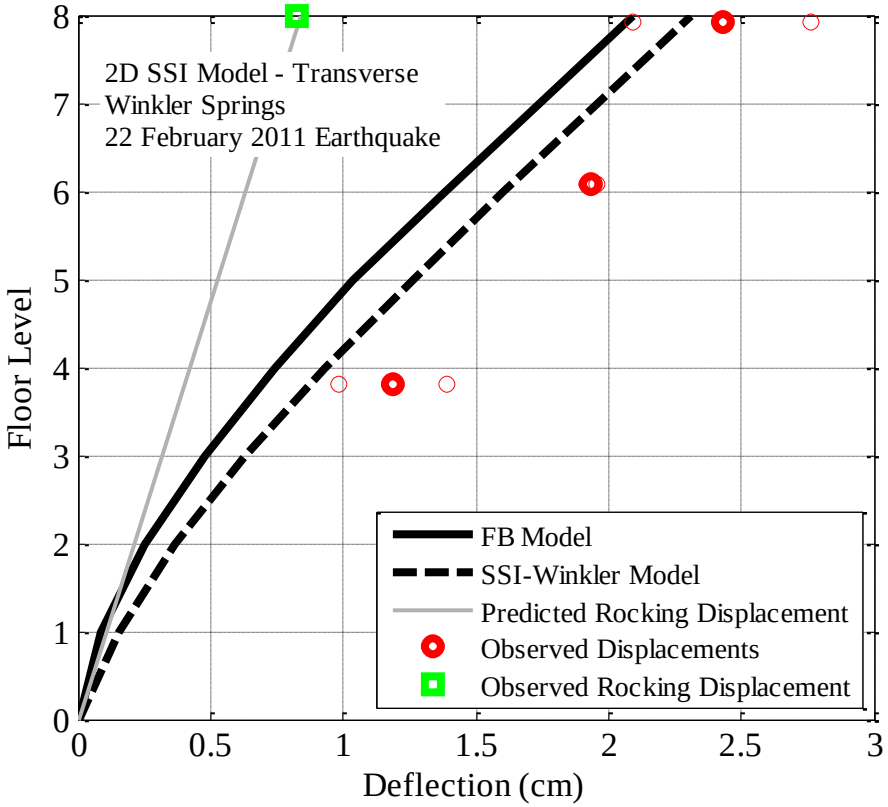


Figure 6-29: Comparison of the maximum deflected shape between observations and the 2D transverse SSI model with Winkler springs for the 22 February 2011 earthquake.

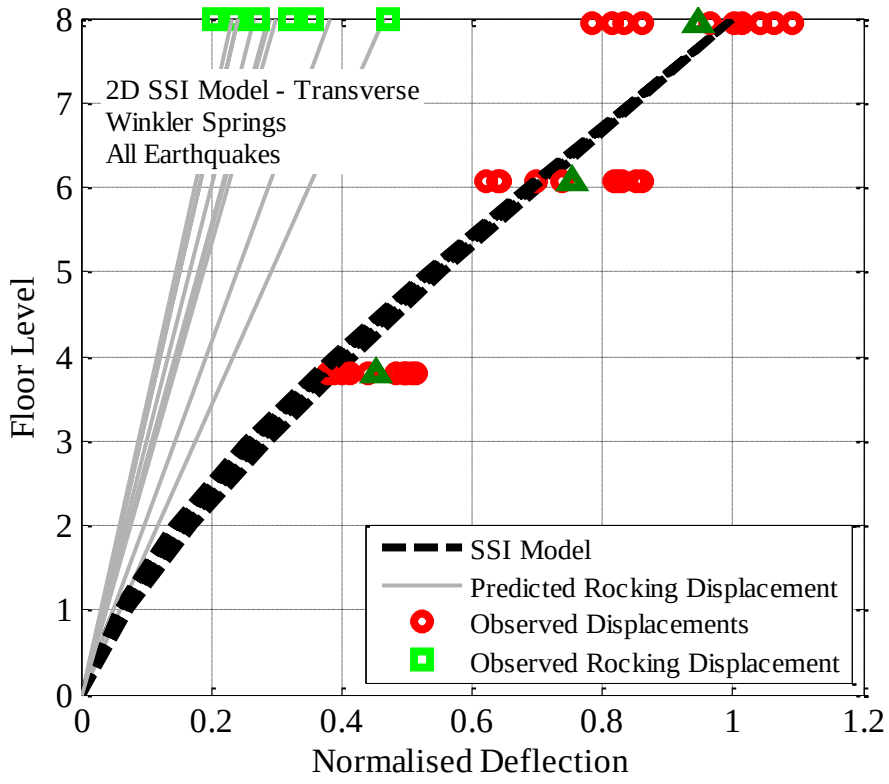


Figure 6-30: Comparison of the maximum deflected shape between observations and the 2D transverse SSI model with Winkler springs for all earthquake.

### 6.5.3 Comparison with 2D fixed base models

#### *6.5.3.1 Longitudinal direction*

The predictive capabilities of the SSI models are compared with fixed base models by calculating the average percentage error of each floors prediction. Table 6-5 shows the comparison between the 2D longitudinal fixed base and SSI models. It can be seen that the responses are very similar with the addition of base flexibility not increasing the predictive capability.

Table 6-5: Average percentage error of the 2D fixed base and SSI longitudinal models compared with observations.

| | **Longitudinal** | |
|---|---|---|
| | **2D FB** | **2D SSI** |
| **8th Floor** | -2.8% | -2.0% |
| **6th Floor** | -4.0% | -4.3% |
| **4th Floor** | -2.6% | -3.2% |
| **Average** | **3.1%** | **3.2%** |

The comparison of the average deflected shape from the two models in Figure 6-31 confirms that the two models predict very similar displacement profiles.

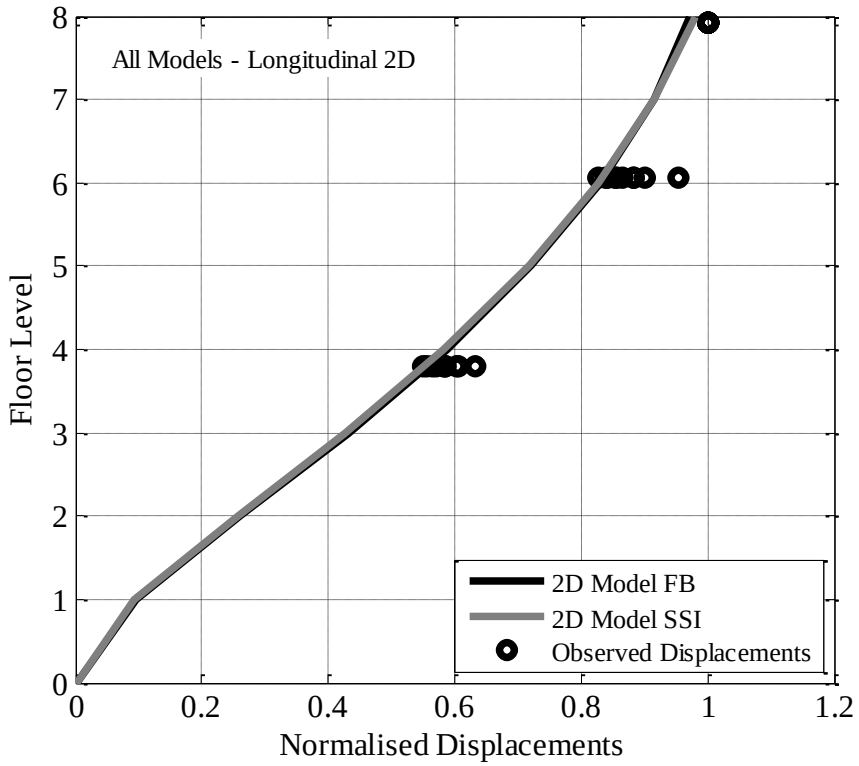


Figure 6-31: Comparison of the normalised maximum deflected shape between the 2D longitudinal fixed base and SSI models for all earthquakes.

### *6.5.3.2 Transverse direction*

The comparison between the transverse fixed base model and the three SSI models can be found in Table 6-6. The rotational and vertical spring SSI models produce only slightly better predictions on each level compared with the fixed base model. The Winkler model has approximately 4% less error on each floor but still under-predicts all floors by approximately 8% on average.

Table 6-6: Average percentage error of the 2D fixed base and SSI transverse models compared with observations.

| | **Transverse** | | | |
|---|---|---|---|---|
| | **2D FB** | **2D SSI - Rot** | **2D SSI - Vert** | **2D SSI - Winkler** |
| 8th Floor | -6.3% | -4.8% | -5.0% | 0.2% |
| 6th Floor | -15.5% | -14.0% | -14.3% | -10.3% |
| 4th Floor | -15.2% | -13.0% | -13.3% | -10.8% |
| **Average** | **12.3%** | **10.6%** | **10.9%** | **6.9%** |

Figure 6-32 clearly shows how the rotational spring and two vertical spring SSI models do not significantly change the predicted shape compared with the fixed base model. The Winkler beam model slightly increases the displacements on each floor however all models still significantly under-predict the lower floor observations.

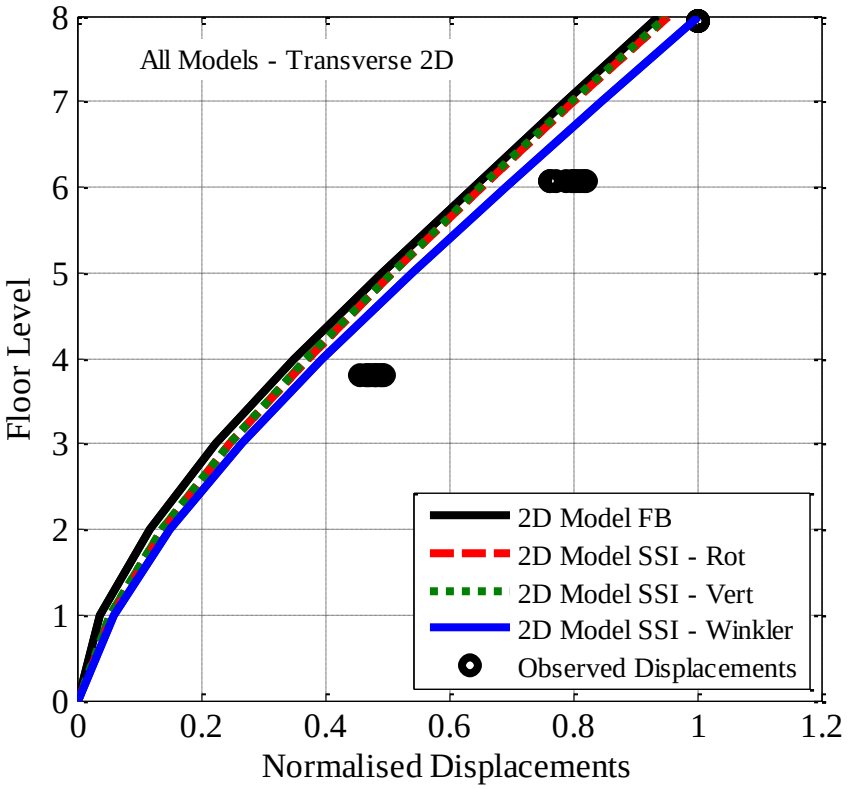


Figure 6-32: Comparison of the normalised maximum deflected shape between the 2D transverse fixed base and SSI models for all earthquakes.

Typically the effect of the inclusion of SSI into a model would increase the fundamental period. However, in this case the period of the model was kept constant by changing the element stiffness. In order to demonstrate the typical SSI effect, a comparison is shown in Figure 6-33 which compares a fixed base model and SSI model with the same element stiffness. The SSI model is the transverse Winkler beam model which has a period of 0.59 seconds. The fixed base model is the 2D transverse model which, like the SSI model, has the effective stiffness equal to 80% of gross stiffness. The period of the fixed base model is 0.51 seconds. The difference between the two models is significant with the with the fixed base model under-predicting the eighth floor displacement by over 20%.

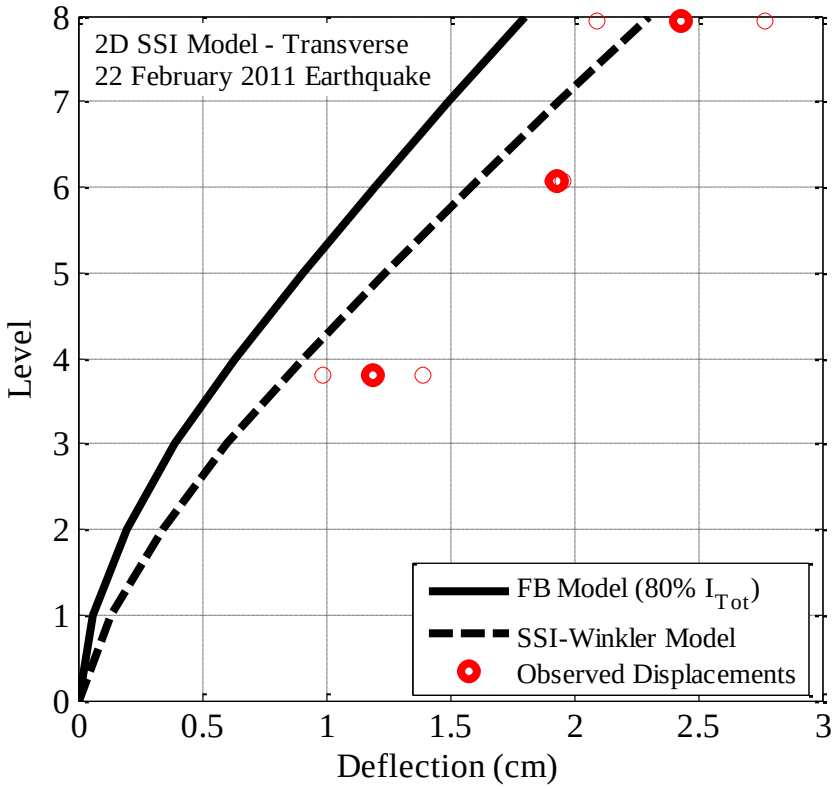


Figure 6-33: Comparison of the maximum deflected shape between observations and the 2D transverse SSI Winkler spring model with the same gross stiffness for the 22 February 2011 earthquake.

## 6.6 Conclusions

This chapter has provided a detailed examination of simple soil-structure interaction models for the prediction of the seismic response of the UC Physics Building in the Canterbury earthquakes. The 1D and 2D models from the previous chapter were adjusted to allow for base flexibility and predictive capability of the new SSI models were compared with observations. A summary of the main findings from this chapter are detailed below:

- The shear strength of the soil was found using data from two CPT's performed in the vicinity of the building. The shear strength between 2-8m was found to be 109 GPa. This value was used to find the stiffness of the vertical and rotational springs for the longitudinal and transverse direction based on Gazetas (1991).
- The 1D fixed base models were adjusted to allow for base flexibility using the rotational springs. The stiffness of the springs was adjusted until the predicted base rotation matched the observed rotation. Calculated values of observed degraded stiffness were compared with the predicted reduction factor prescribed by FEMA356 (2000) in the longitudinal direction and with both FEMA356 (2000) and Paolucci *et al.* (2009) in the transverse direction. It was found that in the longitudinal direction that the observed degradation was significantly lower than the predicted due to the assumption that the foundation would rotate as a uniform body. This did not significantly affect the results as SSI was negligible in this direction. In the transverse direction, the FEMA356 prescription under-predicted the degradation while the Paolucci *et al.* (2009) method predictions matched the observations. The maximum displacement profile predicted by the 1D longitudinal SSI model had an average error of 5.8%, which was worse than the 1D fixed base model. The average error in the 1D transverse SSI model was 7.1%, which was a significant improvement on the average error of 11.6% in the fixed base model.
- Three different 2D SSI models considered in the transverse direction which included; a rigid base with a rotational spring, a rigid base with two vertical springs and a rigid with multiple vertical springs. Only one SSI model, with vertical springs, was used in the transverse direction as it was assumed that the foundation would not rotate as a rigid system. The predicted degraded stiffness was under-predicted by FEMA356 in both models while Paolucci *et al.* (2009) slightly over-predicted the degradation in the transverse model. It was found that the 2D longitudinal SSI model provided similar predictions to the fixed base model suggesting that there was minimal SSI in that direction. The average percentage error of the longitudinal 2D SSI model was 3.2%. The 2D transverse SSI models had average errors of 10.6%, 10.9% and 6.9%. These are all lower than the 2D fixed base model, however, only the Winkler model was significantly better.

## 6.7 References

Computers and Structures, I. (1998). Soil-structure interaction- At a finite distance from a structure the absolute displacements must approach the free-field displacements.

Federal Emergency Management Agency. (2000). *Prestandard and Commentary for the Seismic Rehabitation of Buildings. FEMA356.* Washington, D.C.

Gajan, S., Raychowdhury, P., Tara C. Hutchinson, Kutter, B. L., & Stewart, J. P. (2010). Application and Validation of Practical Tools for Nonlinear Soil-Foundation Interaction Analysis. *Earthquake Spectra,* **26**(1), *111-129*.

Gazetas, G. (1991). Foundation Vibrations. In H. Y. Fang (Ed.), *Foundation Engineering Handbook, 2nd Edition* (Chapter 15. pp. 553-593): Kluwer / Springer.

Kausel, E. (2010). Early historyofsoil–structureinteraction. *Soil DynamicsandEarthquakeEngineering,* **30**, *822-832*.

Moghaddasi, M., Cubrinovski, M., Chase, J. G., Pampanin, S., & Carr, A. (2012). Stochastic Quantification of Soil-Shallow Foundation-Structure Interaction. *Journal of Earthquake Engineering,* **16**(6), *820-850*.

Mylonakis, G., & Gazetas, G. (2008). Seismic soil-structure interaction: Beneficial or detrimental. *Journal of Earthquake Engineering,* **4**(3), *277-301*.

Standards New Zealand. (2006). *Part 1 - The Design of Concrete Structures. NZS3101.*

Paolucci, R., Prisco, C. D., Figini, R., Petrini, L., & Vecchiotti, M. (2009). Interazione Din Non Lin Terreno-Struttura Nell'ambito Della Prog Sismica Agli Spostamenti. *Progettazione Sismica, IUSS Press, Pavia: 1–12*.

Robertson, P. K. (2012). *Interpretation of In-situ Tests - Some Insights*. Paper presented at the 4th International Conference on Geotechnical and Geophysical Site Characterization (ISC'4), Proto de Galinhas, Pernambuco - Brazil.

Seed, H. B., & Idriss, I. M. (1970). Soil moduli and damping factors dynamic response analyses. *Rept. EERC 70-10. University of California, Berkeley*.

Stewart, J. P., Seed, R. B., & Fenves, G. L. (1999a). Seismic soil-structure interaction in buildings. I: Analytical aspects. *J. Geotech. & Geoenv. Engrg., ASCE,* **125 (1)**, *pp 26-37*.

Stewart, J. P., Seed, R. B., & Fenves, G. L. (1999b). Seismic soil-structure interaction in buildings. II: Empirical findings. *J. Geotech. & Geoenv. Engrg, ASCE,* **125 (1)**, *pp 38-48*.

Sullivan, T. J., Salawdeh, S., Pecker, A., Corigliano, M., & Calvi, M. M. (2010). Soil-Foundation-Structure Interaction Considerations for Performance-Based Design of RC Wall Structures on Shallow Foundations. *Soil-Foundation-Structure Interaction – Orense, Chouw & Pender*(Taylor & Francis Group, London, ISBN 978-0-415-60040-8).

Wolf, J. P. (1994). *Foundation vibration analysis using simple physics models*. Englewood Cliffs, NJ: PTR Prentice Hall

# 7 EFFECT OF NON-LINEAR & TORSIONAL BEHAVIOUR ON MODEL PREDICTION

## 7.1 Overview

This chapter examines the effects of non-linear material modelling in the numerical model of the UC Physics Building in comparison with the observed response. Moment curvature relationships are found for the key structural elements and two simplified relationships are used to represent this behaviour. A bi-linear approximation is used for the wall elements while a tri-linear relationship with a degrading stiffness is used for the beam members. The nonlinear constitutive models are considered for the elements in the 2D models over a finite region where plastic behaviour is likely to occur in the beams and walls. These nonlinearities are considered for both the longitudinal and transverse fixed base 2D models as well as the transverse 2D SSI model. The displacement response series and maximum displacement profiles are compared with the observations for each model. The maximum element curvatures on each floor are found and compared for all models considered thus far (fixed base linear, fixed base non-linear, SSI linear and SSI non-linear) in order to identify the effect of each assumption on the curvature profile.

This chapter also examines the effect of allowing for global torsional behaviour in numerical modelling. A three dimensional (3D) fixed base model is constructed by combining the two dimensional models from each direction. The observed torsional behaviour from Chapter 4 was inferred as a result of the connection from the UC Physics Building to the adjacent lift shaft structure (Link Building). The Link Building is modelled as a MDOF structure and is connected to the 3D model using a series of horizontal springs. The observed torsional rotation from each earthquake event is compared with the predicted torsion angle from the 3D model.

## 7.2 Non-linear material models

### 7.2.1 Bi-Linear model

The simplest way to represent the non-linear (NL) material behaviour, is with a bi-linear relationship. The initial slope of the bi-linear model represents the linear behaviour of the member. The relationship changes when the yield moment is reached and the new stiffness is equal a reduced percentage of the initial stiffness. The dashed line in Figure 7-1 shows the actual moment curvature relationship for the longitudinal beam and was found using Cumbia (Montejo & Kowalsky, 2007). The solid line shows the best fit bi-linear approximation. This is also shown for the transverse coupling beam in Figure 7-2.

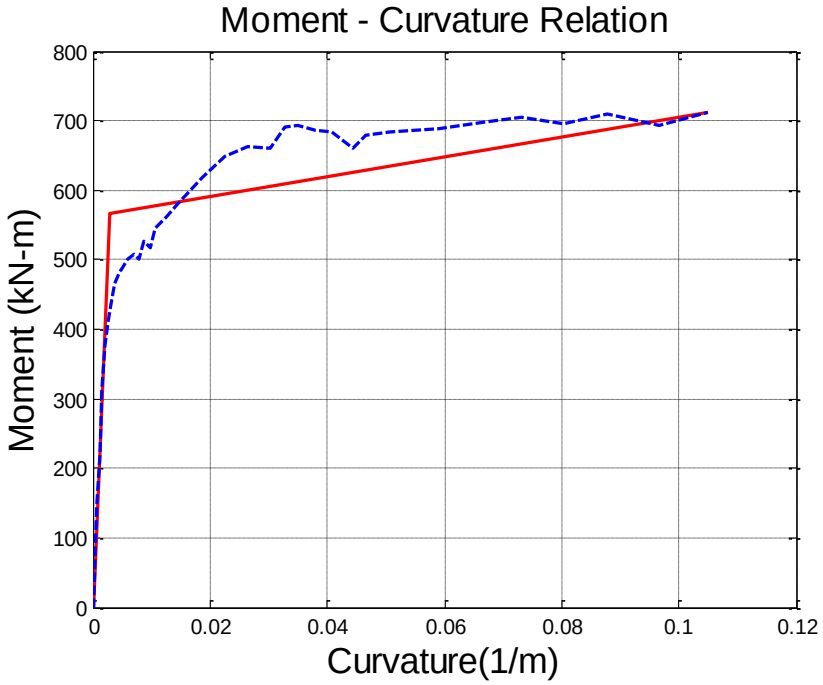


Figure 7-1: Bi-linear moment curvature relationship for the longitudinal beam.

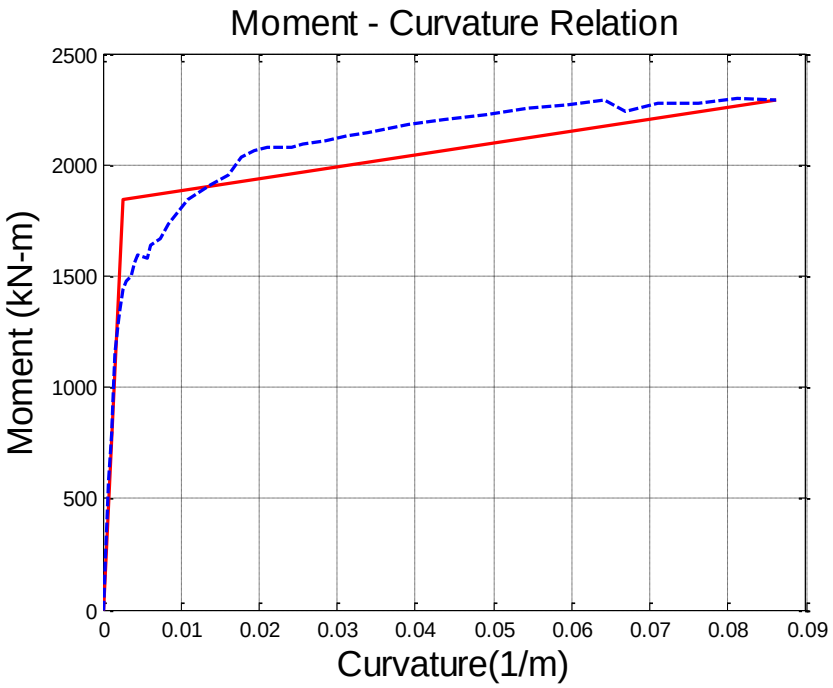


Figure 7-2: Bi-linear moment curvature relationship for the transverse coupling beam.

A summary of the bi-linear properties for all members in both models can be found in Table 7-1. The walls have a higher ratio of post yield to initial stiffness (r) compared with the beams due to their relatively high axial load. The yield moment and initial stiffness are the two most important parameters in determining the non-linear behaviour of the martial (Otani, 1984).

Table 7-1: Bi-linear model properties.

| Element | My (kN.m) | r |
|---|---|---|
| Long - Wall | 5,500 | 0.05 |
| Long - Beam | 567 | 0.01 |
| Trans - C-Wall1 | 61,000 | 0.05 |
| Trans - C-Wall2 | 32,000 | 0.05 |
| Trans - C-Beam | 1,812 | 0.01 |

### 7.2.2 Tri-linear degrading stiffness model

The cyclic behaviour of the bi-linear model produces a hysteresis loop with a large area providing a large level of hysteretic damping. This can sometimes be unrealistic for concrete, as once it has cracked, the initial stiffness will never again be reached, therefore a different model is required which represents this. An example of an inelastic tri-linear model is shown in Figure 7-3; this model has three different stiffness values for loading as well as a reduced stiffness for unloading. The behaviour

predicted by the tri-linear model is more similar to the cyclic behaviour of reinforced concrete with different levels of stiffness derived from the behaviour of the reinforced concrete after cracking and steel yielding respectively (Stojadinovic & Thewalt, 1996). The area enclosed in this hysteresis loop is much smaller compared with the bi-linear model, therefore providing less damping. This hysteresis model is very similar to the modified Takeda model (Takeda *et al.*, 1970), with the addition of a tri-linear backbone curve.

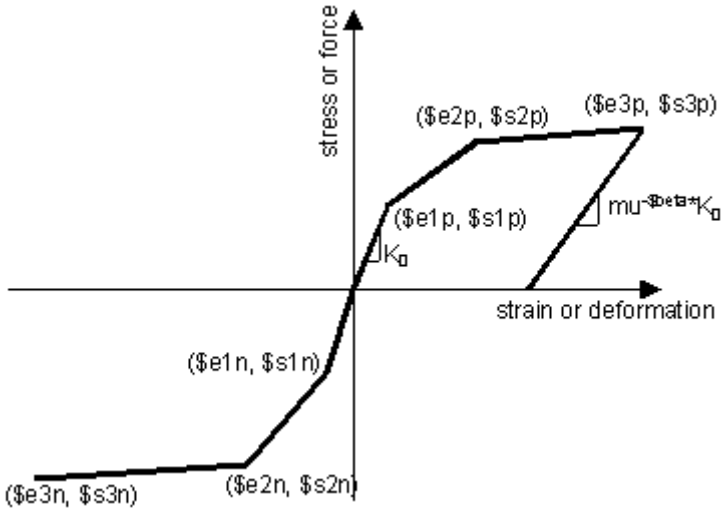


Figure 7-3: Tri-linear degrading hysteresis model (Opensees (2013))

The most important members in the non-linear analysis are the beam elements in each model. This is where most of the non-linear behaviour is expected to occur, therefore tri-linear models will be used in these locations in order to more accurately model the concrete behaviour. The tri-linear model is shown in Figure 7-4 and Figure 7-5 for the longitudinal and transverse beams, respectively. The properties of the two beam models are listed in Table 7-2 where My is the yield moment, $r_1$ is the ratio of post yield stiffness to initial stiffness, Mu is the ultimate yield moment and $r_2$ is the ratio of the final stiffness to the initial stiffness.

Table 7-2: Tri-linear model properties.

| **Element** | **My (kN.m)** | **$r_1$** | **Mu (kN.m)** | **$r_2$** |
|---|---|---|---|---|
| Long - Beam | 413 | 0.05 | 663 | 0.01 |
| Trans - Beam | 1,441 | 0.06 | 2,066 | 0.01 |

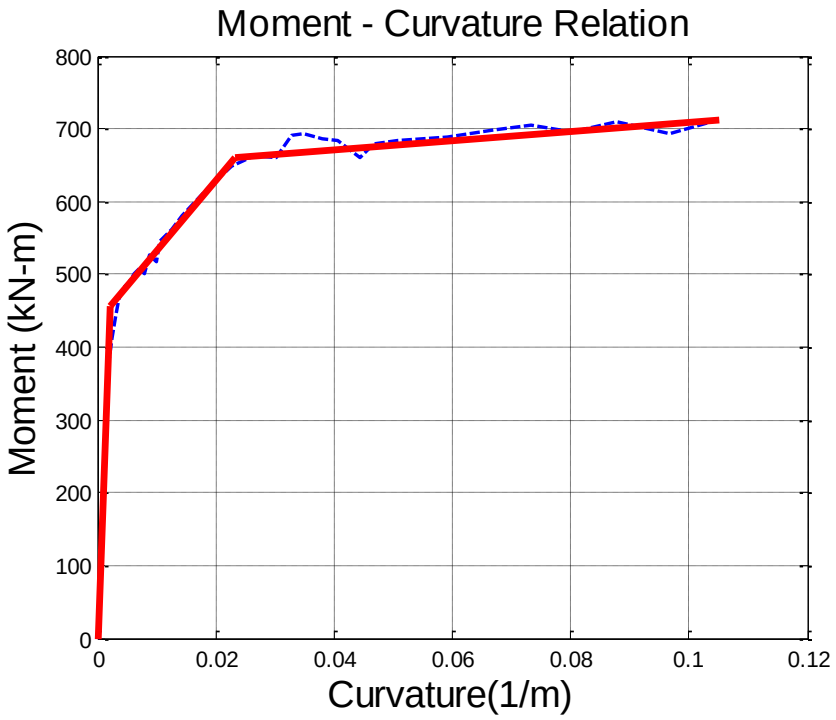


Figure 7-4: Tri-linear moment curvature relationship for the longitudinal beam.

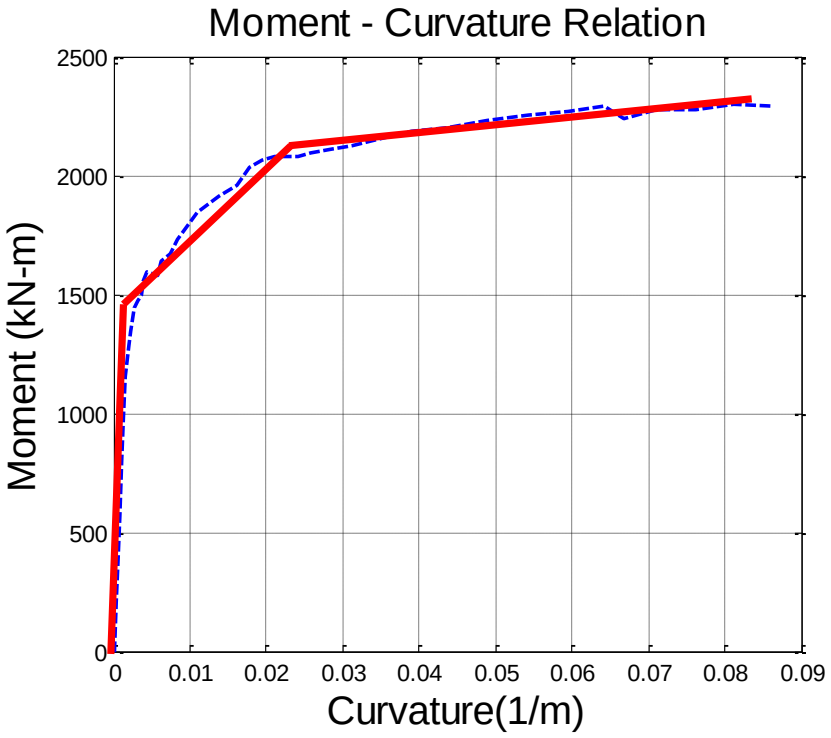


Figure 7-5: Tri-linear moment curvature relationship for the transverse coupling beam.

## 7.3 2D fixed base non-linear models

The wall elements in the longitudinal and transverse non-linear models have bi-linear moment curvature relationships while the beam elements in both models have the tri-linear relationship. The length of the plastic hinge zone in all models is equal to half the depth of the member (Park & Paulay, 1975).

### 7.3.1 Longitudinal model

The maximum deflected shape of the NL longitudinal model was initially tested under the 16 April 2011 earthquake with the results shown in Figure 7-6. As expected, the non-linear response is identical to the linear response as the level of shaking was relatively small during this earthquake, resulting in the members remaining elastic.

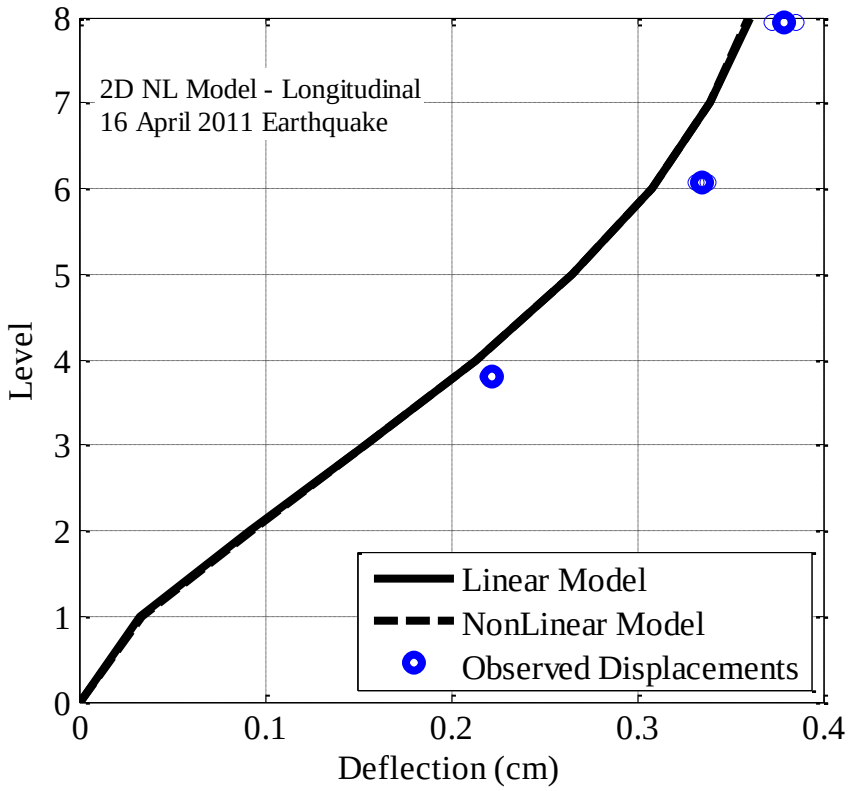


Figure 7-6: Comparison of the maximum deflected shape between observations and the 2D longitudinal NL model for the 16 April 2011 earthquake. Note that the thin circles represent the observed end shear wall displacements while the thick circles represents the average of the two responses.

In order to reach the yielding point of the non-linear constitutive models, the earthquake loading must be large enough. It is during the strong ground motion records, such as 4 September 2010, where non-linear behaviour is expected to have occurred. The predicted displacement response series for the 4 September 2010 earthquake from the longitudinal non-linear model along with the observed

response is shown in Figure 7-7. It can be seen that the response is very similar for most of the response however, the predictions for the large cycle motion is larger than the observed displacements.

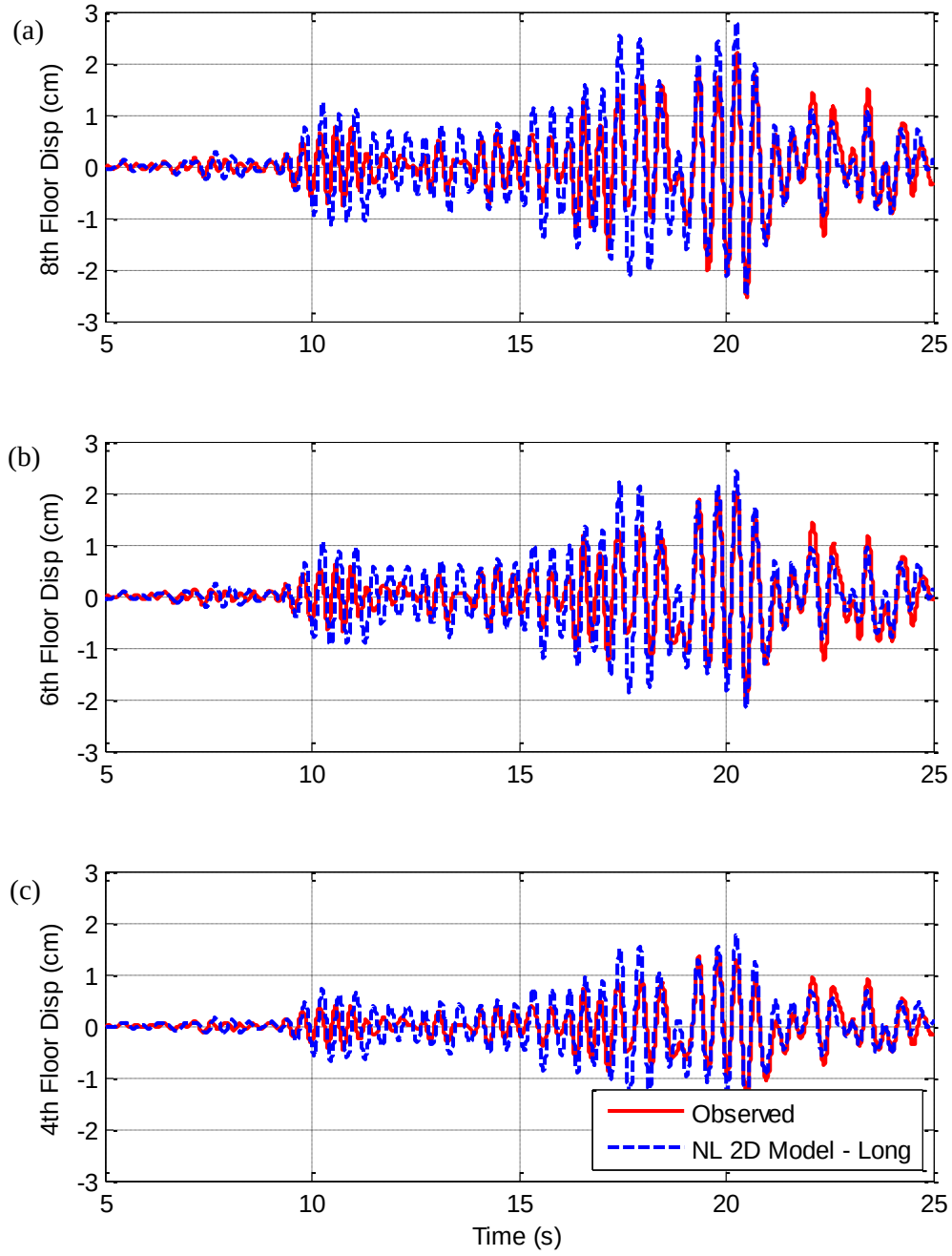


Figure 7-7: Comparison between the displacement time histories of the observations and 2D longitudinal non-linear model for the 4 September 2010 earthquake: (a) 4$^{th}$; (b) 6$^{th}$; and (c) 8$^{th}$ floor responses.

The effect of allowing for non-linear behaviour is shown in the maximum displacement response profile given in Figure 7-8 for the linear and non-linear models. The difference between the peak displacement profile indices of the two analyses indicates that there has been some non-linear

behaviour occurring which has reduced the stiffness of the elements. This has not provided better predictions for this earthquake as the linear model already over-predicted the response.

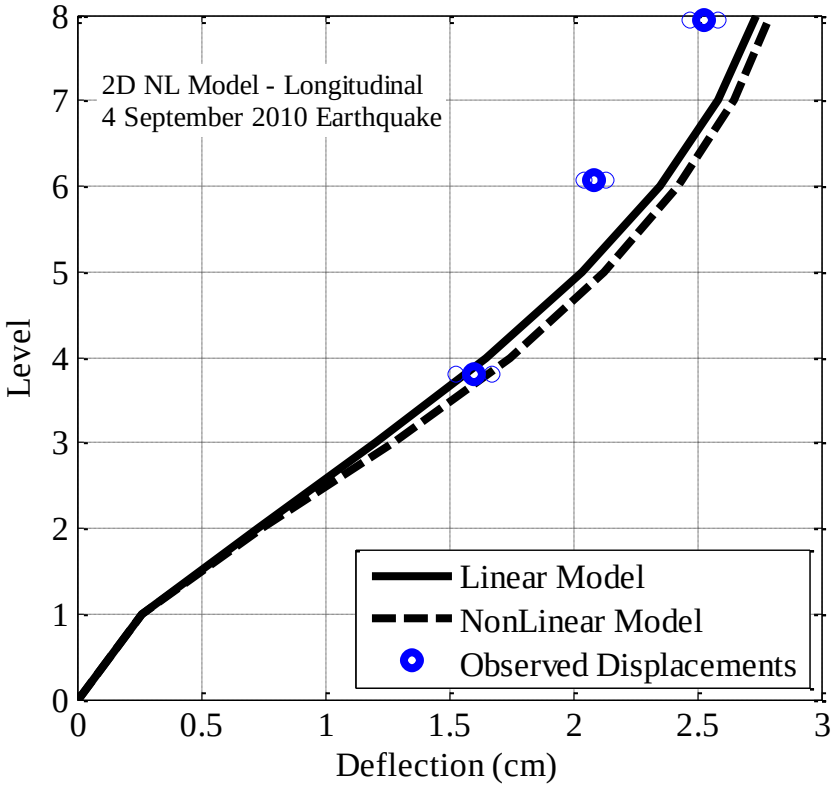


Figure 7-8: Comparison of the maximum deflected shape between observations and the 2D longitudinal NL model for the 4 September 2010 earthquake. Note that the thin circles represent the observed end shear wall displacements while the thick circles represents the average of the two responses.

Figure 7-9 illustrates the moment-curvature responses for the plastic hinges zones from the base of the wall and eight beams. It can been seen in the figure that the first three floor beams have some non-linear behaviour. The maximum curvature occurred in the second floor beam while the base of the wall and top five level beams all remain linear throughout the earthquake.

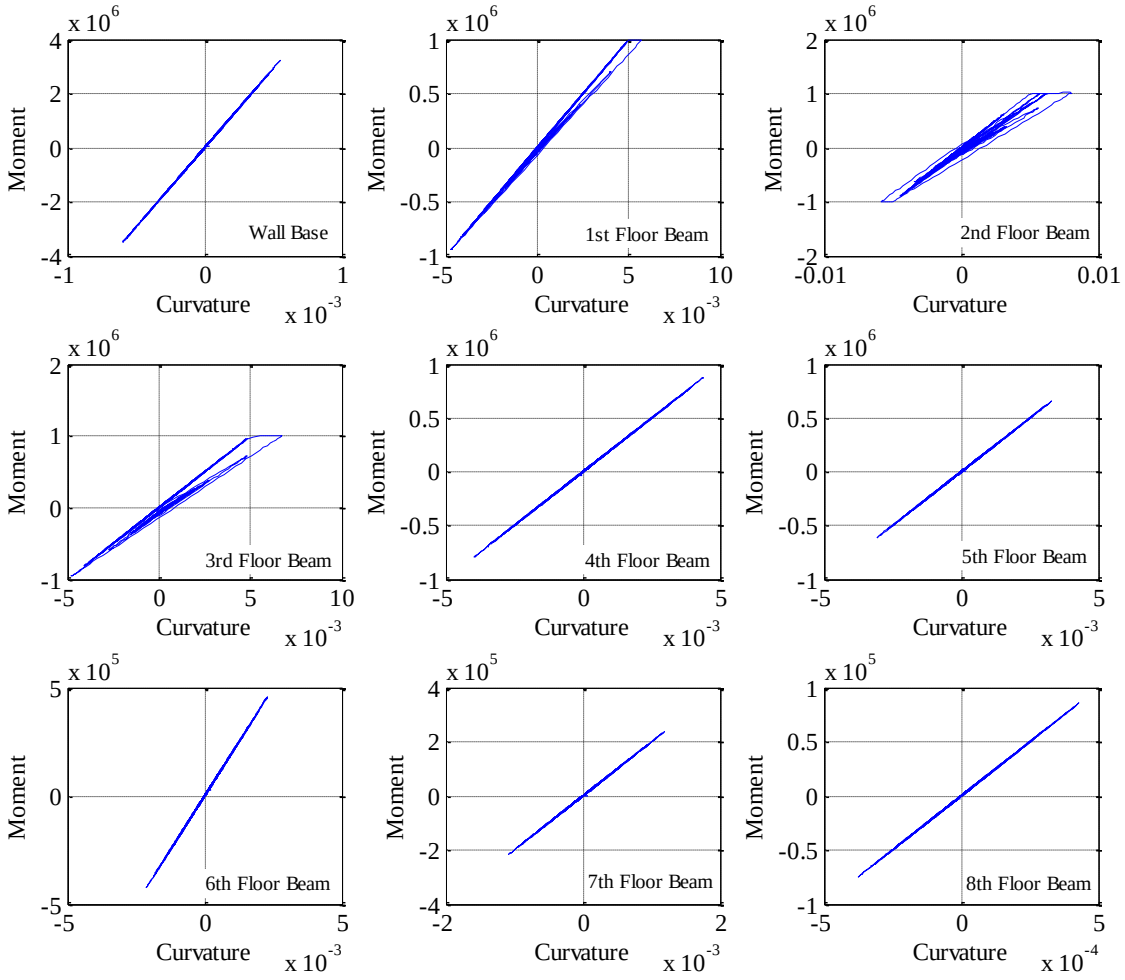


Figure 7-9: Moment curvature plots from the plastic hinge zone for the base of the wall and end of the beams on all floors in the longitudinal direction for the 4 September 2010 earthquake.

The comparison between the predicted deflected shape from the fixed base linear and non-linear longitudinal models for all earthquake events is shown in Figure 7-10. It can be seen that the predicted response varies between over and under-prediction of the observed response for each event. Only the 4 February 2011 earthquake appears to have a different non-linear response.

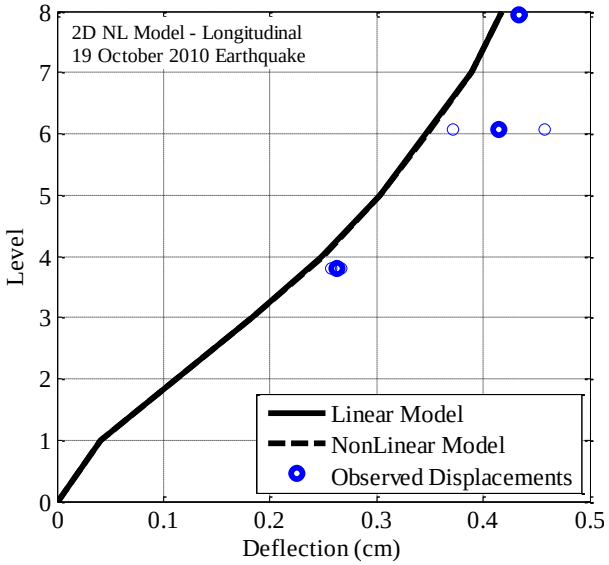
2D NL Model - Longitudinal
19 October 2010 Earthquake
Level
Deflection (cm)
Linear Model
NonLinear Model
Observed Displacements

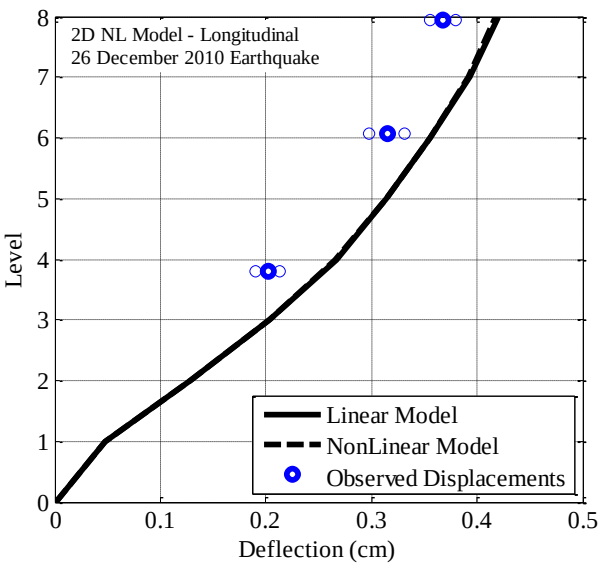
2D NL Model - Longitudinal
26 December 2010 Earthquake
Level
Deflection (cm)
Linear Model
NonLinear Model
Observed Displacements

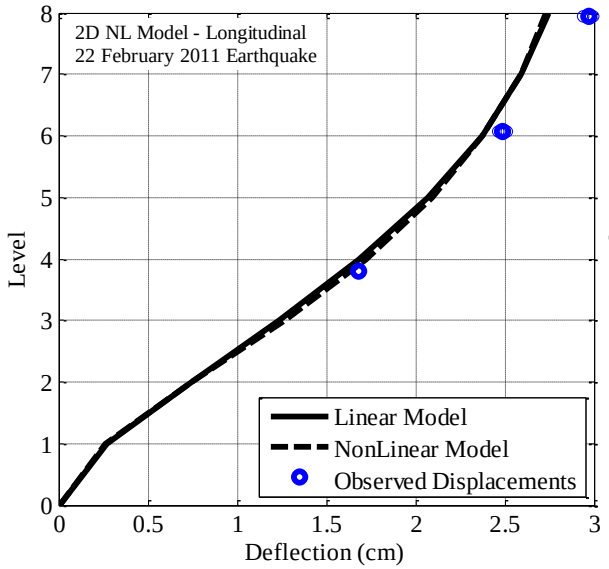
2D NL Model - Longitudinal
22 February 2011 Earthquake
Level
Deflection (cm)
Linear Model
NonLinear Model
Observed Displacements

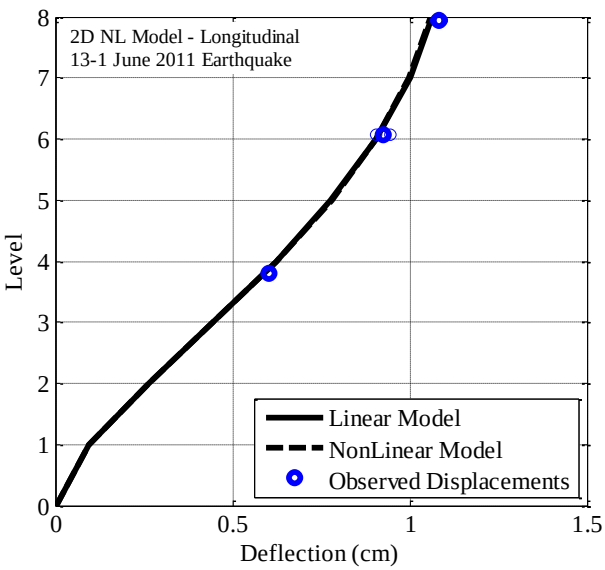
2D NL Model - Longitudinal
13-1 June 2011 Earthquake
Level
Deflection (cm)
Linear Model
NonLinear Model
Observed Displacements

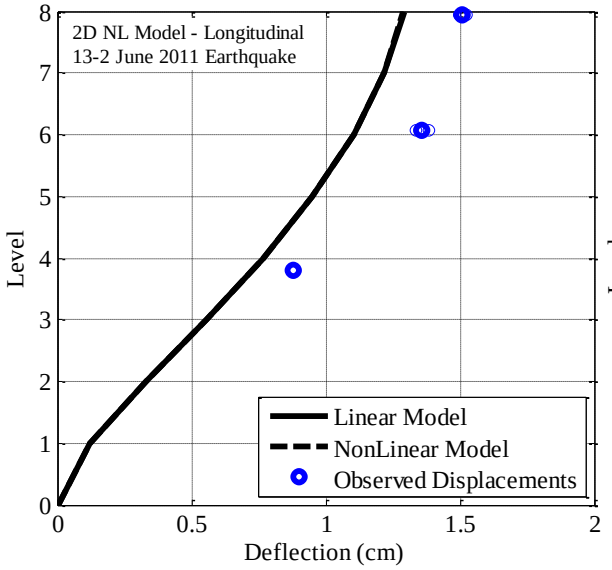
2D NL Model - Longitudinal
13-2 June 2011 Earthquake
Level
Deflection (cm)
Linear Model
NonLinear Model
Observed Displacements

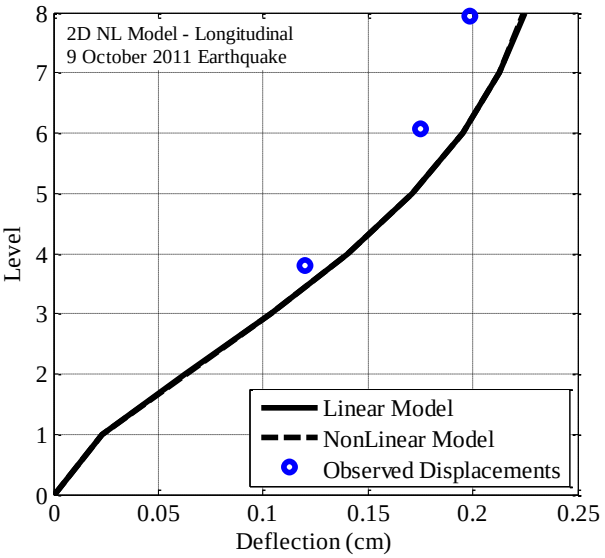
2D NL Model - Longitudinal
9 October 2011 Earthquake
Level
Deflection (cm)
Linear Model
NonLinear Model
Observed Displacements

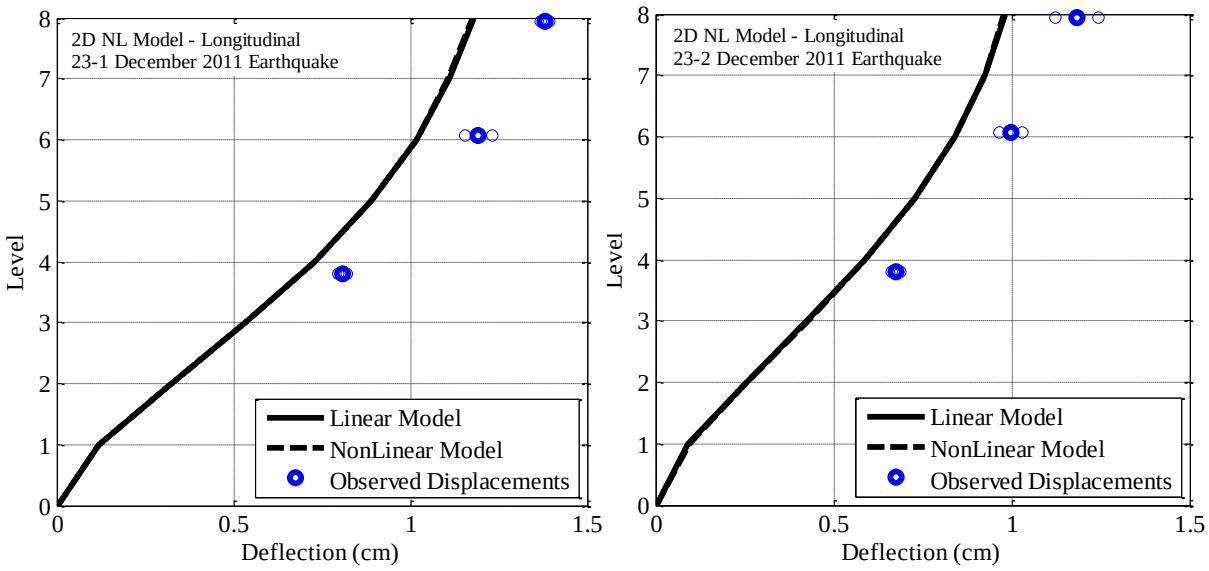


Figure 7-10: Comparison of the maximum deflected shape between observations and the 2D longitudinal NL model for all earthquakes.

The normalised predictions from the NL longitudinal model are shown in Figure 7-11. The average predicted displacements pass through the average observed displacement on each of the three floors with a distribution of approximately ±20%. There is also some variation in the predicted deflect shape with a range of ±5%.

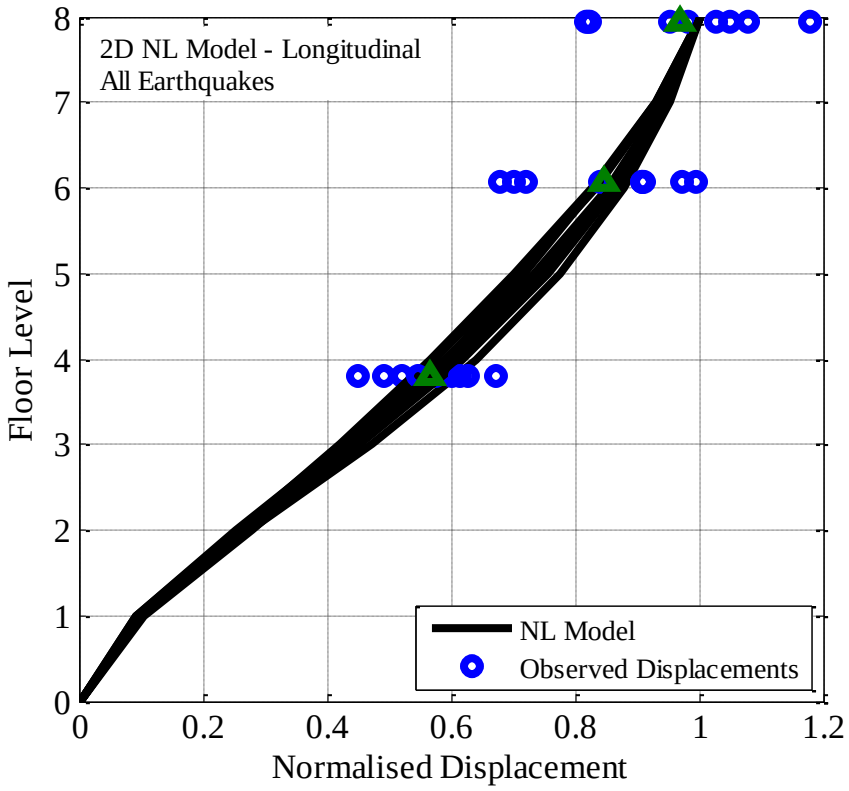


Figure 7-11: Comparison of the normalised maximum deflected shape between observations and the 2D longitudinal NL model for all earthquakes.

### 7.3.2 Transverse model

The fixed base, NL transverse model was also initially tested under small ground motion loading to check that it produced the same predictions as the linear model. This is shown in Figure 7-12 for the 16 April 2011 earthquake and, as expect, there is no difference between the two lines.

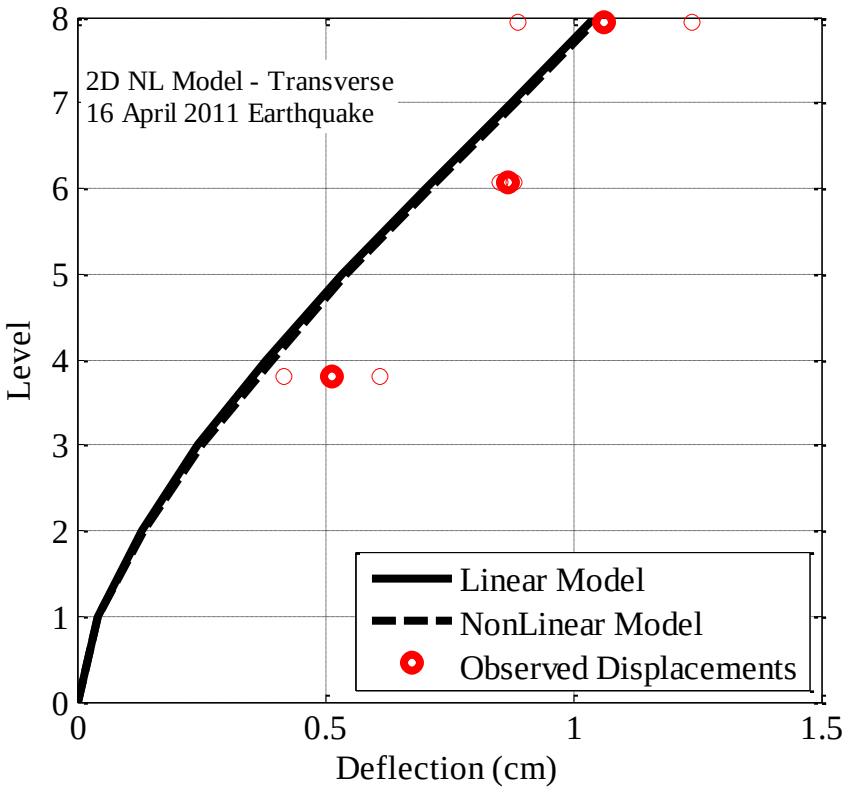


Figure 7-12: Comparison of the maximum deflected shape between observations and the 2D transverse NL model for the 16 April 2011 earthquake. Note that the thin circles represent the observed end shear wall displacements while the thick circles represents the average of the two responses.

In order to investigate any possible non-linear behaviour, the fixed-base NL model was subjected to the largest ground motion which occurred during the 4 September 2010 earthquake (i.e. Figure 4-4 in Chapter 4). The predicted transverse displacement response under the 4 September 2010 earthquake loading is shown in Figure 7-13. The NL model appears to match the observations very well with only the peak response at 19 seconds under-predicted. Another slight difference is the apparent increase in period of model after 22 seconds which does not match the observations.

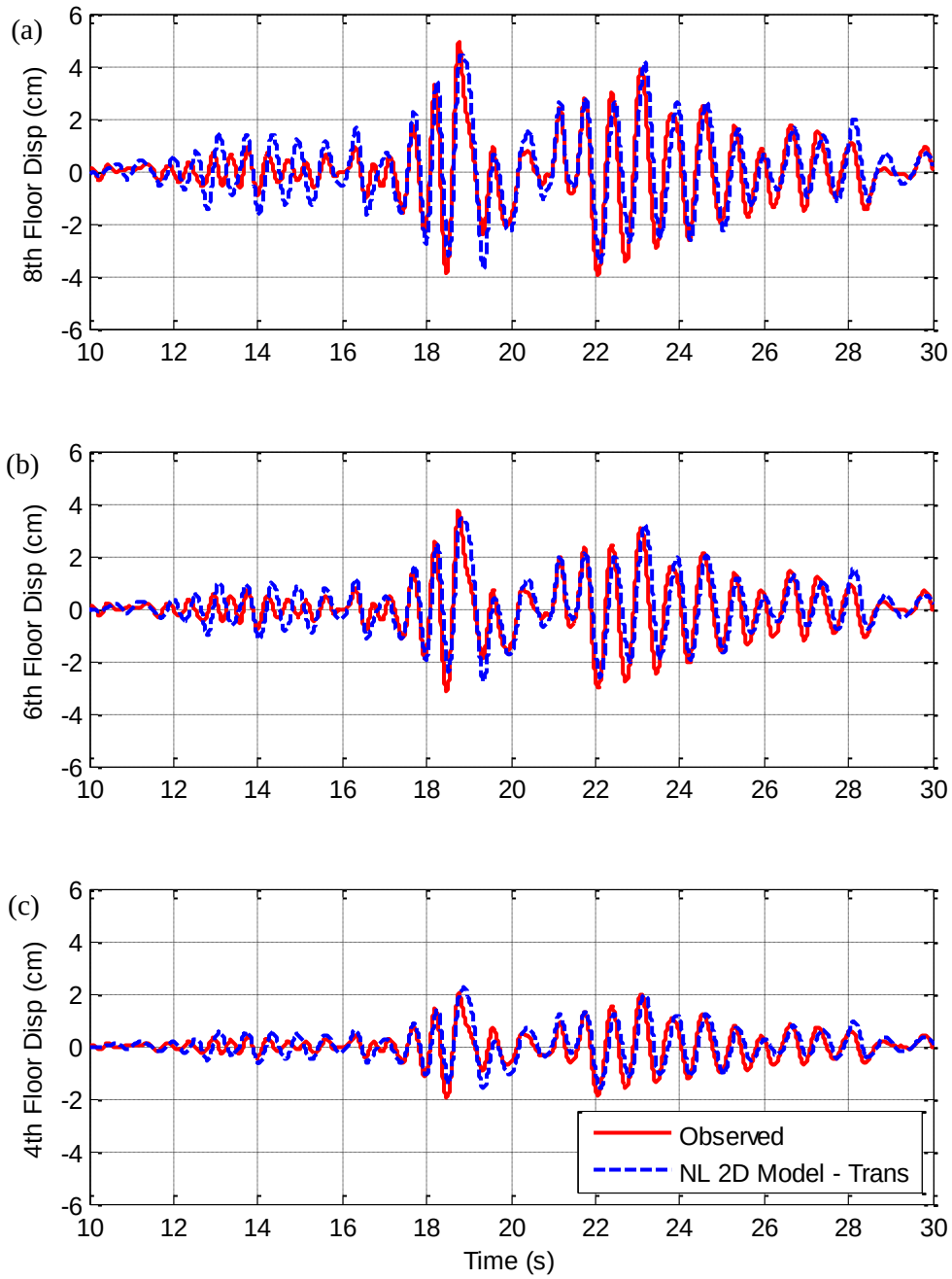


Figure 7-13: Comparison between the displacement time histories of the observations and 2D transverse non-linear model for the 4 September 2010 earthquake: (a) 4th; (b) 6th; and (c) 8th floor responses.

The effect of the non-linear behaviour can be more clearly seen in Figure 7-14 which compares the maximum displacement profiles of the linear and non-linear models. The non-linear behaviour has significantly reduced the maximum displacements response, particularly on the upper floors.

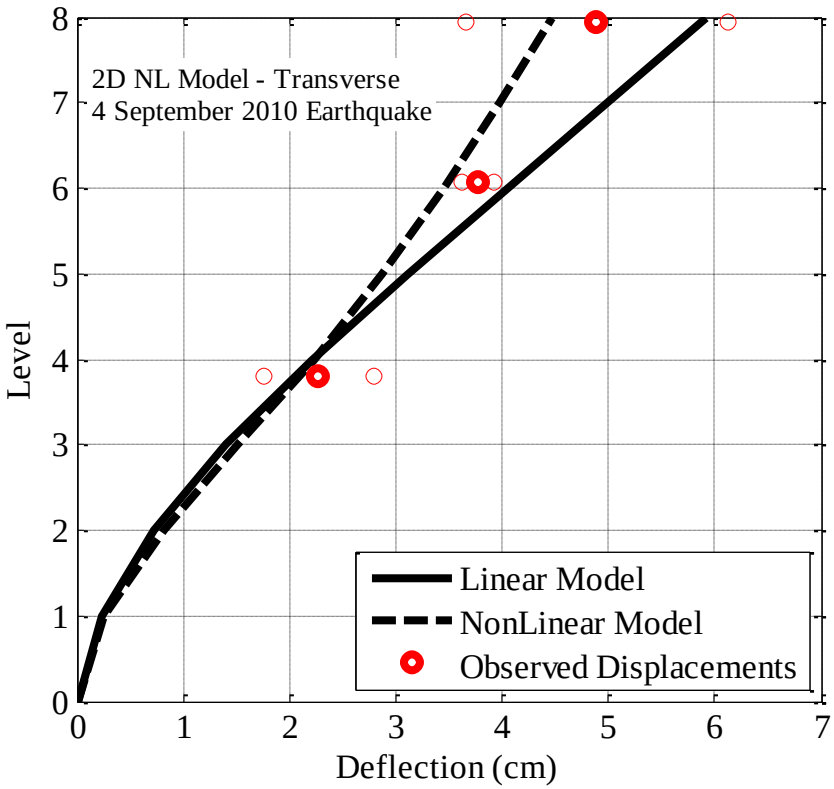


Figure 7-14: Comparison of the maximum deflected shape between observations and the 2D transverse NL model for the 4 September 2010 earthquake. Note that the thin circles represent the observed end shear wall displacements while the thick circles represents the average of the two responses.

The moment-curvature relationships for the non-linear elements in the transverse direction under the 4 September 2010 earthquake are shown in Figure 7-15. It can be seen that the first six floor beams have significant non-linear behaviour while the top two floor beams and wall base remain linear elastic. The maximum curvatures were predicted to occur in the second and third floor beams.

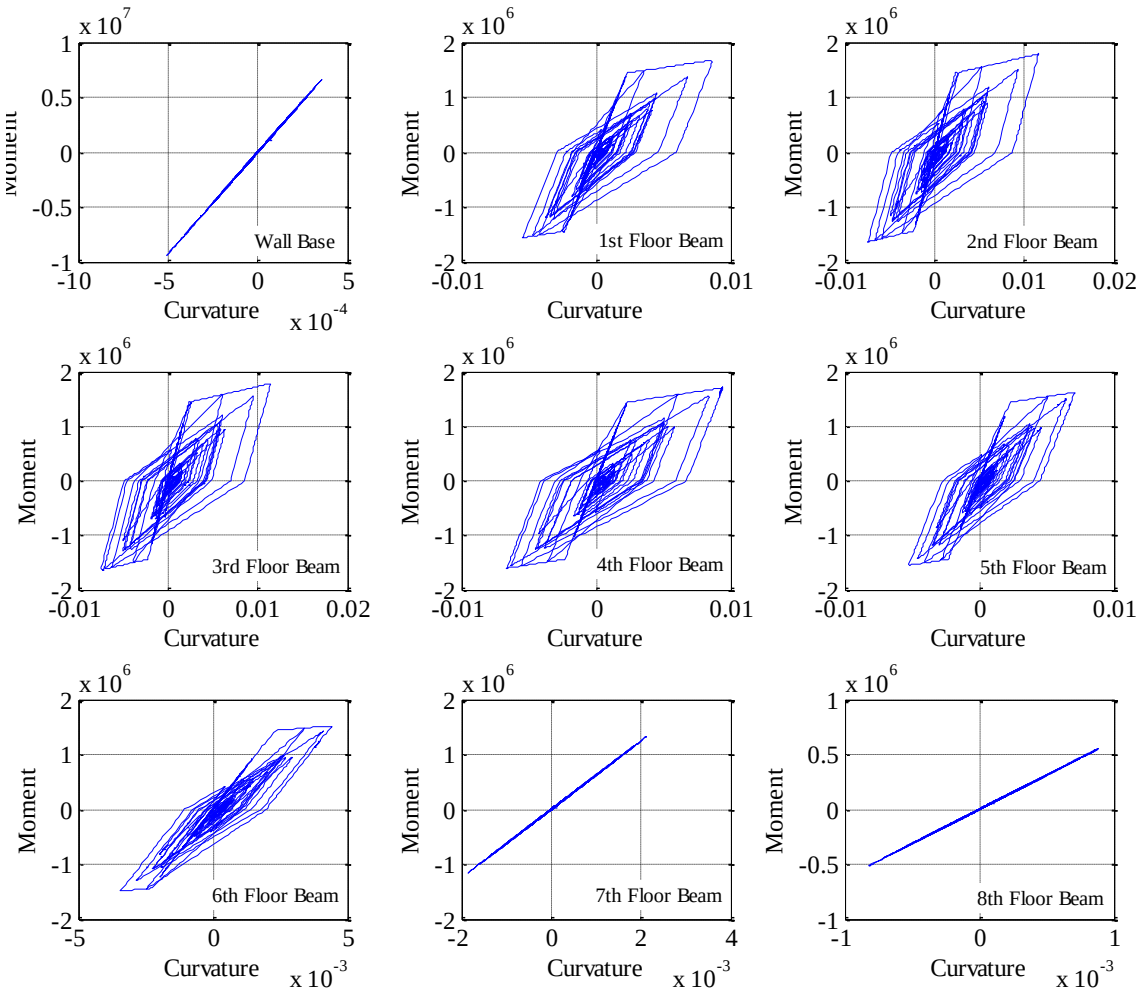


Figure 7-15: Moment curvature plots from the plastic hinge zone for the base of the wall and end of the beams on all floors for the transverse fixed base model in the 4 September 2010 earthquake.

The comparison between the predicted deflected shape from the fixed base linear and non-linear transverse models for all earthquake events is shown in Figure 7-16 It can be seen that the predicted response under-predicts the observed response for all events. There are multiple events where it appears that there was a small non-linear response including 26 December 2010, 22 February 2011, 13-1 June 2011, 13-2 June 2011 and 23-2 December 2011.

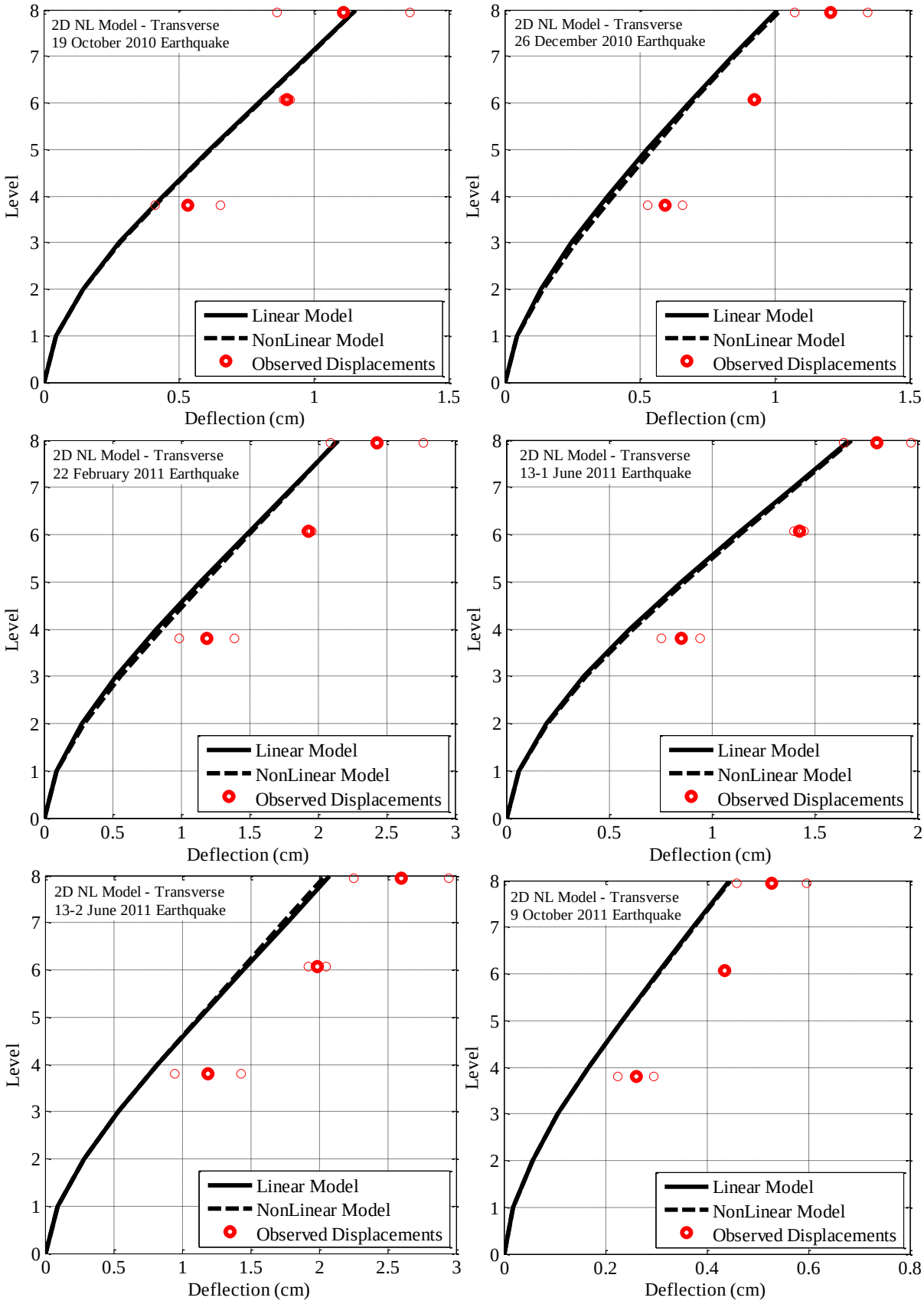
2D NL Model - Transverse
19 October 2010 Earthquake
2D NL Model - Transverse
26 December 2010 Earthquake
2D NL Model - Transverse
22 February 2011 Earthquake
2D NL Model - Transverse
13-1 June 2011 Earthquake
2D NL Model - Transverse
13-2 June 2011 Earthquake
2D NL Model - Transverse
9 October 2011 Earthquake
Linear Model
NonLinear Model
Observed Displacements
Level
Deflection (cm)

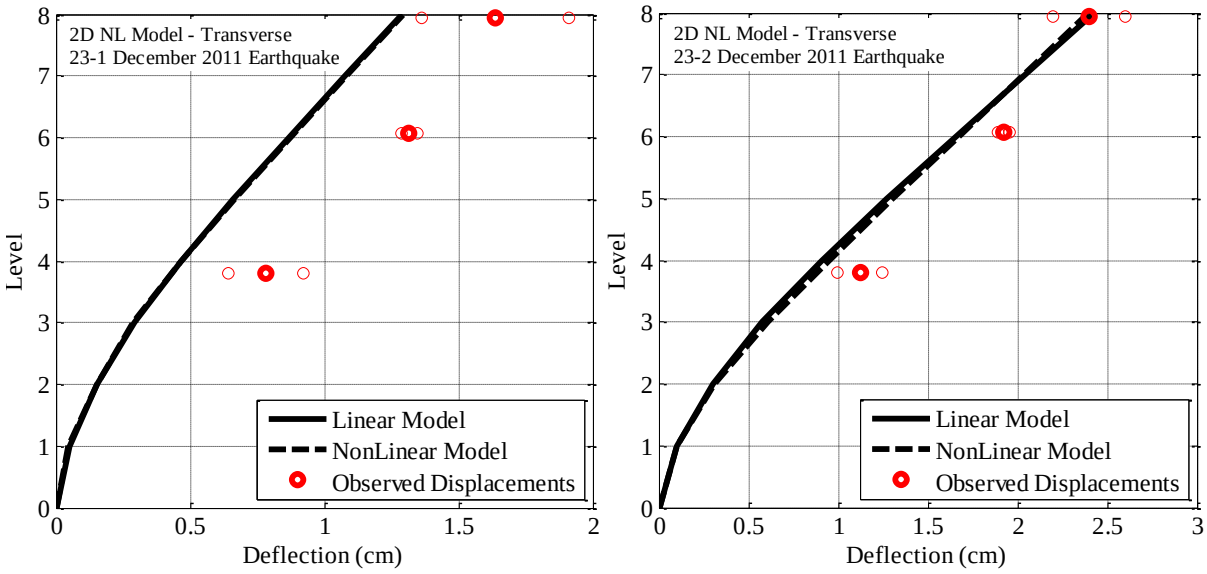


Figure 7-16: Comparison of the maximum deflected shape between observations and the 2D transverse NL model for all earthquakes.

The fixed base, non-linear transverse response for all earthquakes is shown in Figure 7-17. The non-linear maximum displacement response of the smaller ground motion records is expected to be the same as the linear response as no non-linear behaviour would have occurred. The deflected shapes, from all but one earthquake, are all similar with the exception being the 4 September 2010 earthquake. It was predicted that there was significant non-linear behaviour during this earthquake which resulted in the deflected shape profile changing. The under-prediction of the other events is likely the result of neglecting SSI effects and hence this is considered in the next section.

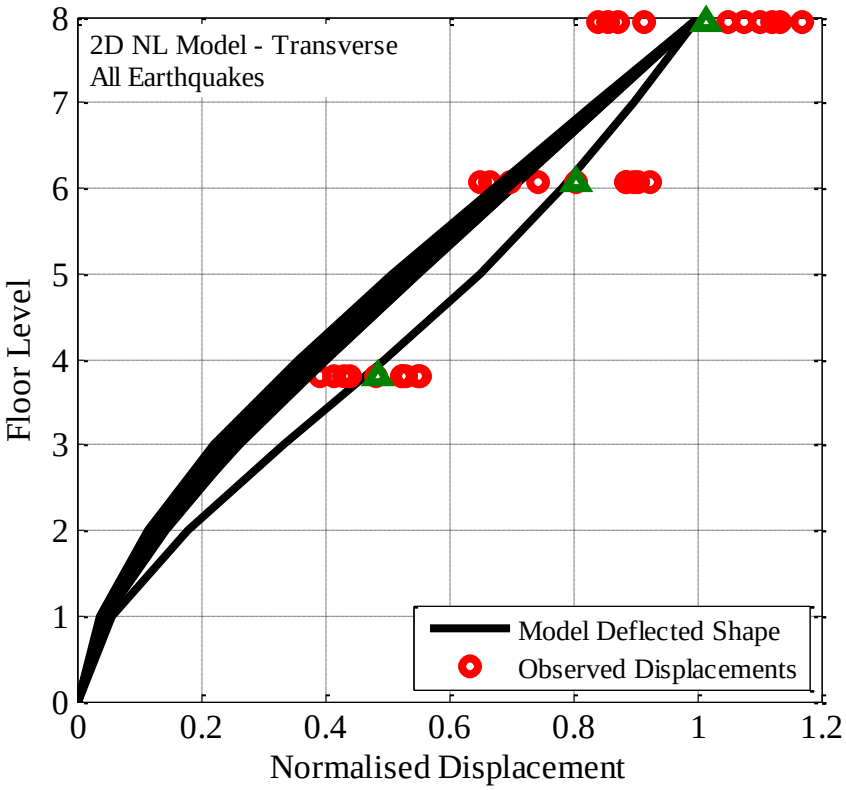


Figure 7-17: Comparison of the normalised maximum deflected shape between observations and the 2D transverse NL model for all earthquakes.

## 7.4 2D non linear SSI model

It was decided that due to the lack of SSI effects inferred in the longitudinal direction (refer to Figure 6-10 in Chapter 6), that only the transverse SSI model would be adjusted to allow for non-linear behaviour. The non-linear beam elements from the transverse non-linear model were combined with the SSI elements from the transverse Winkler beam model. It was shown in Chapter 6 that the Winkler beam SSI model provided the best predictions out of the three SSI models considered.

Figure 7-18 illustrates the displacement response history of the NL SSI transverse model for the 4 September 2010 earthquake. The model predicts the response very well except for the small amplitude response in the first 18 seconds. The predicted rotational response shown in Figure 7-18 (d), does not match the observed response. However, the large peaks between 18-22 seconds do not resemble a rocking response of the base and could be a result of differential settlement. As this type of behaviour was not accounted for in the modelling process, it was decided that the predicted rocking response was sufficient for this event.

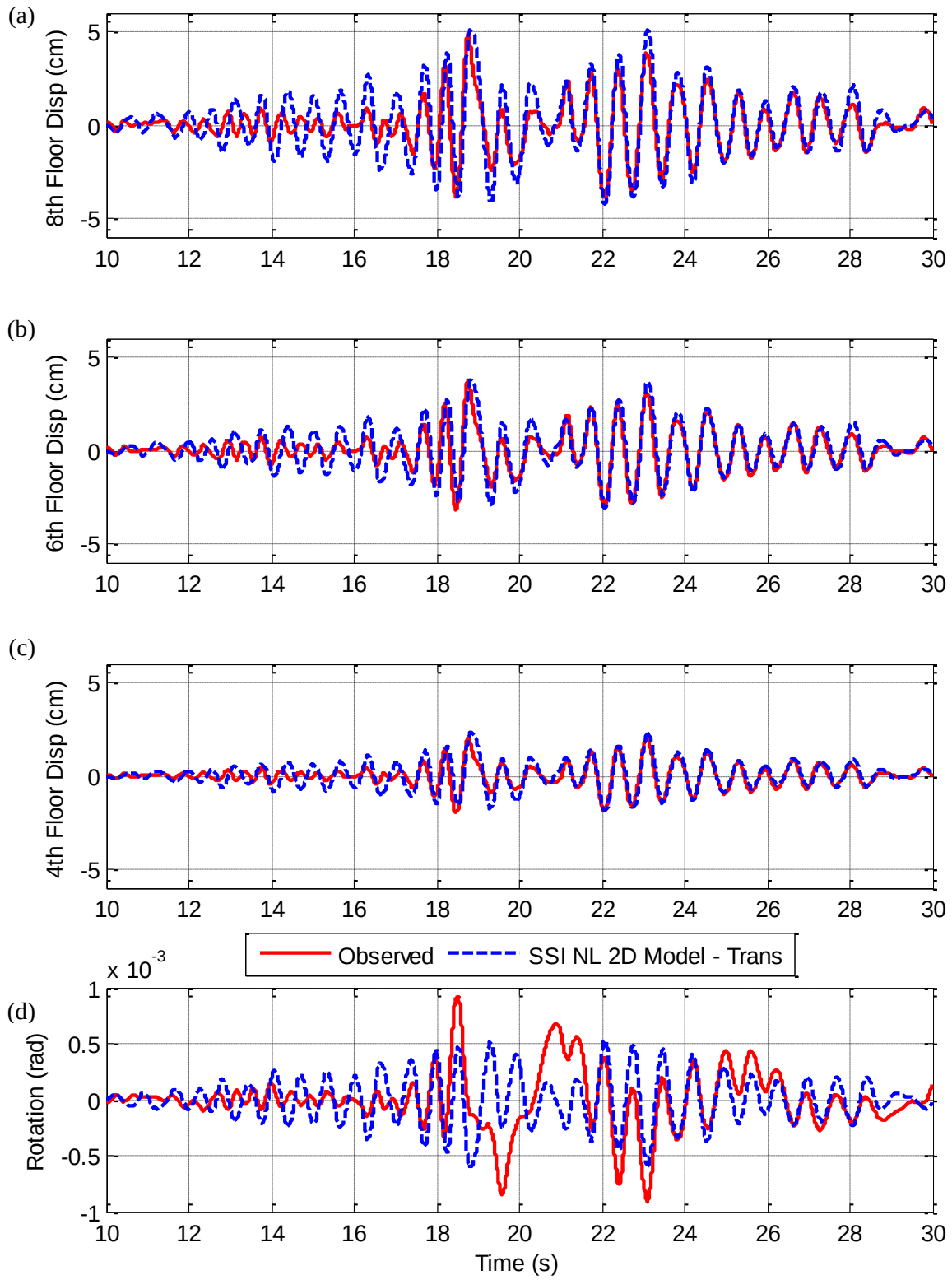


Figure 7-18: Comparison of the (a) 8th; (b) 6th, and (c) 4th floor responses and (d) .rotational response histories and the observations for 2D transverse NL SSI model in the 4 September 2010 earthquake.

The maximum displacement predictions from the NL SSI transverse model for the 4 September 2010 earthquake are shown in Figure 7-19. It can be seen non-linear behaviour has again reduced the response of the higher floors similar to the fixed base NL model in Figure 7-14. The predicted

response is very similar to the observations on all floors however, the predicted rocking displacement under-predicts the observed rocking due to reasons explained earlier.

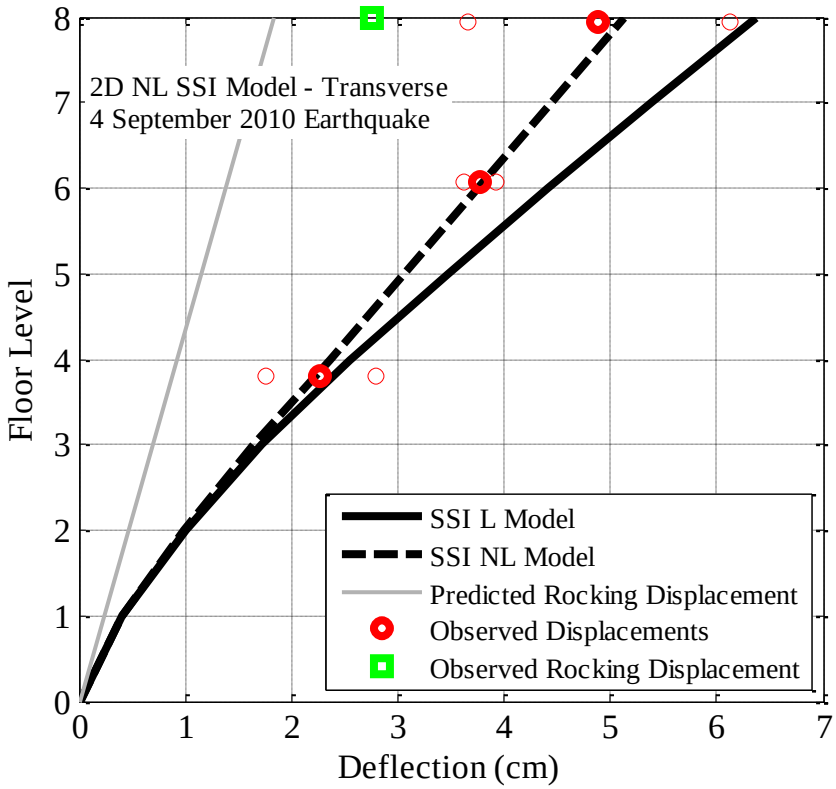


Figure 7-19: Comparison of the maximum deflected shape between observations and the 2D transverse NL SSI model for the 4 September 2010 earthquake.

The moment-curvature relationships for the NL SSI transverse model under the 4 September 2010 earthquake are shown in Figure 7-20. The first six floor beams all have non-linear behaviour in this model while the other beams and wall base remain linear. The predicted curvatures in the SSI transverse model is equal to approximately half of those found in Figure 7-15 from the fixed base transverse model. The decrease in the maximum curvatures of lower floor beams is due to the rotation at the base in the SSI model. This results in lower rotational demands in the beams due to relative displacements within the structure itself (Mylonakis & Gazetas, 2008).

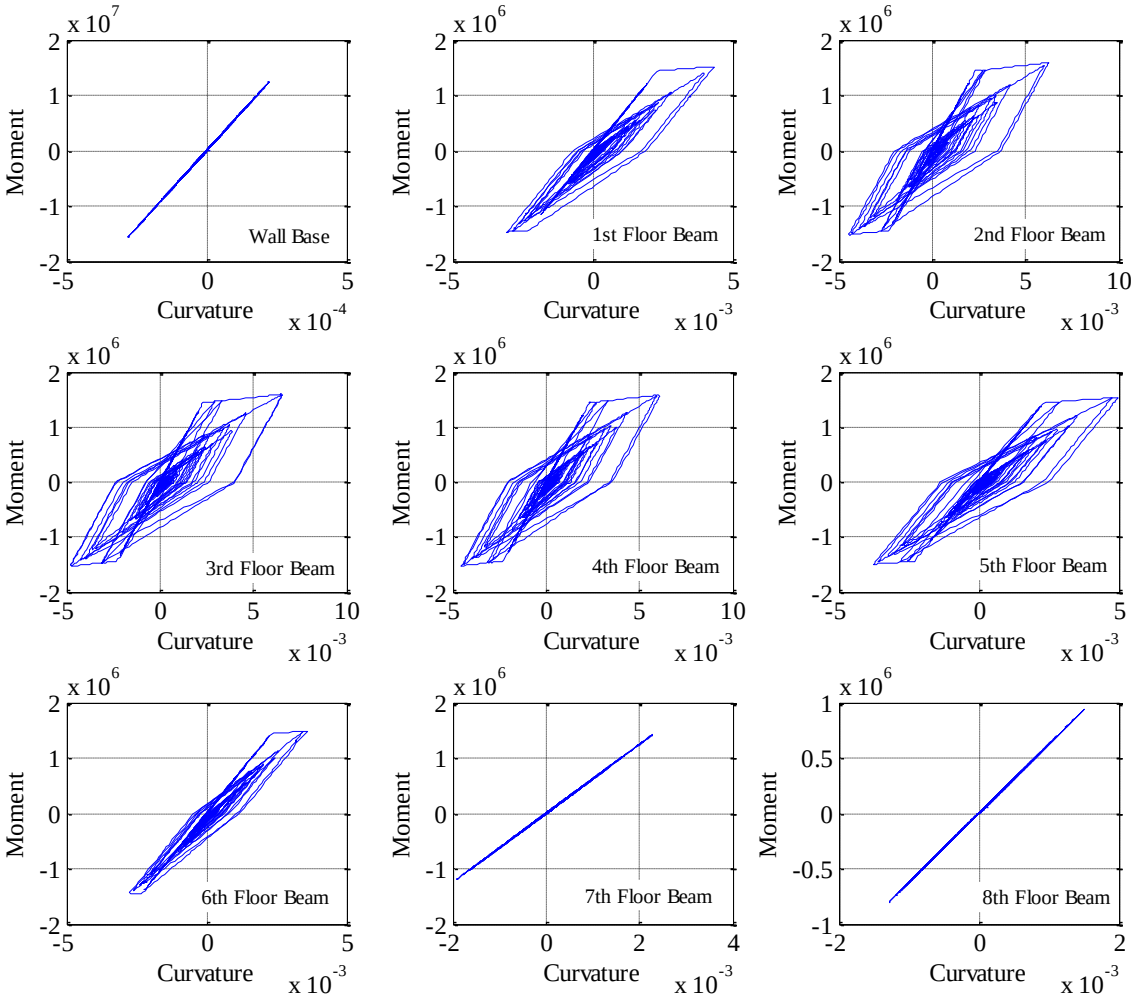


Figure 7-20: Moment curvature plots from the plastic hinge zone for the base of the wall and end of the beams on all floors for the transverse SSI model in the 4 September 2010 earthquake.

The comparison between the predicted deflected shape from the SSI linear and non-linear transverse models for all earthquake events is shown in Figure 7-21. It can be seen that the predicted response under-predicts the observed response for all events. There are multiple events where it appears that there was a small non-linear response including 26 December 2010, 22 February 2011, 13-1 June 2011 and 13-2 June 2011 and a significant non-linear response during the 23-2 December 2011.

**Effects of Non-Linear & Torsional Behaviour on Model Prediction**

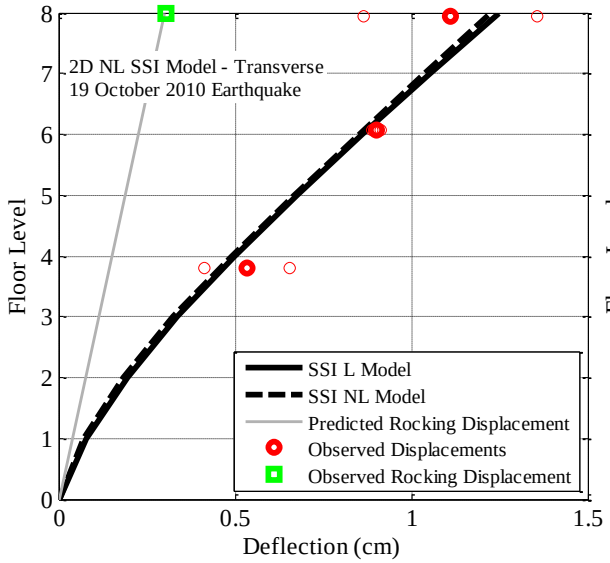


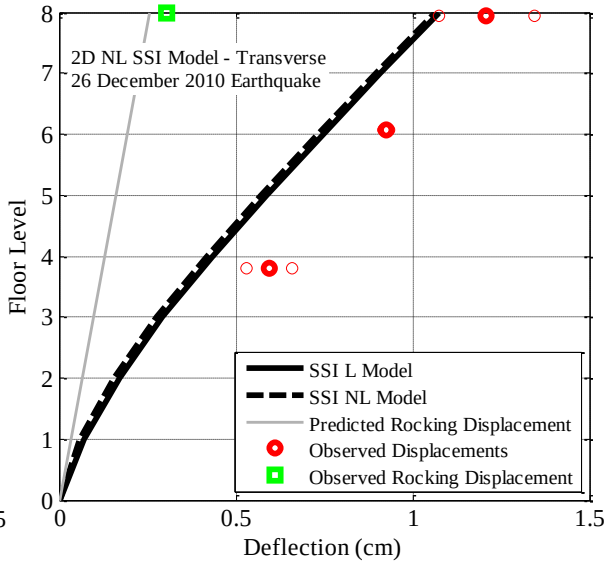


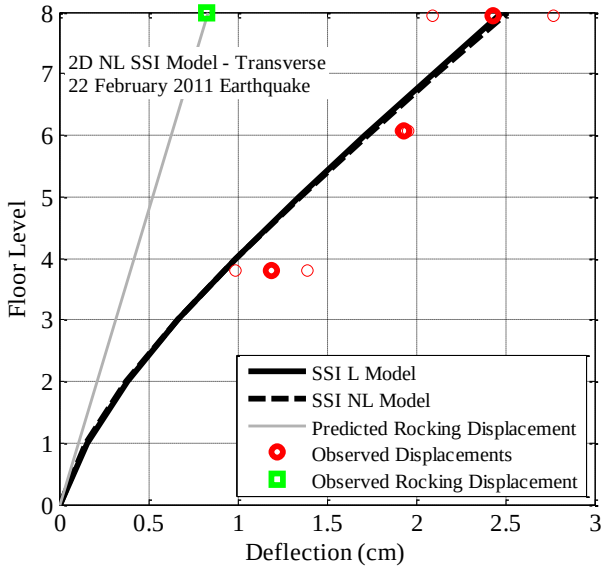


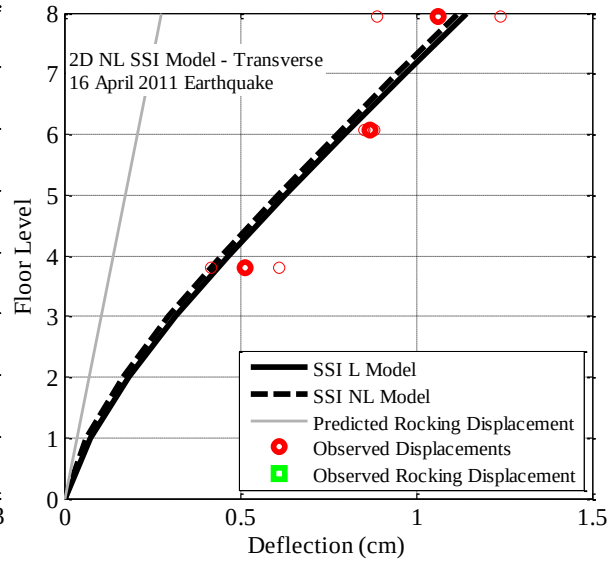


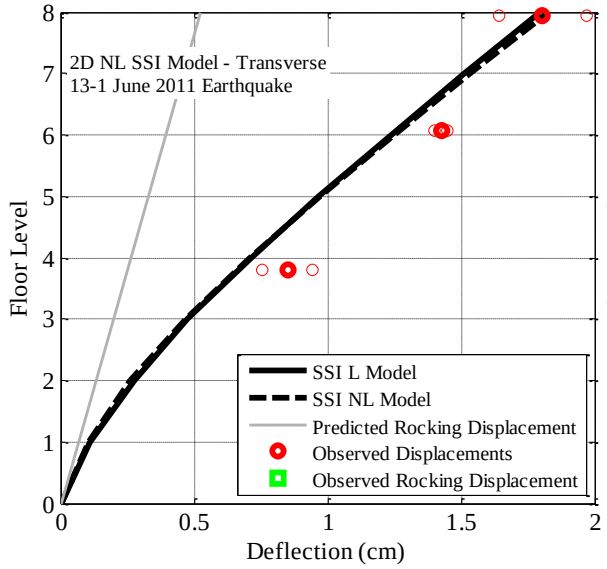


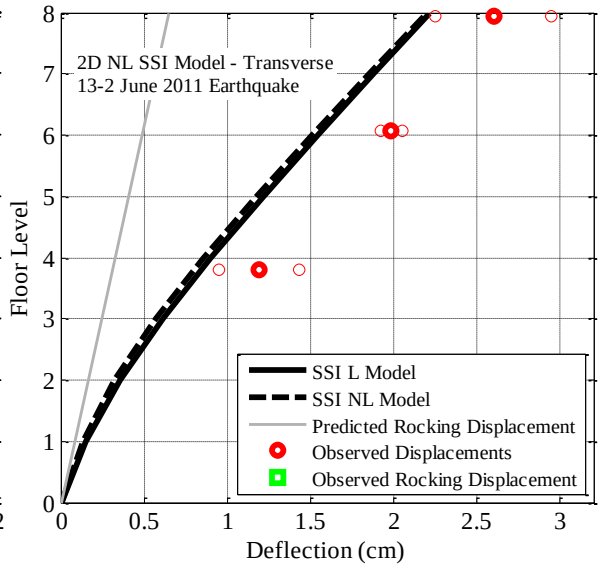

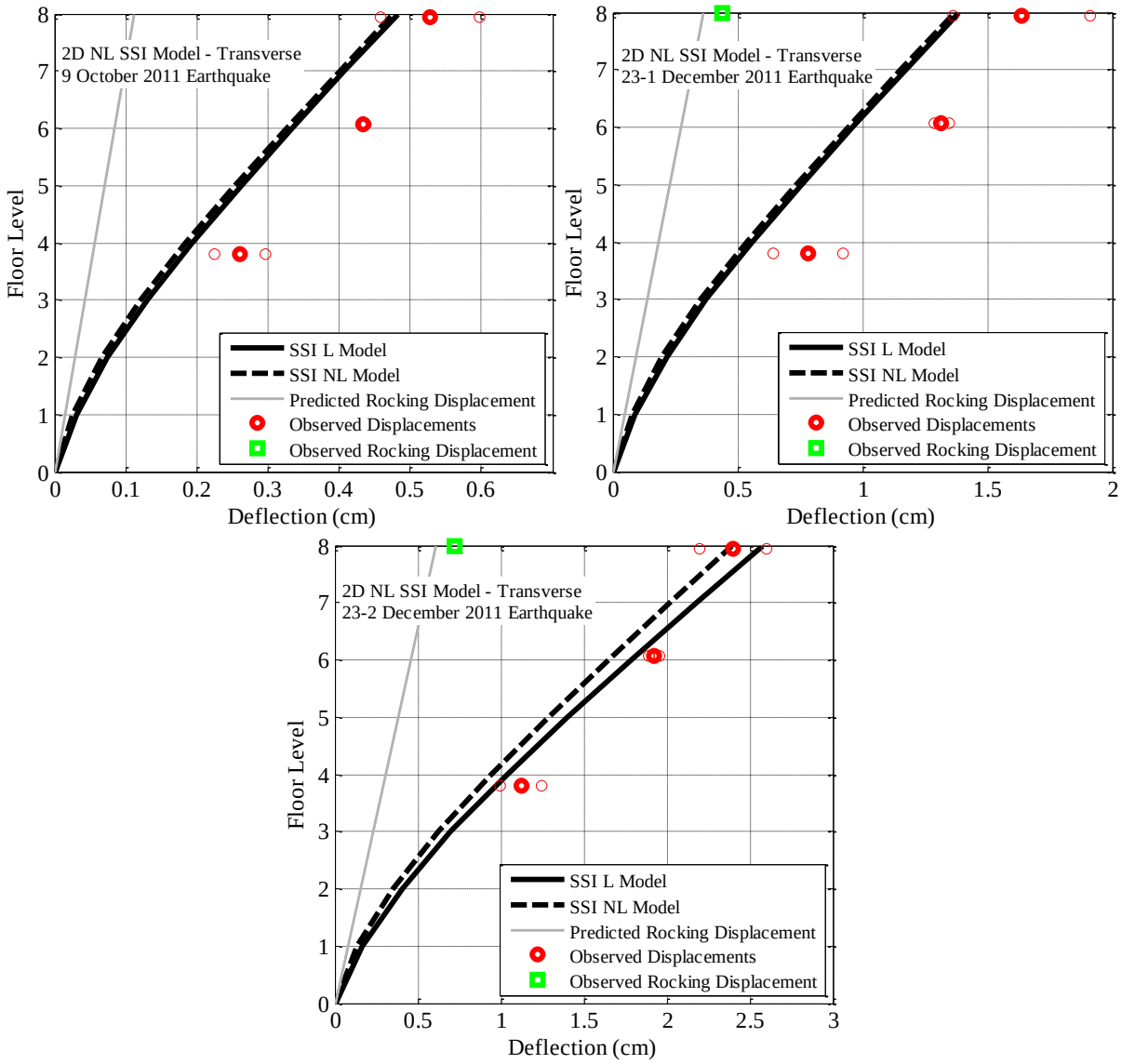


Figure 7-21: Comparison of the maximum deflected shape between observations and the 2D transverse NL SSI model for all earthquakes.

The normalised response of the NL SSI transverse model for all earthquakes is shown in Figure 7-22. The normalised deflected shape from each event is very similar and even with the inclusion of SSI and NL behaviour, the model still under-predicts the maximum response of the fourth and sixth floors. The predicted rocking displacements still match the observed rocking except for the 4 September 2011 earthquake.

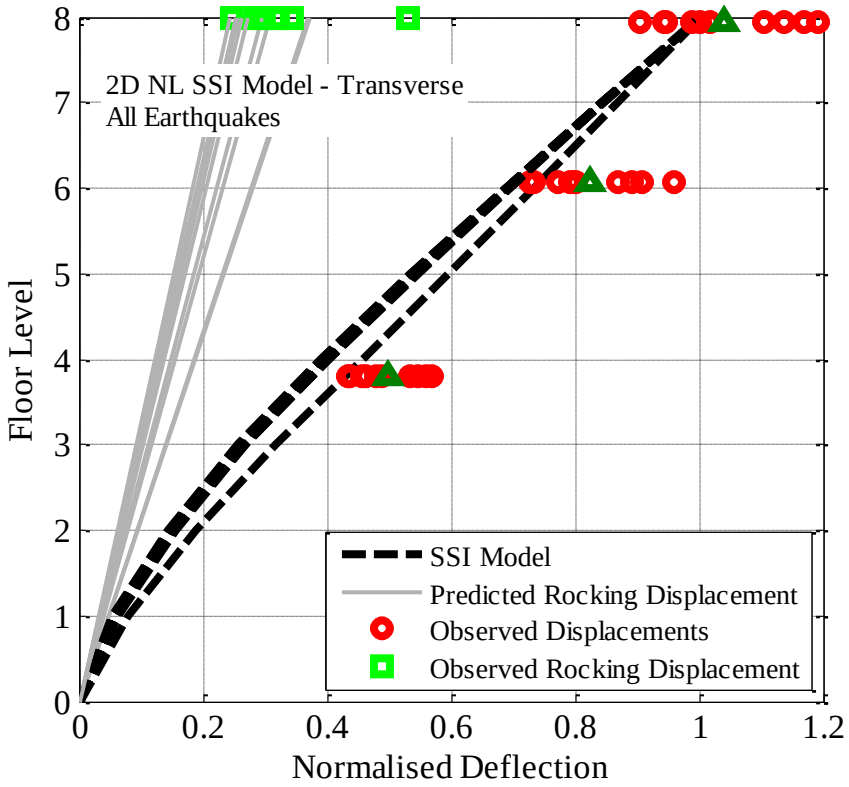


Figure 7-22: Comparison of the normalised maximum deflected shape between observations and the 2D transverse NL SSI model for all earthquakes.

## 7.5 Sequential earthquake loading

The transverse non-linear response for all earthquakes shown in Figure 7-17 and Figure 7-22 assumes that the building had no damage (residual displacements or curvatures) at the start of the analysis. This would not be the case in reality as the initial state of the structure should include the residual displacements (if any) after the 4 September 2010 earthquake. The effect of the sequential loading was examined using the SSI linear and non-linear models under the 22 February 2011 earthquake. The non-linear response under the 22 February earthquake alone was compared with a combined earthquake consisting of the 4 September 2010 earthquake plus the 22 February 2011 earthquake.

The acceleration record from the combined earthquakes is shown in Figure 7-23 (a). Figure 7-23 (b) shows the displacement time series for the fourth floor for the observations, 22 February 2011 earthquake only and the combined response. There is a gap of ten seconds between the acceleration time series from the two earthquakes in order to allow time for the building to come to rest before the second earthquake (Raghunandan *et al.*, 2012). Figure 7-23 (c) compares the response of both models to the 22 February 2011 earthquake. It can be seen that the combined earthquake response has an increased effective period after the initial large displacement cycle (at 69 seconds) which causes the model to be out of phase with the observations from that point onwards. Although this type of

loading is more realistic, it relies on the final state of the building being correct after the initial earthquake. This error could be attributed to the uncertainty in defining the parameters in the constitutive models.

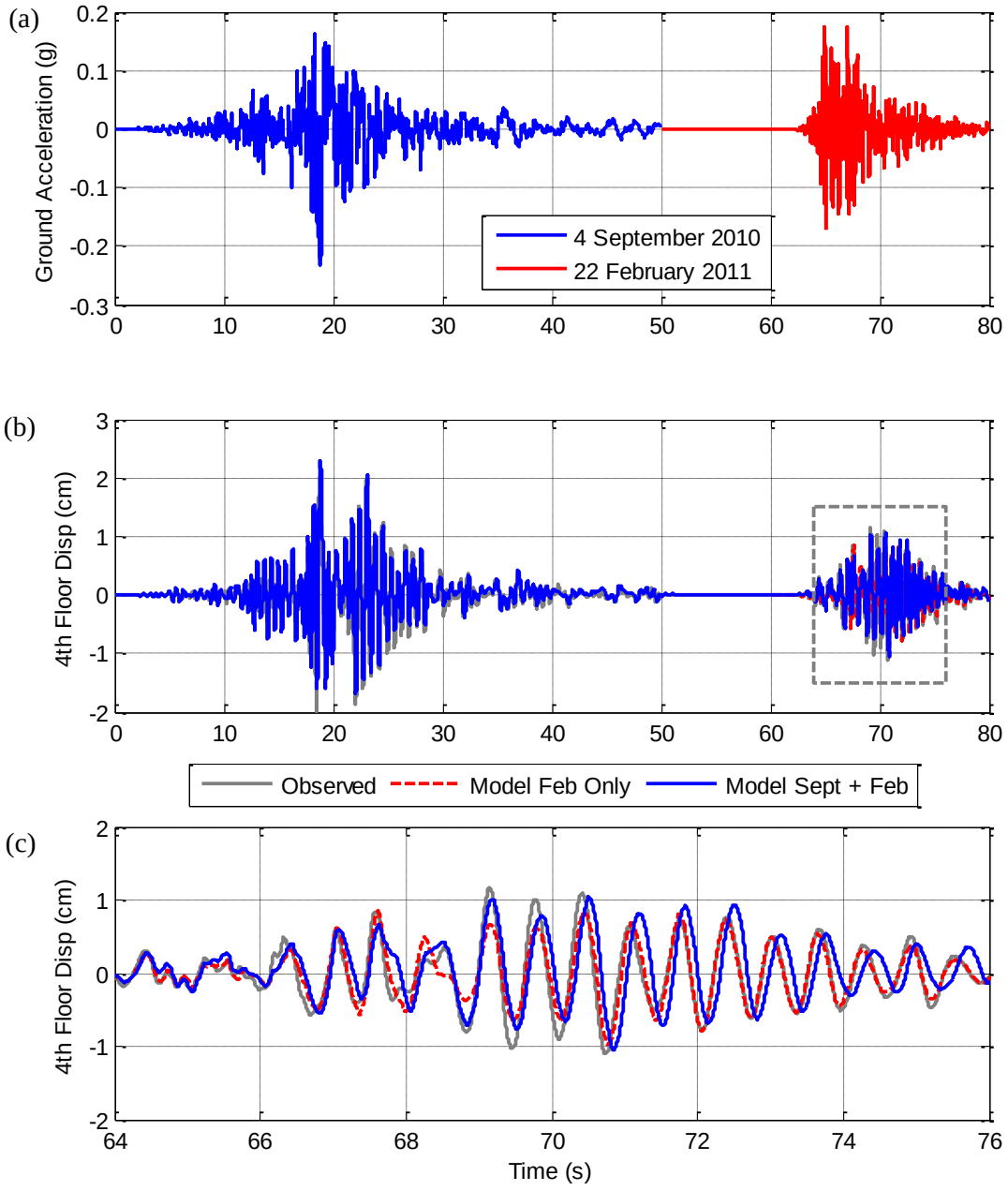


Figure 7-23: (a) Combined 4 September 2010 and 22 February 2011 earthquake acceleration time series. (b) and (c) Fourth floor displacement response predicted by non-linear transverse model for the 22 February 2011 earthquake only and the 4 September 2010 plus 22 February 2011 earthquakes.

The change to the maximum displacement response for the combined earthquake sequence is shown in Figure 7-24. It can clearly be seen that the combined earthquake loading has significantly increased the maximum deflected shape however, as shown in Figure 7-23, the displacement response appears to have a larger period causing the predicted response to be out of phase with the observations and therefore less accurate.

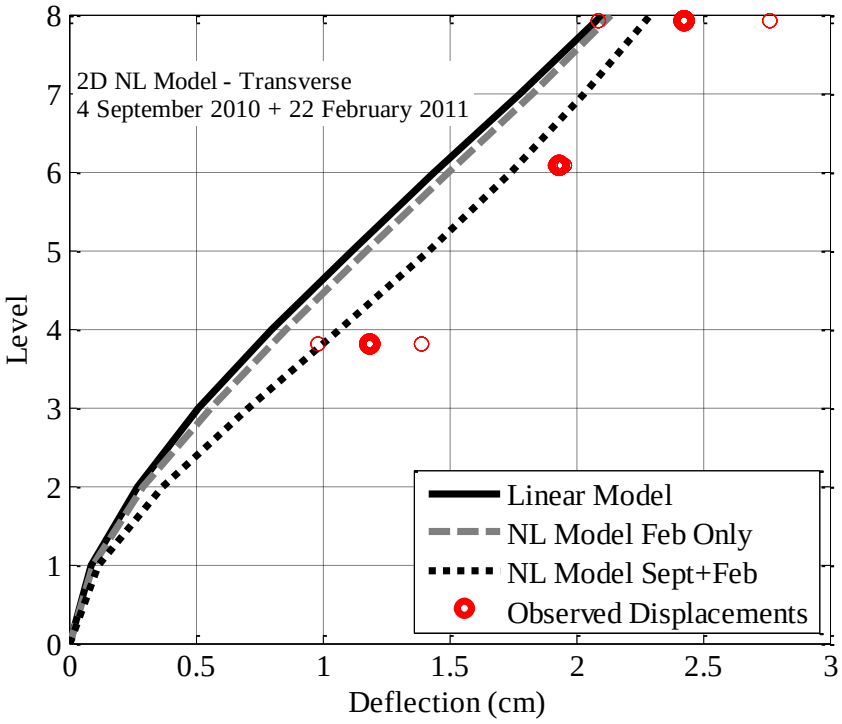


Figure 7-24: Comparison of the maximum deflected shape between observations and the 2D transverse NL model for the 22 February 2011 earthquake after initially being loaded under the 4 September 2010 earthquake.

## 7.6 Comparison of all 2D models

In order to compare the predictions of all three longitudinal models and four transverse models, a new comparison measure is used. This is done using the error ratio which is calculated by dividing the predicted displacement on the fourth, sixth and eighth floors by the observed displacement on the same floor. If the prediction is the same as the observation, then the error ratio will be one. Therefore a perfect model prediction would be straight line equal to one. This method is used to examine the predictive capability of all the longitudinal and transverse models.

### 7.6.1 Longitudinal models

Figure 7-25 shows the error ratio from the three longitudinal models for all events. The longitudinal models considered were the fixed base linear, SSI linear and fixed base non-linear models. The different markers show the error ratio from each earthquake event while the solid lines show the

average error ratio from each model. The dotted lines show the standard deviation of the error ratios for each model. It can be seen in the figure that the average error from all models is very similar however, they all under-predict the displacement by approximately 5% on each floor. The standard deviation of the error ratios is generally on the order of 10-15% indicating that one can be 66% confident (i.e. ± 1 σ) that the model prediction is within 10-15% of the true response.

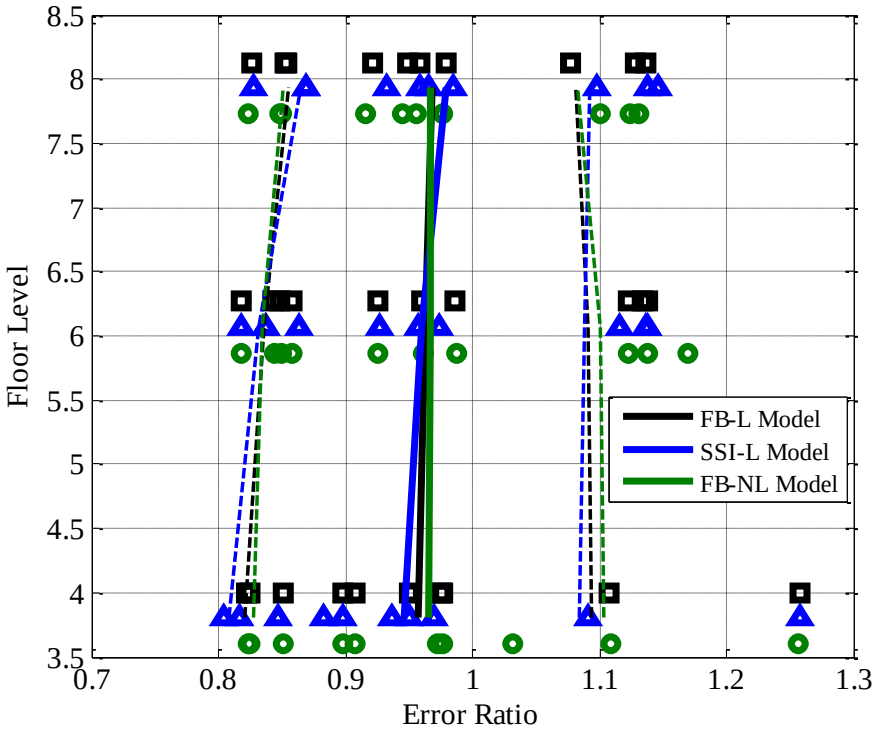


Figure 7-25: Error ratio from all earthquakes for the fixed base linear and non-linear longitudinal models. Solid lines represent the average error ratio for each model, while dashed lines represent the [16th, 84th] percentile range. The observed error ratios have been offset vertically in the y-axis for clarity.

The average percentage error from the three longitudinal models can be found in Table 7-3. The three models have similar average errors and however, the best model appears to be the NL fixed base model with an average error of 2.7%.

Table 7-3: Average percentage error of all 2D Longitudinal models compared with observations.

| | **Longitudinal** | | |
|---|---|---|---|
| | **2D FB - L** | **2D SSI - L** | **2D FB - NL** |
| 8th Floor | -2.8% | -2.0% | -2.7% |
| 6th Floor | -4.0% | -4.3% | -3.6% |
| 4th Floor | -2.6% | -3.2% | -1.8% |
| **Average** | **3.1%** | **3.2%** | **2.7%** |

The effect of the base flexibility and non-linear behaviour can be investigated by plotting the maximum predicted curvature of the eight beams and wall base for all earthquakes. This allows for further examination of the effect from the base flexibility and NL assumptions on the curvature demand of the members. Figure 7-26 shows the predicted curvature demand of the members for the four models in the 4 September 2010 earthquake. It can be seen that the SSI has practically no effect on the curvature demand, while the non-linear behaviour causes increases curvature on all floors expect the top three.

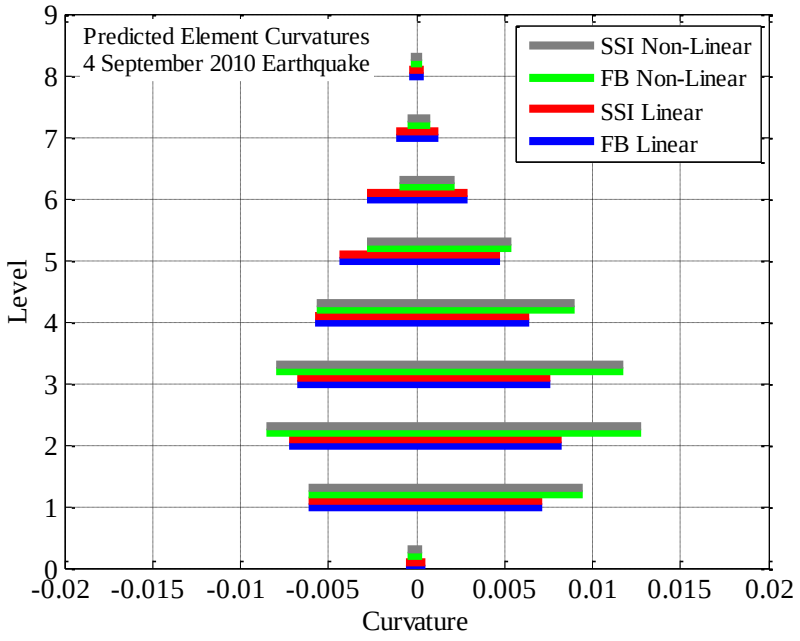


Figure 7-26: Maximum base and beam curvatures from the four 2D longitudinal models for the 4 September 2010 earthquake.

The maximum curvature versus level for the 22 February earthquake is shown in Figure 7-27. In this case, the non-linear behaviour causes and increase to the curvature demand on all floors. The effect of SSI again has no influence on the curvature demand of the beam and wall members.

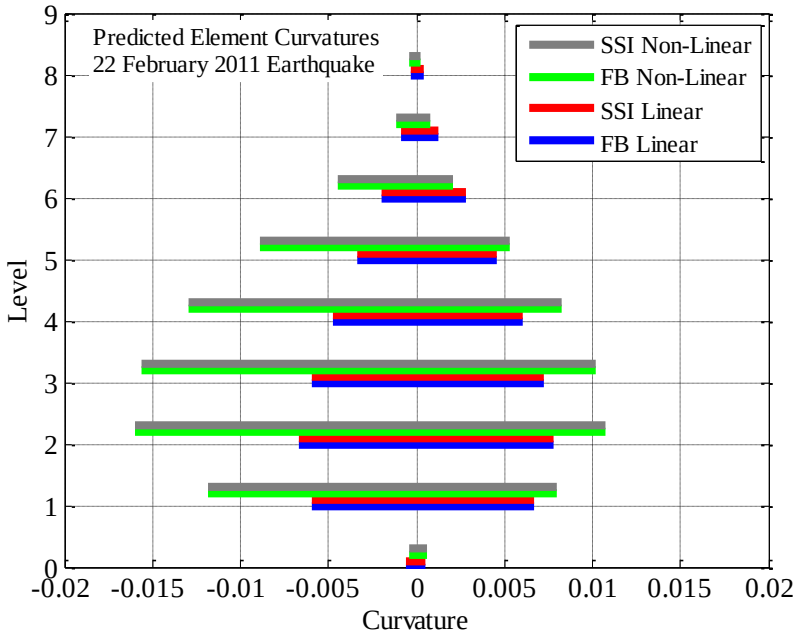


Figure 7-27: Maximum base and beam curvatures from the four 2D longitudinal models for the 22 February 2011 earthquake.

The maximum predicted curvature versus level is plotted for all other earthquakes in Figure 7-28. It can be seen that there was non-linear behaviour in four of the other earthquakes as the curvature in the non-linear models is different than the linear models. The SSI also has no effect on the on the predicted curvature demand for all earthquakes.

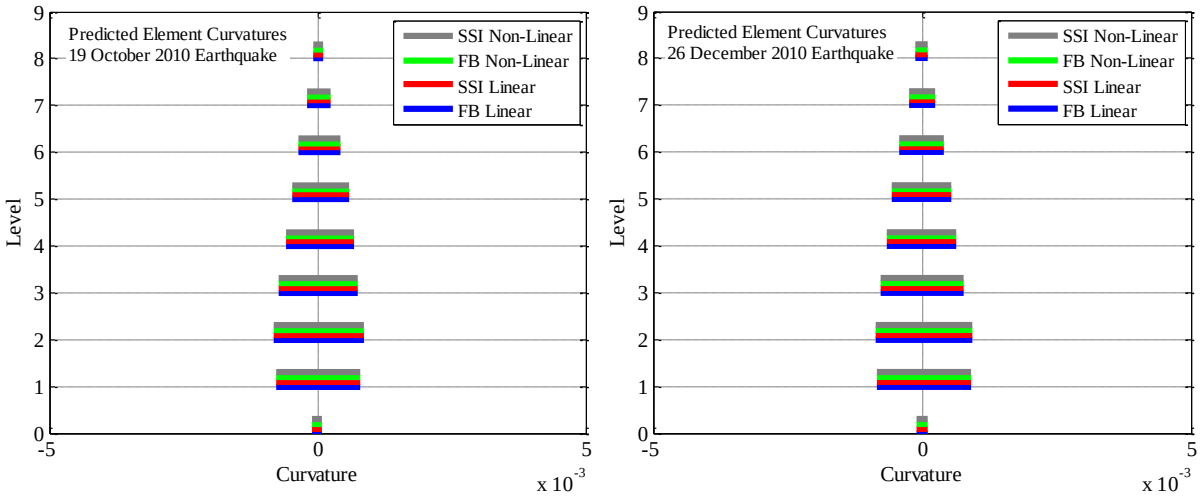

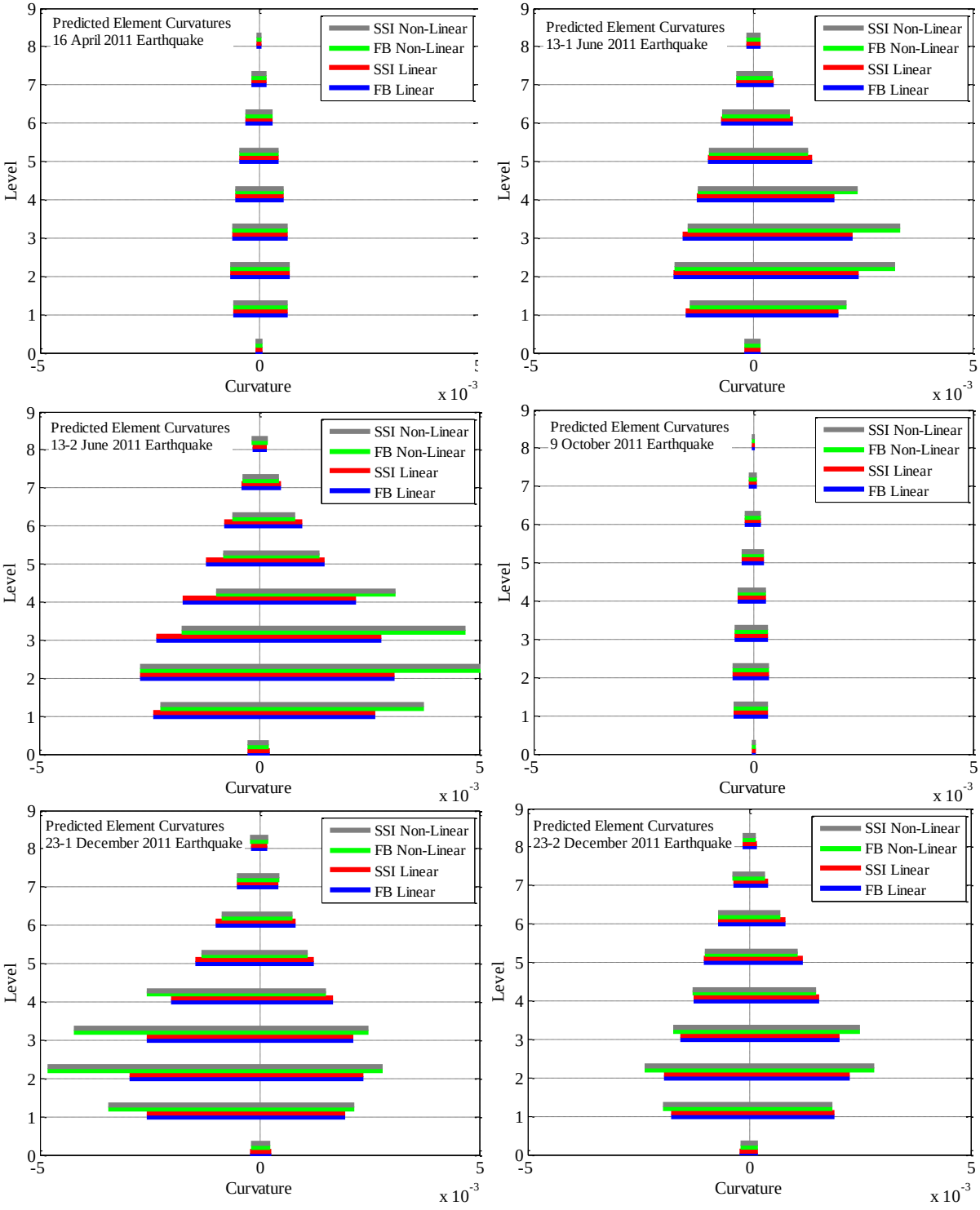


Figure 7-28: Maximum base and beam curvatures from the four 2D longitudinal models for all earthquakes.

### 7.6.2 Transverse models

The error ratios for each earthquake event along with the average from the four transverse models are shown in Figure 7-29. The four transverse models that are compared include the fixed base linear model, SSI linear model, fixed base NL model and SSI NL model. The main difference between the four models is from the inclusion of the SSI effect where the two models with SSI produce predictions 10% better than the fixed base modes. The inclusion of NL behaviour has a minimal effect on the overall prediction accuracy however, as shown previously it significantly improved the 4 September 2010 event predictions.

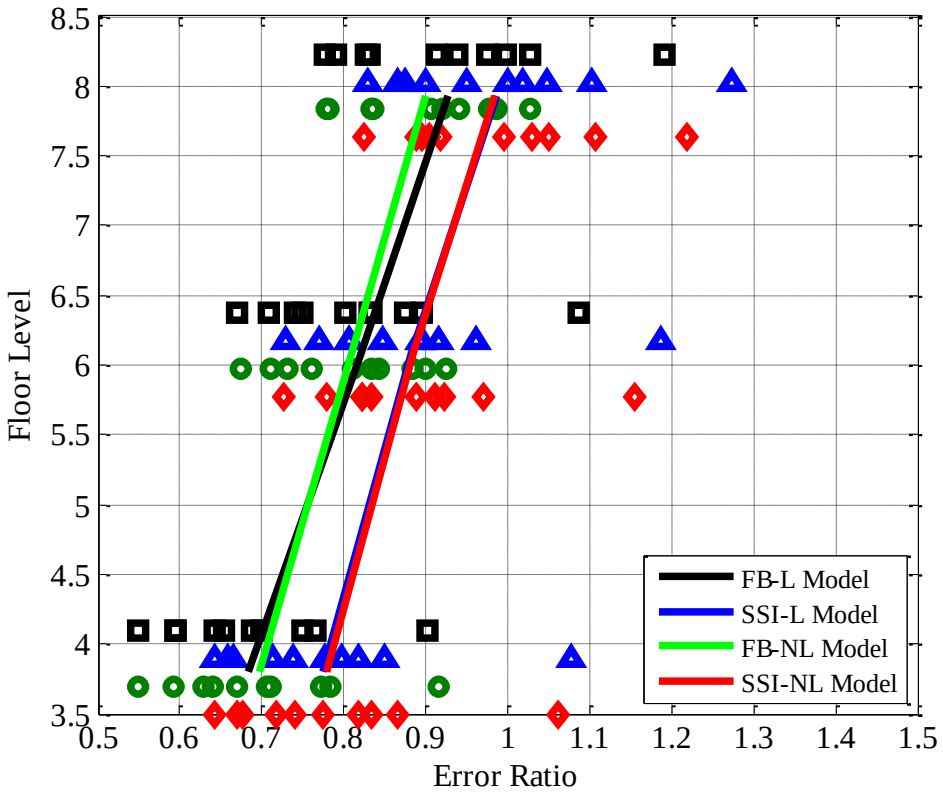


Figure 7-29: Error ratio from all earthquakes for the fixed base linear and SSI non-linear transverse models. Solid lines represent the average error ratio for each model. The observed error ratios have been offset vertically in the y-axis for clarity.

The average floor error ratio and the corresponding standard deviation or each model is shown in Figure 7-30. The standard deviation of the error ratios is generally on the order of 10-15%. The predictions from the SSI models are within one standard deviation for the displacements above the sixth floor however, below this all models are outside this confidence range.

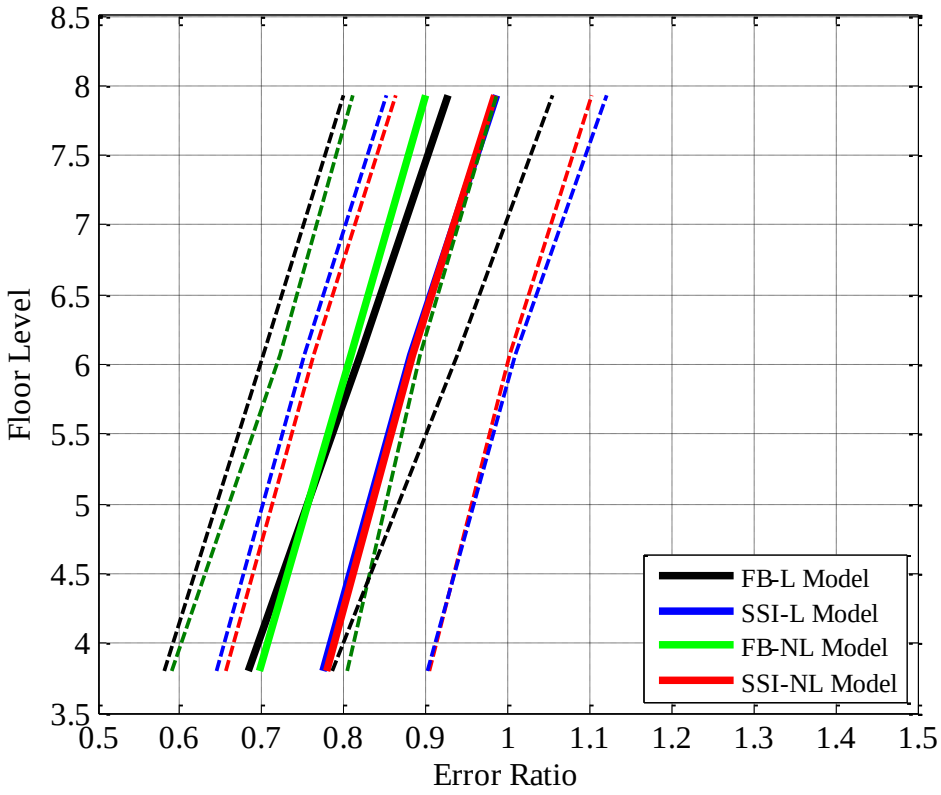


Figure 7-30: Average error ratio with standard deviation from all earthquakes for the fixed base linear and SSI non-linear transverse models. Solid lines represent the average error ratio for each model, while dashed lines represent the [16th, 84th] percentile range.

The average error ratio of all four of the transverse models (FB-L, SSI-L, FB-NL, SSI-NL) are compared in Table 7-4 It can be seen that the inclusion of the SSI provides the more significant increase in displacement compared with the non-linear effect. It appears that the SSI non-linear model provides the best predictions in the transverse direction with an average error of 6.3% per floor. The SSI linear model is also reasonably accurate with an average error of 7.3%.

Table 7-4: Average percentage error of all 2D Transverse models compared with observations.

| | **Transverse** | | | |
|---|---|---|---|---|
| | **2D FB - L** | **2D SSI - L** | **2D FB - NL** | **2D SSI - NL** |
| 8th Floor | -6.3% | 0.2% | 1.5% | 1.3% |
| 6th Floor | -15.5% | -10.5% | -16.3% | -8.2% |
| 4th Floor | -15.2% | -11.2% | -14.3% | -9.3% |
| **Average** | **12.3%** | **7.3%** | **10.7%** | **6.3%** |

The maximum predicted curvature versus level for all four transverse models during the 4 September 2010 earthquake is shown in Figure 7-31. The maximum curvature occurs in the second or third floor

beams for all models. It can been seen that the base flexibility in the SSI models causes a reduction in the maximum curvature for both the linear and non-linear models.

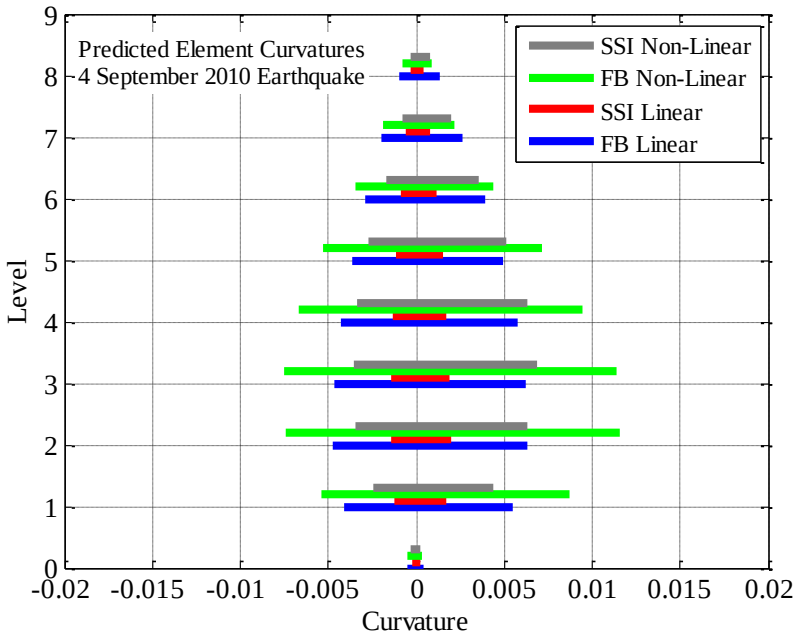


Figure 7-31: Maximum base and beam curvatures from the four 2D transverse models for the 4 September 2010 earthquake.

The maximum curvature profile for the 22 February 2011 earthquake, shown in Figure 7-32, is similar to the 4 September earthquake with SSI effects decreasing the beam curvatures on all floors. It can be seen that for the two models considering SSI (i.e. SSI-NL and SSI-L) provide essentially the same result, indicating that there was negligible NL behaviour. For the FB models (i.e. FB-NL and FB-L) a minor increase in curvatures on some levels due to non-linear behaviour was observed.

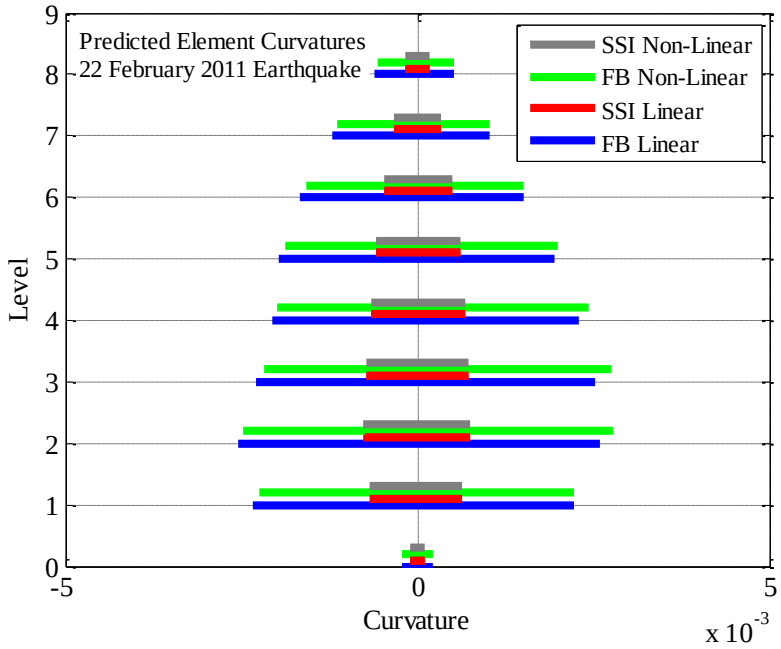


Figure 7-32: Maximum base and beam curvatures from the four 2D transverse models for the 22 February 2011 earthquake.

The maximum curvature profiles for the other earthquakes is shown Figure 7-33. It can be seen that the SSI reduces the predicted beam curvatures for all earthquakes. The second 13 June 2011 earthquake and second 23 December 2011 earthquake also have increased curvatures in the non-linear fixed base models.

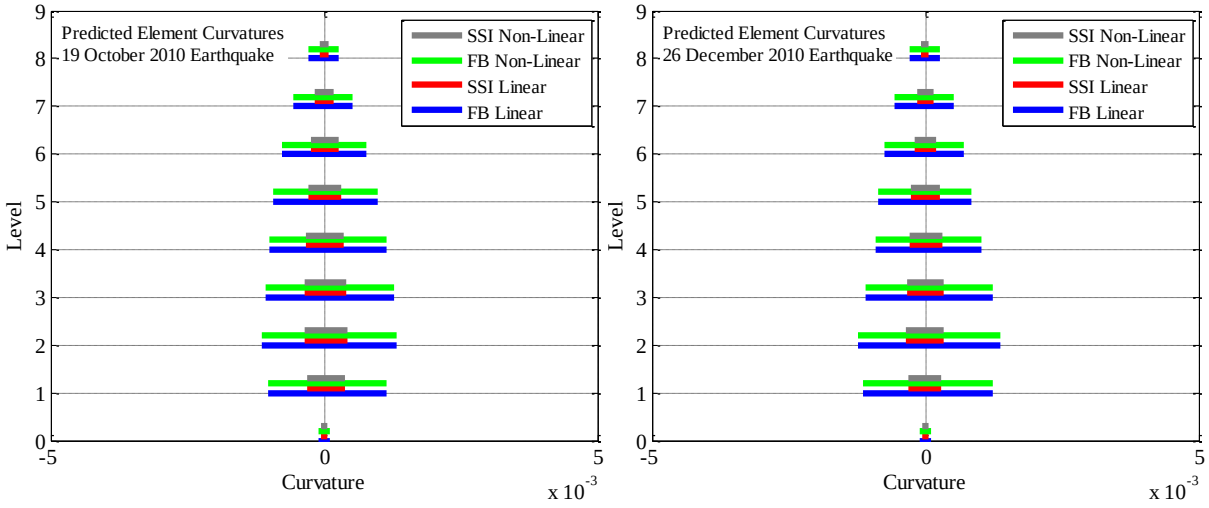

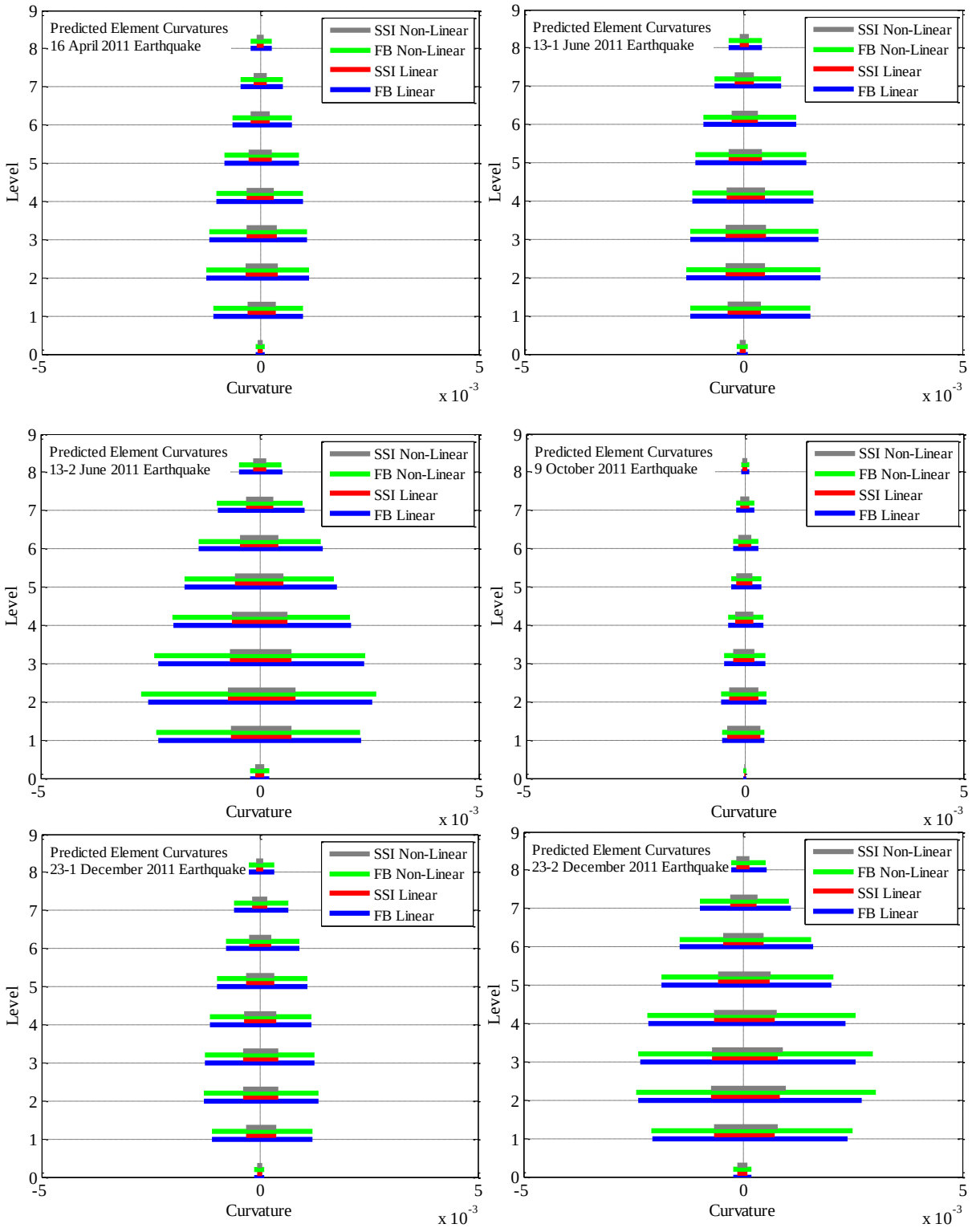


Figure 7-33: Maximum base and beam curvatures from the four 2D transverse models for all earthquakes.

## 7.7 Prediction of torsional response

A three dimensional (3D) model of the UC Physics Building was developed by combining two longitudinal frames plus three transverse walls with a rigid floor on each level. For simplicity, each system had zero stiffness out of plane, so the response in each direction was governed by the behaviour of the systems previously considered in the 1D and 2D modelling. The model at this stage should produce the same displacements as the 2D models in each direction. The model was then adjusted so that the floors could twist torsionally about the vertical axis as a result of differential stiffness that appeared to exist in the actual structure.

The connection between the Physics Building and the Link Building is meant to act as a seismic gap so that the two buildings can respond separately during an earthquake. In reality, three factors that could potentially result in the interaction of the Physics and Link Buildings include: (i) the seismic gap not being 'perfect' as thin steel plates and services pipes connect the two buildings at each floor level; (ii) the foundation, which is a continuous system connecting all three buildings (Chemistry, Link and Physics); and (iii) each building having foundations which are designed in a different manner (Chemistry and Link Building foundations consist of a full basement which is fully embedded while the Physics Building foundation is a half basement filled with gravel is only partially embedded).

In order to try and replicate the contribution of the Link Building on the Physics Building, a simple multi degree-of-freedom (MDOF) model representing the transverse behaviour of the Link Building was constructed using the structural plans. The MDOF was placed at the south-west end of the 3D model and attached to the model using a zero length springs connected to each frame, which have non-zero stiffness in the transverse direction only. The stiffness of the springs was adjusted until the desired torsional behaviour was reached. Once the required spring stiffness was calculated, simple calculations were performed in order to determine what could possibly cause this level of restraint. The 3D model was then used to predict the displacement of both ends of the structure which is directly compared with the observed displacements from each shear wall. The amount of torsional rotation predicted from each earthquake and the period of the torsional mode are also be compared with the observations.

### 7.7.1 Development of 3D analysis model

Initially, the floor diaphragm was fixed against torsional rotation so that the 3D model could be compared with the relevant 2D model in each direction. The first four modes of the 3D model are shown in Figure 7-34 (a) to (d). The first and third modes relate to the transverse direction and are the first two translational modes in that direction. The second and fourth modes are in the longitudinal

direction and are again the first two translational modes for that direction. The periods of the modes are identical to the individual 2D models which shows that the 3D model is working correctly as a combination of the two 2D models.

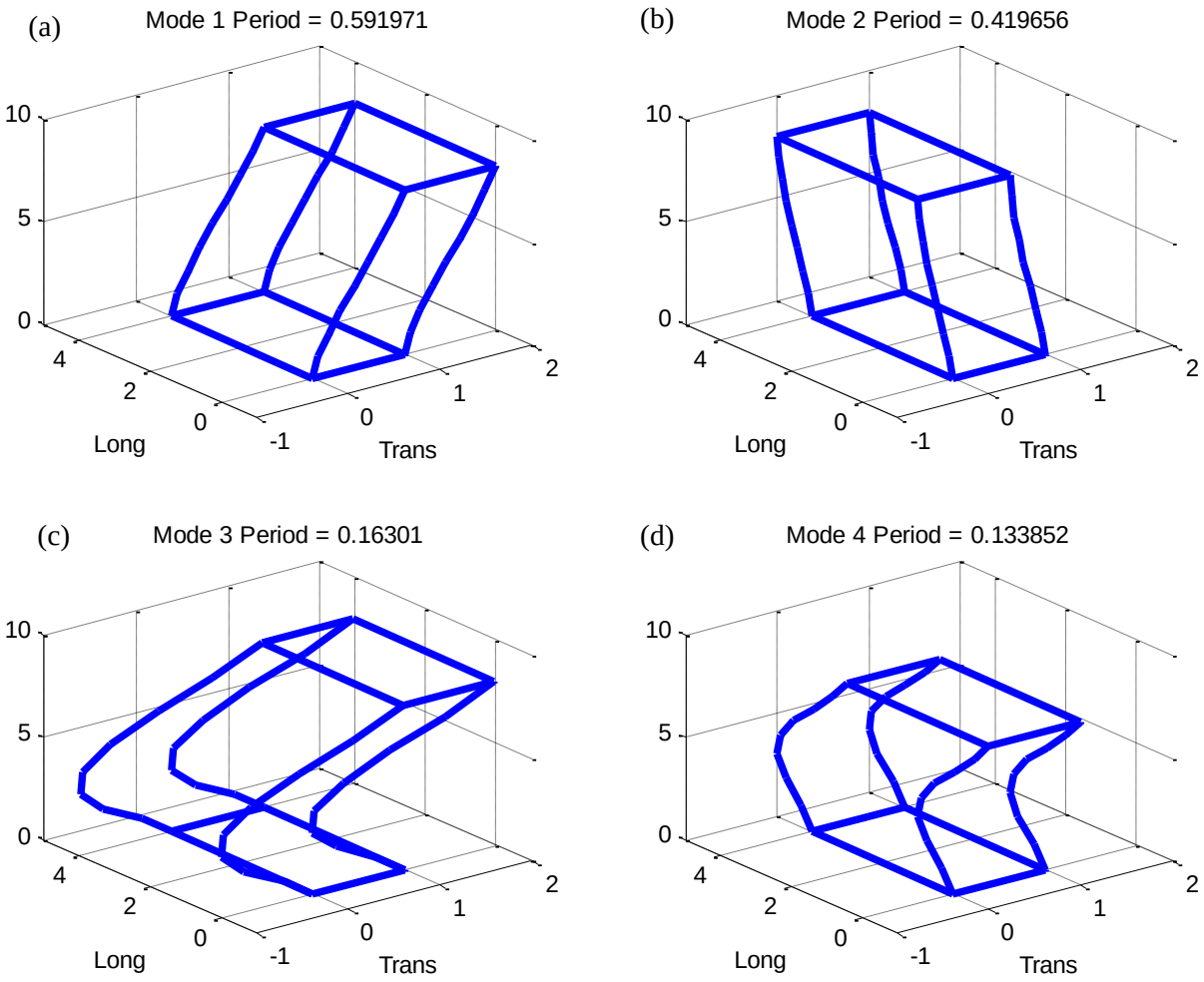


Figure 7-34: (a) First, (b) second, (c) third and (d) fourth mode shape and period for the 3D model with no torsion.

The maximum response of the longitudinal and transverse directions for the 3D model is shown in Figure 7-35. This response is similar to the maximum response of the two individual models in each direction. The observed displacements are now displayed as the two individual observations from each end of the building. These values can now be directly compared with the models predicted displacement from each end of the building. However, in this case where the floor is fixed from torsional movement, the prediction from each end of the model will be the same, as shown in the figure.

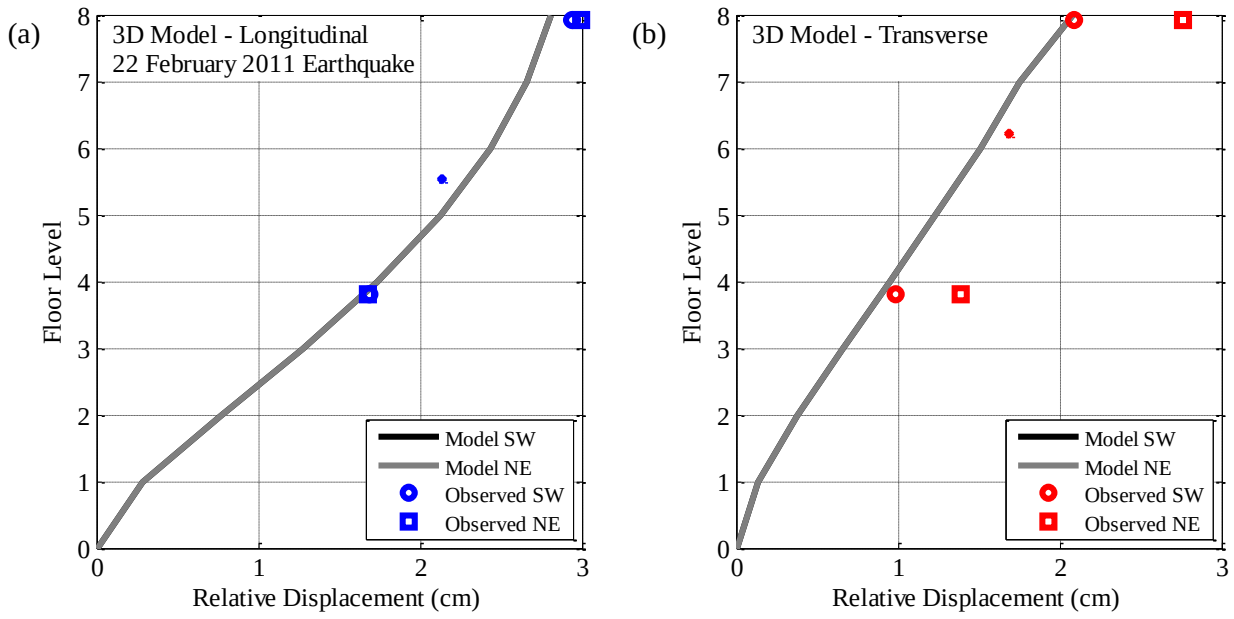


Figure 7-35: Comparison of the maximum deflected shape between observations and the 3D model with no torsion in the (a) longitudinal and (b) transverse direction for the 22 February 2011 earthquake.

The next step was to remove the torsional fixity of the floor so that the torsional behaviour could be predicted. This allowed for the calculation of the torsional mode as shown in Figure 7-36 (b) as the second mode of the structure with a period of 0.48 seconds. The third structural mode is now the first translational mode in the longitudinal direction and the fourth mode of the 3D model is now the second translational mode in the transverse direction.

The Link Building was modelled as a MDOF in the transverse direction with the mass and stiffness properties determined by the structural drawings. The fundamental period of the Link Building was equal to 0.43 seconds (in comparison, the fundamental period of the transverse direction of the Physics Building was 0.59 seconds). This was connected to the 3D Physics Building model using horizontal springs in the transverse direction. The stiffness of the springs was determined using trial and error and the resulting stiffness used was equal to 8,000 kN/m. The torsional period of the model (0.46s) is between the two torsional periods observed calculated in Chapter 4 using spectral and Fourier analyses which were 0.50s and 0.43s respectively. There was however, a large variability in calculated torsional period in both methods which shows how hard it is to determine the fundamental period especially for small amplitude ground motion records where the torsional mode may not even be excited.

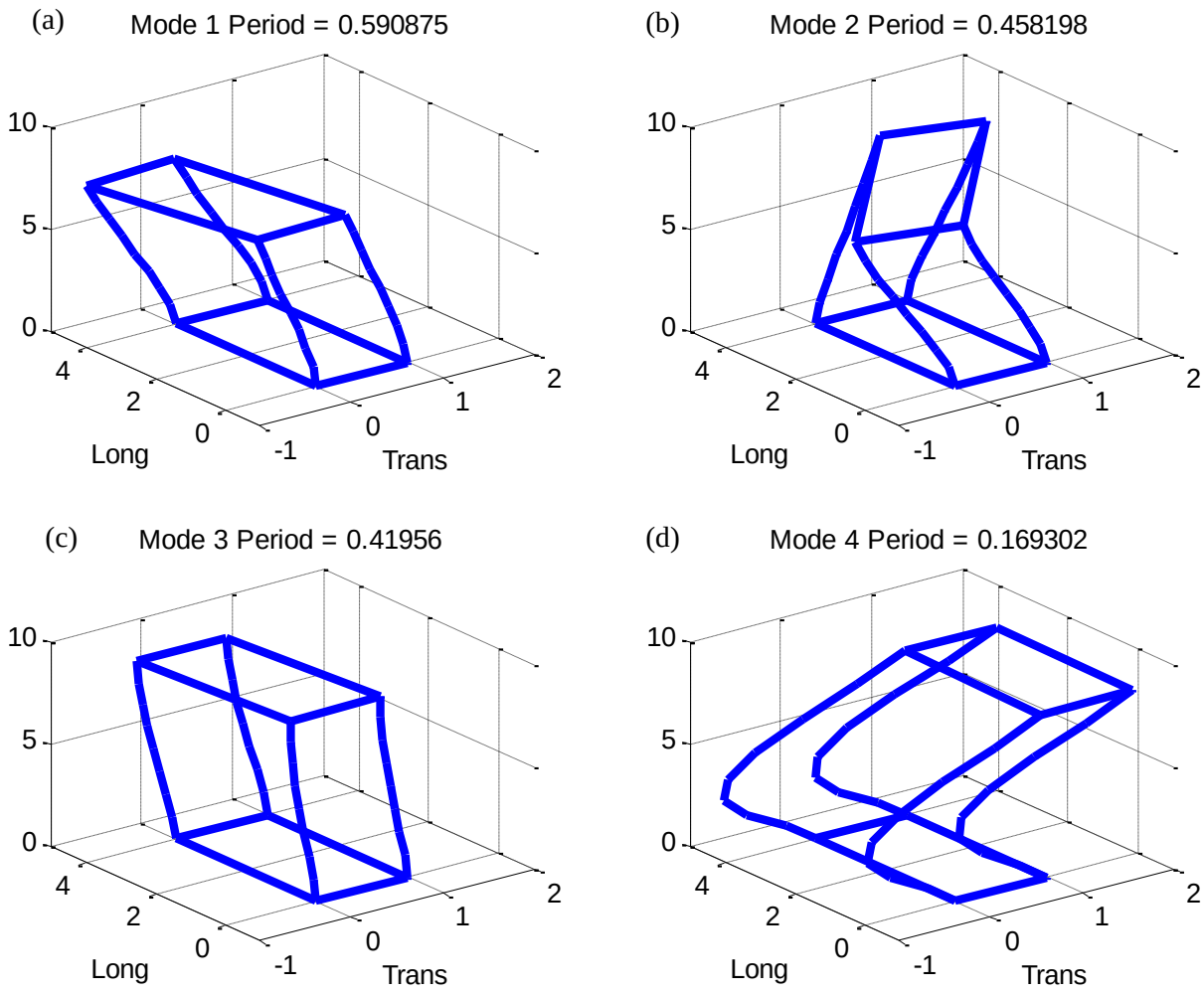


Figure 7-36: (a) First, (b) second, (c) third and (d) fourth mode shape and period for the 3D model with torsion.

### 7.7.2 Comparison between observed and predicted torsion

The maximum displacement response of the 3D torsional model in each direction for the 22 February 2011 earthquake is shown in Figure 7-37. It can be seen that in the transverse direction that the response at each end of the model is different with the north-east (NE) end producing larger displacements compared with the south-west (SW) end which has the horizontal springs attached to the MDOF. The response at the NE end from the 3D model is larger than the predicted response from the 2D model. This is a result of the torsional mode increasing the edge displacements of the 3D model (Chopra & Llera, 1996). The predicted displacements at both ends are still less than the observations however, if SSI was allowed for as in Chapter 6, then the predictions would be expected to be closer. Due to time constraints, a combined 3D SSI model was not considered in this research. In the longitudinal direction, the predicted displacement profile is the same as the 2D fixed base model as the torsional mode is purely in the transverse direction.

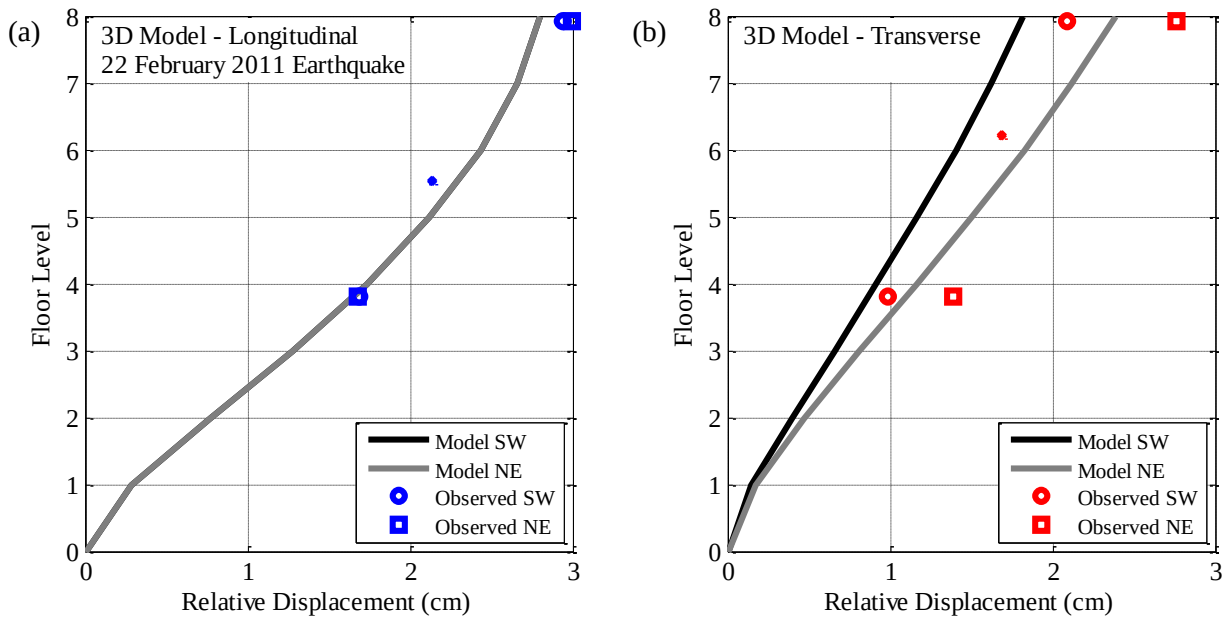


Figure 7-37: Comparison of the maximum deflected shape between observations and the 3D model with torsion in the (a) longitudinal and (b) transverse direction for the 22 February 2011 earthquake.

The displacement response series from the fourth and eighth floors can be compared with the responses from both ends of the model. This is shown in Figure 7-38 for the 22 February 2011 earthquake. The 3D model predicts the displacement response series at both ends very well, picking up the peak response as well as the subsequent steady state response.

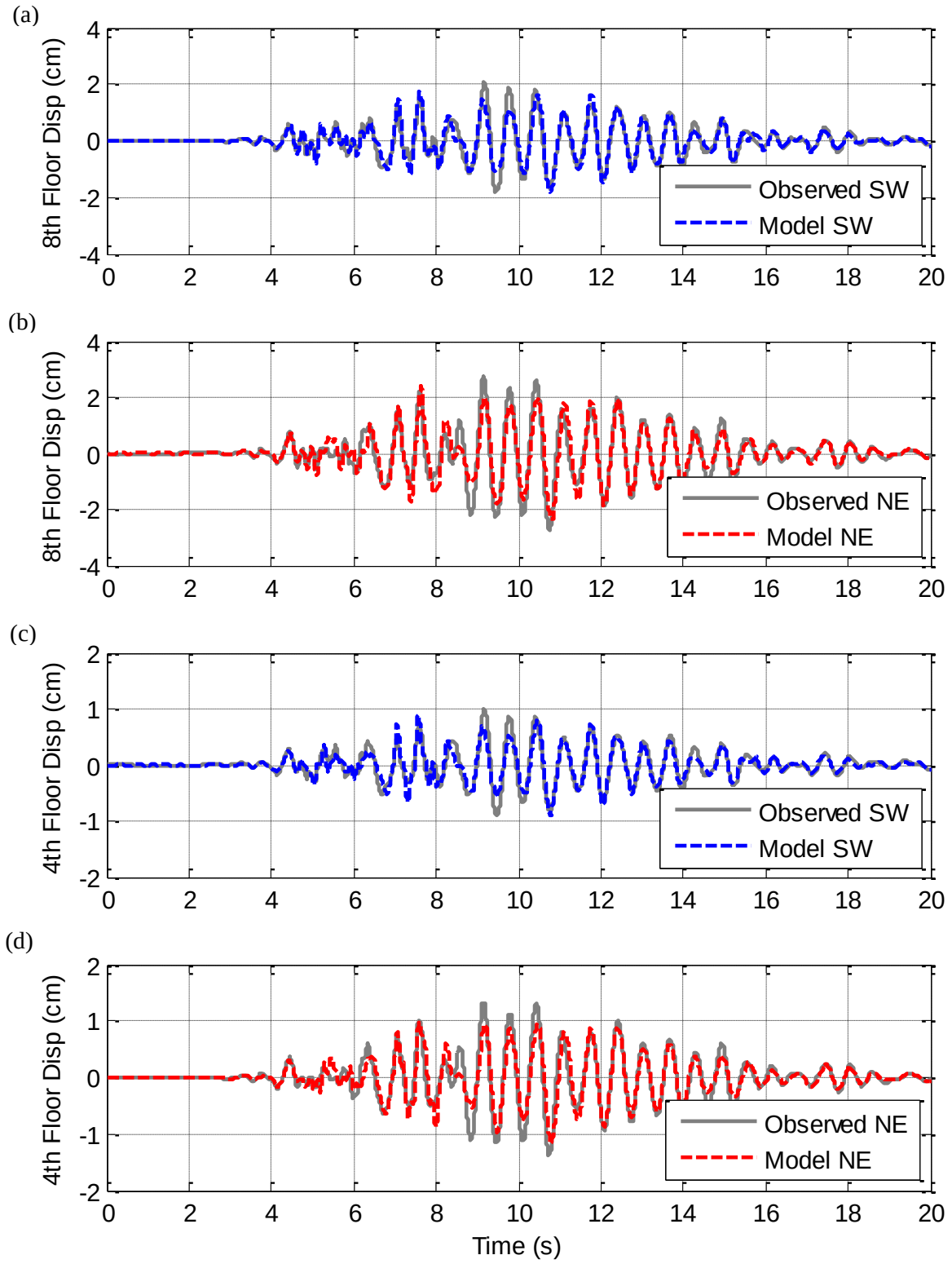


Figure 7-38: Comparison of the eighth and fourth floor transverse displacement time series for the (a) and (c) SW and (b) and (d) NE ends of the structure from the 3D torsional model for the 22 February 2011 earthquake.

The maximum response of the 3D model to the 4 September 2010 earthquake and 13 June 2011 earthquake is shown in Figure 7-39 and Figure 7-40 respectively. The displacement time series response for the 4 September 2010 earthquake and 13 June 2011 earthquake is shown in Figure 7-41

and Figure 7-42 respectively. It can be seen that a good prediction is obtained in both events without NL or SSI effects considered. This implies that 3D effects are quite important and that the 2D models are not able capture this, therefore importance of NL and SSI effects may be overstated in the previous chapters.

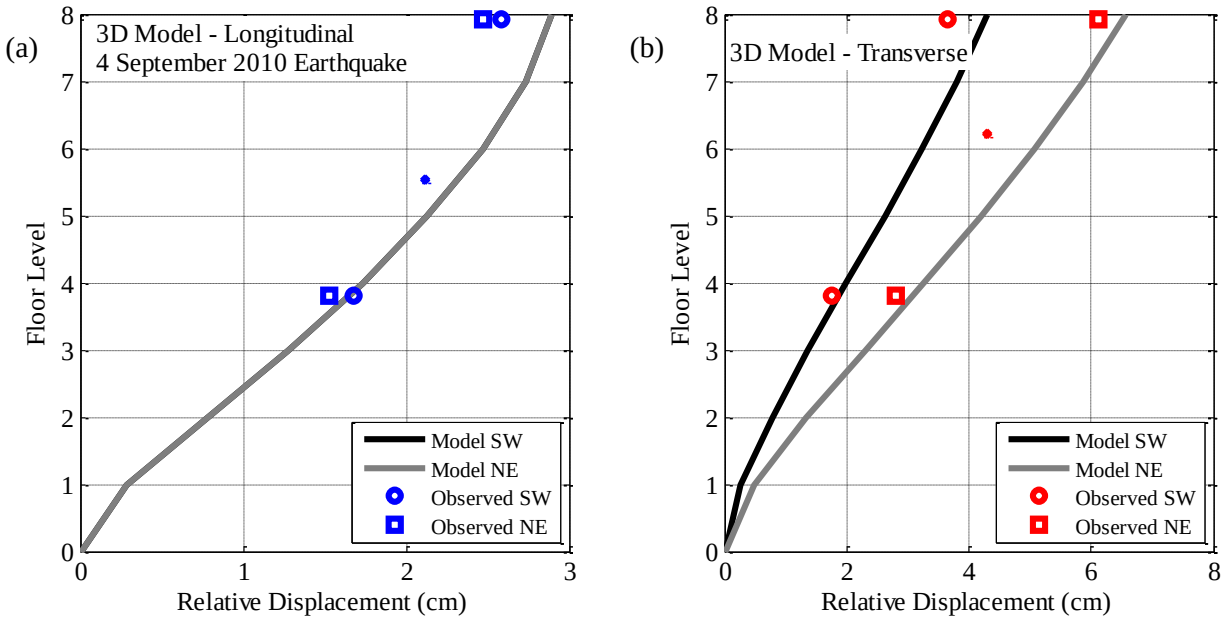


Figure 7-39: Comparison of the maximum deflected shape between observations and the 3D model with no torsion in the (a) longitudinal and (b) transverse direction for the 4 September 2010 earthquake.

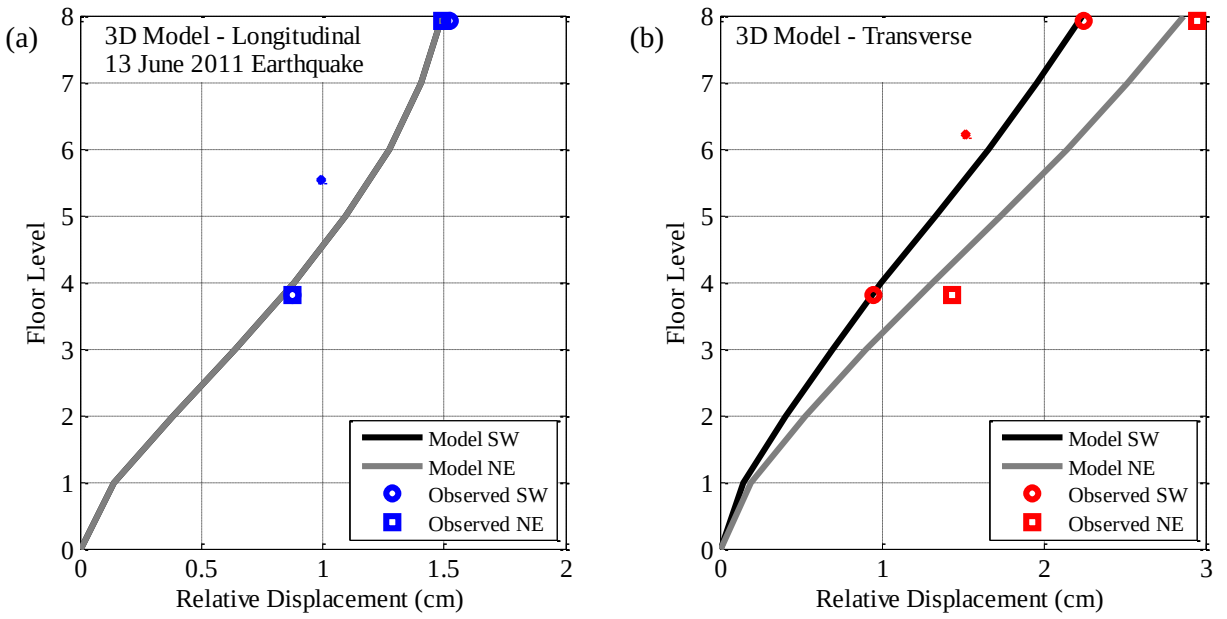


Figure 7-40: Comparison of the maximum deflected shape between observations and the 3D model with no torsion in the (a) longitudinal and (b) transverse direction for the 13 June 2011 earthquake.

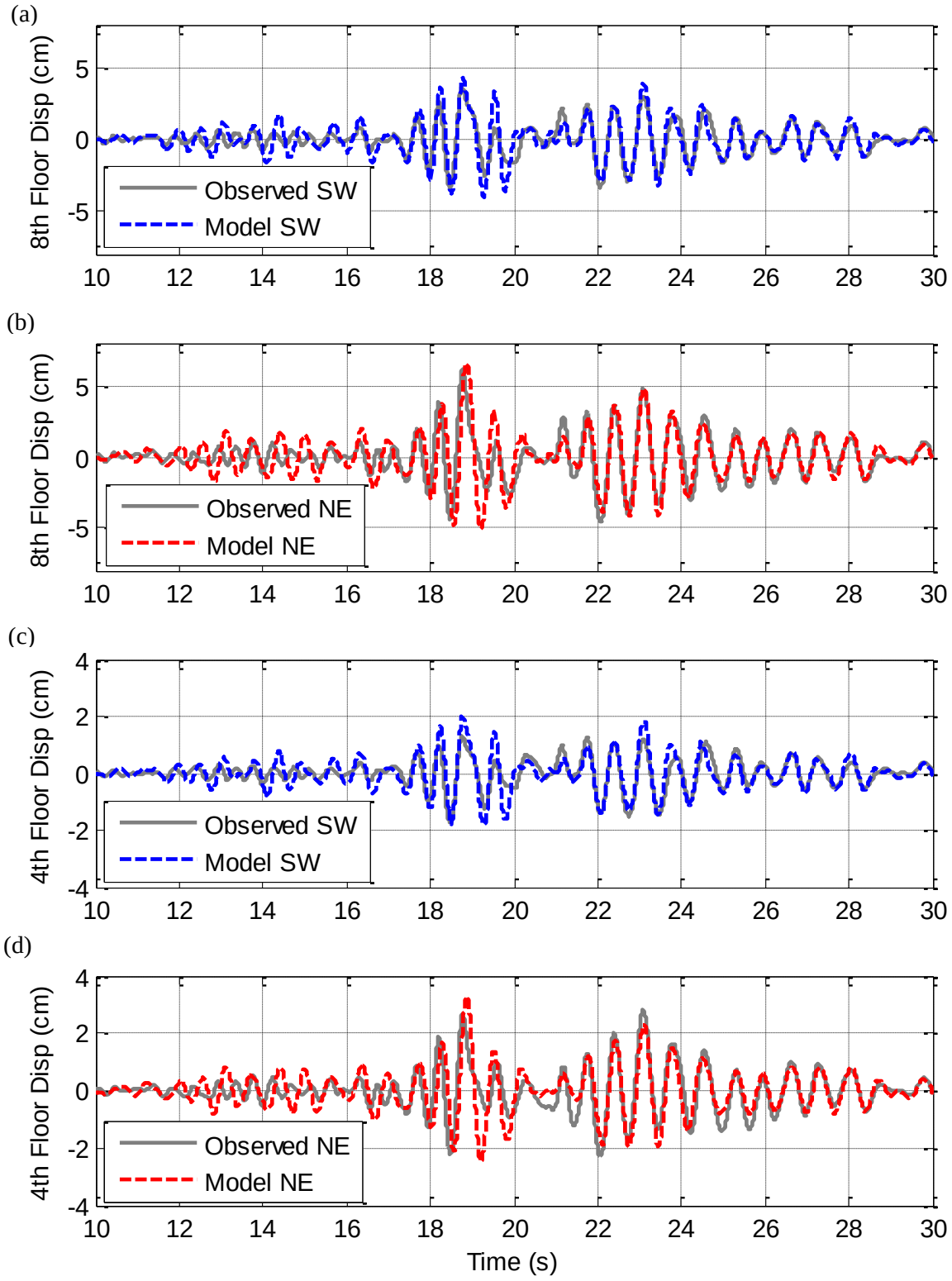


Figure 7-41: Comparison of the eighth and fourth floor transverse displacement time series for the (a) and (c) SW and (b) and (d) NE ends of the structure from the 3D torsional model for the 4 September 2010 earthquake.

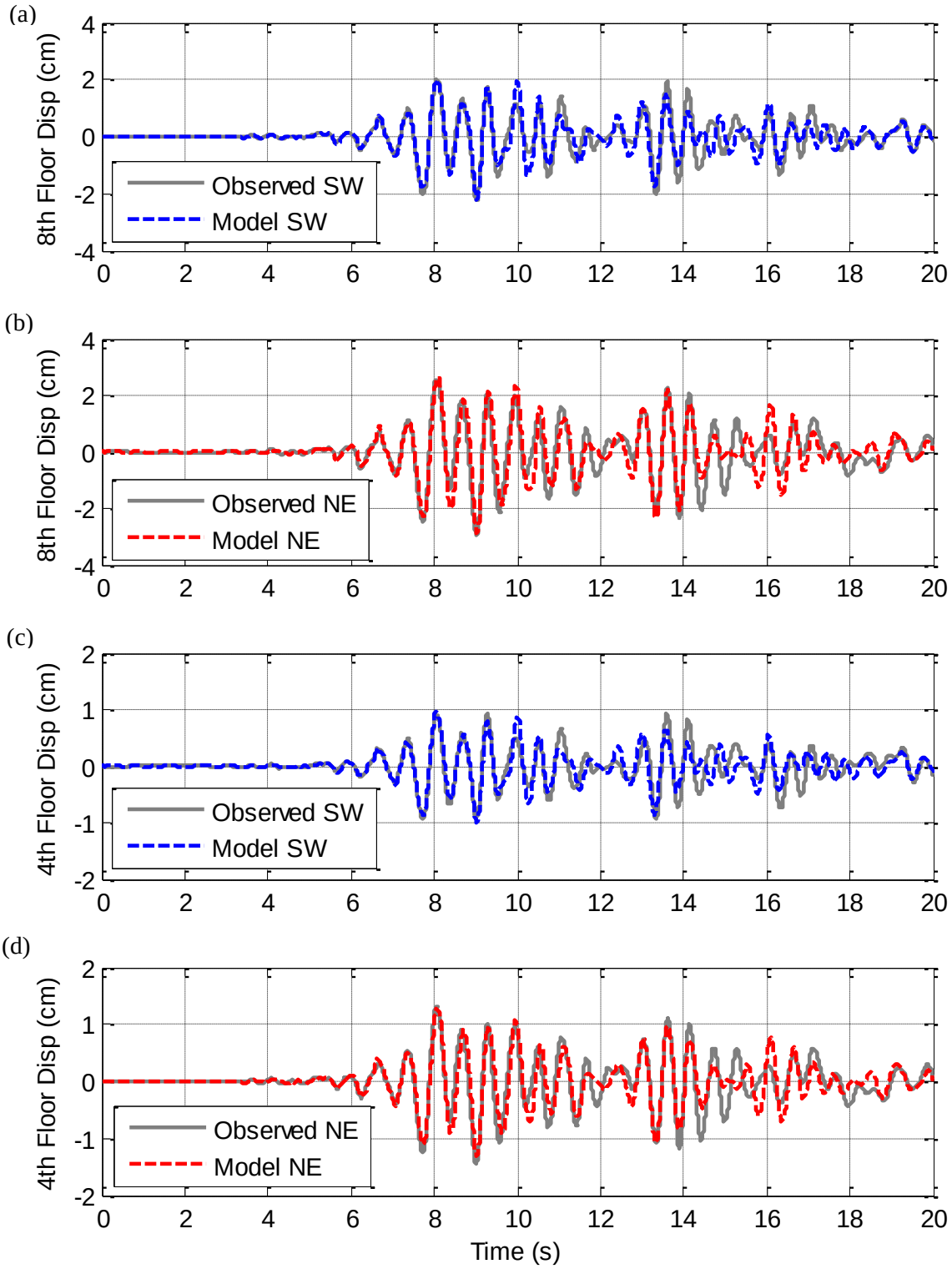


Figure 7-42: Comparison of the eighth and fourth floor transverse displacement time series for the (a) and (c) SW and (b) and (d) NE ends of the structure from the 3D torsional model for the 13 June 2011 earthquake.

When the south-west end of the Physics Building move relatively to the Link Building, the springs connecting the two apply a restoring force to try and bring the two back together. This resorting force

is equal to the spring stiffness multiplied by the relative displacement between the two buildings. The relative displacement between the eighth and fourth floors is shown in Figure 7-43.

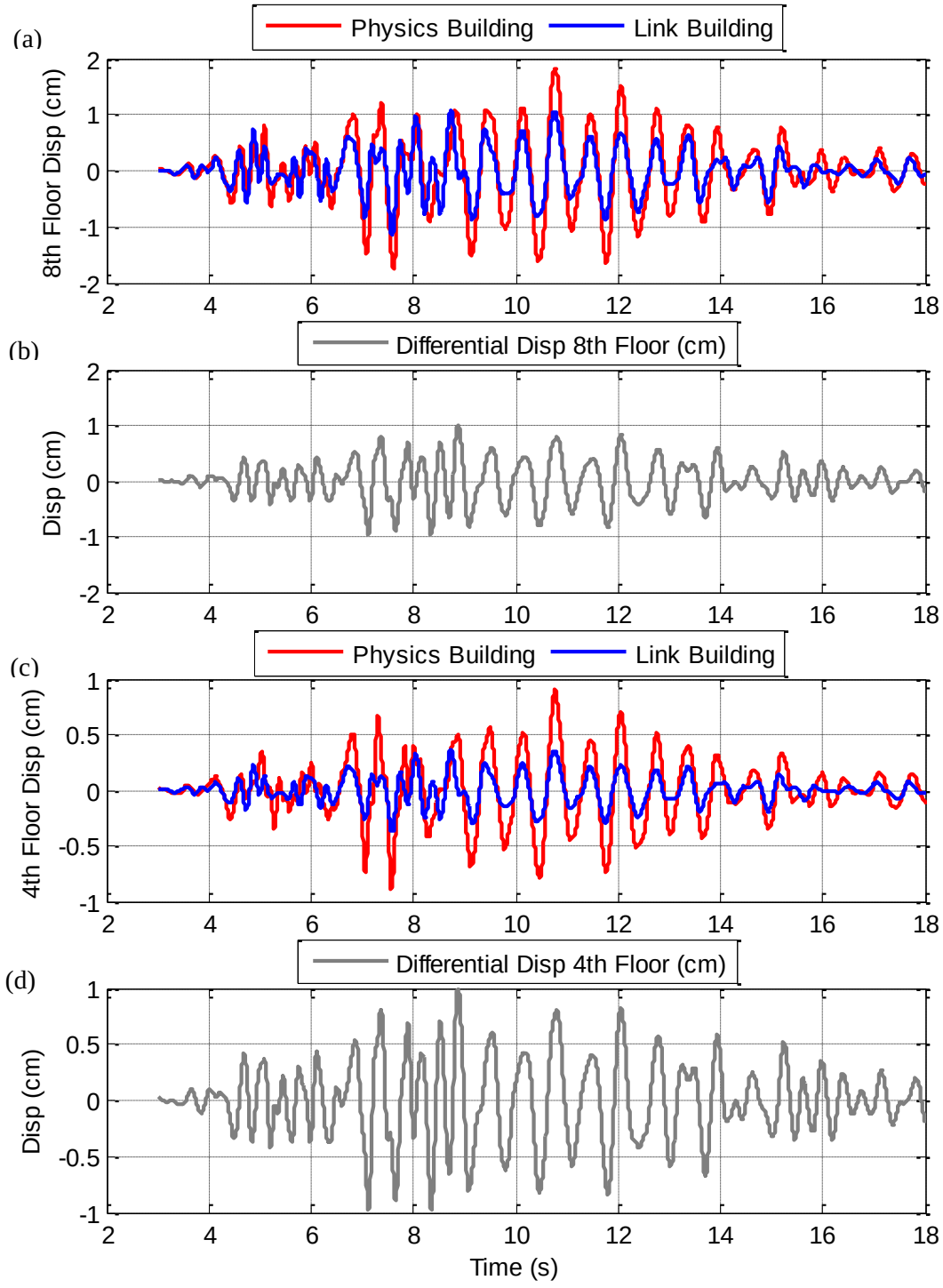


Figure 7-43: Differential displacement between the Link Building and the Physics Building on the (a) and (b) eighth and (c) and (d) fourth floors for the 22 February 2011 earthquake.

Using the spring stiffness (K) of 8,000 kN/m (2 springs per floor) and the maximum relative displacement between the two buildings ($D_{max}$),the maximum resorting force can be calculated to be:

$$F_{max} = 2 \times K \times D_{max}$$

$$F_{max} = 2 \times 8{,}000\ N/mm \times 10\ mm$$

$$F_{max} = 1.6 \times 10^5\ N$$

The spring stiffness represents the contribution of many factors which restrict the movement of the SW end of the Physics Building and at present it is not self-evident what is the cause of this restraint. However, the cross sectional area of steel undergoing plastic deformation required to match this level of shear stiffness can be approximated. This can be calculated using the following equation:

$$\tau_p = \frac{F}{A}$$

where, $\tau_p$ is the plastic shear stress in the steel (assumed to be 150 MPa for grade 300 steel (Gorenc *et al.*, 2012)) and A is the cross sectional area of steel subject to the shear force.

$$A = \frac{F}{\tau_p}$$

$$A = \frac{1.6 \times 10^5\ N}{150 \times 10^6 N/m^2}$$

$$A = 1.1 \times 10^{-3} m^2$$

This is a very small area of steel which implies that only a small connection between buildings can result in a large torsional response. For example, if the steel plates which cover the seismic gap through the doors are 1.0m wide, then a thickness of 1mm would be sufficient to provide this area. Clearly the connection of any unforeseen restraints between the Physics and Link buildings would not be rigid, (i.e. there would be some 'slop' in the restraint) it can be seen that very little restraint is required to result in the observed torsional response.

The maximum angle of torsional twist predicted by the model can be compared with the observed torsion angle. The observed torsional effects were discussed in more detail in Chapter 4. The comparison between predicted and observed angles of torsion can be found in Figure 7-44 for each earthquake. It can be seen that the two angles are very close and are within 30% for all earthquakes.

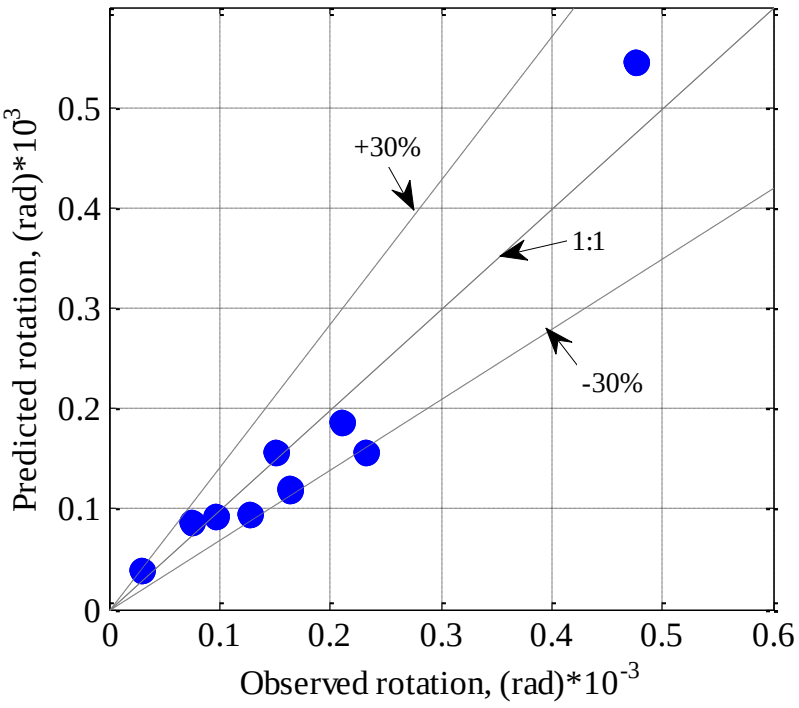


Figure 7-44: Predicted vs observed torsion rotation angle from 3D model.

## 7.8 Conclusions

This chapter has provided a detailed examination of simple conventional non-linear modelling for the prediction of the seismic response of the UC Physics Building in the Canterbury earthquakes. The 2D models were adjusted to allow for non-linear material behaviour and the predictions from the models were compared with observations. A 3D model of the UC Physics Building was also constructed and used to predict torsion using spring connections to a model of the Link Building. The predicted torsion was compared with the observed torsional response. A summary of the main findings from this chapter are detailed below:

- A bi-linear constitutive model was used to represent the material non-linear behaviour of the base of the wall, while a tri-linear degrading model was used to represent the behaviour of the beams. Material non-linearity was modelled using lumped plasticity in the zones where non-linear behaviour is most likely to occur. Non-linear elements were added to the longitudinal fixed base model and the fixed base and SSI transverse models.
- In the longitudinal direction, the fixed base non-linear model had the smallest average percentage error which was equal to 0.7%. The best longitudinal model was the non-linear SSI model which had an average percentage error of 6.3%, however, this model still under-predicted the response of the fourth and sixth floors by approximately 9%.
- The effect of sequential earthquake loading was investigated by comparing the non-linear response of the 22 February 2011 earthquake only and the response to the combined 4 September 2010 and 22 February 2011 earthquakes. It was found that the combined response was dependant on the final state of the 4 September 2010 earthquake. This resulted in an increase in the fundamental period of the structure during the 22 February 2011 earthquake causing it to be out of phase with the observations.
- The maximum curvature demand on each floor was compared for the four different models (FB-L, SSI-L, FB-NL, and SSI-NL) in each direction. This meant that the effect of adding the SSI and non-linear behaviour on the maximum curvatures could be examined for each earthquake event. In the longitudinal direction, the addition of SSI had no effect on the maximum curvature, however, the non-linearitie's increased the curvature for the lower floor beams in the larger earthquakes. In the transverse direction, the addition of SSI decreased the maximum curvatures for the beams on each floor during all earthquakes. The non-linearitie's in the transverse direction also increased the curvatures for the larger amplitude ground motion events.
- Finally, a three dimensional (3D) model was developed in order to determine if the observed torsional behaviour could be modelled. A 3D model was constructed using the two 2D models connected with a rigid floor. The contribution of the Link Building was modelled as a

multi degree-of-freedom model connected to the 3D model with transverse springs. The springs had a stiffness of 8,000 kN/m. This allowed for the prediction of the torsional period which was equal to 0.46 s. The 3D model was able to predict the different response of both end shear walls and the predicted deflected shape appeared to follow the observed deflections better than the 2D models. This results suggested that the 3D effects were quite important and that the 2D models were not able capture this. The predicted maximum torsional angle was also compared with the observed angle and the prediction was within 30% for all earthquakes.

## 7.9 References

Chopra, A. K., & Llera, J. C. D. L. (1996). *Accidental and Natural Torsion in Earthquake Response and Design of Buildings*. Paper presented at the 11 WCEE, Acapulco.

Gorenc, B., Syam, A., & Tinyou, R. (2012). *Steel Designers' Handbook*. Sydney: NewSouth Publishing

Montejo, L. A., & Kowalsky, M. J. (2007). CUMBIA—Set of codes for the analysis of reinforced concrete members. *CFL Technical Rep. No. IS-07 1*.

Mylonakis, G., & Gazetas, G. (2008). Seismic soil-structure interaction: Beneficial or detrimental. *Journal of Earthquake Engineering,* **4**(3), *277-301*.

Otani, S. (1984). *Hysteresis Model of Reinforced Concrete for Earthquake Response Analysis*. Paper presented at the 8 WCEE, San Francisco.

Park, R., & Paulay, T. (1975). *Reinforced concrete structures*. New York: John Wiley & Sons.769.

Raghunandan, M., Liel, A. B., Ryu, H., Luco, N., & Uma, S. R. (2012). *Aftershock Fragility Curves and Tagging Assessments for a Mainshock-Damaged Building*. Paper presented at the 15 WCEE, Lisbon.

Stojadinovic, B., & Thewalt, C. R. (1996). *Energy Balannced Hysteresis Models*. Paper presented at the 11 WCEE, Acapulco.

Takeda, T., Sozen, M. A., & Nielsen, N. N. (1970). Reinforced Concrete Response to Simulated Earthquakes. *ASCE, Journal of the Structural Division,* **96**(No. ST12).

# 8 CONCLUSIONS

The main objective of this research was to examine the predictive capability of numerical seismic response models using various conventional assumptions adopted in earthquake engineering practice. This University of Canterbury (UC) Physics Building was utilized as a case study because of the numerous strong ground motions which this building was subjected to during the Canterbury earthquake sequence during which the seismic response was recorded with an instrumental array. Initially, a detailed understanding of the observed seismic response of the UC Physics Building was found using the recorded acceleration records. Numerical models were then developed with increasing complexity in order to examine the predictive capability of each. The effect of various design assumptions was identified by comparing predicted displacements from the numerical models with the observed recorded behaviour. In particular the effects of 1D, 2D and 3D modelling, non-linear constitutive models, and soil-structure-foundation interaction were examined. A summary of the main conclusions from the various chapters is provided below with design recommendations based on this case study.

## 8.1 Observed response

Chapter 4 provided a detailed overview of the observed response of the UC Physics Building from the ground motions generated in the Canterbury earthquake sequence. The findings from that chapter were:

- Ten of the largest earthquake events from the 2010-11 Canterbury earthquake sequence were selected in order to understand the seismic response of the UC Physics Building. This included the two largest events of the 4 September 2010 earthquake with a magnitude of 7.2 and the 22 February 2011 earthquake with a magnitude of 6.2.
- The largest PGA, PGV and PGDs at the base of the structure were recorded during the 4 September 2010 earthquake and were found to be 0.25g, 42.3cm/s and 13.5cm, respectively. Six out of the ten ground motions selected had PGA values greater than 0.1g. The largest level of acceleration recorded in the building itself was on the eighth floor during the 22 February 2011 earthquake and equal to 0.76g. Rocking behaviour was observed in the

building during the earthquakes with the maximum angle of rocking equal to $1x10^{-2}$ rad in the transverse direction and $1.9x10^{-3}$ rad in the longitudinal direction during the 4 September 2010 earthquake. Significant torsional behaviour was also observed in the transverse building response for al earthquakes. The maximum angle of torsional movement was observed during the 4 September 2010 earthquake and was equal to 48 $x10^{-3}$ rad.

- The fundamental period of the building was found in each orthogonal direction using both pseudo-spectral and Fourier analysis. Both analytical methods produced practically the same result in the longitudinal direction where the fundamental period was found to be 0.42 s. It was found that, on average, the fundamental period in the transverse direction was 0.59 s. The fundamental period of the rocking motion was found to be 0.61s in the transverse direction and 0.45 s in the longitudinal direction. These periods were very similar to the fundamental period of the translational motion in each direction. The period of the torsional motion was found to lie in the range of 0.43s to 0.50s.

## 8.2 Comparison of observations with design codes

Chapter 5 provided an overview of seismic design code prescriptions and compared the observed response of the UC Physics Building with the prescribed values. The key findings from this chapter are detailed below:

- Response spectra produced by the recorded ground motions from each earthquake were compared with the design spectra in both horizontal and vertical directions. The 4 September 2010 and 22 February 2011 earthquakes produced horizontal and vertical response spectra values above the design level for certain periods. All other earthquakes were within the design spectra envelope.
- The empirical formula for the amplification of peak horizontal floor accelerations with respect to the height of the building was compared with the observed amplification. It was found that a maximum ratio of three prescribed by the NZ code provided a good match with the eighth floor observations. However, all observations from the fourth floor were less than the prescribed value, suggesting that the code is over-conservative in this range for this particular structure.
- An estimate of the fundamental period prescribed by 1170.5 was compared with the observed fundamental period in both horizontal directions. The predicted values were both significantly larger than the observed period.
- The percentage of gross stiffness required to match the observed period was compared with suggested effective stiffness values for reinforced concrete from NZS3101. The percentage

of gross stiffness required was dependent on whether the model included soil-structure interaction or not. In the longitudinal direction, 21% of the gross stiffness was required to match the observed period while 28.5% was required in the transverse direction. These values were both significantly less than the prescribed stiffness reduction however, the percentage increased to 80% in the transverse direction when SSI was included.

## 8.3 Numerical modelling

### 8.3.1 1D vs 2D modelling

Chapter 5 provided a detailed overview of conventional modelling practices and how they compare with the observed behaviour of the UC Physics Building during the 2010-2011 Canterbury earthquakes. The key findings from this chapter are detailed below:

- The 1D and 2D numerical models were constructed with the same fundamental period and they predicted similar deflected shapes. The slight difference in the deflected shape between the two models in the longitudinal direction was due to the inability of the 1D model to capture the interaction between the horizontal and vertical elements. The longitudinal frame is made up of ten bays by eight stories and the vertical elements in the 1D model were not sufficient to replicate this interaction. The two transverse models had the same deflected shape, however, the transverse system consisted of shear walls so the 1D model was able to represent this behaviour. Both transverse models under-predicted the maximum deflected shape because they did not account for soil-structure interaction or non-linear behaviour.
- It is worth noting that although the 1D model was comparable with the 2D model when predicting the deflected shape, it is significantly more difficult to define the appropriate stiffness of the elements in the 1D model. The elements in a 2D model represent real structural members such as beams and columns, whereas, the vertical elements in a 1D model represent the stiffness contribution of the beams and columns combined. Therefore it would be easier to make a 2D model in the first instance so that the fundamental period of the structure can be found before making a 1D model with the same period (should computational issues make running a dynamic 2D analysis problematic). For this research this was not required as the fundamental period was already known from observations.

### 8.3.2 Soil-structure interaction

Chapter 6 provided a detailed examination of simple soil-structure interaction models for the prediction of the seismic response of the UC Physics Building in the Canterbury earthquakes. The 1D and 2D models from the previous chapter were adjusted to allow for base flexibility and the predictive capability of the SSI models was compared with observations. A summary of the main findings from this chapter are detailed below:

- A rotational spring was added to the base of 1D models with a stiffness defined by Gazetas (1991), based on the soil and foundation properties of the UC Physics Building. The predictions from the transverse 1D SSI model were significantly closer to the observed response compared with the fixed base model. The longitudinal 1D SSI model did produce better predictions as the rotational spring had a very high stiffness due to long foundation in that direction. This therefore suggested that there was noteworthy SSI occurring the in the transverse direction, but not the longitudinal direction. In the transverse direction three different 2D SSI models were examined, two based on the 1D Gazetas rotational spring and one base on a Winkler beam system. It was found that the two Gazetas spring methods produced similar predictions, however, they did not increase the deflected shape significantly. The Winkler spring method did improve the fixed base predictions, but the model still under-predicted the average observed displacement on each floor.
- The stiffness of the rotational and vertical springs in the SSI models was adjusted to allow for soil strength degradation based on the equivalent linear approach. The observed degradation was compared with that predicted by Paolucci *et al.* (2009) and FEMA 356 (2000) methods. It was found that FEMA356 prescription under-predicted the amount of degradtion while the Paolucci *et al.* (2009) method slightly over-predicted the degradation.
- Based on this research, the best way to initially model SSI would be to use a 1D model as was able to sufficiently model the observed SSI. A 1D model can be easily constructed based on a 2D model, as described in the previous section. The 1D model can be adjusted to allow for SSI using a Gazetas (1991) rotational spring and the response can be compared with a fixed base 1D model. If the SSI model does not significantly change the fixed base predictions, then SSI does not need to be included in a 2D model analysis. However, if the 1D SSI is significant then a 2D SSI model should be constructed in order to determine the combined effect of SSI and non-linear behaviour.

### 8.3.3 Non-linear effects and torsional behaviour

Chapter 7 provided a detailed examination of simple conventional non-linear modelling for the prediction of the seismic response of the UC Physics Building in the Canterbury earthquakes. The 2D

models were adjusted to allow for non-linear material behaviour and the predictions from the models were compared with observations. A 3D model of the UC Physics Building was also constructed and used to predict global torsion effects using spring connections to a model of the Link Building. The predicted torsion was compared with the observed torsional response. A summary of the main findings from this chapter are detailed below:

- Material non-linearities were modelled using a lumped plasticity approach for the 2D models. A bi-linear relationship was used to model the moment-curvature behaviour at the base of the walls while a tri-linear degrading relationship was used to model the beam behaviour. The choice of constitutive model become more important as the amount of non-linear behaviour increased. The non-linear 2D models provided better predictions for some earthquakes, however this was not always the case. The predictive capability of the non-linear (NL) model significantly changed with both the choice of constitutive model and parameters (yield moment and curvature) in the model. It should also be noted that although the effect of non-linear modelling was minimal for study, the demand was also relatively low. This was shown in the comparison between observed and design spectra in Chapter 5 where the demand was only slightly above the design level for the 4 September 2010 earthquake. It would be expected that the effect of non-linear modelling would be more important had the demand been higher.
- In the transverse direction, a combined SSI NL model was constructed based on the fixed base NL model and SSI linear model. The combined model was able to produce the best predictions in the transverse direction. It was noted that while allowing for non-linear behaviour increased the predicted beam curvatures for larger events, allowing for SSI deceased the beam curvatures for all events. This has an important implication in design as allowing for SSI means the model can withstand large inter-storey drifts with reduced demand on the beam plastic hinge regions.
- A 3D model of the Physics Building connected to a 1D model of the Link Building was developed to attempt to predict the torsional response observed in Chapter 4. The connection between the Physics and Link buildings was modelled with springs in the transverse direction with the spring stiffness determined based on trial and error. It was found that the model was able to predict the differential end displacements of the building in the transverse direction as well as the maximum torsion angle for most events. In order to model this behaviour without the observed results, the torsional response could be found by varying the stiffness of the springs, within a feasible range, so the worst case design demands on critical components could be found.